Electrochemical and structural studies of organometallic acetylide complexes

Rachel Louise Roberts

University of Durham

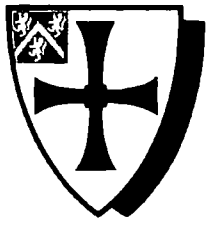

Electrochemical and Structural Studies of Organometallic Acetylide Complexes

Submitted by

Rachel Louise Roberts, M.Sci. Hons (Dunelm)

(Van Mildert College)

Department of Chemistry

A thesis submitted in part fulfilment of the requirements for the degree of Doctor of Philosophy at the University of Durham

2005

Abstract

This thesis describes the synthesis and properties of systems of the general type ML_x-bridge-ML_x, and related 'mixed-valence' derivatives.

The efficacy of the 1,1'-ferrocenediyl unit (Fc') as a bridge between two redox-active metal centres, is investigated by examination of the properties of a series of complexes, 1,1'-{Cp'(PP)RuC≡C}$_2$Fc', and the related binuclear model systems Ru(C≡CFc)(PP)Cp'. Whilst interactions through an ethyndiyl bridge occur between one Ru(PP)Cp' moiety and a ferrocenyl centre, in the 1,1'-{Cp'(PP)RuC≡C}$_2$Fc' systems no interaction between the terminal Ru(PP)Cp' groups is observed.

A comparative study of the redox and spectroscopic properties of the family of complexes [{Ru}$_2$(μ-C≡CXC≡C)]$^{n+}$ [{Ru} = Ru(PPh$_3$)$_2$Cp, Ru(dppe)Cp*; X = 1,4-C_6H_4, 1,4-$C_{10}H_6$, 9,10-$C_{14}H_8$; n = 0, 1, 2] is presented, together with those of the related mononuclear compounds. Comparison of the results with DFT calculations of the electronic structure allows the properties of the diethynylaryl-bridged, bimetallic complexes to be rationalised in terms of a significant contribution of the diethynylaryl bridging ligand to the SOMO.

The electronic properties of the 1,12-diethynyl carborane-bridged species 1,12-{Ru(dppe)Cp*}$_2$(μ-C≡C-$CB_{10}H_{10}$C-C≡C), and the related mononuclear complex Ru(C≡C-$CB_{10}H_{10}$CH)(dppe)Cp*, are assessed by a combination of electrochemical and spectroscopic techniques. The results allow a comparison of the 'three-dimensional' aromatic spacer 1,12-$C_2B_{10}H_{10}$ with the phenylene analogue.

Explorations of the acetylide chemistry of the Fe(dppe)$_n$ fragment are described. The resulting air stable complexes provide a convenient entry point to the acetylide chemistry of the octahedral iron fragment.

The details of additional crystal structures obtained by single crystal X-ray diffraction methods, together with a brief description of the chemistry associated with them, are presented in the appendix.

Acknowledgements

I would like to thank Dr Paul Low for his supervision, support and advice during the course of my Ph.D. I would also like to thank Professor Judith Howard for her guidance and encouragement throughout the last four years.

Thanks must also go to the past and present members of Lab 100 for making the lab such a great place to be over the last four years, namely Dr Olivia Koentjoro, Dr Michael Paterson, Dr Richard Cordiner, Mr W. M. Khairul Wan-Mohamed-Zin, Mr Julian Farmer, Dr Donocadh Lydon, Dr Mark Smith, Dr Mark Fox, and to the project students Hanilore Lonsdale, Gavin Forrest, Sophia Anderton, Matthew Feroze and Victoria Jeffries. Special thanks go to Olivia, Mike and Richard for their friendship and support from the beginning.

I would like to thank everyone in the crystallography group for their endless patience, and help with the structural aspects of this thesis. Special thanks go to Dr David Albesa-Jove, Dr Victoria Money, Dr Horst Puschmann, Dr Amber Thompson and Dr Mike Probert, whose help has been invaluable.

I would like to thank Dr František Hartl for providing me with the opportunity to work in The Netherlands and for his help and advice throughout my time there, and since. I would also like to thank the members of the molecular photonics group, UvA, especially Mr Taasje Mahabiersing, Mr Ron Jukes and Mr Zoran Popovic, for making me so welcome and for helping making my time in Amsterdam so enjoyable. Funding from the Marie Curie Fellowship award is gratefully acknowledged.

Many thanks are due the departmental technical staff for all their help and assistance over the course of this project. Thanks are also extended to people with whom aspects of this work was carried out in collaboration with; to Professor Michael Bruce and the Bruce group, for the compounds described in Chapter 2 and to Dr Andrew Beeby, Dr Laurent Porrès and Dr Simon Fitzgerald for their help with the Raman spectroscopic measurements.

Last but not least, many thanks go to my friends and family for all the encouragement and support they have shown me during my time at university. Special thanks are given to the girls of 2 High Wood View, namely Miss Rachel Slater, Miss Amy Thompson and Miss Lucy Wheatley for being such great housemates and for their friendship over the past three years.

Memorandum

The work presented in this thesis was carried out at the University of Durham between October 2002 and September 2005. This thesis is the work of the author, except where acknowledged by reference and has not been submitted for any other degree.

Part of this work has been presented at:

University of Durham, Departmental Final Year Postgraduate Symposium, 2005

University of Durham, Departmental Final Year Postgraduate Poster Competition, 2005

Metal Containing Molecules, 3rd Chianti Electrochemistry Meeting, Sienna, Italy, 2004

37th Universities of Scotland Inorganic Conference (USIC), University of Strathclyde, 2003

RSC Coordination Chemistry Discussion Group Meeting, Manchester, 2003

Statement of Copyright

Abbreviations

Å	angstroms
abs	absorption
Ar	aryl
av	average
bpy	2,2' - bipyridine
bpe6	1,2-bis(phosphorinan-1-yl)ethane
^{n}Bu	normal butyl
^{t}Bu	tertiary butyl
ca.	circa
cm^{-1}	wavenumber (reciprocal centimetres)
cod	cyclooctadienyl
Cp	cyclopentadienyl
Cp^{Me}	methylcyclopentadienyl
Cp*	pentamethylcyclopentadienyl
CV	cyclic voltammetry
Cy	cyclohexyl
dbpe	1,2-bis(di^{n}butylphosphino)ethane
depe	1,2-bis(diethylphosphino)ethane
DFT	density functional theory
dippe	1,2-bis(diisopropylphosphino)ethane
diph	1,2-bis(methylphenylphosphino)benzene
dmpe	1,2-bis(dimethylphosphino)ethane
dpe	H_2P-$(CH_2)_2$-PH_2
dppe	1,2 - bis(diphenylphosphino)ethane
dppf	1,1' - bis(diphenylphosphino)ferrocene
dppm	1,2 - bis(diphenylphosphino)methane
DPV	differential pulse voltammetry
ε	extinction coefficient (spectroscopy) or energy (DFT results)
ESR	electron spin resonance
ES(+)-MS	positive-ion electrospray mass spectrometry
Et	ethyl
eV	electron volts

Fc	ferrocenyl
Fc'	1,1'-ferrocendiyl
g	grams
HOMO	highest occupied molecular orbital
HS	high spin
IR	infra-red
IVCT	intervalence charge transfer
K	Kelvin
K_c	comproportionation constant
LMCT	ligand-metal charge transfer
LS	low spin
LUMO	lowest unoccupied molecular orbital
$[ML_x]$	general metal-ligand fragment
M	metal or molarity
Me	methyl
MeOH	methanol
mg	milligrams
min	minutes
MLCT	metal-ligand charge transfer
mM	millimolar
MMCT	metal-metal charge transfer
mmol	millimoles
MO	molecular orbital
ν	wavenumber (for infra-red spectra)
$\bar{\nu}$	wavenumber (for electronic absorption spectra)
NIR	near infra-red
NLO	non-linear optics or non-linear optical
nm	nanometres
NMR	nuclear magnetic resonance
OTE	optically transparent electrode
OTTLE	optically-transparent thin layer electrode
PE	potential energy
Ph	phenyl
ppm	parts per million
^{i}Pr	isopropyl

pyr	pyrazine
Rc	ruthenocenyl
SCE	standard calomel electrode
SOMO	semi-occupied molecular orbital
TBA	tetra-butyl ammonium
Tp'	hydridotris(3,5-dimethylpyrazolyl)borate
UV-vis	ultraviolet-visible
V_{ab}	electronic coupling constant
X	halide or spacer within a diyn(di)yl bridge

Table of contents

Chapter 2: 1,1'-Ferrocenediyl-Bridged Complexes

Chapter 3: Diethynylaryl-Bridged Complexes

Appendix 1: Additional Crystal Structures

Chapter 1

1.1 Mixed-Valency and Mixed-Valence Compounds

Mixed-valence complexes, where two otherwise identical elements in the same complex are in formally different oxidation states, can arise as a consequence of the synthetic pathway, or can be generated from isovalent precursors by electrochemical or chemical redox processes. The classification system introduced by Robin and Day is widely used in the description of mixed-valence systems and distinguishes three general classes based on the strength of interactions between the redox active sites.[1]

Those compounds in which the interactions between sites are negligible, for example because of the distance between them, are termed Class I mixed-valence complexes. Class I complexes display properties associated with each valence state in isolation. Systems in which moderate coupling between the redox sites permits electron exchange, but in which the charge is transiently localised, are termed Class II. In addition to properties arising from localisation of the unpaired electron Class II species also exhibit characteristics arising from the electron transfer process. In Class III systems the redox centres are so strongly coupled that the odd-electron is delocalised and only a single, average valence state can be assigned to the two centres. Class III compounds are not, strictly speaking, "mixed-valence" systems, but are perhaps better described as "valence averaged" species, which display unique characteristics that cannot be assigned to either individual oxidation state.

Potential energy surfaces

The difference in the classes can be illustrated by examining the potential energy surfaces that can be used to describe them. The potential energy surface of a mixed-valence system can be constructed by utilising parabolic functions to initially represent the non-interacting states in a Class I system (**Figure 1.1a**). Electronic coupling of these two states to give a Class II system leads to a splitting at the intersecting region (**Figure 1.1 b**). This splitting gives rise to two different energy surfaces, a lower lying surface which features two minima, with each minimum

corresponding to localisation of the charge on one redox centre, and a higher lying state.

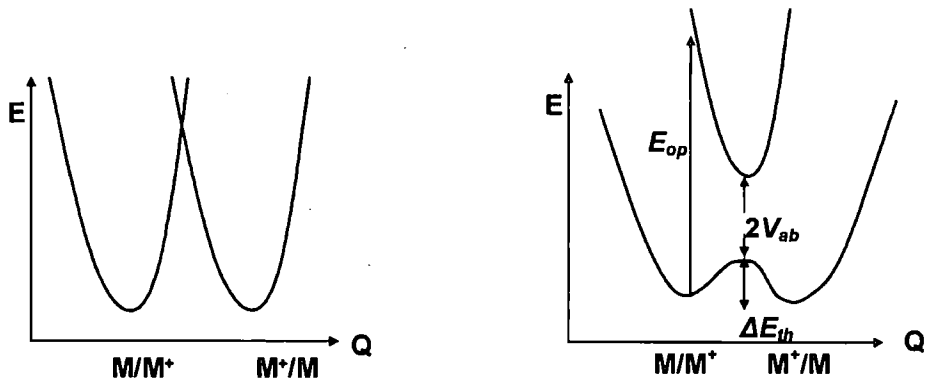

(a) (b)

Figure 1.1 Representations of typical potential energy surfaces for Class I (**a**) and Class II (**b**) complexes (Q = reaction coordinate).

In Class II systems there are two processes by which electron transfer can occur, a thermal process and an optical process (**Figure 1.2**). Although the states before and after electron transfer are indistinguishable there is an activation barrier, ΔE_{th}, to the thermal electron exchange process, and an energy, E_{op}, associated with photo-induced charge transfer.

The activation barrier arises as a consequence of the differing solvent and substituent environments at M and M^+. As a result of this difference, the electron transfer is accompanied by nuclear rearrangement at each site. As electronic motion occurs on a much shorter time-scale than nuclear motion (the Franck Condon principle), this nuclear rearrangement gives rise to the electron transfer activation barrier ΔE_{th}. For thermal electron transfer, rearrangement of the substituents and solvent about M and M^+ precedes the electron transfer step, and the electron transfer occurs within an

activated complex in which the bond lengths and solvent environment in M and M^+ are the same. The total reorganisation energy, λ, is the sum of these inner (substituents) and outer (solvent) sphere terms.

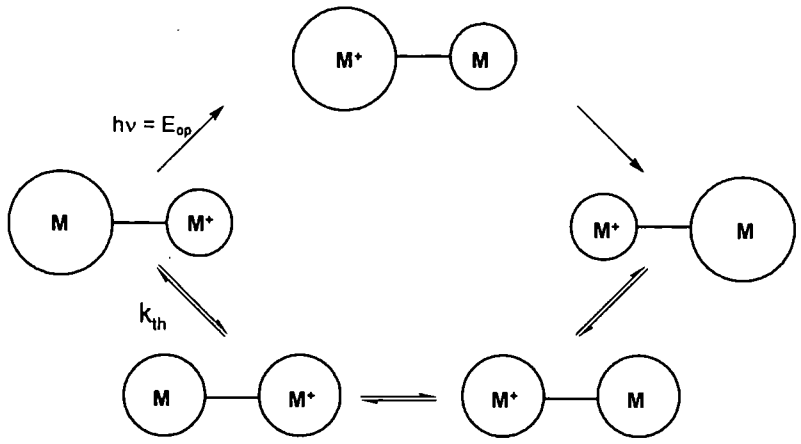

Figure 1.2 Representation of optical and thermal electron transfer pathways

The thermal activation energy barrier can be related to the coupling parameter, V_{ab}, and λ by Equation 1.1

$$\Delta E_{th} = \left(\frac{\lambda}{4} - V_{ab}\right) + \frac{V_{ab}^{\ 2}}{\lambda} \qquad \textbf{Equation 1.1}$$

Electron transfer can occur without prior rearrangement of the complex if the system is photoexcited, from one minima of the lower lying state to the upper PE surface, by absorption of light of the appropriate energy, E_{op}, to form the excited state.[2]

$$E_{op} = \lambda = h\nu = 4\Delta E_{th} \qquad \textbf{Equation 1.2}$$

In the case of symmetric complexes, the rate constant for the intramolecular electron transfer process, k_{th}, can be obtained from Equation 1.3

$$k_{th} = \kappa \nu_n e^{\left(\frac{-\Delta E_{th}}{RT}\right)}$$ **Equation 1.3**

Where κ is the adiabatic factor and ν_n is the nuclear frequency factor.

As the extent of electronic coupling, and hence V_{ab}, increases, ΔE_{th} decreases. When the electronic coupling is sufficiently strong (Class III system) the lower lying state becomes a single minimum state (**Figure 1.3**) and the unpaired electron is delocalised between the two redox active sites.

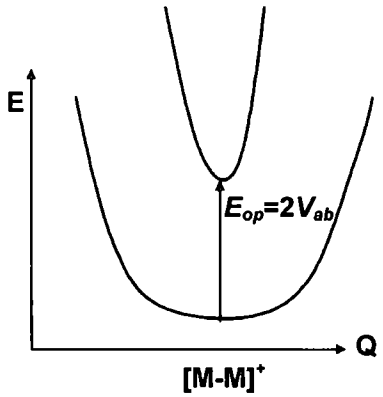

Figure 1.3 Representation of the typical potential energy surfaces for Class III complexes

Hush Theory

For both Class II and Class III systems the absorption bands due to the optical electron transfer process are found in the NIR region of the electromagnetic spectrum, and can be analysed to provide information on the nature of the mixed-valence system. Theoretical treatments were developed by Hush which predicted the occurrence of this IVCT band and allow thermal parameters to be extracted from

analysis of the energy and shape of the absorption band.[3] For Class II systems a Boltzmann distribution of vibrational states over the ground state surface, and hence a Gaussian shape to the absorption band (centred at $\bar{\nu}_{max}$ with a band width at half height $\Delta\bar{\nu}_{1/2}$), is assumed. Analysis of this IVCT band allows extraction of the electronic coupling term V_{ab} using Equation 1.4

$$V_{ab} = \frac{0.0205}{r}\sqrt{\varepsilon_{max}\Delta\bar{\nu}_{1/2}\bar{\nu}_{max}} \qquad \textbf{Equation 1.4}$$

where ε_{max} is the molar extinction coefficient of the IVCT band, and r is the intramolecular electron transfer distance (in Å). Although estimates of r can be difficult when the redox-active orbitals are significantly delocalised, r is often assumed to be the intra-molecular M-M distance.

The bandwidth at half-height, $\Delta\bar{\nu}_{1/2}$ (cm^{-1}), of the optical transition is related to the energy of the transition, $\bar{\nu}_{max}$, by Equation 1.5

$$\Delta\bar{\nu}_{1/2} = \sqrt{2310\bar{\nu}_{max}} \qquad \textbf{Equation 1.5}$$

Comparison of the observed ($\Delta\bar{\nu}_{1/2(obs)}$) and calculated ($\Delta\bar{\nu}_{1/2}$) bandwidths at half height can provide an indication of the class of a mixed-valence compound. In strongly coupled Class III systems the ground state potential energy surfaces are no longer parabolic in shape, leading to an asymmetry of the absorption band and a 'cut-off' at $h\nu = 2V_{ab}$, on the low energy side of the band (**Figure 1.4**). This cut-off results in narrower bands than would be predicted by Equation 1.5, and hence, complexes with asymmetric (non-Gaussian) shaped bands, that are significantly narrower than the Hush relationship predicts, are assumed to belong to Class III.[4, 5]

Figure 1.4 Representations of typical optical transition bands illustrating the 'cut-off' observed for Class III complexes

In the case of Class III systems V_{ab} is related to the energy of the optical transition by Equation 1.6

$$E_{op} = \bar{\nu}_{max} = 2V_{ab} \qquad \textbf{Equation 1.6}$$

In addition to the problems in analysis that can arise from the band cut off in Class III complexes, for strongly coupled systems multiple transitions are often observed in the NIR region. For transition metal complexes with low symmetry at the metal sites, and multiple orbital interactions across the bridge, bands can arise due to the formally forbidden dπ-dπ transitions, which gain intensity through spin orbit coupling and metal ligand orbital mixing (**Figure 1.5**), in addition to bands arising from IVCT processes.

Figure 1.5 Representation of the multiple bands that may be observed in the NIR region and the transitions that can give rise to these bands

The Creutz-Taube Ion

Many mixed-valence materials of contemporary interest are derived from a common $[L_xM]$-B-$[ML_x]$ structure, in which two redox-active metal fragments ML_x, are linked by some bridging ligand B. The mixed-valence state can be generated by a one electron oxidation (or reduction) of the overall assembly.

Perhaps the classic example of this type of complex is the ruthenium based complex $[\{(NH_3)_5Ru\}_2pyr]^{5+}$ (**Figure 1.6**), also known as the Creutz-Taube ion.[6]

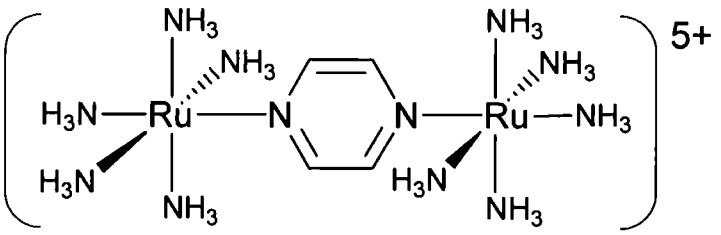

Figure 1.6 The Creutz-Taube ion

The complex has also been isolated as the +4 and +6 ions, where in each case both ruthenium centres are in identical oxidation states (Ru^{II}/Ru^{II} or Ru^{III}/Ru^{III} respectively). In the +5 ion the two ruthenium centres have formally differing oxidation states (Ru^{II}/Ru^{III}) and the mixed-valence complex formed has properties that do not arise from either the Ru^{II} or Ru^{III} centres.

The properties of the Creutz-Taube ion have been studied and determination of the Robin-Day Class (Class II or Class III) of this mixed-valence complex has been the subject of much debate. The electronic absorption spectrum of the mixed-valence complex reveals a narrow, solvent-independent band in the NIR region suggesting a Class III classification would be appropriate. The EPR data suggests that the odd-electron occupies an orbital that lies along this Ru-pyr-Ru axis, again consistent with assignment to a Class III complex.[6-9] Mössbauer spectroscopy has shown that there are equal numbers of Ru^{II} and Ru^{III} centres which occur in the mixed-valence species and the molecular structure of the tosylate salt reveals that slightly different geometries exist at each ruthenium centre suggesting Class II behaviour.[10, 11] Recent theoretical work has supported both the Class III and Class II designations,[12, 13] and the debate surrounding the Creutz-Taube ion has highlighted the ambiguity of complexes which fall at the Class II/Class III divide and prompted suggestions that such compounds should be given their own classification.[14] There have been numerous reviews of inter-valence electron transfer discussing theoretical aspects of these processes and further discussion will not be made here.[2, 4, 15, 16]

The fascination with the Creutz-Taube ion has led to a host of studies of mixed-valence compounds featuring various combinations of metals, supporting ligands and bridging moieties. The diversity of redox centres and bridging structures presents an almost limitless combination of $[ML_x]$-B-$[ML_x]$ systems and many of these systems, and their related mixed-valence derivatives, have been prepared and studied.[17-44] In the interests of the presentation of a concise and relevant introduction to the field, the review that follows will focus exclusively on the mono-nuclear metal containing moieties and acetylenic-based bridging ligands that are most relevant to the complexes presented in this thesis.

1.2 C_n bridges

Many mixed-valence materials of contemporary interest are systems in which two redox-active metal fragments are linked by some bridging ligand. There has been a great deal of interest in systems bridged by one-dimensional carbon allotropes built exclusively from C≡C units, and bimetallic species bridged by polycarbon ligands derived from polyynes was comprehensively reviewed recently.[36, 45] The following section reviews this area with particular attention to the properties of the mixed-valence species derived from such systems, and serves to highlight the particular attention that has been paid to the question of how the nature of the ML_x fragment can influence the electronic structure, and characteristics of the associated mixed-valence states, in bimetallic complexes derived from a common bridge motif.

Polyacetylide-bridged bis-ferrocenes

The electrochemical response of diferrocenylacetylene, the simplest of the family of polyacetylide-bridged bis-ferrocenes $Fc(C{\equiv}C)_nFc$, (**1.1/n**) is characterised by two reversible oxidation waves with a separation of *ca.* 140 mV,[46, 47] which has been taken as measure of moderate degree of interaction between the ferrocene centres.

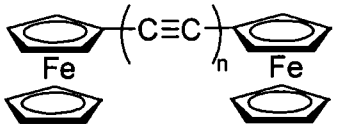

1.1/n

Figure 1.7 Polyacetylide-bridged bis-ferrocenes $Fc(C{\equiv}C)_nFc$, **1.1/n**

Elongation of the polycarbon chain results in a decrease in ΔE, the diacetylene derivative $Fc(C{\equiv}C)_2Fc$ **1.1/2** is characterised by two reversible one electron

oxidations with a separation of approximately 100 mV.[47, 48] The cyclic voltammogram of the more electron rich derivative 1,4-bis(octamethylferrocenyl)butadiyne displayed two oxidation waves with a ΔE of 150 mV, the increased separation from the parent complex **1.1/2** attributed to the electron donating effects of the methyl groups on the Cp ligand.[49] Moving through the series, the value of ΔE decreases sharply with increasing chain length becoming a single, two electron event in the octatetrayne (n = 4) (**Table 1.1**).

Table 1.1 The electrochemical properties of bis(ferrocenyl)polyynes **1.1/n**

n	E_1/V	E_2/V	ΔE/mV	conditions	reference
1	-0.11	0.08	190	0.1M NBu_4ClO_4 in CH_2Cl_2, 100 mV/s, vs FcH/FcH^+	50
	0.625	0.755	130	0.2M NBu_4BF_4 in CH_2Cl_2, 100 mV/s, vs SCE	47
2	0.14	0.23	90	0.1M NBu_4ClO_4 in CH_2Cl_2, 100mV/s, vs FcH/FcH^+	50
	0.58	0.68	100	0.2M NBu_4BF_4 in CH_2Cl_2, 100 mV/s, vs SCE	47
	0.486	0.586	100	0.1M NBu_4PF_6 in 1:1 CH_2Cl_2:NCMe, vs Ag/AgCl, 100 mV/s	51
	0.58	0.69	110	0.1M NBu_4PF_6 in CH_2Cl_2, Cp^*_2Fe [0.0765 V vs SCE]	48
3			60		48
4	0.601			0.1M NBu_4PF_6 in 1:1 CH_2Cl_2:NCMe, vs Ag/AgCl	52
6	0.652			0.1M NBu_4PF_6 in 1:1 CH_2Cl_2:NCMe, vs Ag/AgCl	52

The spectroscopic properties of **1.1/1** and its oxidation products have also been evaluated. In early work, low-intensity bands were observed in the mixed-valence complexes $[\mathbf{1.1/1}]^+$ (λ_{max} = 1560 nm, ε = 670 M^{-1} cm^{-1}) and $[\mathbf{1.1/2}]^+$ (λ_{max} = 1180 nm, ε = 570 M^{-1} cm^{-1}), which were not present in either the neutral or fully oxidised dicationic derivatives, and were assigned to Hush-type IVCT transitions.[47, 53] These transitions were studied in more detail utilising both the electrochemically produced and chemically isolated mixed-valence species, leading to the conclusion that the mixed-valence ions had localised valence sites and that the observed IVCT properties were consistent with Hush treatment for optical electron transfer with slight deviations possibly arising from partial delocalisation.[46, 54, 55]

C_2-bridged bimetallic complexes

Generally, incorporation of the redox group directly into the conjugation system of the bridge results in increased electronic interaction between the remote termini. Systems in which the metal centres are linked by a dicarbon bridge are relatively well explored,[56-65] and examples of the three limiting valence structures (M-C≡C-M, M=C=C=M, M≡C-C≡M) are known. However, as is the case with other poly-carbon-bridged complexes, the acetylenic sub-structure dominates the chemistry of these bimetallic dicarbon complexes. Despite their prevalence, few of these dicarbon complexes have been investigated using electrochemical methods, or had the electronic structure of their redox-generated products explored. For example, the bimetallic species $(^tBuO)_3W{\equiv}C\text{-}C{\equiv}W(O^tBu)_3$, in which the two tungsten centres are linked by a triple bond to the bridging C_2 moiety, displayed two irreversible one-electron oxidation processes.[66] The bimetallic acetylide complex $\{Re(CO)_5\}_2(\mu\text{-}C{\equiv}C)$ also displays two irreversible oxidations, but at considerably higher potentials, consistent with the nature of the supporting ligands.[64] However, in the absence of a wider range of complexes with a more subtle and systematic range of metal-ligand end-caps, conclusions about the electronic structure of these metal-stabilised dicarbon complexes has largely rested on computational investigations. The theoretical treatments of the variation in valence bond representations appropriate for

$[ML_x](\mu\text{-}C_2)[ML_x]$ systems as a function of metal d-electron counts has been reviewed recently.[67]

Probably the most thoroughly explored example of this type of complex comes from the Berke group. The electrochemical response of **1.2**, $\{Mn(dmpe)Cp^{Me}\}_2(\mu\text{-}C{\equiv}C)$, (measured from the dication $[\mathbf{1.2}][\mathbf{PF_6}]_2$) was characterised by three reversible waves, two oxidation waves corresponding to production of $[\mathbf{1.2}]^+$ $Mn^{II/II}$-$Mn^{II/III}$, -1.835 V and $[\mathbf{1.2}]^{2+}$ $Mn^{II/III}$-$Mn^{III/III}$, -0.847 V, and a reduction to the monoanionic species, $Mn^{II/II}$-$Mn^{II/I}$, -2.824 V (vs Fc/Fc^+). The comproportionation constant for formation of the monocation ($\Delta E_{1/2}$ = 0.988 V) K_c = 8.6 x 10^{16} indicates the high thermodynamic stability of the radical cation.[68] The UV-vis spectra of $[\mathbf{1.2}]^{n+}$ (n = 0-2) were characterised by an intense band and shoulder between 400-500 nm, with a second band of low intensity being observed at higher energy in the neutral and monocationic derivatives. The monocationic derivative was classified as a Robin-Day Class III mixed-valence system on the basis of the characteristics of NIR absorption bands, IR spectroscopy and magnetic properties, a conclusion which was supported by DFT calculations.

Electrochemical data has been used to provide some insight into the nature of interactions between heterometallic centres mediated by the dicarbon moiety. The heterometallic species $\{Cp^*Re(NO)(PPh_3)\}(\mu\text{-}C{\equiv}C)\{Pd(PEt_3)_2(Cl)\}$ (**1.3**) and $\{Cp^*Re(NO)(PPh_3)\}(\mu\text{-}C{\equiv}C)\{Rh(PPh_3)_2(CO)\}$ (**1.4**) were prepared by the sequential deprotonation and metallation of $Re(C{\equiv}CH)(NO)(PPh_3)Cp^*$. The cyclic voltammogram of **1.4** was characterised by a chemically reversible one-electron oxidation and a second, irreversible one-electron oxidation assigned to the Re and Pd centres respectively, following comparison of the observed potentials with those of mononuclear models, with the radical cation produced by the one-electron oxidation having a localised structure.[69]

C_4-bridged bimetallic complexes

By far the most common systems in this series MC_nM are those bridged by the diyndiyl dianion $[C{\equiv}CC{\equiv}C]^{2-}$ and a range of bimetallic complexes bearing both identical (**Table 1.2a**) and differing (**Table 1.2b**) metal end-caps have been produced.

Table 1.2 a) Diyndiyl-bridged systems $[ML_x]$-C_4-$[ML_x]$

ML_x	reference
$Mo(CO)_3Cp$	70
$Mo(CO)_2Tp'$	71
$W(CO)_3Cp$	70
$W(CO)_2Tp'$	71
$W(CO)_3Cp^*$	72
$W(O)_2Cp^*$	72
$Mn(dmpe)_2I$	73
$Mn(C{\equiv}CH)(dmpe)_2$	74
$Re(NO)(PPh_3)Cp^*$	75
$Re(NO)(P(tol)_3)Cp^*$	76
$Re(NO)(P(C_6H_4\text{-}4\text{-}^tBu)_3)Cp^*$	76
$Re(CO)_3(bipy)$	77
$Fe(CO)_2Cp$	78
$Fe(CO)_2Cp^*$	65
$Fe(dppe)Cp^*$	79
$Fe(dippe)Cp^*$	80
$Ru(PPh_3)_2Cp$	81
$Ru(PPh_3)(PMe_3)Cp$	82
$Ru(dppe)Cp$	83
$Ru(dppm)Cp^*$	84
$Ru(dppe)Cp^*$	84
cis-$RuCl(bpy)_2$	85
trans-$Rh(CO)(P^iPr_3)_2$	86
trans-$RhH(=C=C(H)C_6H_5)(P^iPr_3)_4$	86
trans-$RhH(C{\equiv}CC_6H_5)(P^iPr_3)_3$	86
trans-$RhHCl(P^iPr_3)_2$	87
trans-$RhHCl(py)(P^iPr_3)_3$	87
trans-$IrCl(CO)(NCMe)(PPh_3)_2$	88
$Ni(CN)(NH_3)_3$	89
$Ni(PPh_3)Cp$	78
$PdCl(PnBu_3)_2$	90
$PtCl(PnBu_3)_2$	91
$PtMe(cod)$	92
$Pt(C_6F_5)(P(tol)_3)_2$	93
$Au(PCy_3)$	94

Table 1.2 b) Diyndiyl-bridged systems $[ML_x]$-C_4-$[ML'_x]$

ML_x	ML'_x	reference
$Fe(CO)_2Cp$	$Fe(CO)(PPh_3)Cp$	95
Fe(dppe)Cp*	$Fe(CO)_2Cp^*$	96
Fe(dppe)Cp*	$Fe(CO)_2(\eta^5\text{-}C_5Ph_5)$	96
Fe(dippe)Cp*	$Fe(CO)_2Cp^*$	80
Mo(CO)(dppe)Cp	$Mo(CO)_2(PPh_3)Cp^{CO2Me}$	97

The tungsten complex $\{W(CO)_3Cp^*\}_2(\mu\text{-}C{\equiv}CC{\equiv}C)$ (**1.5**) was oxidised chemically using H_2O_2/H_2SO_4 to give the bis(dioxo) complex $\{W(O)_2Cp^*\}_2(\mu\text{-}C{\equiv}CC{\equiv}C)$ (**1.6**) via a bis(oxo-peroxo) intermediate.[72] Whilst both **1.5** and **1.6** displayed an irreversible electrochemical response, comparisons of the structural parameters with those of the related mono-nuclear diynyl models suggested pronounced metal-carbon mixing in the case of the complex featuring d^4 (i.e. **1.5**), but not d^0 (i.e. **1.6**), metal centres. These conclusions were consistent with DFT calculations of $W(C{\equiv}CC_6H_5)(O)_2Cp^*$ reported at the same time,[98] and attributed to the poor energy match of the metal and acetylide orbitals.

Whilst the majority of $[L_xM]$-C_4-$[ML_x]$ complexes isolated have been shown to have bridging ligands with predominantly diyndiyl character, the compounds $Tp'(CO)_2M{\equiv}CC{\equiv}CC{\equiv}M(CO)_2Tp'$ [M = Mo (**1.7**), W (**1.8**)] which display a bis-carbyne C_4 bridging unit can be produced from $M(\equiv CCH_3)(CO)_2Tp'$ by a sequence of deprotonation and oxidation steps.[71] In both the tungsten and molybdenum analogues, electrochemical studies revealed two reversible oxidation processes with separations of 0.278 V (K_c = 5 x 10^4) and 0.239 V (K_c = 1 x 10^4), respectively. The authors attributed these relatively small values of the comproportionation constant to a limited contribution from the carbon bridge orbitals to the HOMO in the mono-oxidised species.[99]

The diyndiyl complex $\{MnI(dmpe)_2\}_2(\mu\text{-}C{\equiv}CC{\equiv}C)$ (**1.9**) and the related complex $\{Mn(C{\equiv}CH)(dmpe)_2\}_2(\mu\text{-}C{\equiv}CC{\equiv}C)$ (**1.10**) (**Figure 1.8**) could be electrochemically

oxidised in two fully reversible steps to produce the respective mono- (Mn^{III}/Mn^{II}) and di-cations (Mn^{III}/Mn^{III}).[73, 74] In the case of **1.10** an additional irreversible reduction near the solvent edge was observed and assigned to the Mn^{II}/Mn^{II}-Mn^{II}/Mn^{I} couple. The large value of the comproportionation constant in each case (**1.9**, 1.9 x 10^{10}; **1.10**, 7.5 x 10^{9}) indicates the thermodynamic stability of the monocations towards disproportionation. Correspondingly, the paramagnetic species **1.9** could also be chemically oxidised sequentially to the corresponding mono- and di-cations using ferrocinium. Two ν(C≡C) stretches were observed in the IR spectrum of the neutral species, in contrast, the IR spectrum of the dication shows no stretches in the ν(C≡C) region, but has a broad band in the ν(C=C) region indicative of the cumulenic structure adopted by the bridging ligand in $[\mathbf{1.9}]^{2+}$.

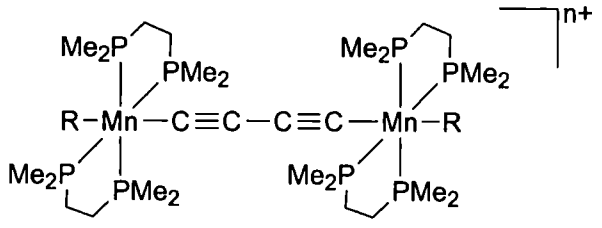

Figure 1.8 The binuclear manganese complexes **1.9** [R = I] and **1.10** [R = (C≡CH)].

The electrochemical response of the related complexes {Mn(C≡CR)(dmpe)$_2$}(μ-C≡CC≡C) [R = $SiMe_3$, **1.11a**; R = $SiEt_3$, **1.11b**; R = Si^iPr_3, **1.11c**; R = $Si(^tBu)Me_2$, **1.11d**] was characterised by two fully reversible anodic processes, which produce the thermodynamically stable monocations (Mn^{III}/Mn^{II}) and dications (Mn^{III}/Mn^{III}) respectively (**Table 1.3**).[100, 101] The structure of the mono-oxidised derivative $[\mathbf{1.11b}]^+$ was also determined by single crystal X-ray diffraction with the bond lengths along the bridging carbon chain best being described by adoption of a partial cumulenic resonance structure. The behaviour of all of these Mn_2C_4 systems upon oxidation is consistent with the composition of the HOMOs as the anti-bonding combination of the metal d and diyndiyl π-systems. Sequential depopulation of this

orbital (**Figure 1.9**) accounts for the progressive migration of the ligand structure which, in valence bond terms, would be described as diyndiyl (C≡CC≡C) to cumulenic (C=C=C=C).

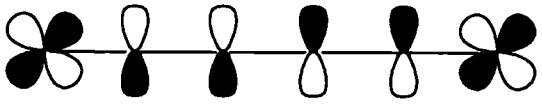

Figure 1.9 Representation of the frontier orbitals in the Mn_2C_4 diyndiyl complexes

Table 1.3 Electrochemical response of **1.11a-d**

	E_1/V	E_2/V	ΔE/mV	K_c	reference
1.11a	-0.816	-0.271	545	2.2×10^9	100
1.11b	-0.843	-0.286	557	3.5×10^9	101
1.11c	-0.857	-0.294	563	4.4×10^9	101
1.11d	-0.849	-0.289	560	4.0×10^9	101

The luminescent rhenium complex $\{Re(CO)_3(^tBu_2\text{-bpy})\}_2(\mu\text{-}C{\equiv}CC{\equiv}C)$ (**1.12**) undergoes three irreversible oxidations, together with a bpy-centred reduction near -2.0V (vs Fc/Fc^+). In contrast to the vast majority of diyndiyl complexes that feature metal centres supported by more electron-donating phosphine and Cp ligands, the first two oxidation events in **1.12** were assigned to carbon-centred processes. Only a single rhenium centred oxidation event was observed +1.84 V.[77] An optical transition near 750 nm, not present in mono-nuclear models, was suggested as being of predominantly $(d\pi)Re \rightarrow \pi^*(C{\equiv}CC{\equiv}CRe)$ or $\pi(C{\equiv}CC{\equiv}CRe) \rightarrow \pi^*(^tBu_2\text{-bpy})$ in character. A more extended ReC_4Re-centred orbital was not considered in this work.

The introduction of more electron-donating ligands around the rhenium centre leads to more reversible electrochemical behaviour, with more metal d character in the redox-active frontier orbitals. The compounds $\{Re(PR_3)(NO)Cp^*\}_2(\mu\text{-}C{\equiv}CC{\equiv}C)$ [R = C_6H_5 (**1.13**), 4-C_6H_4Me (**1.14**), 4-$C_6H_4{}^tBu$ (**1.15**)] were obtained as diastereotopic mixtures by the Glaser coupling of the corresponding rhenium ethynyls $Cp^*(NO)(PR_3)Re\text{-}C{\equiv}CH$.[75, 76, 102, 103] Absolute stereochemistry was assigned for **1.13** after fractional crystallisation of the (SS,RR) diastereomer and single crystal X-ray diffraction study (**Figure 1.10**).

The electrochemical response of **1.13** was characterised by two chemically reversible, one-electron oxidations, with a separation of 0.53 V (K_c = 1.1 x 10^9) assigned to the Re^I/Re^{II} couples. The paramagnetic, mono-oxidised species [**1.13**][PF_6], was isolated by the treatment of $\{Re(PPh_3)(NO)Cp^*\}_2(\mu\text{-}C{\equiv}CC{\equiv}C)$ with $AgPF_6$ or by comproportionation of [**1.13**][PF_6]$_2$ and **1.13**. A combination of IR, NIR and ESR spectroscopy indicated delocalisation of the odd electron over both metal centres.

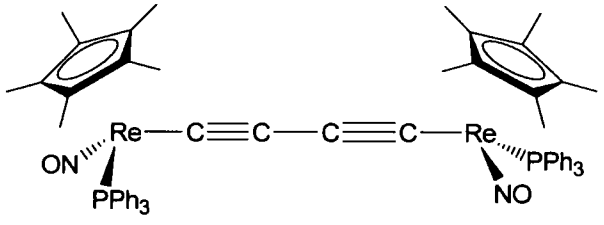

Figure 1.10 The dirhenium complex **1.13**.

Similarly, the electrochemical response of **1.14** was characterised by two chemically reversible one-electron oxidations with a separation of 0.53 V (K_c = 1.1 x 10^9), with each oxidation being 230 mV more facile than that of the triphenylphospine analogue **1.13**. The mono-oxidised derivative was isolated as the SbF_6^- salt and a combination

of ESR spectroscopy and the observation of a single ν(NO) band in the IR spectra again indicated delocalisation of the odd electron over both rhenium end groups.[76]

The binuclear iron complexes $\{Fe(CO)(L)Cp\}_2(\mu\text{-}C{\equiv}CC{\equiv}C)$ (L = CO, **1.16a**; L = PPh_3, **1.16b**) were prepared by a number of routes including, for **1.16a**, the reaction of Li_2C_4 with two equivalents of $FeCl(CO)_2Cp$, by reaction of $Cp(CO)_2Fe\text{-}C{\equiv}CC{\equiv}CH$ initially with BuLi and then the metal halide $FeCl(CO)_2Cp$, and by the CuI-catalysed reaction of $FeCl(CO)_2$ with $HC{\equiv}CC{\equiv}CH$.[78, 95, 104] Although the electron-withdrawing nature of the carbonyl supporting groups does not aid electrochemical investigations of acetylide complexes featuring this moiety, the carbonyl ligands do provide an excellent indirect measure of the electronic nature of the metal centre through the characteristic frequencies of the ν(CO) bands. The observation that the ν(CO) band of one iron fragment was affected by substitution of one CO by PPh_3 on the second fragment was taken as evidence that the butadiyndiyl ligand was efficient at conveying electronic information between the two termini in the ground-state of these 36-electron species.

The Lapinte group have reached the same general conclusion following a thorough study of the unsymmetrical di-iron complexes $\{Cp^*(dppe)Fe\}(\mu\text{-}C{\equiv}CC{\equiv}C)\{Fe(CO)_2Cp^*\}$ (**1.17**) and $\{Cp^*(dppe)Fe\}(\mu\text{-}C{\equiv}CC{\equiv}C)\{Fe(CO)_2(\eta^5\text{-}C_5Ph_5)\}$ (**1.18**).[96] The cyclic voltammograms of both complexes displayed two oxidation waves due to the oxidation of the neutral complexes to the mono and dications respectively, the second redox process becoming reversible at faster scan rates. Comparison of the electrochemical parameters with those of the corresponding mononuclear systems confirmed a degree of 'electronic communication' between the metal centres across the carbon bridge, which may, in the most general sense, be attributed to a polarisation of the carbon bridge brought about by the combination of a strongly electron-donating Fe(dppe)Cp* end-cap with the more electron-withdrawing $Fe(CO)_2(\eta^5\text{-}C_5Ph_5)$ or $Fe(CO)_2Cp^*$ moiety.

Initial reports of the electrochemical response of the symmetrical iron complex $\{Fe(dppe)Cp^*\}_2(\mu\text{-}C{\equiv}CC{\equiv}C)$ (**1.19**) described two well-separated, reversible, one-

electron oxidation processes (ΔE = 0.72 V, K_c = 1.6 x 10^{12}).[79, 105, 106] The description of the electrochemical properties of closely related ruthenium complexes that exhibited four sequential oxidation events (*vide infra*) prompted a re-investigation of the electrochemical properties of **1.19**, and a third oxidation at higher potential was duly observed.[80] Treatment of the neutral species with one equivalent of $[Cp_2Fe][PF_6]$ allowed isolation of the mixed-valence complex **[1.19][PF$_6$]** as a green solid and comparison of the IR spectrum of **[1.19][PF$_6$]** with the neutral **1.19** and dicationic **[1.19][PF$_6$]$_2$** derivatives could be made. The neutral complex displayed ν(C≡C) bands at 1880 and 1955 cm^{-1} and the monocation at 1880 and 1973 cm^{-1}, further oxidation to the dicationic derivative resulted in the observation of bands at higher energy (1950, 2160 cm^{-1}). These results, and data obtained from Mössbauer spectroscopy, were taken to indicate a weak contribution from the π orbitals of the bridging ligand to delocalisation of the odd electron, and a predominantly metal-centred HOMO. This conclusion was supported by DFT level electronic structure calculations. A band in the NIR region of the electronic spectrum of **[1.19][PF$_6$]** was observed that was not present in either **1.19** or **[1.19][PF$_6$]$_2$** and was assigned to an intervalence transition. Treatment of the band envelope as an IVCT transition in a Class III mixed-valence complex gave a large value of the coupling constant V_{ab} (0.47 eV).

Although the relatively high oxidation potential of **[1.19]$^{3+}$** hampered efforts to obtain samples of this material for study, electrochemical analysis of the related species {Fe(dippe)Cp*}$_2$(μ-C≡CC≡C) (**1.20**), containing the more electron releasing dippe ligand, revealed three well separated, reversible redox processes, which were respectively 0.29, 0.14 and 0.14 V more facile than the equivalent processes observed for **1.19**.[80] The first two oxidation waves were described in terms of metal centred oxidation events and attributed sequential Fe^{II}/Fe^{III} couples. The separation between the oxidation waves was also found to increase in **1.20** with respect to that observed for **1.19**, the consequential increase in comproportionation constant demonstrating the improved stability of the monocation with the increase in electron density at the metal centres. The third oxidation was identified as a bridge-centred redox process forming the trication radical, **[1.20]$^{3+}$**, which could be accessed chemically and was structurally characterised by single crystal X-ray diffraction.

The molecular structure of the isolated triply-oxidised derivative $[\mathbf{1.20}]^{3+}$ revealed two PF_6^- anions located at both edges of the trication and the third positioned equidistant from the metal centres. The bond distances along the carbon chain were found to be intermediate between those determined for butadiyne and butatriene. Comparison of the bond lengths along the chain with those determined for **1.19**[107] and the mixed-valence derivative [**1.19**][PF_6] (**Figure 1.11**) indicated a progressive lengthening of the C(1)-C(2) bond ('triple bond') and shortening of the bond between C(2)-C(3) upon oxidation. The observed structural parameters are at odds with the initial description of increasing diyndiyl character in the carbon bridge as oxidation proceeds, which was based on IR data alone.[79]

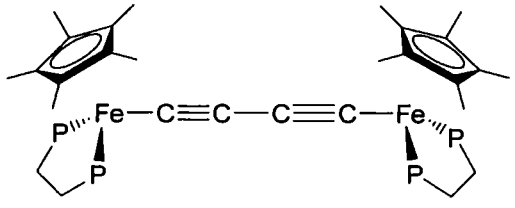

[Fe]——C_1——C_2——C_3——C_4——[Fe]

1.19	1.889(3)	1.221(4)	1.373(4)	1.220(4)	1.884(3)
[1.19][PF_6]	1.830(8)	1.236(9)	1.36(1)	1.236(9)	1.830(8)
[1.20][PF_6]$_3$	1.79(1)	1.27(1)	1.33(1)	1.27(1)	1.79(1)

Figure 1.11 Structural parameters for the related complexes **1.19**, [**1.19**][PF_6] and [**1.20**][PF_6]$_3$

The ^{57}Fe Mössbauer spectrum of $[\mathbf{1.20}]^{3+}$ was characterised by a single doublet, indicating the equivalence of the two iron termini on the Mössbauer timescale. Examination of the NIR spectrum of $[\mathbf{1.20}]^{3+}$ did not show any absorption in this region. The bond lengths observed from the crystal structure and this spectroscopic

data are consistent with the proposed carbon-centred radical, which may be approximated by the resonance structures shown in **Figure 1.12**, and not an Fe^{III}/Fe^{IV} mixed-valence system.

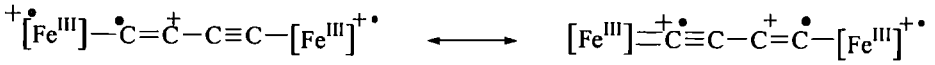

Figure 1.12 Resonance structures for $[\{Fe(dippe)Cp^*\}_2(\mu\text{-}C{\equiv}CC{\equiv}C)]^{3+}$

The symmetrical binuclear complex $\{Ru(PPh_3)_2Cp\}_2(\mu\text{-}C{\equiv}CC{\equiv}C)$ (**1.21**) undergoes four stepwise one-electron oxidation processes. The first three being quasi-reversible redox events, and the fourth being an irreversible process.[81, 108-110] The K_c values for the odd electron species $[\mathbf{1.21}]^+$ and $[\mathbf{1.21}]^{3+}$ are 1.5 x 10^{11} in each case, and the monocation $\mathbf{1.21}[PF_6]$ can be produced by chemical oxidation of the neutral species with $AgPF_6$ or by comproportionation of **1.21** and $\mathbf{1.21}[PF_6]_2$. A similar electrochemical response to that in **1.21** was observed in the mixed phosphine complex $\{Ru(PPh_3)(PMe_3)Cp\}_2(\mu\text{-}C{\equiv}CC{\equiv}C)$ (**1.22**) with the more electron donating PMe_3 ligands resulting in significantly lower potentials than in **1.21** and with K_c values for $[\mathbf{1.22}]^+$ and $[\mathbf{1.22}]^{3+}$ of 2.1 x 10^{10} and 2.7 x 10^8, respectively.[110]

Spectroscopic data and theoretical calculations on this family of compounds demonstrate that the oxidation affects the metal centre as well as the carbon atoms of the diyne bridge leading to the conclusion that the electron removed is delocalised over the Ru-C_4-Ru chain.[110] The ν(CC) frequencies move to progressively lower energy upon oxidation, consistent with a greater involvement of the diyndiyl ligand in the redox-active orbitals than was observed in the iron analogues **1.19** and **1.20**. This generalisation is consistent with DFT calculations which suggest an approximately equal weighting of ruthenium and carbon (diyndiyl) in the frontier orbitals of **1.21** and related ruthenium species.

The properties of this family of ruthenium diyndiyl complexes is not overly sensitive to the nature of the phosphine and cyclopentadienyl supporting ligands, and the more electron-rich complexes $\{Ru(dppe)Cp^*\}_2(\mu\text{-}C{\equiv}CC{\equiv}C)$ (**1.23**) and $\{Ru(dppm)Cp^*\}_2(\mu\text{-}C{\equiv}CC{\equiv}C)$ (**1.24**) behave in a manner entirely analogous to the Cp derivatives **1.21** and **1.22** described above (**Table 1.4**).[84, 111] Chemical oxidation of **1.23** with $[Cp_2Fe][PF_6]$ afforded the mono and dications, **[1.23]**$[PF_6]$ and **[1.23]**$[PF_6]_2$, and examination of the IR spectra obtained revealed a progressive decrease in energy of the ν(C≡C) band **1.23** > **[1.23]**$[PF_6]$ > **[1.23]**$[PF_6]_2$, consistent with the evolution of a more cumulenic structure along the C_4 bridge. This observation was in agreement with the structures obtained by single crystal X-ray diffraction studies which confirmed the best description of the C_4 chain in the neutral species as being in terms of a diyndiyl representation (**A**), with a cumulenic description being more appropriate following oxidation to the dication (**B**) (**Figure 1.13**).

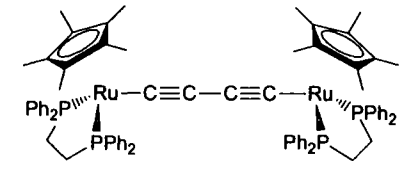

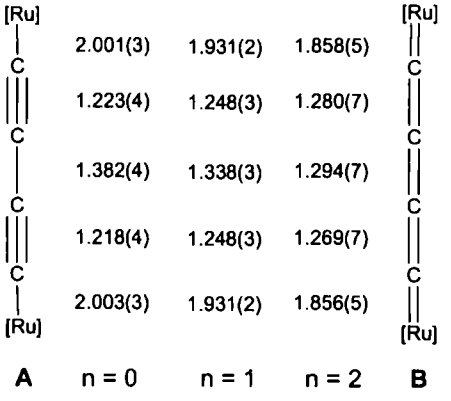

Figure 1.13 Representation of $[\mathbf{1.23}]^{n+}$. Bond lengths (Å) are given for **1.23** (n = 0), $[\mathbf{1.23}]^+$ (n = 1) and $[\mathbf{1.23}]^{2+}$ (n = 2)

The changes in the electronic spectra of **1.23** and **1.24** upon oxidation were assessed by spectroelectrochemical techniques, and revealed very similar spectra in each case. Upon oxidation to the monocationic derivatives a number of overlapping bands were observed in the NIR region, these band envelopes could be deconvoluted to give three Gaussian-shaped bands, of very similar energy, in each case. Analysis of the lowest energy band obtained, yielded a value of V_{ab} = 0.63 eV in each case.

The unsymmetrical binuclear ruthenium species {$Cp(PPh_3)_2Ru$}(μ-C≡CC≡C){Ru(dppe)Cp} (**1.25**) and {$Cp(PPh_3)_2Ru$}(μ-C≡CC≡C){Ru(dppe)Cp*} (**1.26**) both undergo three reversible oxidation processes and a fourth irreversible oxidation. The first two oxidations are *ca.* 100 mV more facile in the Cp* derivative but with similar values of K_c for the monocation in each case (**1.25**, ΔE = 0.64 V, K_c = 6.53 x 10^{10}; **1.26**, ΔE = 0.67 V, K_c = 2.09 x 10^{11}) (**Table 1.4**).[83]

Table 1.4 Electrochemical properties of diruthenium complexes.

	E_1/V	E_2/V	$\Delta E_{1/2}$/mV	K_c	E_3/V	E_4/V	reference
1.21	-0.23	0.41	640	6.53 x 10^{10}	1.03	1.68[a]	81, 108-110
1.22	-0.26	0.33	590	2.1 x 10^{10}	0.97	1.46	110
1.23	-0.43	0.22	650	9.64 x 10^{10}	1.04	1.51[b]	84, 111
1.24	-0.48	0.15	630	4.46 x 10^{10}	1.04	1.41	84, 111
1.25	-0.22	0.42	640	6.53 x 10^{10}	1.07	1.52[a]	83
1.26	-0.33	0.34	670	2.09 x 10^{11}	1.03	1.56[a]	83

[a]peak potential for irreversible process. [b]partially reversible.

The related complex {$Cp(dppf)Ru$}$_2$(μ-C≡CC≡C) (**1.27**) was characterised by five redox events in its cyclic voltammogram. Reversible waves at -0.680 V and -0.030 V were attributed to stepwise oxidation of Ru^{II}/Ru^{II} to Ru^{II}/Ru^{III} and Ru^{III}/Ru^{III}, $\Delta E_{1/2}$ = 0.650V, K_c = 9.74 x 10^{10}. Other waves were assigned to oxidation of the Fe^{II} centres

in the dppf ligand and further oxidations of the Ru^{III} centres.[112] Coordination of the carbon chain in **1.27** by Cu^{I}(NCMe) groups results in less chemically reversible redox chemistry, but the influence of the copper centre on the electronic structure of the six-atom Ru-C_4-Ru assembly was not assessed.

The compound {*cis*-RuCl(bpy)$_2$}$_2$(μ-C≡CC≡C) (**1.28**) undergoes two reversible oxidations, attributed to the Ru^{II}/Ru^{III} couples, with a potential difference of 0.52 V (K_c = 6.13 x 10^8). The cyclic voltammogram of this complex also displayed two irreversible oxidation at potentials above 2V, attributable to the Ru^{III}/Ru^{IV} couple, and two ligand centred reduction processes.[85]

C_4-bridged heterometallic complexes

A number of diyndiyl species that contain heterometallic metal end caps have been produced (**Table 1.5**). The task of evaluating ground state interactions between different metal centres through ethynyl-based bridging ligands, using electrochemical methods, can be complicated by differing interpretations of the observed electrochemical response of the system, in terms of either metal centred redox events (i.e. simple donor-acceptor systems), or redox processes which involve more extensively delocalised orbitals. Solvation effects can also alter E^0 values, and it is important to bear in mind that direct comparisons of electrode potentials of bimetallic complexes with those of model compounds is only valid if the relative solvation energies of the compounds in their various oxidation states do not differ significantly.[113, 114]

Table 1.5. Heterometallic diyndiyl-bridged systems $[ML_x]$-C_4-$[M'L'_x]$

ML_x	$M'L'_x$	reference
$W(CO)_3Cp$	$Mo(CO)_3Cp$	115
$W(CO)_3Cp$	$Mn(CO)_5$	115
$W(CO)_3Cp$	$Ru(CO)_2Cp$	115
$W(CO)_3Cp$	$Ru(PPh_3)_2Cp$	115
$W(CO)_3Cp$	$Rh(CO)(PPh_3)_2$	116
$W(CO)_3Cp$	$Ir(CO)(PPh_3)_2$	116
$W(CO)_3Cp$	$Au(PPh_3)$	115
$Re(NO)(PPh_3)Cp^*$	*trans*-$Rh(CO)(PPh_3)_2$	69
$Re(NO)(PPh_3)Cp^*$	*trans*-$Pd(PEt_3)_2Cl$	69
$Fe(CO)_2Cp$	$W(CO)_3Cp$	95
$Fe(CO)_2Cp$	$Mo(CO)_3Cp$	95
$Fe(CO)(PPh_3)Cp$	$W(CO)_3Cp$	95
$Fe(CO)(PPh_3)Cp$	$Mo(CO)_3Cp$	95
$Fe(CO)_2Cp$	$Fe(CO)(PPh_3)Cp$	95
$Fe(dppe)Cp^*$	$Fe(CO)_2Cp^*$	96
$Fe(dppe)Cp^*$	$Fe(CO)_2(\eta^5\text{-}C_5Ph_5)$	96
$Fe(dippe)Cp^*$	$Fe(CO)_2Cp^*$	80
$Fe(dppe)Cp^*$	$Re(NO)(PPh_3)Cp^*$	117
$Fe(dppe)Cp^*$	$Ru(dppe)Cp^*$	118
$Fe(dppe)Cp^*$	$Ru(PPh_3)_2Cp$	118
Cu(triphos)	$Au(P(tol)_3)$	119
$(Cp(CO)_3W\text{-}C{\equiv}CC{\equiv}C\text{-}Au)(\mu\text{-}$ dppm)Au	$W(CO)_3Cp$	120
$Pt(C{\equiv}CC{\equiv}CH)(dppe)$	$Au(PPh_3)$	121

The electrochemical response of {Cp*(NO)(PPh_3)Re}(μ-C≡CC≡C){$PdCl(PEt_3)_2$} (**1.29**) was characterised by a chemically reversible oxidation at 0.32 V and a second irreversible oxidation at 1.29 V (Fc/Fc^+ as internal reference, E^0 = +0.56 V). These were assigned, by comparison with model complexes, to metal-localised redox events on rhenium and palladium, respectively.[69] Electrochemical studies of the related complex {Cp*(NO)(PPh_3)Re}(μ-C≡CC≡C){Fe(dppe)Cp*} (**1.30**) revealed two chemically reversible oxidations with a separation of 0.73 V, corresponding to formation of the radical cation $[\mathbf{1.30}]^+$ and the dication $[\mathbf{1.30}]^{2+}$ respectively, and a third oxidation at the solvent edge attributed to the formation of the trication $[\mathbf{1.30}]^{3+}$.[117] By comparison with the related monometallic complexes Fe(C≡CC≡C$SiMe_3$)(dppe)Cp* and Re(C≡CC≡C$SiMe_3$)(NO)(PPh_3)Cp* the first oxidation was presumed to be predominantly iron-centred in character and the second to have dominant rhenium character. The oxidations are 0.12 V and 0.50 V more favourable than in the respective mononuclear complexes. Comparison with the homometallic binuclear complexes **1.13** and **1.19** revealed that the iron fragment Fe(dppe)Cp* is more electron releasing than the rhenium fragment Re(PPh_3)(NO)Cp* introducing an inherent "polarisation" to the carbon bridge.

The mixed-valence complex $[\mathbf{1.30}]^+$ and the dicationic derivative $[\mathbf{1.30}]^{2+}$ could be chemically isolated as the PF_6^- salts and the spectroscopic properties examined. The IR ν(C≡C) bands were observed at significantly lower frequencies in the radical cation (*ca.* 125 cm^{-1}) than in the neutral complex, indicative of a lowering of the bond order upon oxidation. Mössbauer spectroscopy indicated that the iron centre in $[\mathbf{1.30}]^+$ is best described as being in the Fe^{III} oxidation state, and that oxidation to the dication $[\mathbf{1.30}]^{2+}$ results in a further decrease of electron density around the iron centre. The electronic (UV-vis-NIR) spectrum of $[\mathbf{1.30}]^+$ displayed a broad and weak band in the NIR region which is absent in **1.30** and $[\mathbf{1.30}]^{2+}$ and was attributed to a photoinduced $Re^{II} \rightarrow Fe^{III}$ transition, and the radical cation $[\mathbf{1.30}]^+$ assigned to a Robin-Day Class II system.

The electronic and spectroscopic properties of the mixed metal complexes {Cp*(dppe)Ru}(μ-C≡CC≡C){Fe(dppe)Cp*} (**1.31**) and {$Cp(PPh_3)_2Ru$}(μ-

C≡CC≡C){Fe(dppe)Cp*} (**1.32**) were compared with those of the analogous homometallic complexes.[118] The cyclic voltammograms of **1.31** and **1.32** show three chemically reversible waves at -0.59, 0.18, 0.99 V and -0.51, 0.30, 1.00 V respectively. When compared with the homometallic species **1.19** the first oxidation process in **1.31/1.32** is less favourable (0.10/0.18 V) suggesting that replacement of one iron centre by a ruthenium centre decreases the energy of the HOMO. The second oxidation in **1.31/1.32** is more favourable than the first oxidation in the mononuclear model complexes $Ru(C{\equiv}CC{\equiv}CSiMe_3)(dppe)Cp^*$ and $Fe(C{\equiv}CC{\equiv}CSiMe_3)(dppe)Cp^*$. The mono- and di-cationic derivatives $[\mathbf{1.31}]^{n+}$ and $[\mathbf{1.32}]^{n+}$ (n = 1, 2) could be chemically isolated as the PF_6^- salts. Infra-red spectroscopy of the neutral complexes displayed a single ν(C≡C) stretch at *ca.* 1965 cm^{-1} in each case. In contrast the IR spectra of the cationic species displayed two ν(CC) bands indicating a decrease in symmetry of the complexes upon oxidation. The frequencies of the ν(CC) bands decreased upon oxidation, consistent with a decrease in bond order of the (CC) 'triple bond'.

^{57}Fe Mössbauer spectroscopic studies of the mono-oxidised derivatives showed that the iron centre is affected by the first oxidation and that the iron centre in $[\mathbf{1.31}]^+$ and $[\mathbf{1.32}]^+$ is best described as having an oxidation state between Fe^{II} and Fe^{III}, suggesting that the unpaired electron is delocalised over the whole $[Ru]C_4[Fe]$ unit. Electronic absorption spectroscopy of $[\mathbf{1.31}]^{n+}$ and $[\mathbf{1.32}]^{n+}$, generated spectroelectrochemically, revealed a relatively intense band envelope within the NIR region which was not present in the neutral and dicationic derivatives.

Clearly, the nature of the metal centre plays a significant role in tuning the properties of complexes featuring the diyndiyl ligand. The spectroscopic and electrochemical behaviour of these systems are both sensitive to the degree of overlap between the metal dπ and diyndiyl π based orbitals, which may be mediated by not only the metal d-electron count, but also by the supporting ligands and the nature of the metal itself.

Polyyndiyl-bridged systems

Studies of $[L_xM]$-C≡CC≡C-$[ML_x]$ complexes have also been extended to the polyyndiyl analogues of these systems. Gladysz and co-workers have carried out the most systematic analysis of the effect of chain length on the electrochemical properties of polyyndiyl complexes by investigations of the series of complexes $[Re(PPh_3)(NO)Cp^*]_2[\mu\text{-}(C\equiv C)_n]$ **1.33/n** (n = 3-10).[102, 122, 123] With the exception of **1.33/10** each compound displayed two one-electron oxidations, the reversibility of which decreased with increasing chain length. The first oxidation becomes thermodynamically less favourable as the length of the bridging carbon chain increases. The second oxidation is similarly affected but less strongly. Consequently the radical cations formed on mono-oxidation become progressively less stable as the chain length increases. In the C_{20} analogue, **1.33/10,** only a single, possibly two-electron, oxidation is observed (**Table 1.6**). The behaviour of this family of complexes is consistent with the gradual decrease in the contribution to the high lying occupied carbon centred orbitals from the atoms at the termini, and consequently the more limited overlap of the metal and carbon dπ-π orbitals.

Table 1.6. Electrochemical properties of **1.33/n**

	E_1/V	E_2/V	$\Delta E_{1/2}$/mV	K_c	reference
1.13	0.01	0.54	530	1.1×10^9	103, 122, 123
1.33/3	0.10	0.48	380	3.0×10^6	122, 123
1.33/4	0.24	0.52	260	59×10^3	122, 123
1.33/5	0.43	0.63	200	2.6×10^3	122, 123
1.33/6	0.46	0.65	190	1.7×10^3	122, 123
1.33/8	0.57	0.66	90	34	122, 123
1.33/10	0.64				122, 123

The octatetrayndiyl complex $\{Fe(dppe)Cp^*\}_2\{\mu\text{-}(C\equiv C)_4\}$ **1.34** undergoes two reversible oxidation processes at -0.23 and 0.20 V (vs. Fc/Fc^+, 0.420 V).[124, 125] The

separation of 0.43 V (K_c = 2 x 10^7) is somewhat less than the 0.71 V observed for the diyndiyl complex **1.19**, in agreement with the trend observed in **1.33/n**. The mono-oxidised species could be chemically isolated as the PF_6^- salt [**1.34**]PF_6. The IR spectra of **1.34** and [**1.34**]PF_6 both display two ν(C≡C) bands, the bands being at lower energy in the oxidised derivative (**1.34**, 2109/1949 cm^{-1}, [**1.34**]PF_6, 1879/1784 cm^{-1}). The electronic spectra of [**1.34**]PF_6 displayed a strong band in the NIR region, analysis of this band revealed a band width narrower than would be predicted by Hush theory, and the monocation was classified as a Robin-Day Class III mixed-valence system.[124]

The electrochemical response of the binuclear ruthenium complex *trans*-[Cl(dppe)$_2$Ru(C≡C)$_6$Ru(dppe)$_2$Cl] **1.35** showed two reversible oxidation waves at -0.05 V and +0.18 V corresponding to formation of [**1.35**]$^+$ and [**1.35**]$^{2+}$ respectively, the separation of 230 mV yielding a K_c value of 10^4.[126] However, the mixed-valence derivative was not isolated and spectroscopic properties of the oxidised members of this family of complexes have yet to be described.

A systematic series of dinuclear platinum complexes with varying chain length, *trans, trans*[(C$_6$F$_5$)(*p*-tol$_3$P)$_2$Pt(C≡C)$_n$Pt(*p*-tol$_3$P)$_2$(C$_6$F$_5$)] (**1.36/n**) (n = 2, 3, 4, 6, 8, 10, 12) and the related complexes *trans, trans*[(C$_6$F$_5$)(PEt$_3$)$_2$Pt(C≡C)$_n$Pt(PEt$_3$)$_2$(C$_6$F$_5$)] (**1.37/n**) (n = 4, 6) have been prepared (**Figure 1.14**).[127, 128]

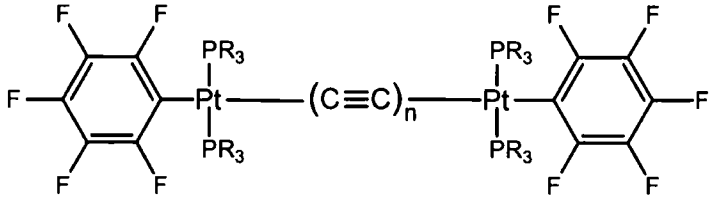

Figure 1.14

The electrochemical responses of a number of members of the series were investigated and the data is summarised in **Table 1.7**. In keeping with the trends observed for the rhenium complexes **1.33/n**, the oxidation processes became less reversible and less thermodynamically favourable as the chain length increased.

Table 1.7 Electrochemical responses of polyyne-bridged dinuclear platinum complexes.[127-129]

	E_{pa}/V	E_{pc}/V	E°/V
1.36/2	0.940	0.862	0.901
1.36/3	1.156	1.066	1.111
1.36/4	1.261	1.143	1.202
1.36/6	1.467	1.306	1.387
1.36/8	1.514		
1.37/4	1.294	1.206	1.250

A series of related complexes, in which the polyyndiyl bridges are protected by alkyl chains, have also been prepared.[129, 130] In this class of complex an sp carbon chain bridging two Pt centres is surrounded by two sp^3 carbon chains which twist in a double helix about the bridge (**Figure 1.15**).

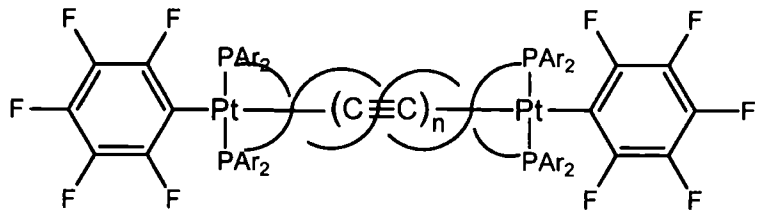

Figure 1.15 Pt-capped sp carbon chain surrounded by a double helix of sp^3 carbons, $(CH_2)_m$ (n = 3, m/Ar = $8/C_6H_4CH_3$, $10/C_6H_5$, $11/C_6H_5$, $12/C_6H_5$, $14/C_6H_4CH_3$, $16/C_6H_5$ (observed *in situ*); n = 4, m/Ar =$10/C_6H_5$, $11/C_6H_5$ $14/C_6H_5$, $14/C_6H_4CH_3$, $14/C_6H_4{}^tBu$; n = 6, m/Ar = $18/C_6H_5$).

The electrochemical responses of the representative compounds $Pt(C{\equiv}C)_3Pt$ $10/C_6H_5$ (m = 10, Ar = C_6H_5) and $Pt(C{\equiv}C)_3Pt$ $12/C_6H_5$ (m = 12, Ar = C_6H_5) demonstrated more reversible couples than the unshielded analogues. The *p*-$C_6H_4CH_3$ derivative $Pt(C{\equiv}C)_3Pt$ $14/C_6H_4CH_3$ however, displayed a much less reversible couple than the unshielded derivative.

The cyclic voltammogram of the rhenium analogue $Cp^*Re(NO)(PPh_2(CH_2)_6CH{=}\overline{CH)(C{\equiv}CC{\equiv}CC{\equiv}CC{\equiv}C)((CH_2)_6PPh_2)}(ON)ReCp^*$ was characterised by two one-electron oxidations, in a similar manner to other Re polyynyl systems. The two oxidations processes were only partially reversible and were slightly more thermodynamically favourable than the PPh_3 analogue (**1.33/4**).[131, 132]

The extension of the polycarbon chain from C_4 to C_n may be regarded as arising from the insertion of C≡C groups into the generic C≡C-C≡C bridge (for even values of n). In the section that follows, this analogy is extended to include a wider range of C≡CXC≡C systems in which aromatic groups are used to extend the conjugated pathway between the ethynyl-bonded metal centres.

1.3 Diethynyl Aromatic Bridges

Introduction of aromatic moieties within the bridging carbon chain in **1.1/2**, to produce complexes such as **1.38** (**Figure 1.16**), results in a change in the electrochemical properties, so that an apparently single, quasi-reversible oxidation process is observed. A relatively large peak-peak separation was observed in several cases which probably indicates the presence of two closely spaced redox processes, however these bridges are clearly not as well-suited to the task of promoting interactions between the remote ferrocene moieties.[133-135] The oxidation potentials of these complexes are sensitive to the nature of the aromatic group within the ethynyl-based bridges, which may suggest involvement of the bridge in the redox active orbital.[49, 133-139]

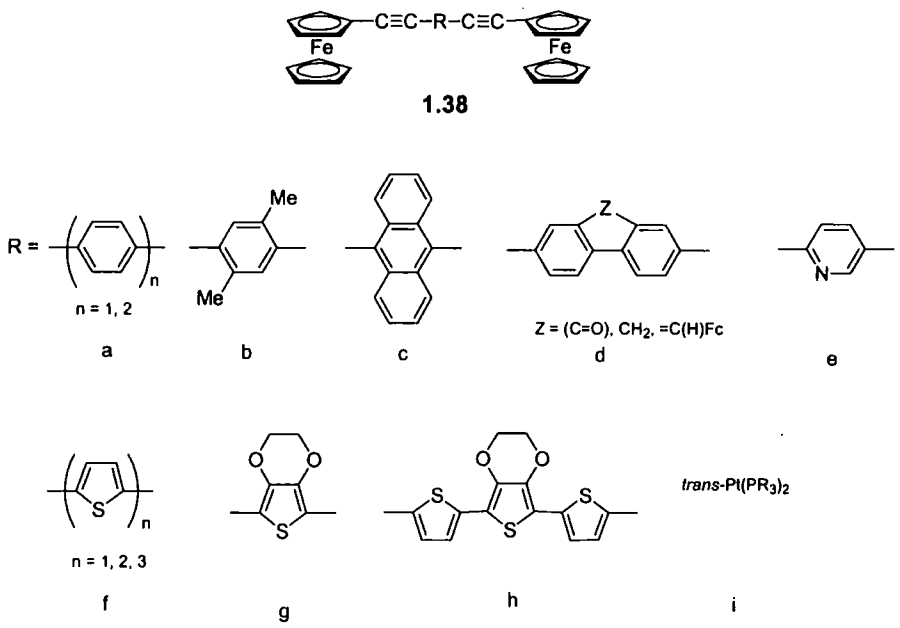

Figure 1.16

In the case of the 2,5-diethynylpyridine-bridged system **1.38e** the ferrocenyl centres are formally non-degenerate, but only a single oxidation process was observed with ΔE_p (64 mV) consistent with essentially independent, and identical, redox behaviour at these sites. However, methylation of the pyridine nitrogen centre in **1.38e** results in a significant splitting of the oxidation events (ΔE = 161 mV) when the non-coordinating electrolyte $[NBu_4][B(C_6F_5)_4]$ is employed in CH_2Cl_2. This switching in behaviour and localisation of charge on the distinct ferrocenyl termini has been suggested as the basis for a single molecule transistor which would pass charge by electron hopping, not through-bond coupling of the redox sites.[140]

The magnitude of the redox wave separation, ΔE, is also sensitive to the regiochemistry of the substitution around the aromatic ring. For example the 1,8- (**1.39**) and 1,5- (**1.40**) substituted bis(ferrocenylethynyl)naphthalene derivatives (**Figure 1.17**) both display two reversible one-electron oxidation couples arising from sequential oxidation of the two ferrocenyl moieties. The value of ΔE is significantly larger in the case of **1.39** (109 mV) than **1.40** (60 mV), this difference being attributed to a combination of through-bond and through-space factors.[48]

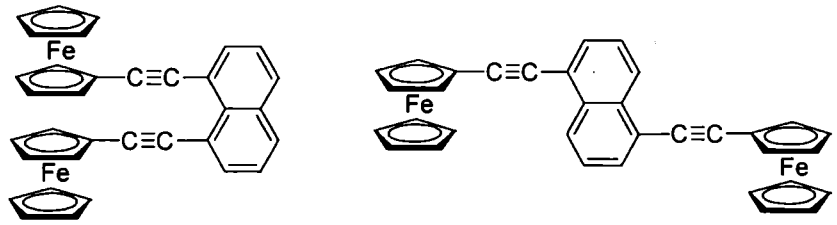

Figure 1.17 bis(ferrocenylethynyl)naphthalene derivatives

Whilst ethynyl aromatic spacers are poor at promoting electronic interaction between Fc probes, incorporation of the redox active probe group directly into the ligand π-system results, as seen in the $(C\equiv C)_n$ containing systems, in greater interactions between the remote sites. There are numerous examples of the preparation and

characterisation of metal complexes, and related polymers, featuring the $\{ML_x\}(\mu\text{-}C{\equiv}CArC{\equiv}C)\{ML_x\}$ motif, however, surprisingly few of these studies have also incorporated electrochemical methods, and addressed the nature of the mixed-valence compounds which may be derived from them.

The electrochemical properties of the series of related complexes *trans*-$[\{MCl(PP)_2\}_2(\mu\text{-}1,4\text{-}C{\equiv}CC_6H_4C{\equiv}C)]$ (M/PP = Fe/dmpe, **1.41**; Ru/dppe, **1.42**; Ru/dmpe, **1.43**; Fe/depe, **1.44**; Ru/dppm, **1.45**; Os/dppm, **1.46**) have been evaluated. The symmetrical diiron(II) complex *trans*-$[\{FeCl(dmpe)_2\}_2(\mu\text{-}1,4\text{-}C{\equiv}CC_6H_4C{\equiv}C)]$ (**1.41**), bearing strongly electron-donating dimethylphosphinoethane ligands, was found to undergo two sequential, one-electron oxidation processes in CH_2Cl_2 containing 0.2 M $[NBu_4][ClO_4]$. These oxidation processes were separated by 0.2 V ($K_c = 2.4 \times 10^3$) and as a result the Fe^{II}/Fe^{III} monocation was assumed to be a Class II mixed-valence species. The diffusion controlled behaviour of these oxidation events was taken as an indication that no significant structural rearrangement accompanies the redox steps. An irreversible, two-electron, anodic process was also observed at higher potentials. Both the mono and dications were found to be ESR active, but only broad unresolved lines were obtained at low temperatures.[141]

The electrochemical response of the diruthenium complex *trans*-$[\{RuCl(dppe)_2\}_2(\mu\text{-}1,4\text{-}C{\equiv}CC_6H_4C{\equiv}C)]$ (**1.42**) was characterised by two successive reversible oxidation waves, with a separation of 0.36 V, which was taken by the authors as evidence for communication between the two ruthenium centres via the 1,4-diethynyl benzene bridge.[142] The related dmpe complex *trans*-$[\{RuCl(dmpe)_2\}_2(\mu\text{-}1,4\text{-}C{\equiv}CC_6H_4C{\equiv}C)]$ (**1.43**) displayed two chemically reversible oxidation processes and was found to have a K_c value of 1.2×10^5.[143] The diiron complex *trans*-$[\{FeCl(depe)_2\}_2(\mu\text{-}1,4\text{-}C{\equiv}CC_6H_4C{\equiv}C)]$ (**1.44**) displayed two one electron oxidations with $\Delta E_{1/2} = 0.16$ V, $K_c = 5.1 \times 10^2$, and was assigned to Robin and Day Class II mixed-valence system.[144] The redox response for the related ruthenium and osmium complexes *trans*-$[RuCl(dppm)_2\}_2(\mu\text{-}1,4\text{-}C{\equiv}CC_6H_4C{\equiv}C)]$ (**1.45**) and *trans*-$[OsCl(dppm)_2\}_2(\mu\text{-}1,4\text{-}C{\equiv}CC_6H_4C{\equiv}C)]$ (**1.46**) were similar with two oxidation events being observed in each case. Both **1.45** and **1.46** display similar values of $\Delta E = 0.30$ V and $K_c = 1.2 \times 10^5$, but these are significantly different to the iron analogue, serving to highlight the

importance the nature of the metal centre, and the degree of overlap between the metal dπ and diyndiyl π based orbitals, in influencing the electrochemical behaviour of these systems. A shift of *ca.* 100 cm^{-1} to lower wavenumber was observed in the IR spectra of the monocations with respect to the related neutral complex in all cases with ν(C≡C) values in the monocation intermediate between those of an acetylide (M-C≡C-R) and an allenylidene (M^+=C=C=CR'_2). Bulk electrolysis of the Fe, Ru and Os complexes allowed the electronic spectra of the mixed-valence species to be collected. These displayed two MLCT bands below 860 nm and a broad, weak IVCT band in the NIR. These NIR bands were treated by Hush theory and as a result all three complexes were assigned as Robin-Day Class II mixed-valence compounds.[144] The electrochemical response of **1.45** was also measured under slightly different conditions and similar values of ΔE = 0.32, K_c = 2.6 x 10^5, were obtained and again the mixed-valence system was assigned to Class II.[145]

The electrochemical response of a number of related pseudo octahedral complexes $\{ML_x\}_2(\mu\text{-}1,4\text{-}C{\equiv}CC_6H_4C{\equiv}C)$ has also been evaluated. The diiron complex $\{Fe(dppe)Cp\}_2(\mu\text{-}1,4\text{-}C{\equiv}CC_6H_4C{\equiv}C)$ **1.47** (**Figure 1.18**) was characterised by two reversible redox events with a separation of 0.26 V corresponding to a comproportionation constant of 2.6 x 10^4.[146] This value of ΔE is less than the value associated with the first two oxidation waves in the acetylenic bridged species $\{Fe(dppe)Cp^*\}_2(\mu\text{-}C{\equiv}CC{\equiv}C)$ (**1.19**) (ΔE = 0.71 V, K_c = 1 × 10^{12}),[79] but is still sufficiently large to allow the chemical isolation of $[\mathbf{1.47}]^+$ and $[\mathbf{1.47}]^{2+}$ as PF_6^- salts.

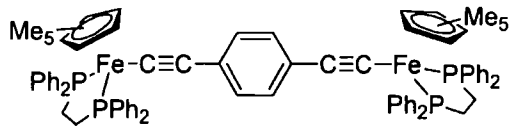

Figure 1.18 The diiron complex **1.47**

The 35-electron mixed-valence complex **[1.47]**[PF_6] was isolated and characterised by CV, and Mössbauer, ESR and IR spectroscopy. The behaviour of the mixed-valence form **[1.47]**$^+$ is complicated by an apparently conformationally-based distinction between valence-trapped and detrapped forms of the compound. The Mössbauer spectrum of **[1.47]**$^+$ contained three sets of doublets, characteristic of Fe^{II} and Fe^{III} centres, and an intermediate valence state indicative of the detrapped state. The relative proportions of these doublets varied between batches of the complex, but were temperature independent between 77 and 280 K. At lower temperatures (5 K) an increase in the amount of Fe^{II} relative to that of the detrapped state was observed, and attributed to stabilisation of a bridge-localised radical. IR spectroscopy of the oxidised species in both solid and solution state were consistent with this description and the complex was assigned as borderline Class II/Class III in terms of the Robin-Day classification.[146] The ESR spectrum of the dicationic species **[1.47]**$^{2+}$ exhibits three broad **g** tensor components without the characteristic hyperfine coupling that might be expected of metal centred radicals. When taken together with a decreased ν(C≡C) frequency from that observed in the neutral species, these data support a description of **[1.47]**$^{2+}$ which involves an appreciable contribution from the cumulated canonical form (**Scheme 1.1**).[146]

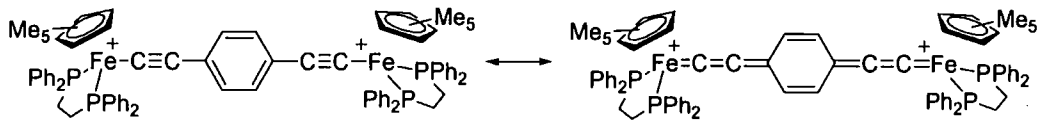

Scheme 1.1

The nature of the metal end-capping group plays a significant role in determining the magnitude of coupling in these systems, for example, in contrast to **1.47**, the 1,4-diethynylbenzene-bridged diplatinum species [$Pt(C_6H_3\{CH_2NMe_2\}_2$-2,6]$_2$(μ-1,4-$C{\equiv}CC_6H_4C{\equiv}C$)[147] **1.48** (**Figure 1.19**) was shown by cyclic voltammetric

measurements to display redox behaviour associated with independent metal sites. Only a single, irreversible oxidation wave was observed in the cyclic voltammogram of **1.48**, corresponding to the removal of a total of four electrons in two, more or less simultaneous, $Pt^{II/IV}$ oxidation steps.

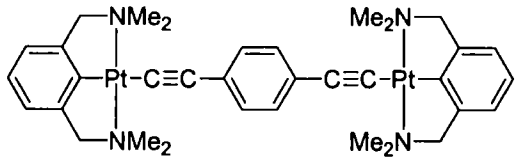

Figure 1.19 The 1,4-diethynylbenzene-bridged diplatinum species, **1.48**

The wealth of knowledge concerning metal acetylide chemistry has resulted in the development of many convenient synthetic routes to metal complexes $[ML_x]C{\equiv}CC_6H_4C{\equiv}CH$, and hence heterometallic systems of general form $[ML_x](\mu\text{-}C{\equiv}CC_6H_4C{\equiv}C)[M'L'_x]$. For the most part, studies of the nature of the electronic interactions in these systems have been limited to examination of the electrochemical response of the bimetallic systems, and comparisons of the resulting electrode potentials with those of mononuclear models. It is often found that the electrochemical response of these heterometallic systems can be interpreted in terms of the isolated metal centres, and upon oxidation genuine MMCT transitions can be observed, which are related to the IVCT process in weakly coupled mixed-valence compounds. Less common are highly delocalised systems, in which an electron (or hole) is delocalised over the heterometallic centres and the bridge.

The mixed metal complexes $[\{(NN)(CO)_3Re\}(\mu\text{-}C{\equiv}C\text{-}C_6H_4\text{-}C{\equiv}C)\{Pt(NNN)\}]OTf$, **1.49** (NN = bpy, $^tBu_2$bpy, $(CF_3)_2$bpy, NO_2phen; NNN = tpy, $^tBu_3$tpy, not all combinations) displayed two irreversible oxidation waves at *ca.* +1.0 and +1.4 V, assigned to oxidation of the alkynyl ligand, and to metal centred oxidation from Pt^{II}

to Pt^{III}, respectively. Two quasi-reversible reduction couples at *ca.* -1.0 and -1.5 V (vs SCE) were ascribed to successive ligand-centred reductions of the terpyridine ligand. In addition a quasi-reversible oxidation couple observed at *ca.* +1.9 V was assumed to be the result of an EC mechanism.[148]

The electrochemical responses of the platinum/ruthenium mixed metal complexes *trans*-[{(dppm)$_2$(Cl)Ru}(μ-C≡CC$_6$H$_4$C≡C){Pt(PEt$_3$)$_2$C$_6$H$_5$}] **1.50** and *trans*-[{Cp(PPh$_3$)$_2$Ru}(μ-C≡CC$_6$H$_4$C≡C){Pt(PEt$_3$)$_2$(C$_6$H$_5$)}] **1.51** (**Figure 1.20**) were also investigated. Complex **1.50** displayed an irreversible wave at 0.07 V attributed to oxidation of the ruthenium centre, whilst in the cyclic voltammogram of **1.51** a quasi-reversible oxidation wave at -0.13 V due to oxidation of the Ru centre was observed. This was significantly lower than the model complex Ru(C≡CC$_6$H$_5$)(PPh$_3$)$_2$Cp[149] indicating that the platinum fragment transfers electron density to the ruthenium centre.[150]

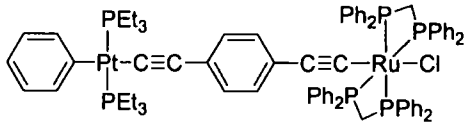

1.50

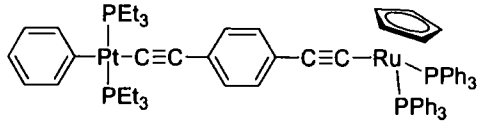

1.51

Figure 1.20

The related complex [{(bpy)(CO)$_3$Re}(μ-C≡CC$_6$H$_4$C≡C){Fe(dppe)Cp*}] **1.52** displayed a quasi-reversible wave due to reduction of the rhenium site at -1.49 V, which is only 0.02 V less favourable than the reduction in Re(C≡CC$_6$H$_4$C≡CH)(CO)$_3$(bpy), and a fully reversible oxidation wave due to oxidation at the iron centre at -0.19 V, some 0.04 V more favourable than the oxidation of Fe(C≡CC$_6$H$_5$)(dppe)Cp*, indicating a simple relationship in which both metal centres act as moderately electron-donating substituents. A third, partially reversible, oxidation wave corresponding to formation of the dication [**1.52**]$^{2+}$ was observed near the solvent edge.[151] The monocation [**1.52**]$^{+}$ could be isolated as the

PF_6^- salt and comparison of the IR spectra of the neutral and cationic derivatives revealed that upon oxidation, the stretching mode attributed to the Fe-C≡C fragment shifted to lower energy (by 58 cm^{-1}) whilst the band associated with the Re-C≡C fragment shifted to higher energy (by 30 cm^{-1}). The electronic spectrum of both **[1.52]**$^+$ and **1.52** were also measured. **1.52** was characterised by absorption bands at 290, 390 and 420 nm which were assigned to intra-ligand π-π* transitions and MLCT transitions. Upon oxidation these MLCT bands were replaced by two less intense bands at slightly lower energies. In addition, a band at *ca.* 830 nm assigned to LMCT transition and a weak absorption in the NIR region were observed. The NIR band envelope could be deconvoluted, assuming Gaussian profiles, to reveal the presence of two absorption bands the highest energy of which was assigned to a Re^{I}-Fe^{III} MMCT transition.[151]

The electrochemical response of {RuCl(dppm)$_2$}(μ-C≡CC_6H_4C≡C){OsCl(dppm)$_2$} was characterised by two oxidation processes, which were assigned to the sequential oxidation of the Os and Ru fragments.[150] These oxidation processes both occurred at less positive potentials than the oxidation processes observed in the model mononuclear complexes *trans*-[MCl(C≡CC_6H_4C≡CH)(dppm)$_2$] (M = Ru, Os), which was taken to be indicative of bridge-mediated donation of electron density between the metal end-caps.[150, 152]

The influence of the aromatic moiety within the bridge has also been considered by examination of the electrochemical properties of a series of complexes featuring a common metal-ligand combination and a range of diethynyl aromatic bridging moieties, which in some cases may also be compared with the analogous polyyndiyl bridged complexes.

The series of iron complexes {Fe(dppe)Cp*}$_2$(μ-C≡CXC≡C) (X = C≡CC≡C **1.34**, 2,5-thiophene **1.53**) were both characterised by two reversible oxidation waves corresponding to the two Fe^{II}/Fe^{III} couples. Comparison of the electrochemical response revealed a greater separation of the two $Fe^{II/III}$ oxidation processes in the case of the polyyndiyl ligand than in the diethynylthiophene derivative (0.43 V vs

0.34 V).[124, 153] The electronic spectra for both of the mono-oxidised species exhibited overlapping transitions in the NIR region of the spectrum which were deconvoluted into two (**1.53**) or three (**1.34**) Gaussian-shaped bands. These bands were treated according to Hush theory and the coupling parameter V_{ab} obtained. Despite the difference in the values of K_c, analysis of the lowest energy band revealed little difference in the coupling parameter (**1.53**; V_{ab} = 2515, **1.34**; V_{ab} = 2520 cm^{-1}). This serves to illustrate the *absence* of a relationship between K_c and V_{ab}, despite many claims to the contrary in the literature. Whilst only a single band is observed in the neutral and dicationic species [**1.53**] and $[\mathbf{1.53}]^{2+}$, the IR spectra of $[\mathbf{1.53}]^{+}$ revealed two distinct ν(C≡C) stretches at lower energy than in the neutral complex.[153]

A combination of electrochemical and spectroscopic techniques, and semi-empirical calculations, has demonstrated that coupling between two *trans*-$MCl(dppm)_2$ fragments (M = Fe, Ru, Os) through diethynylaromatic ligands, C≡CArC≡C, follows the order Ar = 2,5-C_4H_2S > 1,4-C_6H_4 > 2,5-C_5H_3N > 1,3-C_6H_4. This order was attributed to the relative energy change associated with the adoption of a quinoidal structure in the mixed-valence system.[143, 144] The nature of the metal fragment also influenced the strength of coupling between the centres with the ruthenium fragments being more strongly coupled than the analogous Fe or Os species, this being attributed to the better interactions between the π-donating ligand the metal centre.[154]

The series of ruthenium complexes [{Ru(dppf)Cp}(μ-C≡C-R-C≡C)] (R = 1,4-C_6H_4, **1.54**; 1,4- $C_{10}H_6$, **1.55**; 9,10-$C_{14}H_{10}$, **1.56**) (**Figure 1.21**) were synthesised by reaction of RuCl(dppf)Cp with the appropriate $Me_3SiC{\equiv}C\text{-}R\text{-}C{\equiv}CSiMe_3$ ligand and KF. For each complex two one-electron oxidation processes were observed corresponding to stepwise oxidation of the ruthenium centres. The separations of these oxidation events (260-290 mV) were smaller than in the related diyndiyl system (**1.27**), and whilst these data point to the relative stability of the mixed-valence complexes derived from these systems, more careful analysis of the spectroscopic properties of these systems is required before any conclusions may be drawn about the underlying electronic structures.

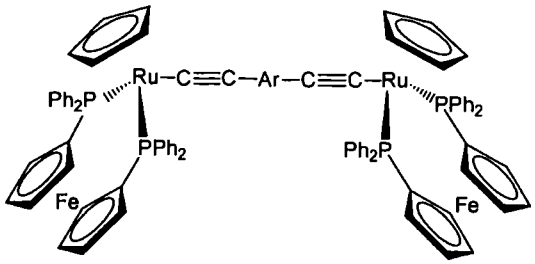

Figure 1.21

The monocations $[\mathbf{1.55}]^+$ and $[\mathbf{1.56}]^+$ were isolated as the PF_6^- salts. The electronic absorption spectra of the monocationic species displayed an absorption in the NIR region, which was assigned to an IVCT transition, the slight solvent dependency of these bands leading to an assignment of the monocations as Robin-Day Class II systems, with coupling parameters in the range of 0.12 - 0.14 eV.[112] The complications in the NIR spectra of mixed-valence compounds derived from low-symmetry organometallic end-caps, such as the Ru(dppf)Cp fragment, has been commented upon earlier (see Section 1.1), and the validity of treating the whole band envelope as a single transition is, of course, questionable. This point is addressed in more detail later in this thesis.

In all systems where the organometallic redox probes are linked by C≡CArC≡C bridging ligands, *meta*-substitution patterns lead to less strongly electronically-coupled systems. For example, for 1,3,5-tris(ferrocenylethynyl)benzene (**Figure 1.22**), in which the ferrocenyl moieties are arranged in mutually *meta* positions around the aromatic ring, only a single anodic process was detected by cyclic voltammetry and was shown by controlled potential coulometry to consume three electrons per molecule.[49, 135, 155]

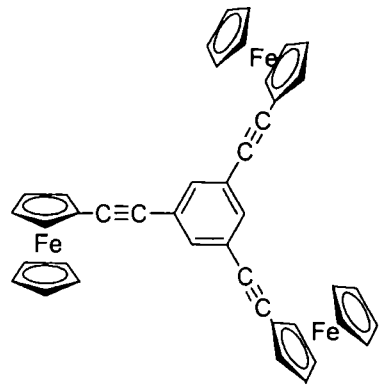

Figure 1.22

As with 1,4-substituted systems, incorporation of the metal centre directly into the conjugated ligand framework can result in more significant interactions between the redox active termini. Electrochemical studies of complexes such as **1.57, 1.58** and **1.59** (**Figure 1.23**) have lead to the observation of ΔE values of up to 180 mV.[156-159]

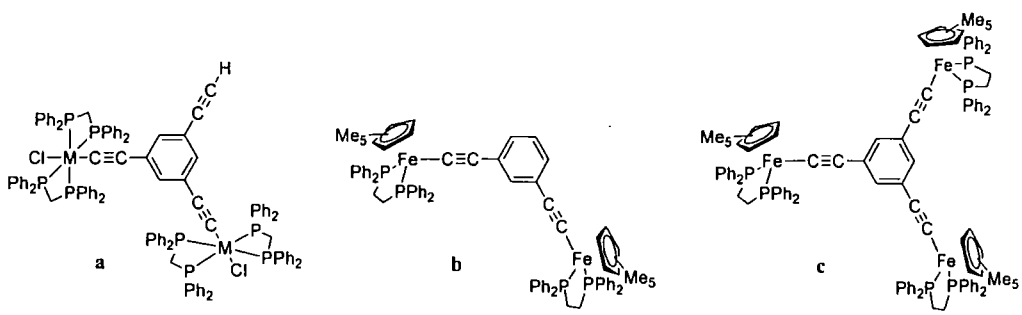

Figure 1.23 a) 1.57, b) 1.58 and **c) 1.59**

The IR spectrum of the mixed-valence cation $[\mathbf{1.58}]^+$ is characterised by two $\nu(C\equiv C)$ bands which correspond to vibrations associated with Fe^{II}-C≡C and Fe^{III}-C≡C moieties. These two distinct bands indicate that electron transfer between the sites is slow on the IR timescale, although DFT analysis suggests an appreciable amount of

the unpaired spin density resides on the aromatic portion of the bridging ligand. The presence of distinct Fe^{II} and Fe^{III} centres is also indicated by Mössbauer spectroscopy.[160] In the electronic spectrum weak, solvent independent bands were observed in the NIR region under the tail of the LMCT bands. By assuming Gaussian line shapes the absorption was deconvoluted into two bands, one assigned to a ligand-field transition associated with the Fe^{III}(dppe)Cp* fragment and the second to the Fe^{II}-Fe^{III} IVCT transition. The Gaussian line-fit of the IVCT band displayed a half-height bandwidth close to that predicted by Equation 1.5. The value of V_{ab} of 0.020 eV (160 cm^{-1}) was obtained from Equation 1.4, assuming the Fe...Fe separation to be a reasonable estimate of the electron transfer distance.[160]

The interpretation of the mixed-valence behaviour in the trinuclear species **[1.59]**$^{+}$ must take into account the electron transfer between three sites, and a modified form of Equation 1.5 is employed, as given in Equation 1.7.[161]

$$V_{ab} = 2.06\times10^{-2}\frac{\sqrt{\nu_{max}\varepsilon_{max}\nu_{1/2}}}{r\sqrt{2}} \qquad \textbf{Equation 1.7}$$

Within the limits of the various assumptions made, the coupling in **[1.59]**$^{+}$ was found to be the same as that in **[1.58]**$^{+}$. The electronic spectrum of the diradical **[1.59]**$^{2+}$ displayed three bands in the NIR region, one assigned to the LF transitions associated with the formally Fe^{III} centre, and the remaining attributed to IVCT type processes assumed to originate from the magnetic interactions between the two S = 1/2 centres.[160]

The results summarised in this introductory chapter serve to illustrate the manner in which the properties of mixed-valence systems can be modified and tuned through careful choice of metal, supporting ligands and the nature of the bridge, and highlight the necessity for a thorough examination of spectroscopic as well as electrochemical data in the assessment of mixed-valence characteristics. Throughout this thesis, spectroscopic (UV-vis-NIR-IR, Raman) data has been obtained *via* conventional and spectroelectrochemical methods. The changes in characteristic spectroscopic

signatures and structural features of the bridge and the metal centres as a function of the oxidation state are related to the underlying electronic structure of the compounds. A short introduction to these techniques follows.

1.4 Concepts and Techniques

Electrochemical methods

In this thesis cyclic voltammetry has been used to evaluate the electrochemical response of the compounds under study. Cyclic voltammetry is a linear sweep voltammetric method in which a potential is applied to a working electrode which is immersed in a solution of the species under investigation, and varied with time. The potential is swept from an initial potential E_i to some maximum potential E_{max} and then inverted and swept to a second vertex E_{min} where it is again inverted and swept to some final potential E_f (**Figure 1.24**).

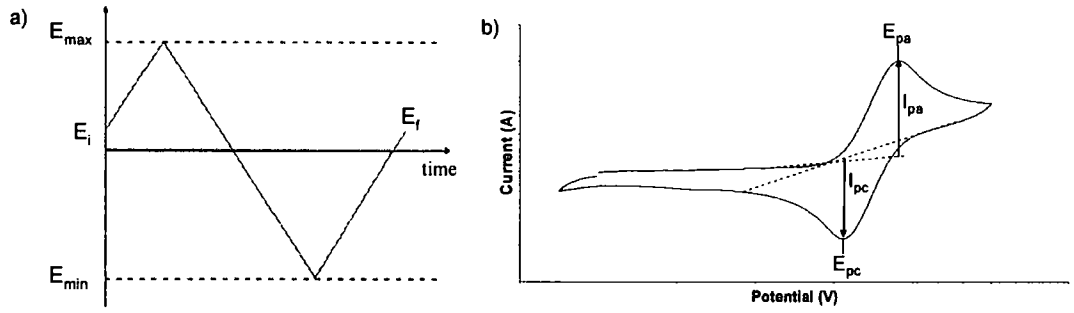

Figure 1.24 a) Potential with time graph and **b)** typical cyclic voltammogram showing: E_i initial potential, E_{max} max potential, E_{min} min potential, E_f final potential, E_{pa} potential of the anodic peak, E_{pc} potential of the cathodic peak, I_{pa} peak current of the anodic wave, I_{pc} peak current of the cathodic wave.

For electrochemically reversible redox systems the relationship E_{pa}-E_{pc} = 57/n mV (where n is the number of electrons consumed in the redox process) should hold,

however in organic solvents there is often resistance due to passage of current through the solution between the working and reference electrodes. This resistance R leads to a shift in the potential of the working electrode by an amount equal to I_pR and results in a broadening of the peaks and a larger value of E_{pa}-E_{pc} than might be predicted. For an electrochemically reversible redox event the relationships $I_p \propto \nu^{1/2}$ (ν = scan rate), E_p is independent of ν and $I_{pa}/I_{pc} = 1$ should also be true.

The thermodynamic stability of the mixed-valence state can be calculated from the values of E°_1 and E°_2. The comproportionation constant, K_c, the equilibrium constant for the reaction in **Scheme 1.2** is given by $K_c = e^{\frac{\Delta EF}{RT}}$, where ΔE is the difference in oxidation potentials (E°_1 and E°_2) associated with the first and second oxidation of the parent complex, $[M^{(n)}L_x]$-B-$[M^{(n)}L_x]$.

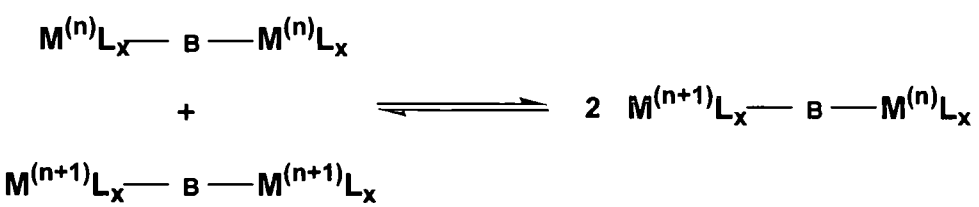

Scheme 1.2

Values of the comproportionation constant range from $K_c \sim 4$ for weakly coupled systems to $>10^{13}$ for the most strongly coupled systems. It is important to note that K_c is a thermodynamic parameter related to the stability of the mixed-valence complex with respect to disproportionation and neither K_c nor ΔE can be used in isolation when determining the class of a mixed-valence system. Rather, information relating to the ground-state interactions of redox centres via bridging ligands may be obtained from comparisons of the electrode potentials in the binuclear systems with

carefully constructed mono-nuclear models that offer similar solvation energies in the oxidation states of interest.

In this study cyclic voltammograms were recorded using an Eco Chemie PGStat 30 controlled by a PC running GPES v4.9 for Windows or using an EG&G PAR Model 283 potentiostat. In the case of measurements using the Eco Chemie PGStat 30, the electrochemical cell used was an EG & G PARC micro-cell fitted with a nitrogen feed for the bubbler and purge inlets (**Figure 1.25**). The working electrodes were EG & G PARC millielectrodes with a 2 mm diameter electrode surface. Counter and pseudo-reference electrodes were platinum wires. Solvents used were deoxygenated by bubbling through with nitrogen prior to measurement and blanketed with nitrogen during measurements. For cyclic voltammograms recorded using the EG&G PAR Model 283 potentiostat, the CH_2Cl_2 solutions contained 10^{-3} M complex and 0.1 M $[NBu_4]PF_6$ (Aldrich; recrystallised twice from absolute EtOH and dried overnight under vacuum at 80 °C) as supporting electrolyte. The solutions were placed in an airtight single-compartment three-electrode cell equipped with a Pt disk working electrode (0.42 mm^2 apparent electrode surface, polished with a 0.25 μm diamond paste), Pt gauze auxiliary electrode and Ag wire pseudo-reference electrode. An internal ferrocene, decamethylferrocene or cobaltocene standard was employed and potentials are quoted against the standard calomel electrode (SCE).[162]

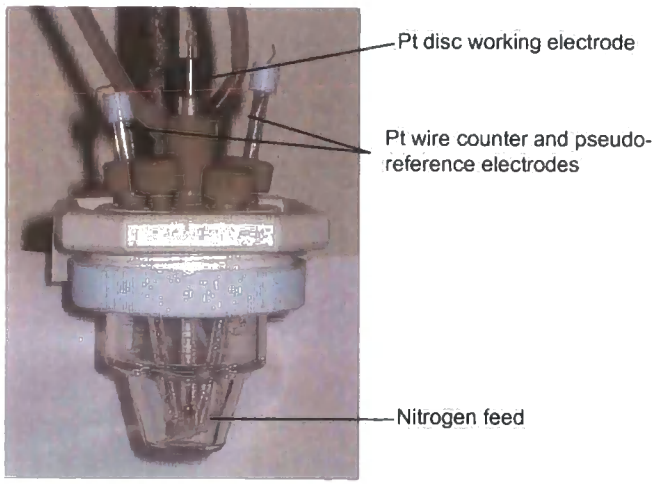

Figure 1.25 Electrochemical cell showing arrangement of electrodes and nitrogen feed

Spectroelectrochemical Methods

In this thesis spectroelectrochemical methods are utilised to obtain vibrational (IR) and electronic absorption spectra of oxidised species. These techniques allow observation of the spectra of electrogenerated species *in situ*, and permit an assessment of differences in the physical and electronic structure of complexes in different redox states.

In order for these observations to be made the beam of the probe light is passed directly through a solution of the electrogenerated species, in close proximity to the working electrode. This allows changes in the electronic or vibrational spectra on oxidation/reduction to be measured directly. In this thesis electrochemical and spectroelectrochemical examples are given in terms of oxidation processes for convenience. To facilitate this procedure, the use of optically transparent metal minigrid working electrode has been adopted. This consists of a fine mesh of a selected metal (platinum is used within this thesis although silver or gold are also commonly used) inserted into a short pathlength cell. Reference and counter electrodes are also included to produce an optically transparent thin layer electrode (OTTLE) cell.[163, 164] The temperature of the cell can be controlled using any one of a variety of variable temperature cell holders and mounts.

The use of a small volume in the electrochemical cell allows bulk electrolysis of the sample to be achieved within a relatively short space of time. In a typical experiment the spectrum of the initial species under study, X, is recorded at a potential at which X is stable followed by a stepwise increase in the applied potential. Spectra are recorded when the system has reached electrochemical equilibrium after each potential step, ultimately providing spectroscopic data associated with X^+. In cases where electrogenerated species are stable by voltammetric measurements but insufficiently stable over the longer time-period required for bulk electrolysis variable-temperature apparatus can be used to reduce the temperature of the solution and hence stabilise the redox product.

The Infra-red spectroelectrochemical studies described in this thesis were conducted using a Nicolet Avatar 360 FT-IR controlled by a PC running OMNIC 5.1b or at the Universiteit van Amsterdam (UvA) using a BioRad FTS-7 spectrometer. Oxidised species were generated using a platinum minigrid working electrode (32 wires/cm) with a platinum wire counter electrode and a silver wire pseudo-reference electrode which are melt-sealed into a smooth polyethylene space sandwiched between two CaF_2 windows to form the OTTLE cell. The working electrode surroundings were masked to avoid spectral interference from the non-electrolysed solution. For variable temperature studies the CaF_2 windows are enclosed within a thermostated Cu block to form the OTTLE cell. The OTTLE cell itself fitted into a double-walled nitrogen bath cryostat permitting the acquisition of spectra over a temperature range of 295-173 K (**Figure 1.26**). The potential during these measurements was controlled by PA4 (EKOM, Czech Republic), Eco Chemie PGStat 30 or home-made potentiostats.

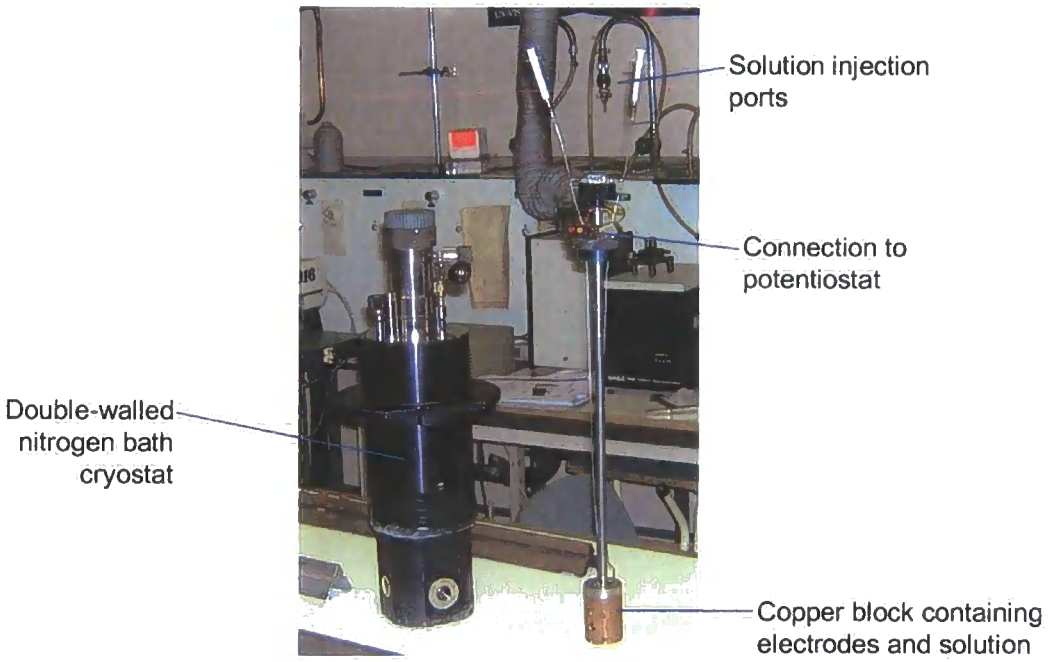

Figure 1.26

UV-vis-NIR spectra were acquired using a Varian Cary-5 spectrophotometer. The OTTLE cell employed to generate the oxidised species consisted of a 30 x 10 x 1 mm quartz cuvette, containing a solution volume of ~0.3 ml in the thin layer region. The three electrode system consisted of a platinum minigrid working electrode (0.06 mm wire diameter, 82 x 82 wires per inch, 65% open area) with platinum wire (0.40 mm diameter) counter and pseudo-reference electrodes (**Figure 1.27a**). The OTTLE cell was held within a Teflon mount which permitted cooling of the solution to sub-ambient temperatures (**Figure 1.27b**). Cooling was achieved by a flow of dry nitrogen gas through a copper coil immersed in liquid nitrogen and subsequently through the interior of the cell mount. The rate of flow of the nitrogen gas was used to control the temperature. Condensation on the cell windows was prevented by the purging of the sample compartment of the spectrometer and the inner space between cell windows with dry nitrogen prior to and during the acquisition of spectra.

a)

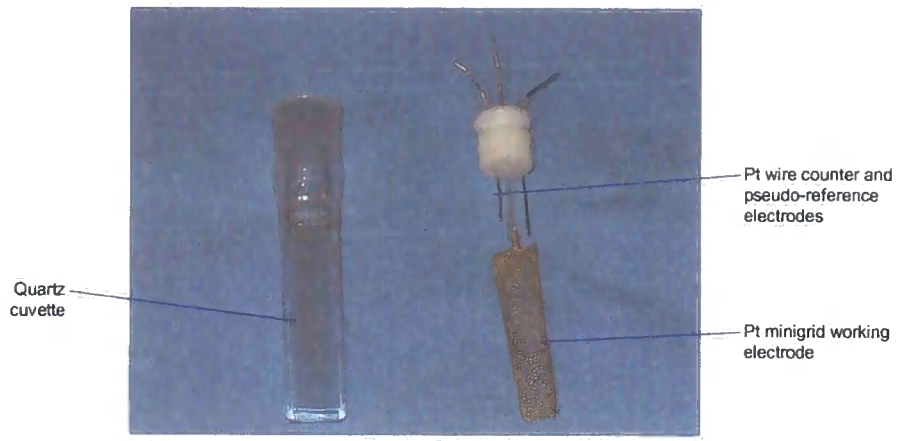

b)

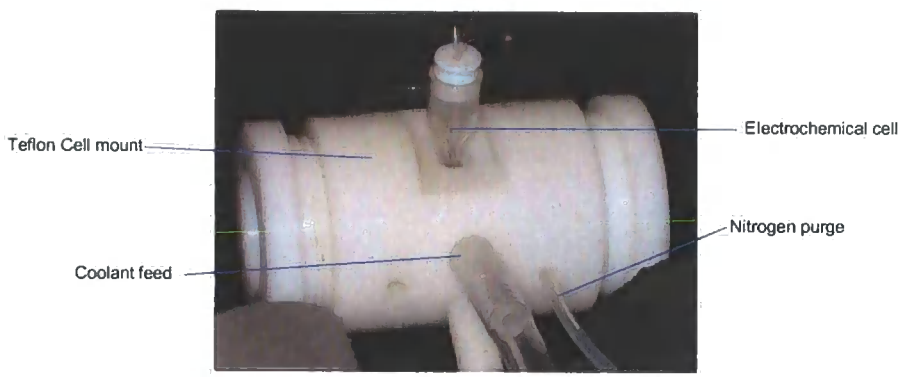

Figure 1.27

Raman Spectroscopy

Raman spectroscopy probes the vibrational energy levels of a compound, through examination of the frequencies and intensities of the radiation scattered by the sample. A typical experiment involves the irradiation of the sample with a monochromatic light source, usually a laser, and recording of the scattered radiation. When the sample is irradiated the interactions between the incident photons and the electron cloud of the molecule, result in light being scattered. Most of this scattered

radiation is of the same frequency as the incident light due to Rayleigh scattering (an elastic process where no energy is transferred to the sample under study). However, a small proportion of photons (*ca.* one in every million) are scattered inelastically, and have a different energy to that of the incident photons. This weak inelastic scattering is termed Raman scattering. The difference in energy between the scattered and incident photons is equal to the energy required to change the vibrational state of the molecule. In Raman scattering, the molecule is virtually promoted to an excited state (either a virtual state or, as in the case of resonance Raman spectroscopy, a real state, *vide infra*). Energy exchange during this process results in two series of Raman bands. Energy can either be transferred from the photon to the molecule (Stokes Raman scattering) or from the molecule to the photon (Anti-Stokes Raman scattering) (**Figure 1.28**).

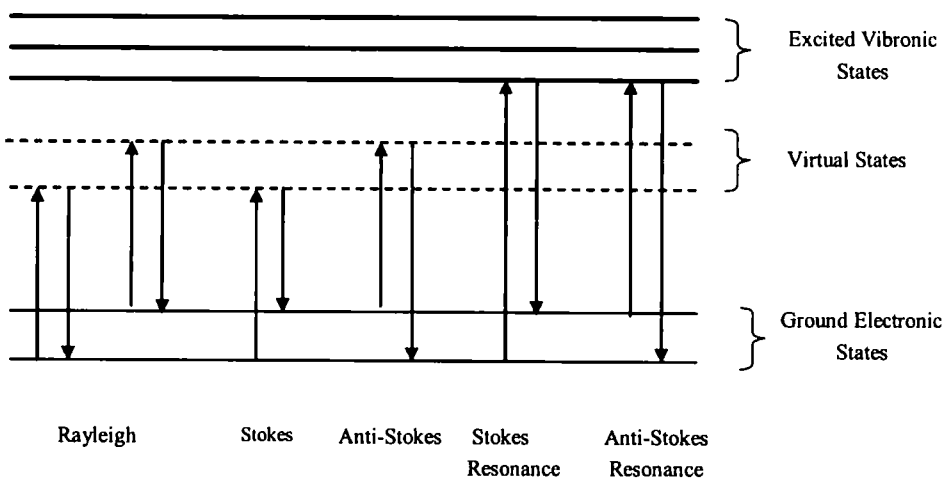

Figure 1.28

The selection rules for Raman spectroscopy are that a vibration mode of a molecule is Raman active if there is a change in the polarisability of the molecule during the vibration.

If the sample under study has an absorption band coincident with the excitation frequency then a resonance Raman effect can be observed resulting in a significant enhancement in the intensity of certain Raman bands. This effect occurs by the promotion of an electron into an excited electronic-vibrational state, accompanied by immediate relaxation into a vibrational level of the ground state. (**Figure 1.28**) Resonance Raman can provide enhancement by a factor of up to 10^4 over normal Raman scattering. It can also be used to probe the structure of a chromophore as only the vibrational modes associated with the chromophore are enhanced.

1.5 Outlook

This introductory chapter has demonstrated the importance that the metal, supporting ligands, and the nature of the bridge play, in determining the properties of mixed-valence systems derived from complexes of the type $[ML_x]$-B-$[ML_x]$. The need for a thorough examination of spectroscopic data, alongside electrochemical data, in the assessment of mixed-valence characteristics has been highlighted.

The following three chapters describe the synthesis and properties of complexes of the type L_nM-C≡C-X-C≡C-ML_n where X is an organometallic spacer, an aromatic organic spacer or a 'three dimensional' aromatic spacer. A combination of electrochemical and spectroscopic and theoretical methods have been utilised to investigate the underlying electronic structures. In addition, in Chapter 5, the synthesis of a series of iron bis(acetylide) complexes, which may provide routes to polymetallic chemistry and discrete oligomers, is described. Appendix 1 describes a number of molecular structures obtained by single crystal X-ray diffraction studies.

1.6 References

1 M. B. Robin and P. Day, *Advan. Inorg. Radiochem.*, 1967, **10**, 247.

2 C. Creutz, *Prog. Inorg. Chem.*, 1983, **30**, 1.

3 N. S. Hush, *Coord. Chem. Rev.*, 1985, **64**, 135.

4 B. S. Brunschwig, C. Creutz, and N. Sutin, *Chem. Soc. Rev.*, 2002, **31**, 168.

5 S. F. Nelson, *Chem. Eur. J.*, 2000, **6**, 581.

6 C. Creutz and H. Taube, *J. Am. Chem. Soc.*, 1969, **91**, 3988.

7 C. Creutz and H. Taube, *J. Am. Chem. Soc.*, 1973, **95**, 1086.

8 C. Creutz and M. H. Chou, *Inorg. Chem. Commun.*, 1987, **26**, 2995.

9 A. Stebbler, J. H. Ammeter, U. Fürholtz, and A. Ludi, *Inorg. Chem.*, 1984, **23**, 2764.

10 C. Creutz, M. L. Good, and S. Chandra, *Inorg. Nucl. Chem. Lett.*, 1973, **9**, 171.

11 U. Fürholtz, S. Joss, A. Bürgi, and A. Ludi, *Inorg. Chem.*, 1985, **24**, 9143.

12 A. Broo and P. Lincoln, *Inorg. Chem.*, 1997, **36**, 2544.

13 A. Bencini, I. Ciofini, C. A. Daul, and A. Ferretti, *J. Am. Chem. Soc.*, 1999, **121**, 11418.

14 K. D. Demadis, C. M. Hartshorn, and T. J. Meyer, *Chem. Rev.*, 2001, **101**, 2655.

15 B. S. Brunschwig, C. Creutz, and N. Sutin, *Coord. Chem. Rev.*, 1998, **177**, 61.

16 J. P. Launay, *Chem. Soc. Rev.*, 2001, **30**, 386.

17 T. Ren and G.-L. Xu, *Comm. Inorg. Chem.*, 2002, **23**, 355.

18 G.-L. Xu, C.-Y. Wang, Y.-H. Ni, T. G. Goodson III, and T. Ren, *Organometallics*, 2005, **24**, 3247.

19 S. K. Hurst and T. Ren, *J. Organomet. Chem.*, 2002, **660**, 1.

20 S. K. Hurst and T. Ren, *J. Organomet. Chem.*, 2003, **670**, 188.

21 G.-L. Xu, M. C. DeRosa, R. J. Crutchley, and T. Ren, *J. Am. Chem. Soc.*, 2004, **126**, 3728.

22 G.-L. Xu, R. J. Crutchley, M. C. DeRosa, Q.-J. Pan, H.-X. Zhang, X. Wang, and T. Ren, *J. Am. Chem. Soc.*, 2005, **127**, 13354.

23 Y. Shi, G. T. Yee, G. Wang, and T. Ren, *J. Am. Chem. Soc.*, 2004, **126**, 10552.

24 G.-L. Xu, G. Zou, Y.-H. Ni, M. C. DeRosa, R. J. Crutchley, and T. Ren, *J. Am. Chem. Soc.*, 2003, **125**, 10057.

25 T. Ren, G. Zou, and J. C. Alvarez, *Chem. Commun.*, 2000, 1197.

26 V. W.-W. Yam and W. K.-M. Fung, *Chem. Commun.*, 1998, 777.

27 V. W.-W. Yam, *Acc. Chem. Res.*, 2002, **35**, 555.

28 V. W.-W. Yam, W.-Y. Lo, C.-H. Lam, W. K.-M. Fung, K. M.-C. Wong, V. C.-Y. Lau, and N. Zhu, *Coord. Chem. Rev.*, 2003, **245**, 39.

29 V. W.-W. Yam, K. K. W. Lo, and K. M.-C. Wong, *J. Organomet. Chem.*, 1999, **578**, 3.

30 P. J. Low, R. Rousseau, P. Lam, K. A. Udachin, G. D. Enright, J. S. Tse, D. D. M. Wayner, and A. J. Carty, *Organometallics*, 1999, **18**, 3885.

31 G. H. Worth, B. H. Robinson, and J. Simpson, *Organometallics*, 1992, **11**, 3863.

32 S. M. Elder, B. H. Robinson, and J. Simpson, *J. Organomet. Chem.*, 1990, **398**, 165.

33 D. Osella, O. Gambino, C. Nervi, M. Ravera, and D. Bertolino, *Inorg. Chim. Acta*, 1993, **206**, 155.

34 R. M. Medina, C. Moreno, M. l. Marcos, J. A. Castro, F. Benito, A. Arnaz, S. Delgado, J. Gonzalez-Velasco, and M. J. Macazaga, *Inorg. Chim. Acta*, 2004, **357**, 2069.

35 N. J. Long and C. K. Williams, *Angew. Chem. Int. Ed.*, 2003, **42**, 2586.

36 M. I. Bruce and P. J. Low, *Adv. Organomet. Chem.*, 2004, **50**, 179.

37 M. D. Ward, *Chem. Soc. Rev.*, 1995, **24**, 121.

38 R. Dembinski, S. Szafert, P. Haquette, T. Lis, and J. A. Gladysz, *Organometallics*, 1999, **18**, 5438.

39 S. B. Falloon, W. Weng, A. M. Arif, and J. A. Gladysz, *Organometallics*, 1997, **16**, 5438.

40 W. Weng, A. M. Arif, and J. A. Gladysz, *Angew. Chem. Int. Ed. Engl.*, 1993, **32**, 891.

41 W. Weng, T. Bartik, and J. A. Gladysz, *Angew. Chem. Int. Ed. Engl.*, 1994, **33**, 2199.

42 T. Bartik, W. Weng, J. A. Ramsden, S. Szafert, S. B. Falloon, A. M. Arif, and J. A. Gladysz, *J. Am. Chem. Soc.*, 1998, **120**, 11071.

43 W. Weng, J. A. Ramsden, A. M. Arif, and J. A. Gladysz, *J. Am. Chem. Soc.*, 1993, **115**, 3824.

44 B. E. Woodworth and J. L. Templeton, *J. Am. Chem. Soc.*, 1996, **118**, 7418.

45 P. J. Low and M. I. Bruce, *Adv. Organomet. Chem*, 2002, **48**, 71.

46 M. J. Powers and T. J. Meyers, *J. Am. Chem. Soc.*, 1978, **100**, 4393.

47 C. Levanda, K. Bechgaard, and D. O. Cowan, *J. Org. Chem.*, 1976, **41**, 2700.

48 C. J. McAdam, J. J. Brunton, B. H. Robinson, and J. Simpson, *J. Chem. Soc., Dalton Trans.*, 1999, 2487.

49 P. Jutzi and B. Kleinebekel, *J. Organomet. Chem.*, 1997, **545-546**, 573.

50 T. Mochida and S. Yamazaki, *J. Chem. Soc., Dalton Trans.*, 2002, 3559.

51 R. D. Adams, B. Qu, M. D. Smith, and T. A. Albright, *Organometallics*, 2002, **21**, 2970.

52 R. D. Adams, B. Qu, and M. D. Smith, *Organometallics*, 2002, **21**, 3867.

53 C. Levanda, D. O. Cowan, C. Leitch, and K. Bechgaard, *J. Am. Chem. Soc.*, 1974, **96**, 6788.

54 G. E. McManis, A. Gochev, R. M. Nielson, and M. J. Weaver, *J. Phys. Chem.*, 1989, **93**, 7733.

55 F. Delgado-Pena, D. R. Talham, and D. O. Cowan, *J. Organomet. Chem.*, 1983, **253**, C43.

56 G. A. Koutsantonis and J. P. Selegue, *J. Am. Chem. Soc.*, 1991, **113**, 2316.

57 H. Ogawa, K. Onitsuka, T. Joh, S. Takahashi, Y. Yamamoto, and H. Yamakazi, *Organometallics*, 1988, **7**, 2257.

58 H. Ogawa, T. Joh, S. Takahashi, and K. Sonogashira, *J. Chem. Soc., Chem. Commun.*, 1985, 1220.

59 M. Akita, M. Terada, S. Oyama, S. Sugimoto, and Y. Moro-oka, *Organometallics*, 1990, **9**, 816.

60 W. A. Herrmann, F. E. Kühn, and C. C. Romao, *J. Organomet. Chem.*, 1995, **495**, 209.

61 M. Appel, J. Heidrich, and W. Beck, *Chem. Ber.*, 1987, **120**, 1087.

62 Y.-L. Yang, L. J.-J. Wang, Y.-C. Lin, T.-W. Tseng, G. H. Lee, and Y. Wang, *Organometallics*, 1997, **16**, 1573.

63 N. A. Ustynuk, V. N. Vinogradova, D. N. Kravtsov, Y. F. Oprunenko, and V. a. Piven, *Mettallo-org. Khim.*, 1988, **1**, 884.

64 J. Heidrich, M. Steimann, M. Appel, W. Beck, J. R. Phillips, and W. C. Trolger, *Organometallics*, 1990, **9**, 1296.

65 M. Akita, M.-C. Chung, A. Sakurai, S. Sugimoto, M. Terada, M. Tanaka, and Y. Moro-oka, *Organometallics*, 1997, **16**, 4882.

66 K. G. Caulton, R. H. Cayton, M. H. Chisholm, J. C. Huffman, E. B. Lobkovsky, and Z. Xue, *Organometallics*, 1992, **11**, 321.

67 N. Ouddaï, K. Costuas, M. Bencharif, J.-Y. Saillard, and J.-F. Halet, *C. R. Chemie*, 2005, **8**, 1336.

68 S. Kheradmandan, K. Venkatesan, O. Blacque, H. W. Schmalle, and H. Berke, *Chem. Eur. J.*, 2004, **10**, 4872.

69 W. Weng, T. Bartik, M. Brady, B. Bartik, J. A. Ramsden, A. M. Arif, and J. A. Gladysz, *J. Am. Chem. Soc.*, 1995, **117**, 11922.

70 M. I. Bruce, M. Z. Ke, and P. J. Low, *Chem. Commun.*, 1996, 2405.

71 B. E. Woodworth, P. S. White, and J. L. Templeton, *J. Am. Chem. Soc.*, 1997, **119**, 828.

72 R. L. Roberts, H. Puschmann, J. A. K. Howard, J. H. Yamamoto, A. J. Carty, and P. J. Low, *Dalton Trans.*, 2003, 1099.

73 S. Kheradmandan, K. Heinze, H. W. Schmalle, and H. Berke, *Angew. Chem. Int. Ed.*, 1999, **38**, 2270.

74 F. J. Fernández, O. Blacque, M. Alfonso, and H. Berke, *Chem. Commun.*, 2001, 1266.

75 Y. Zhou, J. W. Seyler, W. Weng, A. M. Arif, and J. A. Gladysz, *J. Am. Chem. Soc.*, 1993, **115**, 8509.

76 W. E. Meyer, A. J. Amoroso, C. R. Horn, M. Jaeger, and J. A. Gladysz, *Organometallics*, 2001, **20**, 1115.

77 V. W.-W. Yam, V. C.-Y. Lau, and K.-K. Cheung, *Organometallics*, 1996, **15**, 1740.

78 J. Kim, H. Masai, K. Sonogashira, and N. Hagihara, *Inorg. Nucl. Chem. Lett.*, 1970, **6**, 181.

79 N. Le Narvor, L. Toupet, and C. Lapinte, *J. Am. Chem. Soc.*, 1995, **117**, 7129.

80 M. Guillemot, L. Toupet, and C. Lapinte, *Organometallics*, 1998, **17**, 1928.

81 M. I. Bruce, P. Hinterding, E. R. T. Tiekink, B. E. Skelton, and A. H. White, *J. Organomet. Chem.*, 1993, **450**, 209.

82 M. I. Bruce, L. I. Denisovich, P. J. Low, S. M. Peregudova, and N. A. Ustynuk, *Mendeleev Commun.*, 1996, 200.

83 M. I. Bruce, B. G. Ellis, M. Gaudio, C. Lapinte, G. Melino, F. Paul, B. E. Skelton, M. E. Smith, L. Toupet, and A. H. White, *Dalton Trans.*, 2004, 1601.

84 M. I. Bruce, B. G. Ellis, P. J. Low, B. W. Skelton, and A. H. White, *Organometallics*, 2003, **22**, 3184.

85 E. Stein, S. Y. Oki, and E. J. S. Vichi, *J. Braz. Chem. Soc.*, 2000, **11**, 252.

86 O. Gevert, J. Wolf, and H. Werner, *Organometallics*, 1996, **15**, 2806.

87 T. Rappert, O. Nurnberg, and H. Werner, *Organometallics*, 1993, **12**, 1359.

88 P. J. Stang and R. Tykwinski, *J. Am. Chem. Soc.*, 1992, **114**, 4411.

89 R. Nast and F. Z. Urban, *Anorg. Allg. Chem.*, 1957, **289**, 244.

90 K. Sonogashira, S. Kataoka, S. Takahashi, and N. Hagihara, *J. Organomet. Chem.*, 1978, **160**, 319.

91 S. Takahashi, Y. Ohyama, E. Murata, K. Sonogashira, and N. Hagihara, *J. Polym. Sci., Polym Chem. Ed.*, 1980, **18**, 349.

92 A. Klein, K.-W. Klinkhammer, and T. Scheiring, *J. Organomet. Chem.*, 1999, **592**, 128.

93 G. R. Owen, F. Hampel, and J. A. Gladysz, *Organometallics*, 2004, **23**, 5893.

94 C.-M. Che, H.-Y. Chao, V. M. Miskowski, Y. Li, and K.-K. Cheung, *J. Am. Chem. Soc.*, 2001, **123**, 489.

95 A. Wong, P. C. W. Kang, C. D. Tagge, and D. R. Leon, *Organometallics*, 1990, **9**, 1992.

96 F. Coat, M.-A. Guillevic, L. Toupet, F. Paul, and C. Lapinte, *Organometallics*, 1997, **16**, 5988.

97 C. Moreno, A. Arnanz, and S. Delgado, *Inorg. Chim. Acta*, 2001, **312**, 139.

98 Y. F. Cheng, D. L. Phillips, G. A. He, C.-M. Che, and Y. Chi, *Chem. Phys. Lett*, 2001, **338**, 308.

99 D. S. Frohnapfel, B. E. Woodworth, H. H. Thorp, and J. L. Templeton, *J. Phys. Chem. A.*, 1998, **102**, 5665.

100 F. J. Fernández, K. Venkatesan, O. Blacque, M. Alfonso, H. W. Schmalle, and H. Berke, *Chem. Eur. J.*, 2003, **9**, 6192.

101 K. Venkatesan, T. Fox, H. W. Schmalle, and H. Berke, *Organometallics*, 2005, **24**, 2834.

102 M. Brady, W. Weng, and J. A. Gladysz, *J. Chem. Soc., Chem. Commun.*, 1994, 2655.

103 M. Brady, W. Weng, Y. Zhou, J. W. Seyler, A. J. Amoroso, A. M. Arif, M. Böhme, G. Frenking, and J. A. Gladysz, *J. Am. Chem. Soc.*, 1997, **119**, 775.

104 R. Crescenzi and C. Lo Sterzo, *Organometallics*, 1992, **11**, 4301.

105 N. Le Narvor and C. Lapinte, *J. Chem. Soc., Chem. Commun.*, 1993, 357.

106 F. Coat, P. Thominot, and C. Lapinte, *J. Organomet. Chem.*, 2001, **629**, 39.

107 H. Jiao, K. Costuas, J. A. Gladysz, J. F. Halet, M. Guillemot, L. Toupet, F. Paul, and C. Lapinte, *J. Am. Chem. Soc.*, 2003, **125**, 9511.

108 M. I. Bruce, P. Hinterding, P. J. Low, B. W. Skelton, and A. H. White, *J. Chem. Soc., Dalton Trans.*, 1998, 467.

109 M. I. Bruce, B. C. Hall, B. D. Kelly, P. J. Low, B. W. Skelton, and A. H. White, *J. Chem. Soc., Dalton Trans.*, 1999, 3719.

110 M. I. Bruce, P. J. Low, K. Costuas, J. F. Halet, S. P. Best, and G. A. Heath, *J. Am. Chem. Soc.*, 2000, **122**, 1949.

111 M. I. Bruce, B. G. Ellis, B. E. Skelton, and A. H. White, *J. Organomet. Chem.*, 2005, **690**, 792.

112 L.-B. Gao, L.-Y. Zhang, L.-X. Shi, and Z.-N. Chen, *Organometallics*, 2005, **24**, 1678.

113 G. A. Neyhart, J. T. Hupp, J. C. Curtis, C. J. Timpson, and T. J. Meyer, *J. Am. Chem. Soc.*, 1996, **118**, 3724.

114 M. A. Watzky, A. V. Macatangay, R. A. Van Camp, S. E. Mazzetto, X. Song, J. F. Endicott, and T. Buranda, *J. Phys. Chem.*, 1997, **10**, 8441.

115 M. I. Bruce, P. J. Low, M. Z. Ke, B. D. Kelly, B. W. Skelton, M. E. Smith, A. H. White, and N. B. Witton, *Aust. J. Chem.*, 2001, **54**, 453.

116 M. I. Bruce, B. G. Ellis, B. E. Skelton, and A. H. White, *J. Organomet. Chem.*, 2000, **607**, 137.

117 F. Paul, W. E. Meyer, L. Toupet, H. Jiao, J. A. Gladysz, and C. Lapinte, *J. Am. Chem. Soc.*, 2000, **122**, 9405.

118 M. I. Bruce, K. Costuas, T. Davin, B. G. Ellis, J. F. Halet, C. Lapinte, P. J. Low, M. E. Smith, B. W. Skelton, L. Toupet, and A. H. White, *Organometallics*, 2005, **24**, 3864.

119 M. I. Bruce, M. E. Smith, N. N. Zaitseva, B. W. Skelton, and A. H. White, *J. Organomet. Chem.*, 2003, **670**, 170.

120 M. I. Bruce, B. C. Hall, B. E. Skelton, M. E. Smith, and A. H. White, *J. Chem. Soc., Dalton Trans.*, 2002, 995.

121 M. I. Bruce, K. Costuas, J. F. Halet, B. C. Hall, P. J. Low, B. K. Nicholson, B. E. Skelton, and A. H. White, *J. Chem. Soc., Dalton Trans.*, 2002, 383.

122 T. Bartik, B. Bartik, M. Brady, R. Dembinski, and J. A. Gladysz, *Angew. Chem. Int. Ed.*, 1996, **35**, 414.

123 R. Dembinski, T. Bartik, B. Bartik, M. Jaeger, and J. A. Gladysz, *J. Am. Chem. Soc.*, 2000, **122**, 810.

124 F. Coat and C. Lapinte, *Organometallics*, 1996, **15**, 477.

125 F. Coat, F. Paul, C. Lapinte, L. Toupet, K. Costuas, and J. F. Halet, *J. Organomet. Chem.*, 2003, **683**, 368.

126 S. Rigaut, J. Perruchon, L. Le Pichon, D. Touchard, and P. H. Dixneuf, *J. Organomet. Chem.*, 2003, **670**, 37.

127 W. Mohr, J. Stahl, F. Hampel, and J. A. Gladysz, *Chem. Eur. J.*, 2003, **9**, 3324.

128 W. Mohr, J. Stahl, F. Hampel, and J. A. Gladysz, *Inorg. Chem.*, 2001, **40**, 3263.

129 G. R. Owen, J. Stahl, F. Hampel, and J. A. Gladysz, *Organometallics*, 2004, **23**, 5889.

130 J. Stahl, J. C. Bohling, E. B. Bauer, T. B. Peters, W. Mohr, J. M. Martín-Alvarez, F. Hampel, and J. A. Gladysz, *Angew. Chem. Int. Ed.*, 2002, **41**, 1871.

131 C. R. Horn, J. M. Martín-Alvarez, and J. A. Gladysz, *Organometallics*, 2002, **21**, 5386.

132 C. R. Horn and J. A. Gladysz, *Eur. J. Inorg. Chem*, 2003, 2211.

133 W.-Y. Wong, G.-L. Lu, K.-F. Ng, C.-K. Wong, and K.-H. Choi, *J. Organomet. Chem.*, 2001, **637-639**, 159.

134 K. R. J. Thomas, J. T. Lin, and Y. S. Wen, *Organometallics*, 2000, **19**, 1008.

135 H. Fink, N. J. Long, A. J. Martin, G. Opromolla, A. J. P. White, D. J. Williams, and P. Zanello, *Organometallics*, 1997, **16**, 2646.

136 N. Chawdhury, N. J. Long, M. F. Mahon, L.-l. Ooi, P. R. Raithby, S. Rooke, A. J. P. White, D. J. Williams, and M. Younus, *J. Organomet. Chem.*, 2004, **689**, 840.

137 W.-Y. Wong, G.-L. Lu, K.-F. Ng, K.-H. Choi, and Z. Lin, *J. Chem. Soc., Dalton Trans.*, 2001, 3250.

138 W.-Y. Wong, K.-Y. Ho, and K.-H. Choi, *J. Organomet. Chem.*, 2003, **670**, 17.

139 Y. Zhu and M. O. Wolf, *J. Am. Chem. Soc.*, 2000, **122**, 10121.

140 C. Engtrakul and L. R. Sita, *Nano Lett.*, 2001, **1**, 541.

141 L. D. Field, A. V. George, F. Laschi, E. Y. Malouf, and P. Zanello, *J. Organomet. Chem.*, 1992, **435**, 347.

142 O. Lavastre, J. Plass, P. Bachmann, S. Gusemi, C. Moinet, and P. H. Dixneuf, *Organometallics*, 1997, **16**, 184.

143 D. Beljonne, M. C. B. Colbert, P. R. Raithby, R. H. Friend, and J. L. Bredas, *Synth. Met.*, 1996, **81**, 179.

144 M. C. B. Colbert, J. Lewis, N. J. Long, P. R. Raithby, M. Younus, A. J. P. White, D. J. Williams, N. N. Payne, L. Yellowlees, D. Beljonne, N. Chawdhury, and R. H. Friend, *Organometallics*, 1998, **17**, 3034.

145 S. K. Hurst, M. P. Cifuentes, A. M. McDonagh, M. G. Humphrey, M. Samoc, B. Luther-Davies, I. Asselberghs, and A. Persoons, *J. Organomet. Chem.*, 2002, **642**, 259.

146 N. Le Narvor and C. Lapinte, *Organometallics*, 1995, **14**, 634.

147 S. Back, M. Lutz, A. L. Spek, H. Lang, and G. van Koten, *J. Organomet. Chem.*, 2001, **620**, 227.

148 S. C.-F. Lam, V. W.-W. Yam, K. M.-C. Wong, E. C.-C. Cheng, and N. Zhu, *Organometallics*, 2005, **24**, 4298.

149 I. R. Whittall, M. G. Humphrey, D. C. R. Hockless, B. E. Skelton, and A. H. White, *Organometallics*, 1995, **14**, 3970.

150 M. Younus, N. J. Long, P. R. Raithby, and J. Lewis, *J. Organomet. Chem.*, 1998, **570**, 55.

151 K. M.-C. Wong, S. C.-F. Lam, C.-C. Ko, N. Zhu, V. W.-W. Yam, S. Roué, C. Lapinte, S. Fathallah, K. Costuas, S. Kahlal, and J.-F. Halet, *Inorg. Chem.*, 2003, **42**, 7086.

152 C. W. Faulkner, S. L. Ingham, M. S. Khan, J. Lewis, N. J. Long, and P. R. Raithby, *J. Organomet. Chem.*, 1994, **482**, 139.

153 S. Le Stang, F. Paul, and C. Lapinte, *Organometallics*, 2000, **19**, 1035.

154 W. Kaim and V. Kasack, *Inorg. Chem.*, 1990, **29**, 4696.

155 J. B. Flanagan, S. Margel, A. J. Baird, and F. C. Anson, *J. Am. Chem. Soc.*, 1978, **100**, 4248.

156 N. J. Long, A. J. Martin, F. Fabrizi de Biani, and P. Zanello, *J. Chem. Soc., Dalton Trans.*, 1998, 2017.

157 N. J. Long, A. J. Martin, A. J. P. White, D. J. Williams, M. Fontani, F. Laschi, and P. Zanello, *J. Chem. Soc., Dalton Trans.*, 2000, 3387.

158 S. K. Hurst and T. Ren, *J. Organomet. Chem.*, 2002, **660**, 1.

159 T. Weyland, C. Lapinte, G. Frapper, M. J. Calhorda, J.-F. Halet, and L. Toupet, *Organometallics*, 1997, **16**, 2024.

160 T. Weyland, K. Costuas, L. Toupet, J.-F. Halet, and C. Lapinte, *Organometallics*, 2000, **19**, 4228.

161 J. Bonvoisin, J. P. Launay, M. Van der Auweraer, and F. C. De Schryver, *J. Phys. Chem.*, 1994, **98**, 5053.

162 N. G. Connelly and W. E. Geiger, *Chem. Rev.*, 1996, **96**, 877.

163 T. Mahabiersing, H. Luyten, R. Nieuwendam, and F. Hartl, *Collect. Czech. Chem. Commun.*, 2003, **68**, 1687.

164 F. Hartl, H. Luyten, H. A. Nieuwenhuis, and G. C. Schoemaker, *Appl. Spectr*, 1994, **48**, 1522.

Chapter 2

2.1 Introduction

As summarised in Chapter 1, the properties of the mixed-valence state of binuclear ferrocenyl complexes have been extensively investigated. Other complexes in which various ML_x groups are linked to a ferrocenyl group by carbon chains have also been investigated. Studies of the electrochemical responses of the complexes $Fc(C{\equiv}C)_nW(CO)_3Cp$ (n = 1 - 4) demonstrated that lengthening of the carbon chain from two to eight carbons resulted in an increase in oxidation potential of the ferrocenyl moiety of about 0.06 V per C≡C unit.[1] This shift is consistent with an increase in the degree of electron transfer from the Fc nucleus to the chain, and the decreased σ-donor ability of the longer carbon chains. In these complexes the $W(CO)_3Cp$ group does not exhibit any redox properties. The electrochemical responses of the related derivatives $Fc(C{\equiv}C)_2Ru(PP)Cp$ [(PP) = dppm, dppe], in which the Fc and Ru(PP)Cp units are linked by C_4 chains, were characterised by an irreversible oxidation at *ca.* 0.3 V and two quasi-reversible oxidations at *ca.* 0.75 and 0.9 V, which cannot all be associated with oxidation of the ferrocenyl moiety. The chemical complications associated with the oxidation process meant the nature of the oxidised species was not investigated further.[2]

Earlier work by Sato and co-workers was concerned with the complexes $FcC{\equiv}CRu(PP)Cp'$ [Cp' = Cp, (PP) = $(PPh_3)_2$ (**2.1**), dppe (**2.2**), dppf (**2.3**); Cp' = Cp* (PP) = $(PPh_3)_2$ (**2.4**), dppe (**2.5**)] (**Figure 2.1**), in which ferrocenyl groups were linked by a C≡C chain to redox-active, ruthenium-based groups.[3] Electrochemical and spectroscopic studies demonstrated a significant electronic interaction between the two end-caps mediated by the carbon chains and showed that the radical cation produced by one-electron oxidation of the parent complex can be described as having some delocalised character.

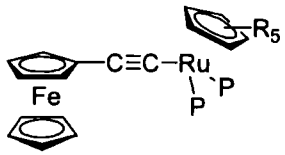

Figure 2.1 The ferrocenyl acetylide complexes FcC≡CRu(PP)Cp'. Cp' = Cp, (PP) = $(PPh_3)_2$ (**2.1**), dppe (**2.2**), dppf (**2.3**); Cp' = Cp* (PP) = $(PPh_3)_2$ (**2.4**), dppe (**2.5**)

The electrochemical response of **2.1-2.3** (0.1M $[NBu_4]ClO_4$ in CH_2Cl_2 as supporting electrolyte, potentials vs $Ag/AgNO_3$ electrode) were characterised by a quasi-reversible peak at *ca.* -0.32 V and a second irreversible peak with E_{pa} falling between 0.29 and 0.38 V (**2.3** displayed an additional wave due to the dppf moiety) and that of **2.4** and **2.5** by a quasi-reversible peak at *ca.* -0.55 V and a second irreversible peak with E_{pa} at 0.29 V and 0.15 V, respectively. A combination of Mössbauer and IR spectroscopy indicated significant delocalisation of the odd electron over the ferrocenyl and Ru(C≡C)(PP)Cp' moieties in the monocations formed by one electron oxidation. The one electron oxidised complexes $[\mathbf{2.1}]^+$, $[\mathbf{2.3}]^+$ and $[\mathbf{2.4}]^+$ displayed broad absorptions in the NIR region. In this previous study the NIR band was attributed to an 'intervalence' transition, the nature of which is somewhat ambiguous. Similar results were observed in the electrochemical response of the related series of complexes FcC≡CFe(PP)Cp', RcC≡CRu(PP)Cp' and Rc'C≡CRu(PP)Cp'.[4,5]

To date, no examples of ferrocene derivatives containing two metal-ethynyl substituents have been reported. To investigate the efficacy of the 1,1'-ferrocenediyl unit (Fc') as a bridge between two redox-active metal centres, a series of complexes of the type Ru(C≡CFc)(PP)Cp' and 1,1'-{Cp'(PP)RuC≡C}$_2$Fc' were prepared, and the electrochemical properties of these systems, and the electronic properties of their oxidation products are presented in this chapter.[†]

[†] The complexes described in this chapter were prepared by the Bruce group and supplied to the author for the electrochemical and spectroelectrochemical investigations that form the body of this chapter.

2.2 Results

The complexes Ru(C≡CFc)(PP)Cp' [Cp' = Cp, PP = $(PPh_3)_2$ (**2.1**), dppe (**2.2**); Cp = Cp*, PP = dppe (**2.5**)] were prepared by the reaction of RuCl(PP)Cp', FcC≡CH and $Na[BPh_4]$ in refluxing methanol, followed by addition of sodium methoxide solution (**Scheme 2.1**). These were identified by their spectroscopic properties (IR, NMR, ES MS) and elemental analyses, and the structures of all were confirmed by X-ray determination.

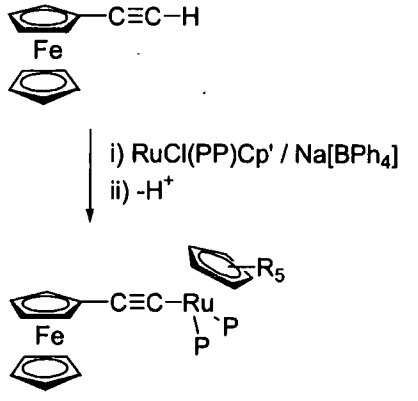

	PP	R
2.1	$(PPh_3)_2$	H
2.2	dppe	H
2.5	dppe	Me

Scheme 2.1 Preparation of the bimetallic complexes **2.1**, **2.2** and **2.5**

As the compound 1,1'-$(HC{\equiv}C)_2$Fc' is rather unstable,[6] a general approach to the synthesis of the disubstituted ferrocenes was developed using the metallo-desilylation reaction of alkynyltrimethylsilanes described earlier.[7] Complexes 1,1'-{Cp'(PP)RuC≡C}$_2$Fc' [Cp' = Cp, PP = $(PPh_3)_2$ (**2.6**), dppe (**2.7**); Cp' = Cp*, PP = dppe (**2.8**)] were prepared in 50-60 % yields by reactions of 1,1'-$(Me_3SiC{\equiv}C)_2$Fc' with the appropriate ruthenium complex RuCl(PP)Cp' in the presence of KF in

MeOH or MeOH-thf mixtures (**Scheme 2.2**). These trimetallic complexes were identified by spectroscopic methods and by X-ray structural determinations of **2.6** and **2.8**.

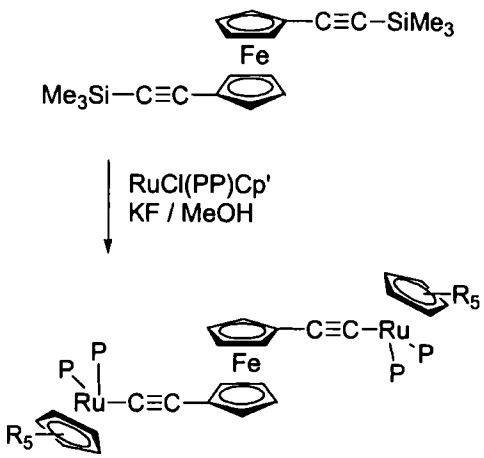

	PP	R
2.6	$(PPh_3)_2$	H
2.7	dppe	H
2.8	dppe	Me

Scheme 2.2 Preparation of the trimetallic species **2.6-2.8** by metallo-desilylation reactions

Although **2.6** proved to be relatively insoluble in common solvents, the more soluble mono-oxidised species [**2.6**]PF_6 was readily obtained by reaction of **2.6** with one equivalent of $[FeCp_2]PF_6$ in a dichloromethane / benzene mixture. The authenticity of [**2.6**]PF_6 was confirmed by microanalysis. Full details of the synthetic and structural work that precedes the electrochemical studies can be found in the publication related to this chapter, together with that of some related derivatives.[8]

Electrochemical studies

The electrochemical responses of the bimetallic complexes **2.1**, **2.2** and **2.5**, and the corresponding trimetallic complexes [**2.6**]PF_6, **2.7** and **2.8** were examined by cyclic

voltammetry. All potentials were converted to the saturated calomel electrode (SCE) scale through reference to an internal ferrocene / ferrocinium or cobaltocene / cobaltocenium standard.[9] At a scan rate $\upsilon \geq 100$ mV s^{-1}, each of the bimetallic complexes were characterised by two chemically reversible oxidation processes, separated by 580-690 mV (**Table 2.1**). Each wave is associated with a one-electron redox process as evidenced by the equal current ratios and peak areas observed in the cyclic voltammograms, and hence number of electrons transferred during each oxidation event. The trimetallic species **[2.6]**PF_6, **2.7** and **2.8** are again characterised by two reversible one-electron redox processes separated by 530-620 mV. A third oxidation process could also be detected near the electrochemical limit of the solvent. The trications generated as a consequence of this third oxidation event were chemically unstable on the time-scale of the voltammetry experiment, as evidenced by the observation of a large number of product waves in the reverse cathodic sweep. The observation of at least two one electron anodic processes indicates some electrochemical distinction of the otherwise identical ruthenium centres.

Table 2.1 Electrochemical details for compounds **2.1**-**2.8**.[a]

	E_1 / V	E_2 / V	ΔE / mV	K_c	E_3 / V
2.1[b]	+0.13	+0.82	690	3.5×10^{11}	
2.2[b]	+0.14	+0.72	580	8.0×10^{9}	
2.5[b]	+0.05	+0.68	630	4.6×10^{10}	+1.21[d]
2.6[c]	-0.04	+0.58	620	2.9×10^{10}	+0.93[d]
2.7	-0.03	+0.50	530	9.5×10^{8}	+0.81[d]
2.8	+0.04	+0.68	640	4.3×10^{10}	+1.29[d]

[a] All electrochemical experiments were performed in 0.1M $[NBu_4]PF_6$ in CH_2Cl_2, referenced to $FeCp_2$ / $[FeCp_2]^+$ = 0.46 V or $CoCp_2/[CoCp_2]^+$ = -0.87 V. [b] Electrochemistry on literature compounds, comparative values in reference 3. [c] As compound **2.6** was not soluble enough for electrochemical studies, these values were obtained from **[2.6]**PF_6. [d] Irreversible

The first oxidation of the bimetallic complexes (**Table 2.1**) occurs at significantly less positive potentials than those of the monometallic models $Ru(C{\equiv}CC_6H_5)(PPh_3)_2Cp$ (0.535 V), $Ru(C{\equiv}CC_6H_5)(dppe)Cp^*$ (0.245 V) or ferrocene (0.46 V) collected under identical conditions, (see Chapter 3) the higher oxidation potential in the model complexes probably being a result of the electron withdrawing effect of the C_6H_5 groups.

The first oxidation of the trimetallic complexes **2.6** and **2.7** were shifted by approximately -0.17 V relative to the first oxidation of **2.1** and **2.2,** and the second oxidation processes were shifted by approximately -0.23 V relative to the appropriate bimetallic analogues. However, the first and second oxidation potentials of the Ru(dppe)Cp* derivative **2.8** are similar to those of **2.5**. The large separation of the redox potentials in both the bi and tri-metallic complexes indicates the high thermodynamic stabilities of the monocations with respect to disproportionation, and leads to large values of the comproportionation constant K_c (10^8 –10^{11}) in each case.

Spectroelectrochemical studies

To explore the nature of the interactions occurring between the metal centres the electronic (UV-Vis-NIR) and vibrational (IR) spectra of the chemically stable, redox-accessible, oxidation states of **2.1**, **2.2** and **2.5-2.8** were obtained using spectroelectrochemical methods. Although each complex in this series gave rise to two redox events that were chemically reversible at room temperature, on the time scale of the cyclic voltammetric experiment, the dicationic species proved to be less robust on the longer time scale required for electrolysis in the spectroelectrochemical cells. This instability of the dication has been observed in similar species on previous occasions.[3-5] Infra-red spectra were therefore collected at –20 °C, using a low-volume cell of standard design.[10, 11] The low volume of the cell served to minimise the time necessary for the experiment, and hence the opportunity for the dications to degrade. The chemical reversibility of each electrogenerated species was established by the recovery of the spectrum associated with the preceding oxidation state, following back-reduction of the sample solution.

In CH_2Cl_2 solution, containing 0.1 M $[NBu_4]PF_6$ as supporting electrolyte, each complex in the series **2.1**, **2.2** and **2.5-2.8** was characterised by a single, weak $\nu(C{\equiv}C)$ band at *ca.* 2080 cm^{-1}. Oxidation of the bimetallic species **2.1**, **2.2** and **2.5** to the corresponding monocations resulted in a shift of the $\nu(C{\equiv}C)$ bands to lower energy ($\Delta\nu \sim 90 - 100$ cm^{-1}) (**Figure 2.2**, **Table 2.2**). This lowering of the $\nu(C{\equiv}C)$ frequency which occurs upon oxidation may be compared with the differences in the $\nu(C{\equiv}C)$ band frequencies of $[Ru(C{\equiv}CC_6H_5)(PP)Cp']^{n+}$ (n = 0, 1; $\Delta\nu \sim 150$ cm^{-1}) (see Chapter 3) and to the related homometallic iron systems, $[FcC{\equiv}CFe(PP)Cp']^{n+}$ (n = 1, 0; $\Delta\nu \sim 100$ cm^{-1}), for which delocalised electronic structures have been proposed.[4]

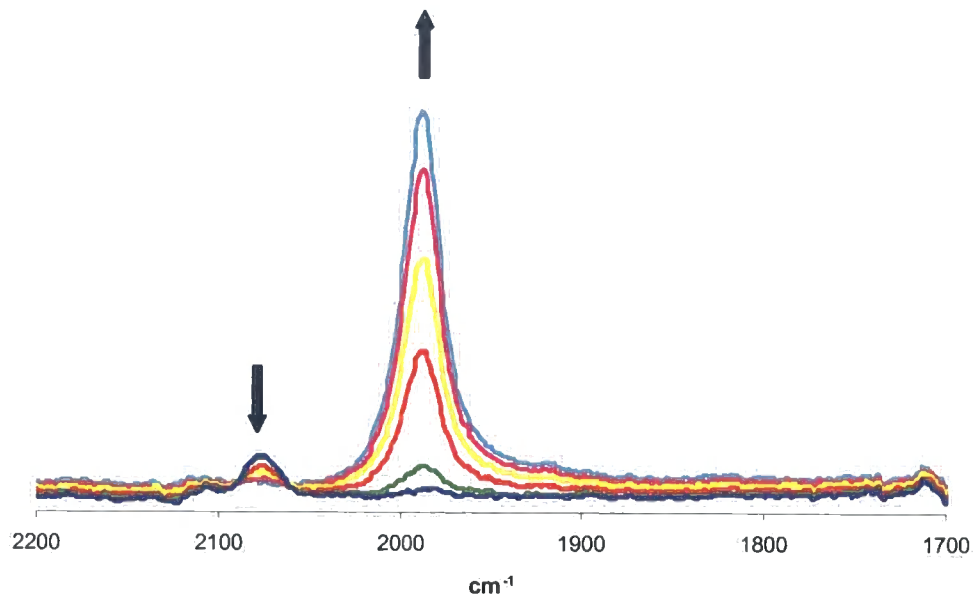

Figure 2.2. Infrared spectra obtained on oxidation of **2.1** → $[\mathbf{2.1}]^+$

The spectra of the trimetallic species $[\mathbf{2.6}]^+$, $[\mathbf{2.7}]^+$ and $[\mathbf{2.8}]^+$ each exhibited a similarly intense ν(C≡C) band at almost the same energy as the corresponding bimetallic species. In addition, a weak band (or shoulder) near 2040 cm^{-1}, not present in the bimetallic species, was also observed (**Figure 2.3 Table 2.2**).

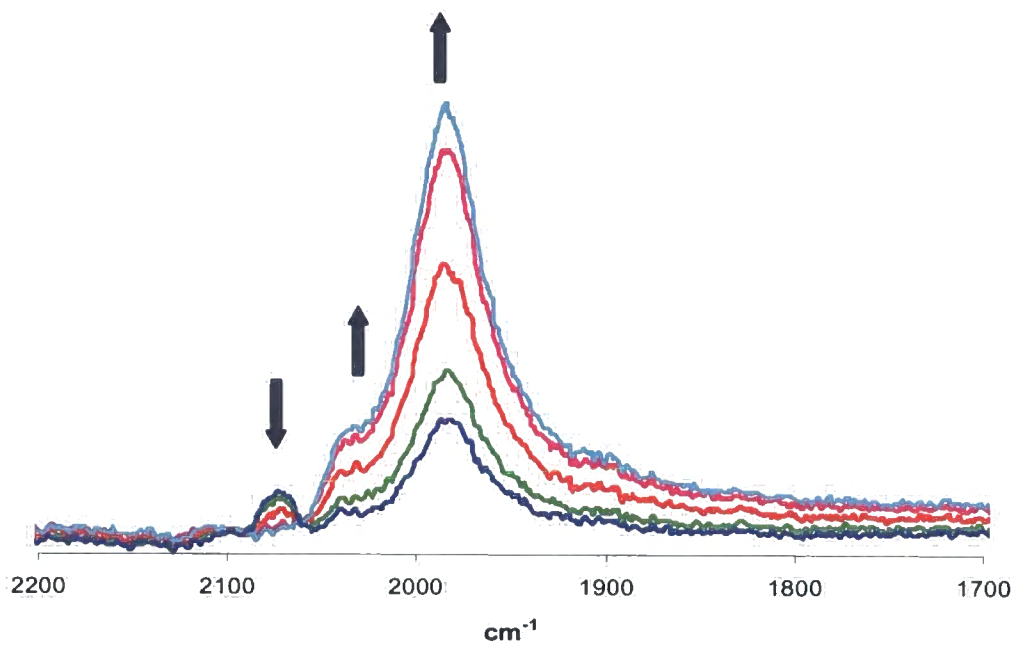

Figure 2.3 Infrared spectra obtained on oxidation of **2.6** → $[\mathbf{2.6}]^+$.

The second oxidation of both the bimetallic and trimetallic species did not result in a decrease in the ν(C≡C) frequency, but rather a partial decrease in the intensity of the bands was observed (**Figure 2.4**, **Figure 2.5**, **Table 2.2**). Whilst the first oxidation process involves orbitals with some C≡C character, evidenced by the decrease in ν(C≡C) upon oxidation, the second oxidation must involve an orbital that does not interact with the acetylene moiety. It is therefore likely that the second oxidation event has considerable ferrocene character.

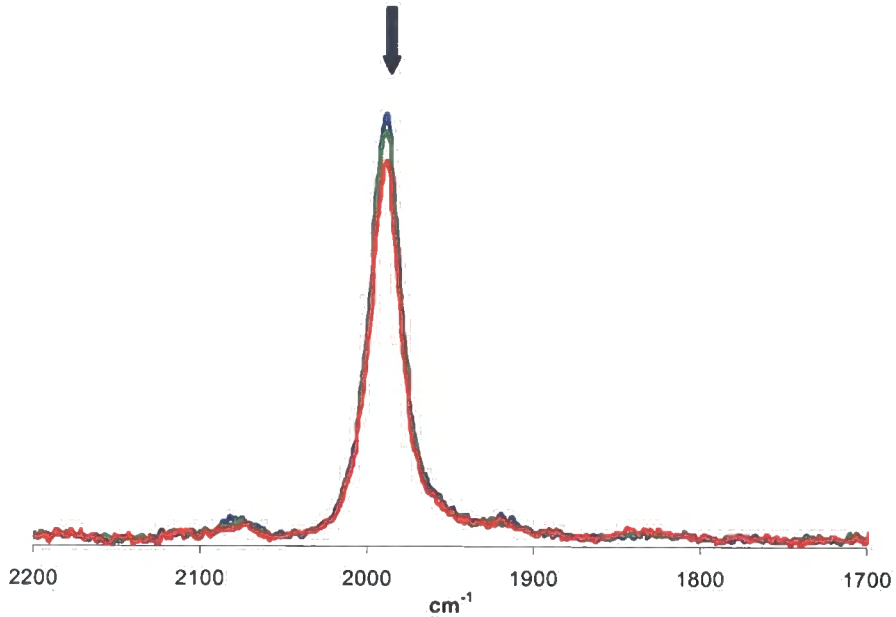

Figure 2.4. Infrared spectra obtained on oxidation of $[\mathbf{2.1}]^{+} \rightarrow [\mathbf{2.1}]^{2+}$.

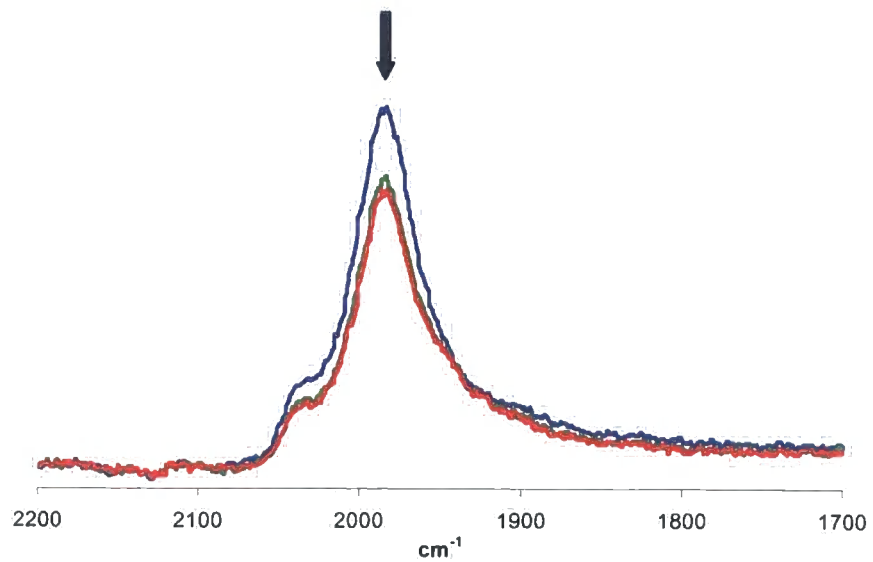

Figure 2.5. Infrared spectra obtained on oxidation of $[\mathbf{2.6}]^{+} \rightarrow [\mathbf{2.6}]^{2+}$.

Table 2.2 Infrared ν(CC) absorptions of ferrocenylethynyl-metal complexes **2.1-2.8** in the oxidation states 0, +1 and +2.

	ν(CC) / cm^{-1}		
	neutral	**+1**	**+2**
2.1	2080	1990	1990
2.2	2082	1990	1990
2.5	2080	1984	1984
2.6	2075	1986, 2039(sh)	1986, 2039(sh)
2.7	2080	1991, 2043(sh)	1991, 2043(sh)
2.8	2076	1981, 2037	1981, 2037

The UV-Vis-NIR spectra of **2.1**, **2.5**, **2.6** and **2.8** and their one-electron oxidised products were collected in an Optically Transparent Electrode (OTE) cell (**Table 2.3**).[12] Whilst the neutral and mono-oxidised species could be generated and observed without difficulty at room temperature, the longer timescale required for electrogeneration in the larger volume OTE cell, and possible intrusion of atmospheric moisture, resulted in decomposition of the dioxidised species and precluded collection of any reliable spectra for these species. Cooling the sample to -30 °C did not alleviate the problem, and any benefit gained by the decreased rate of decomposition reactions brought about by the lower temperature was offset by the slower diffusion-controlled electrolysis in the cell.

The electronic absorption spectrum of **2.1** was characterised by two bands in the UV region, which tail into a broad ferrocene d-d band near 22000 cm^{-1} (**Table 2.3**). The related trimetallic species **2.6** (electrogenerated in the OTE cell from the soluble sample of [**2.6**][PF_6]) exhibited a similar spectrum, the introduction of a second ruthenium acetylide fragment having little effect on the general profile, save for an increase in the intensity of the UV bands relative to the d-d band.

The more electron rich derivative **2.5** was similarly characterised by two bands in the UV region at 37600 cm^{-1} and 28500 cm^{-1} which again overlap a broad ferrocene band at 23000 cm^{-1}. The introduction of the second ruthenium fragment in the trimetallic complex **2.8** again resulted in only a slight shift in position and intensity of the bands.

Table 2.3 Electronic absorption spectra of ferrocenylethynyl-metal complexes **2.1**, **2.5**, **2.6** and **2.8** in the neutral oxidation state.

	Band maxima / cm^{-1} (ε / $dm^3mol^{-1}cm^{-1}$)		
2.1	35000 (17400)	28700 (8550)	~22000 (2220)
2.5	37600 (22600)	28500 (9580)	~23000 (1790)
2.6	34600 (21800)	28700 (9100)	
2.8	37900 (26800)	25800 (14700)	~22000 (2190)

One-electron oxidation of **2.1** to the corresponding monocation (**Figure 2.6**) results in a slight shift in the highest energy bands and the appearance of two new bands in the visible region which do not display vibrational fine structure.

Similar bands in this region have been observed in oxidised (17-e) products derived from Group 8 metal alkynyl complexes and these bands are usually attributed to transitions from occupied orbitals to the stabilised unoccupied orbital set. The assignment of the bands can be made difficult however because of the delocalised nature of the frontier orbitals. Given the substantial acetylide (π^*) character of the LUMO in such complexes,[13, 14] an MLCT description may be used as a reasonable approximation for these transitions. In addition, at least two overlapping transitions are clearly observed in the NIR region of $[\mathbf{2.1}]^+$ (**Figure 2.6**). By considering Hush-style descriptions of the spectra of mixed-valence complexes these bands are assigned to transitions from lower-lying occupied orbitals to the SOMO.

The spectrum of $[\mathbf{2.6}]^+$ displays the same characteristic transitions as observed in the bimetallic analogue $[\mathbf{2.1}]^+$ with bands in the visible region at 33800 and 25100 cm^{-1} and overlapping bands in the NIR region. The lowest energy band is at the same energy in both the bimetallic and trimetallic systems.

As the chemically oxidised sample of $[\mathbf{2.6}]PF_6$ was available the UV-Vis-NIR spectrum of this material was recorded in solvents of different dielectric strength, free from complications arising from the supporting electrolyte necessary for spectroelectrochemical work, to examine the solvatochromic behaviour of the bands in the NIR region. The transitions in $[\mathbf{2.6}]^+$ were found to be independent of the solvent environment. This suggests the monocation may best be described as having a delocalised structure. The spectra of the more electron-rich complexes $[\mathbf{2.7}]^+$ and $[\mathbf{2.8}]^+$ were essentially identical to those of their $Ru(PPh_3)_2Cp$ analogues, although the NIR transitions in $[\mathbf{2.7}]^+$ were not well resolved (**Table 2.4**).

Table 2.4. Electronic absorption spectra of ferrocenylethynyl-metal complexes **2.1**, **2.5**, **2.6** and **2.8** in the oxidation state +1.

	Band maxima / cm^{-1} (ε / $dm^3mol^{-1}cm^{-1}$)				
$[\mathbf{2.1}]^+$	33200	23500	17000	6520	4760
	(17582)	(4656)	(13270)	(6425)	(49560)
$[\mathbf{2.5}]^+$	37700	30900	16100	~6470 [a]	~5130
	(21589)	(11895)	(6906)		(4430)
$[\mathbf{2.6}]^+$	33800	25100	16400	7360	4740
	(33416)	(8858)	(15900)	(5740)	(4130)
$[\mathbf{2.8}]^+$	38610	32800	16300	6540	4590
	(26791)	(18711)	(8997)	(4100)	(4270)

[a] unresolved.

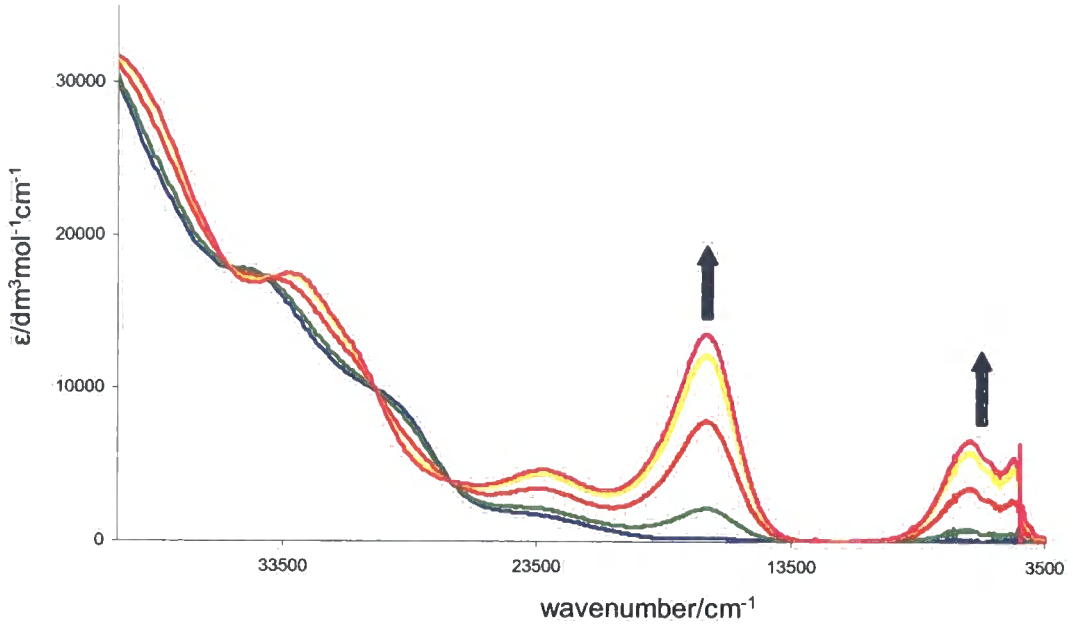

Figure 2.6 UV-vis-NIR spectra obtained on oxidation of **2.1** → $[\mathbf{2.1}]^+$

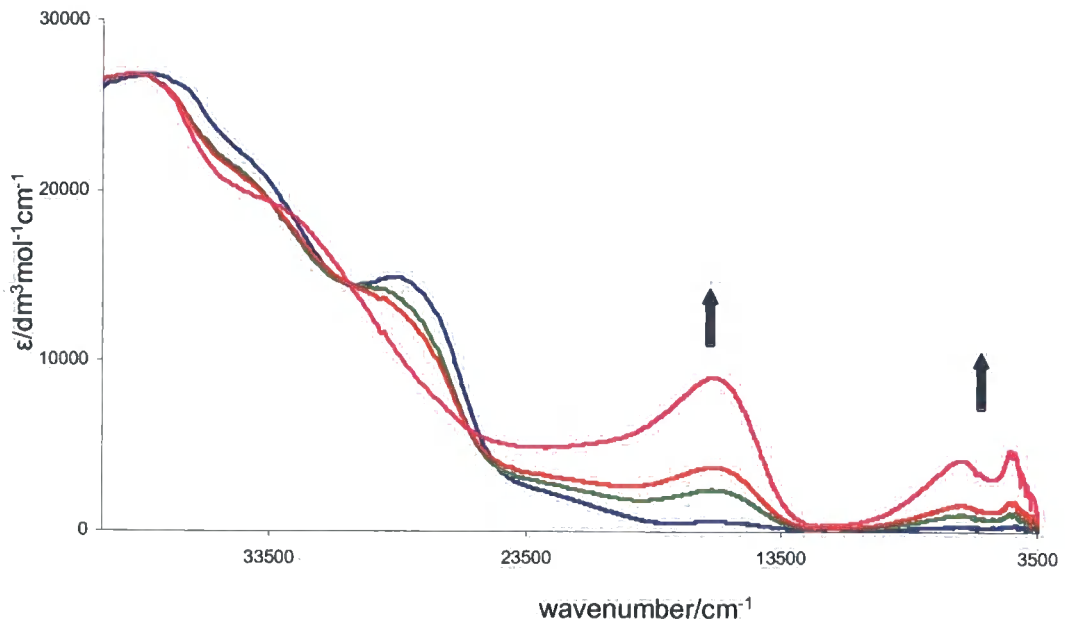

Figure 2.7 UV-vis-NIR spectra obtained on oxidation of [**2.8**] → $[\mathbf{2.8}]^+$.

Mössbauer spectroscopy.

The availability of chemically isolable samples of both **2.6** and [**2.6**]PF_6 allowed further investigation of the nature of the site of oxidation in this complex utilising Mössbauer spectroscopy. The spectrum of **2.6** was recorded at 80 K and contained a unique doublet [IS = 0.539(3) mm s^{-1} *vs* Fe; QS = 2.357(6) mm s^{-1}] very similar to that of ferrocene itself [90 K: IS 0.531(3) mm s^{-1}, QS 2.419(1) mm s^{-1}].[15] Under similar conditions, the Mössbauer spectrum of [**2.6**]PF_6 shows a doublet [IS = 0.548(3) mm s^{-1} *vs* Fe, QS = 0.952(3) mm s^{-1}], accompanied by a small doublet with parameters identical with those of **2.6**, indicating the presence of *ca.* 10% of the neutral complex in the sample. The observation of a doublet associated with [**2.6**]PF_6 is not in keeping with the classic Mössbauer spectra of ferrocenium derivatives, which are characterised by an almost zero value of the quadrupole splitting.[16, 17] This result further supports the concept of a delocalised structure in [**2.6**]PF_6, rather than an oxidation event localised on either the Ru or Fe centres. Again it is unfortunate that the instability precluded a Mössbauer investigation of the two-electron-oxidised forms of these materials.

2.3 Discussion

The combined electrochemical and spectroscopic data allow an assessment of the electronic properties of the trimetallic species **2.6**, **2.7** and **2.8**, and the mixed-valence complexes that may be derived from them, to be made. The observation of two sequential, well separated, one-electron oxidation processes in the voltammograms of the trimetallic compounds, **2.6**, **2.7** and **2.8**, is indicative of the thermodynamic stability of the mono-oxidised species with respect to disproportionation. Comparison of the oxidation potentials of the trimetallic compounds with those of the related bimetallic models indicates higher lying occupied orbitals in the trimetallic compounds.

From the IR spectroelectrochemical experiments the decrease in ν(C≡C) during the first oxidation clearly indicates this process involves orbitals with an appreciable amount of C≡C character. The second oxidation, by contrast has no effect on the C≡C portion of the complex and is centred on the central 1,1'-ferrocenyl moiety. The electronic spectra of the monocationic species were characterised by a series of overlapping bands in the NIR region assigned to transitions from lower-lying occupied orbitals to the SOMO. These transitions were solvent-independent in the case of **[2.6]**PF_6 suggesting a description of the monocation as having a delocalised structure is appropriate.

Taken together, the IR and electronic spectra of the mono-oxidised systems suggest an interpretation of the electronic structure which involves significant delocalisation of the odd electron between the ferrocene centre and one of the ruthenium centres. The observation of a second ν(C≡C) band in the IR spectra of the trimetallic cations $[\mathbf{2.6}]^+$, $[\mathbf{2.7}]^+$ and $[\mathbf{2.8}]^+$, which is not observed in the bimetallic analogues $[\mathbf{2.1}]^+$, $[\mathbf{2.2}]^+$ and $[\mathbf{2.5}]^+$, suggests that electron exchange between the Ru centres through the Fc centre is slow on the IR timescale. The less intense higher-lying shoulder is assigned to the largely non-oxidized Ru(C≡C)(PP)Cp' moiety in the trinuclear monocation, which is shifted relative to the neutral precursor by the electron withdrawing nature of the oxidised fragment. This interpretation is also consistent with the observation of well-separated one-electron anodic waves by cyclic

voltammetry, and with the Mössbauer spectrum of [**2.6**]PF_6, which differs from that of ferrocene and ferrocinium derivatives. Critically, the electronic absorption spectra of the bi- and trimetallic complexes are similar and there is no evidence of a new band in the trimetallic species which can be assigned to a photo-induced $Ru^{II} \rightarrow Ru^{III}$ MMCT process (**Figure 2.6**, **Figure 2.7**).

The second oxidation event, which does not influence the ν(C≡C) frequency in the IR spectra of these compounds, is consistent with a ferrocene-based oxidation process, but unfortunately the two-electron oxidised complexes could not be accessed either chemically or electrochemically for electronic spectroscopic work.

Comparison of the electrochemical and spectroscopic results obtained for $[\mathbf{2.1}]^{n+}$, $[\mathbf{2.2}]^{n+}$ and $[\mathbf{2.5}]^{n+}$ - $[\mathbf{2.8}]^{n+}$ with related diyndiyl complexes [{Ru(PP)Cp'}$_2$(μ-C≡CC≡C)] (Cp' = Cp, PP = $(PPh_3)_2$ **1.21**; Cp' = Cp*, PP = dppe, **1.23**, dppm **1.24**) can give an insight into the role of the central 1,1'-ferrocenyl moiety. The diyndiyl-bridged species **1.21**, **1.23** and **1.24** undergo three reversible oxidation processes and a fourth irreversible, or partly chemically reversible, oxidation. The 35-electron butadiyndiyl complexes $[\mathbf{1.21}]^+$, $[\mathbf{1.23}]^+$ and $[\mathbf{1.24}]^+$, derived from one electron oxidation of the parent complexes, can be described as Class III systems with the odd electron being fully delocalised over the entire molecule.[18-20] If $[\mathbf{2.6}]^+$, $[\mathbf{2.7}]^+$ and $[\mathbf{2.8}]^+$ are considered as being derived from these diyndiyl systems by introduction of a 1,1'-ferrocenyl moiety within the C_4 bridging ligand, the effect of insertion of this group can be assessed. The combined evidence from UV-Vis-NIR and IR spectroelectrochemistry and Mössbauer spectroscopy supports the conclusions that whilst interactions occur between one Ru(PP)Cp' moiety and a ferrocenyl centre within these complexes, through an ethyndiyl bridge, the 1,1'-ferrocenyl group acts as an insulator when inserted into the carbon chain of the archetypal molecular wires {Ru(PP)Cp'}$_2$(μ-C≡CC≡C) and no interaction between the terminal Ru(PP)Cp' groups is observed.

2.4 Experimental Details

General conditions

All reactions were carried out under dry, high purity argon using standard Schlenk techniques. Common solvents were dried, distilled under argon and degassed before use. Ferrocene was used as received.

Instrumentation

Cyclic voltammograms of complexes **2.1**, **2.2**, **2.5**, [**2.6**]PF_6, **2.7**, and **2.8** were recorded with an EG&G PAR Model 283 potentiostat. The CH_2Cl_2 solutions contained 10^{-3} M complex and 0.1 M $[NBu_4]PF_6$ (Aldrich; recrystallised twice from absolute EtOH and dried overnight under vacuum at 80 °C) as supporting electrolyte. The solutions were placed in an airtight single-compartment three-electrode cell equipped with a Pt disk working electrode (0.42 mm^2 apparent electrode surface, polished with a 0.25 μm diamond paste), Pt gauze auxiliary electrode and Ag wire pseudo-reference electrode. In all cases, ferrocene or cobaltocence as used as internal calibrant [$E_{1/2}(FeCp_2/[FeCp_2]^+)$ = +0.46 V vs SCE in CH_2Cl_2; $E_{1/2}(CoCp_2/[CoCp_2]^+$ = -0.87 V vs SCE in CH_2Cl_2]. The IR spectroelectrochemical experiments at variable temperatures were performed with a previously described OTTLE cell positioned in the sample compartment of a Bio-Rad FTS-7 FT-IR spectrometer.[10, 11] The solutions were 5 x 10^{-3} M in analyte and 3 x 10^{-1} M in the supporting electrolyte, $[NBu_4]PF_6$. The UV-Vis-NIR spectroelectrochemical measurements were conducted using an OTE cell similar to that described previously,[12] from CH_2Cl_2 solutions containing 1 x 10^{-1} M $[NBu_4]BF_4$ as supporting electrolyte.

2.5 References

1 M. I. Bruce, M. E. Smith, B. W. Skelton, and A. H. White, *J. Organomet. Chem.*, 2001, **637-639**, 484.

2 M. I. Bruce, F. de Montigny, M. Jevric, C. Lapinte, B. E. Skelton, and A. H. White, *J. Organomet. Chem.*, 2004, **689**, 2860.

3 M. Sato, H. Shintate, Y. Kawata, M. Sekino, M. Katada, and S. Kawata, *Organometallics*, 1994, **13**, 1956.

4 M. Sato, Y. Hayashi, S. Kumakura, N. Shimizu, M. Katada, and S. Kawata, *Organometallics*, 1996, **15**, 721.

5 M. Sato, S. Kawata, H. Shintate, Y. Habata, S. Akabori, and K. Unoura, *Organometallics*, 1997, **16**, 1693.

6 G. Doisneau, G. Balavoine, and T. Fillebeen-Khan, *J. Organomet. Chem.*, 1992, **425**, 113.

7 M. I. Bruce, B. C. Hall, B. D. Kelly, P. J. Low, B. W. Skelton, and A. H. White, *J. Chem. Soc., Dalton Trans.*, 1999, 3719.

8 M. I. Bruce, P. J. Low, F. Hartl, P. A. Humphrey, F. De Montigny, M. Jevric, C. Lapinte, G. J. Perkins, R. L. Roberts, B. E. Skelton, and A. H. White, *Organometallics*, 2005, **24**, 5241.

9 V. V. Pavlishchuk and A. W. Addison, *Inorg. Chim. Acta*, 2000, **298**, 97.

10 F. Hartl, H. Luyten, H. A. Nieuwenhuis, and G. C. Schoemaker, *Appl. Spectr*, 1994, **48**, 1522.

11 T. Mahabiersing, H. Luyten, R. Nieuwendam, and F. Hartl, *Collect. Czech. Chem. Commun.*, 2003, **68**, 1687.

12 C. M. Duff and G. A. Heath, *Inorg. Chem.*, 1991, **30**, 2528.

13 J. E. McGrady, T. Lovell, R. Stranger, and M. G. Humphrey, *Organometallics*, 1997, **16**, 4004.

14 O. F. Koentjoro, R. Rousseau, and P. J. Low, *Organometallics*, 2001, **20**, 4502.

15 R. Basta, D. R. Wilson, H. Ma, A. M. Arif, R. H. Herber, and R. D. Ernst, *J. Organomet. Chem.*, 2001, **637-639**, 172.

16 R. L. Collins, *J. Chem. Phys.*, 1965, **42**, 1072.

17 S. Nlate, J. Ruiz, V. Sartor, R. Navarro, J.-C. Blais, and D. Astruc, *Chem. Eur. J.*, 2000, **6**, 2544.

18 M. I. Bruce, P. J. Low, K. Costuas, J. F. Halet, S. P. Best, and G. A. Heath, *J. Am. Chem. Soc.*, 2000, **122**, 1949.

19 M. I. Bruce, B. G. Ellis, P. J. Low, B. W. Skelton, and A. H. White, *Organometallics*, 2003, **22**, 3184.

20 M. I. Bruce, B. D. Kelly, B. W. Skelton, and A. H. White, *J. Organomet. Chem.*, 2000, **604**, 150.

Chapter 3

3.1 Introduction

As highlighted in Chapter 1, there is currently great interest in the electronic structure of bimetallic complexes featuring unsaturated bridging ligands capable of promoting electronic interactions between the remote metal termini. There are many fundamental questions which such systems pose, not least of which lies in the correlation of the electronic structure of these bimetallic complexes in their various electrochemically accessible redox-states, with the particular combination of metal, supporting ligands and bridging moiety. The use of diethynylaromatic bridging ligands such as 1,4-diethynylbenzene is commonplace, owing to the ready availability of the precursor dialkynes. Initial studies concentrated on polymeric systems which may be derived from these ligands, and complexes such as $[M(P^nBu_3)_2\text{-}C{\equiv}CC_6H_4C{\equiv}C\text{-}]$ (M = Ni, Pd, Pt), first developed by Hagihara and co-workers,[1-4] have been extensively investigated.[5] Such systems have been of particular interest for their technological potential, in particular due to their promising electronic and structural properties including NLO effects,[6-9] luminescence and photoconductivity,[10-13] and liquid crystallinity.[14-17] Initial systems prepared contained metals from group 10, but adaptations of the synthetic methodology used to prepare these systems has resulted in a variety of transition metals being introduced into the polymer backbone and the evaluation of their physical and electronic properties.[18, 19] For example, the rhodium-containing systems $[Rh(X)(PMe_3)_3\text{-}C{\equiv}C\text{-}C_6H_4\text{-}C{\equiv}C\text{-}]_n$ (X = H, $SnMe_3$) and $[Rh(H)(P^nBu_3)_3\text{-}C{\equiv}C\text{-}C_6H_4\text{-}C{\equiv}C\text{-}]_n$ have been produced,[20, 21] with $[Rh(H)(PMe_3)_3\text{-}C{\equiv}C\text{-}C_6H_4\text{-}C{\equiv}C\text{-}]_n$ and $[Rh(H)(P^nBu_3)_3\text{-}C{\equiv}C\text{-}C_6H_4\text{-}C{\equiv}C\text{-}]_n$ being characterised by IR spectroscopy and displaying a $\nu(C{\equiv}C)$ stretch identical to the model complexes $[Rh(C{\equiv}C\text{-}C_6H_4\text{-}C{\equiv}CH)_2(H)(PR_3)_3]$.[20]

The IR spectra of the polymeric complex $[Ru(CO)_2(P^nBu_3)_2\text{-}C{\equiv}C\text{-}C_6H_4\text{-}C{\equiv}C\text{-}]_n$ (**3.1**) displayed a single strong $\nu(C{\equiv}C)$ absorption at 2084 cm^{-1} consistent with the *trans* configuration of the acetylenic units around the metal centre.[22] The energy of this absorption was lower than that observed in the model bimetallic complex $[Cl(P^nBu_3)_2(CO)_2Ru\text{-}C{\equiv}C\text{-}C_6H_4\text{-}C_6H_4\text{-}C{\equiv}C\text{-}Ru(CO)_2(P^nBu_3)_2Cl]$ (2106 cm^{-1}), demonstrative of the increased conjugation in the polymeric system. The energy of the $\nu(C{\equiv}C)$ absorption of $[Ru(CO)_2(P^nBu_3)_2\text{-}C{\equiv}C\text{-}C_6H_4\text{-}C{\equiv}C\text{-}]_n$ was also higher than

that of the related complex featuring only phosphine ligands, $[Ru(depe)_2\text{-}C{\equiv}C\text{-}C_6H_4\text{-}C{\equiv}C\text{-}]_n$ (**3.2**) ($\nu(C{\equiv}C)$ = 2046 cm^{-1}),[23] an observation which highlighted the importance of the metal ancillary ligands in determining the overall electronic structure of the polymer. Optical absorption spectra were recorded, and the band gaps obtained from analysis of these demonstrated that the band gap in **3.1** was much higher than in **3.2**, again providing evidence that the ancillary ligands play a critical role in determining the character of the MLCT process taking place within these systems.

The series of platinum-containing polymers, $[Pt(P^nBu_3)_2\text{-}C{\equiv}CXC{\equiv}C\text{-}]_n$, where X is a variety of aromatic and heteroaromatic spacers, have been comprehensively studied and display donor-acceptor interactions between the Pt centres and the conjugated ligand, the degree of which depends on the electronic nature of the spacer group.[24-31] For the systems involving the aromatic spacers C_6H_4, $C_{10}H_6$ and $C_{14}H_8$, spectroscopic measurements reveal that the electron-rich aryl spacers create strong donor-acceptor interactions, between the Pt^{II} centres and the conjugated ligands, along the rigid backbone of the organometallic polymer. The absorption spectra displayed an absorption band assigned to transitions between the mixed ligand π and platinum 5d orbitals, and the ligand π^* and platinum 6p orbitals. The energy of this transition, and hence the band gap, decreases as the size of the aromatic linker group increases, consistent with there being a greater degree of delocalisation with the anthracene linker compared with the benzene linker group, with values from 2.9 eV (430 nm) for $[Pt(P^nBu_3)_2\text{-}C{\equiv}CC_6H_4C{\equiv}C\text{-}]_n$ to 2.35 eV (530 nm) for $[Pt(P^nBu_3)_2\text{-}C{\equiv}CC_{14}H_8C{\equiv}C\text{-}]_n$ being obtained.[32] Additionally, an increase in the thermal stability of the polymers was observed as the size of the aromatic spacer increased from phenyl, through naphthyl to anthryl. The vibrational spectra of the polymers were characterised by a $\nu(C{\equiv}C)$ band at 2095 (naph) and 2094 (anth) cm^{-1} consistent with the *trans* configuration of the diethynylaromatic ligands around the Pt centre.[32]

More recently discrete bimetallic systems have attracted much interest. However, despite the large number of compounds of this type that are now known, and the great interest in the electronic interactions which such ligands may promote, there are remarkably few examples of spectroscopic characterisation of such systems in the

multiple redox states which may be accessed.[33] The {Fe(dppe)Cp*}$_2$(μ-C≡C-X-C≡C) series is perhaps the most comprehensively studied with the 1,4-diethynylbenzene,[34] 2,5-diethynylthiophene[35] derivatives (**1.47** and **3.3**) being investigated previously and the 9,10-diethynylanthracene[36] derivative (**3.4**) being reported during the preparation of this thesis.

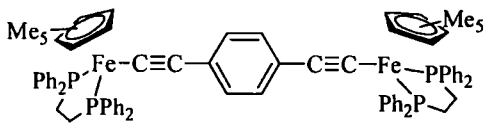

1.47

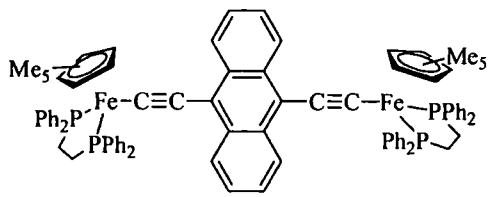

3.4

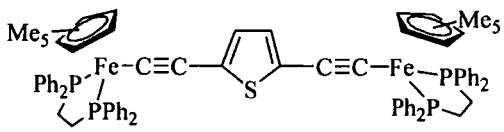

3.3

Figure 3.1. {Fe(dppe)Cp*}$_2$(μ-C≡CC_6H_4C≡C) (**1.47**), {Fe(dppe)Cp*}$_2$(μ-C≡CC_4H_2SC≡C) (**3.3**) and {Fe(dppe)Cp*}$_2$(μ-C≡C$C_{14}H_8$C≡C) (**3.4**)

As mentioned in Chapter 1 the mixed-valence cation **[1.47]**$^+$ was studied (as the PF_6^- salt) by a combination of Mössbauer spectroscopy and IR spectroscopy, which lead to the conclusion that the 1,4-diethynylbenzene ligand is capable of delocalising an unpaired electron between the two iron centres. Magnetic susceptibility measurements of the dicationic species **[1.47]**$^{2+}$ were performed over the range 5-300K and the molar paramagnetic susceptibility was found to be temperature dependent. The results indicated an antiferromagnetic coupling between the two 17-electron iron centres, and this, combined with ESR and IR spectroscopic results, supported a description of **[1.47]**$^{2+}$ which involves an appreciable contribution from the cumulated canonical form.[34]

The electrochemical response of **3.3** was characterised by two chemically reversible oxidation waves at -0.39 V and -0.05 V (vs SCE) and a third process at more positive potentials (1.04 V). In a similar manner the cyclic voltammogram of **3.4** displayed two chemically reversible oxidation waves at -0.40 and -0.04 V (vs SCE) and a third process close to the solvent edge. The first oxidations in **3.4** and **3.3** are 130 mV more facile than that in **1.47,** but the second oxidation potentials are very similar. This results in a larger value of ΔE and hence K_c for $[\mathbf{3.4}]^+$ (ΔE = 360 mV, K_c = 1.3 x 10^6) and $[\mathbf{3.3}]^+$ (ΔE = 340mV, K_c = 5.8 x 10^5) than in $[\mathbf{1.47}]^+$ (ΔE = 260 mV, K_c = 2.6 x 10^4) indicating the increased thermal stability of the mixed valence system in the anthracene and thiophene derivatives with respect to $[\mathbf{1.47}]^+$. Comparison with Cp*(dppe)Fe-(C≡C)$_4$-Fe(dppe)Cp* (**1.34**),[37] indicates that the stability of the mixed-valence species increases in the order $[\mathbf{1.47}]^+ < [\mathbf{3.3}]^+ < [\mathbf{3.4}]^+ < [\mathbf{1.34}]^+$. In the case of **3.4** the increase in stability with respect to $[\mathbf{1.47}]^+$ was taken as evidence for a larger bridging ligand contribution to the HOMO and was supported by DFT calculations on the model complex {Fe(dpe)Cp}$_2$(μ-C≡C$C_{14}H_8$C≡C) which suggested that the HOMO has dominant anthracene character.[36]

Mössbauer spectroscopy revealed that the two iron centres in $[\mathbf{3.4}]^{n+}$ (n = 0, 1, 2) are spectroscopically equivalent in all three oxidation states of the complex and the presence of a unique doublet in the mixed-valence complex [**3.4**][TCNQ] was taken as evidence that $[\mathbf{3.4}]^+$ is best described as a detrapped Class III mixed-valence complex on the Mössbauer timescale. The Mössbauer spectrum of $[\mathbf{3.3}]^+$ exhibited a single doublet with a QS value intermediate between those usually observed for Fe^{II} and Fe^{III} in the Fe(dppe)Cp* fragment. The equivalence of the iron centres was taken to indicate the delocalisation of the odd electron over both metal centres on the Mössbauer timescale.

The IR spectrum of **3.4** was characterised by a single ν(C≡C) band at 2010 cm^{-1}. Oxidation to the monocation resulted in the observation of two weaker bands at lower energy (1964, 1901 cm^{-1}) and further oxidation to the dication was accompanied by a further decrease in intensity and shift to lower wavenumber (1943, 1896 cm^{-1}), the shifts in energy of the ν(C≡C) bands upon oxidation providing

further evidence for a significant contribution of the bridging ligand to the redox-active HOMO.

The IR spectrum of the neutral complex **3.3** displayed a single ν(C≡C) stretch at 2041 cm^{-1} which on oxidation to the monocation $[\mathbf{3.3}]^+$ was shifted to lower energy with a concomitant splitting of the band, resulting in two bands at 1983 and 1910 cm^{-1}, indicating that the two metal sites are not equivalent on the IR timescale. The IR spectrum of the dicationic species $[\mathbf{3.3}]^{2+}$ was characterised by a single band at 1950 cm^{-1}.

The UV-vis spectra of **3.4** (277, 339 nm) and **3.3** (<300, 418 nm) were characterised by bands attributed to intra-ligand π-π* transitions, which were less intense and red-shifted compared to those observed for **1.47** (242, 262 nm). An additional band at 623 nm in **3.4** and at *ca.* 400 nm in **3.3** was ascribed to an MLCT transition, and compared to the similar MLCT band observed in the phenyl system at 413 nm. Spectra of the dications $[\mathbf{3.4}][PF_6]_2$ and $[\mathbf{1.47}][PF_6]_2$ were very similar, displaying LMCT bands at 816 and 702 nm respectively. The mixed-valence complex $[\mathbf{1.47}][PF_6]$ displayed both MLCT and LMCT bands at 546 and 702 nm and the electronic spectrum obtained was intermediate between those of **1.47** and $[\mathbf{1.47}][PF_6]_2$. The spectrum of $[\mathbf{3.3}]^+$ was comparable with an MLCT band observed at 423 nm and LMCT bands at 588 and 653 nm. The spectrum of $[\mathbf{3.4}][PF_6]$ however was very similar to that of the dication $[\mathbf{3.4}][PF_6]_2$, with a unique band at 831 nm which was attributed to an LMCT transition.

In addition to the shifts observed in the UV-vis region of the electronic spectrum, changes in the NIR region were observed upon oxidation. Complex **3.4** does not contain any absorption bands in the NIR region, however the dicationic derivative displayed weak absorptions at 5300 and 7490 cm^{-1}. The NIR spectrum of the mono-oxidised system $[\mathbf{3.4}][PF_6]$ displayed a number of overlapping bands in the NIR region that could be deconvoluted into three Gaussian band shapes, a well defined maximum and two shoulders. The band width at half height of the lowest energy band was found to be *ca.* two times narrower than the value predicted by Hush theory, providing further support for the classification of the mixed-valence system

as Class III. The position of the bands was found to be solvent independent, in agreement with this classification.[36]

The NIR spectrum of $[\mathbf{3.3}]^+$ also displayed a number of overlapping bands which were not present in the neutral or dicationic derivatives and were found to be solvent independent. The band envelope could be deconvoluted into two Gaussian-shaped bands and the lower energy band was significantly narrower than was predicted by Hush theory.[35]

It has been demonstrated, both in Chapter 1, and in the introduction to this chapter, that the properties, and electronic structure, of mixed-valence systems derived from a common $[ML_x](\mu\text{-}C{\equiv}CXC{\equiv}C)[ML_x]$ motif are strongly dependent on the nature of the 'spacer' X. In the remainder of this chapter, a comparative study of the redox and spectroscopic properties of a family of complexes $[\{Ru\}_2(\mu\text{-}C{\equiv}CXC{\equiv}C)]^{n+}$ [{Ru} = $Ru(PPh_3)_2Cp$, Ru(dppe)Cp*; X = 1,4-C_6H_4, 1,4-$C_{10}H_6$, 9,10-$C_{14}H_8$; n = 0, 1, 2] is presented. In any study of cooperative effects in bimetallic systems $[\{ML_x\}(\mu\text{-bridge})\{ML_x\}]$ it is helpful to also consider the properties of closely related monometallic model systems, for example $[\{ML_x\}(\text{bridge-H})]$, in order to help distinguish direct metal-bridge effects from bridge-mediated metal-metal interactions. Together, studies of mono- and bi-metallic complexes, featuring related ligands, allow a thorough investigation of the electronic structure of such complexes, therefore, in this chapter the related mononuclear compounds will also be presented.

3.2 Results

Metal acetylide complexes $Ru(C{\equiv}CR)L_2Cp'$ are often prepared from the reaction of the halide complex $RuClL_2Cp'$ with the appropriate terminal alkyne, via deprotonation of an intermediate vinylidene.[38-40] Utilising this methodology the reactions of $RuClL_2Cp'$ (L = PPh_3, Cp' = Cp, **a**; L_2 = dppe, Cp' = Cp*, **b**) with $HC{\equiv}CC_6H_5$ and NH_4PF_6, in methanol, afford $[Ru(C{=}CH\text{-}C_6H_5)(L_2)Cp']$, which can be deprotonated *in situ* using methoxide, to produce the corresponding acetylide complexes $Ru(C{\equiv}CC_6H_5)L_2Cp'$ (**3.5a**, **3.5b**, **Scheme 3.1**) as yellow solids in good yield.[41-43]

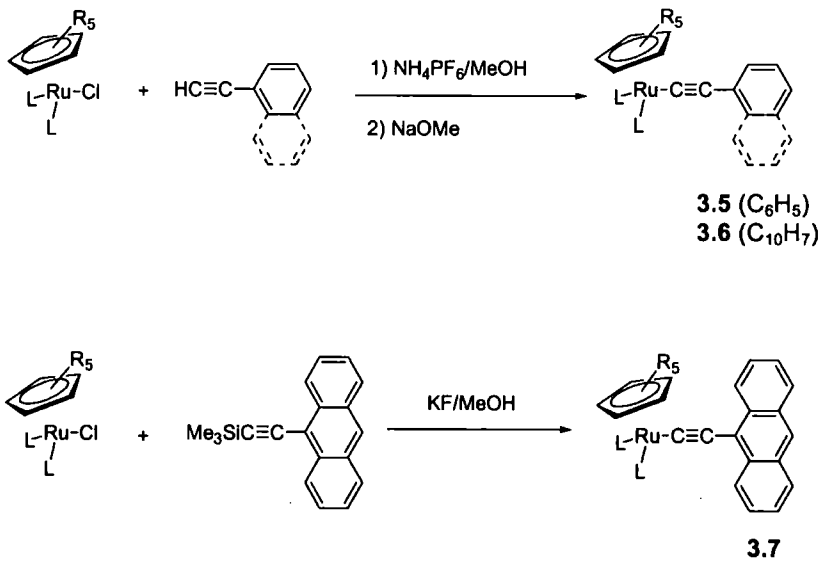

Scheme 3.1 Production of **3.5**, **3.6**, and **3.7** via an intermediate vinylidine or utilising an *in situ* desilylation / metallation procedure

The new complexes $Ru(C{\equiv}CC_{10}H_7)L_2Cp'$ (**3.6a**, **3.6b**) were prepared in an entirely analogous fashion from 1-ethynylnaphthalene, $HC{\equiv}CC_{10}H_7$. However as a result of the thermal and light sensitivity of 9-ethynylanthracene, $HC{\equiv}C_{14}H_9$, the more stable trimethylsilyl-protected derivative was utilised with the *in situ* desilylation /

metallation procedure described previously.[44] In accordance with this procedure, the reaction of $RuClL_2Cp'$ with $Me_3SiC{\equiv}CC_{14}H_9$ and catalytic quantities of KF in MeOH afforded the orange complexes $Ru(C{\equiv}CC_{14}H_9)L_2Cp'$ (**3.7a**, **3.7b**) in good yield (**Scheme 3.1**).

In a similar fashion to that described for the preparation of **3.7** the complexes **3.8**, **3.9** and **3.10** were readily obtained from stoichiometric reactions of $RuCl(PPh_3)_2Cp$ or RuCl(dppe)Cp* with the dialkynes 1,4-bis(trimethylsilylethynyl)benzene (**3.11**), 1,4-bis(trimethylsilylethynyl)naphthalene (**3.12**) and 9,10-bis(trimethylsilylethynyl)anthracene (**3.13**), in the presence of KF in methanol, and isolated as yellow or orange powders in good yield (**Scheme 3.2**).

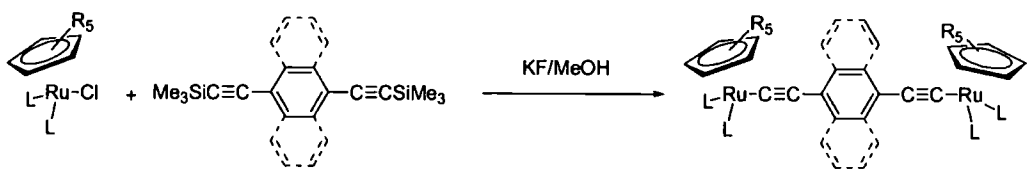

3.11 (C_6H_4)
3.12 ($C_{10}H_6$)
3.13 ($C_{14}H_8$)

3.8 (C_6H_4)
3.9 ($C_{10}H_6$)
3.10 ($C_{14}H_8$)

Scheme 3.2 Production of **3.8**, **3.9**, and **3.10** utilising an *in situ* desilylation / metallation procedure

All complexes (**3.5-3.10**) were characterised by the usual spectroscopic methods, and selected data are summarised in **Table 3.1** and **Table 3.2**. For all compounds the NMR and mass spectra are entirely consistent with the proposed structures. The ^1H NMR spectra contained overlapping resonances from the aromatic protons of the phosphine phenyl groups and the ethynylaromatic ligands. In addition, resonances due to the Cp (**3.5a-3.7a**, **3.9a**, **3.10a**) or Cp* (**3.5b-3.10b**) ligands were observed with very little difference in chemical shift observed within each series respectively.

Table 3.1 Selected spectroscopic data for complexes **3.5-3.10a,b**

	δ_H Cp/Cp* (ppm)	δ_C C_α/C_β (ppm)	δ_P Ph_3/dppe (ppm)	ES(+)-MS	reference
3.5a	4.50	[a]	51.5 [f]	793 [M^+]	43
3.5b	1.55	[a]	82.0 [f]	737 [M^+]	41
3.6a	4.59 [b]	[a]/114.5 [d]	51.6 [f]	842 [M^+]	
3.6b	1.58 [b]	[a]	75.4 [f]	786 [M^+]	
3.7a	4.49 [b]	81.57 [d] /112.70 [d]	51.2 [f]	892 [M^+]	
3.7b	1.71 [b]	[a]	76.1 [f]	836 [M^+]	
3.8b	1.54 [b]	89.27 [e] /99.65 [e]	81.8 [f]	1394 [M^+]	
3.9a	4.42 [b]	[a]	51.5 [f]	1556 [M^+]	
3.9b	1.55 [b]	[a]/110.19 [e]	82.0 [f]	1444 [M^+]	
3.10a	4.51 [b]	[a]	51.1 [f]	1606 [M^+]	
3.10b	1.61 [c]	89.26 [e] /99.60 [e]	82.3 [f]	1494 [M^+]	

[a] not observed. [b] $CDCl_3$, 200 MHz. [c] C_6D_6, 200 MHz. [d] $CDCl_3$, 126 MHz. [e] C_6D_6, 126 MHz. [f] $CDCl_3$, 81 MHz. Details in Experimental Details section.

Coordination of the metal fragments in the bimetallic complexes **3.8-3.10** results in a decrease of *ca.* 90 cm^{-1} in the ν(C≡C) frequency, relative to the trimethylsilyl-protected alkyne. However, the IR spectra of the mono- and bi-metallic complexes are very similar, despite the presence of the additional electron-donating metal fragment in the bimetallic complexes. The supporting phosphine and cyclopentadienyl ligands have a very minor effect on the ν(C≡C) frequency, in contrast to the large effect on oxidation potential (*vide infra*) and, for any given diethynylaryl bridging ligand, the spectra of the $Ru(PPh_3)_2Cp$ and Ru(dppe)Cp* derived complexes were essentially identical. This independence of ν(C≡C) from the supporting ligands around the metal centre supports the concept that metal-alkyne (d-π*) back bonding plays little part in the overall electronic structure of these metal acetylide complexes which feature formal 18 electron counts at each metal centre.[45-47] The trends in ν(C≡C) are more dependent on the nature of the aromatic spacer, with the greater degree of mixing between the filled C≡C orbitals and orbitals of the

aromatic spacer likely accounting for the apparent trend in ν(C≡C) frequencies **3.5** > **3.6** > **3.7** and **3.8** > **3.9** > **3.10**.

Table 3.2 Infra-red[a] (ν(C≡C) /cm^{-1}) data for [**3.5**]$^{n+}$-[**3.10**]$^{n+}$

	n		
	0	**1**	**2**
3.5a	2073		
3.5b	2070		
3.6a	2057		
3.6b	2055		
3.7a	2042		
3.7b	2041	1926	
3.8b	2069	1978	1928
3.9a	2061	1963	1922
3.9b	2056	1967	1914
3.10a	2033	1954	1920
3.10b	2026	1954	1913
3.11	2158		
3.12	2149		
3.13	2149/2123		

[a] measured as solutions in CH_2Cl_2 or in CH_2Cl_2 containing 1 x 10^{-1} M $[NBu_4]BF_4$.

Structural Studies

The molecular structure of **3.10b** was determined, using single crystal X-ray diffraction methods, from crystals grown by slow evaporation of a saturated solution of the complex in C_6D_6 (**Table 3.3, Figure 3.2**). The molecular structure demonstrates the expected 'half-sandwich' geometry around the metal centre observed in related complexes.[48] The Ru-P bonds are longer than observed in the related C_4 complex **1.23** (2.2420(8)- 2.2556(8) Å), probably indicative of the electron withdrawing effect of the central aromatic ring. The Ru-C(1), C(1)-C(2) and C(2)-C(3) bond lengths are consistent with those reported for other complexes of this type and confirm the alternating long-short-long bond lengths associated with the description of the acetylenic moiety. The acetylenic chain displays a slight deviation from linearity [Ru(1)-C(1)-C(2)/C(1)-C(2)-C(3), 178.5(5)/172.8(6)°] probably as a consequence of crystal packing effects.

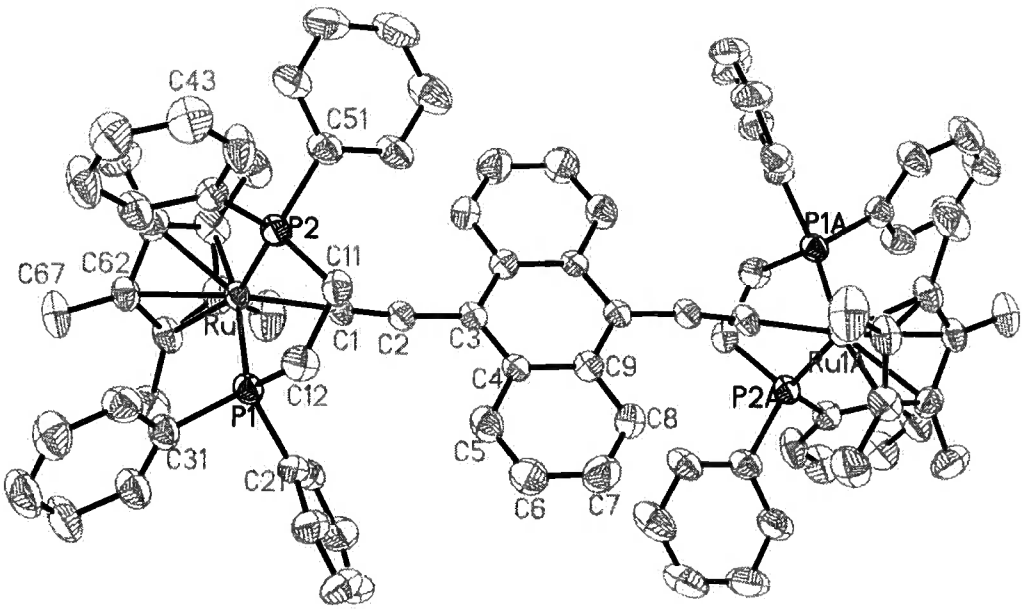

Figure 3.2 Molecular structure of **3.10b** showing labelling scheme, hydrogen atoms are omitted for clarity.

Table 3.3 Selected bond lengths (Å) and angles (°) for **3.10b**.

Ru(1)-C(1)	2.017(6)	C(7)-C(8)	1.348(9)
C(1)-C(2)	1.228(8)	C(8)-C(9)	1.426(9)
C(2)-C(3)	1.416(8)	C(9)-C(3)#1	1.419(8)
Ru(1)-P(1)	2.2597(17)		
Ru(1)-P(2)	2.2602(16)	C(1)-Ru(1)-P(1)	84.37(17)
Ru(1)-C_{Cp} (av)	2.255(7)	C(1)-Ru(1)-P(2)	82.74(17)
C(3)-C(9)#1	1.419(8)	P(1)-Ru(1)-P(2)	83.12(6)
C(3)-C(4)	1.424(9)	Ru(1) -C(1)-C(2)	178.5(5)
C(4)-C(9)	1.426(8)	C(1)-C(2)-C(3)	172.8(6)
C(4)-C(5)	1.431(8)	C(12)-C(11)-P(2)	108.1(4)
C(5)-C(6)	1.360(10)	C(11)-C(12)-P(1)	111.9(4)
C(6)-C(7)	1.393(10)		

Symmetry transformations used to generate equivalent atoms: #1 -x+2,-y+2,-z

Electrochemical Studies

The low solubility of compound **3.8a** has hampered efforts at obtaining reliable electrochemical data.[44] However the Ru(dppe)Cp* derivative **3.8b** and the related complexes **3.5-3.7, 3.9** and **3.10** were amenable to analysis by cyclic voltammetry (**Table 3.4**). Each of the mononuclear complexes **3.5a,b**, **3.6a,b** and **3.7a,b** gave rise to a single oxidation event, which was more chemically reversible in the case of the Ru(dppe)Cp* derived examples (**Table 3.4**). The half-wave potentials associated with oxidation of the complexes derived from the Ru(dppe)Cp* moiety were also more thermodynamically favourable than those associated with the analogous $Ru(PPh)_3Cp$ derivatives, consistent with the relative electron donating properties of the supporting ligand. The nature of the aromatic portion of the ethynyl ligand also plays a significant role in the relative oxidation potentials, with the trend $E_{1/2}$ **3.5** > **3.6** > **3.7** being apparent.

Table 3.4 Oxidation potentials for complexes **3.5-3.7, 3.8b** and **3.9-3.10**.[a]

	E_1/mV	E_2/mV	ΔE/mV	K_c
3.5a	535			
3.5b	315			
3.6a	450[b]			
3.6b	270			
3.7a	340[b]			
3.7b	215			
3.8b	-15	265	280	7.40×10^4
3.9a	160	420	260	3.00×10^4
3.9b	-55	220	275	6.00×10^4
3.10a	-40	275	315	2.70×10^5
3.10b	-165	135	300	1.35×10^5

[a] Data recorded from solutions in CH_2Cl_2 containing 0.1 M NBu_4PF_6 supporting electrolyte and referenced against cobaltocene/cobaltocenium couple at -0.87 V vs SCE. [b] Irreversible even at low temperatures, peak potential reported

The bimetallic complexes **3.8b**, **3.9a**, **3.9b**, **3.10a**, and **3.10b** each undergo two reversible, sequential oxidation processes (E_1 and E_2) with a value of $\Delta E = E_2 - E_1$ of *ca.* 300 mV being observed in all cases. The electrochemical data indicate that all of the singly-oxidised derivatives should be stable with respect to disproportionation, with relatively large ($> 10^4$) values of the comproportionation constant K_c being calculated in each case. It is interesting to note that the singly-oxidised derivatives **[3.10a]**$^+$ and **[3.10b]**$^+$ featuring the anthracene moiety are the most thermodynamically stable members of their respective series.

The trends in electrode potential noted for the mononuclear complexes were also apparent in the bimetallic series, with oxidation of the Ru(dppe)Cp* based complexes being rather more thermodynamically favourable than oxidation of the

analogous $Ru(PPh_3)_2Cp$ derivatives. Again, within each series featuring a consistent metal end-cap, the nature of the aromatic spacer influenced the relative oxidation potentials, with values of both E_1 and E_2 decreasing in the order **3.8** > **3.9** > **3.10**. In each case, the first oxidation potential of the binuclear species is significantly (*ca.* 300 mV) lower than the oxidation potential of the corresponding mononuclear model [e.g. E(**3.5b**) +245 mV > E_1(**3.8b**) -55 mV], indicating a much higher-lying HOMO in the case of the bimetallic complexes.

Spectroelectrochemical studies

In order to probe the effect of oxidation on the physical and electronic structure of the complexes, and in particular to assess the contribution of the bridge π-system to the oxidation processes, a series of spectroelectrochemical experiments were undertaken covering the UV-vis-NIR and IR regions of the spectrum.

Despite the chemical reversibility of the redox events on the timescale of the CV experiments, the mononuclear cations **[3.5a,b]**$^+$, **[3.6a,b]**$^+$ and **[3.7a]**$^+$ were insufficiently stable for meaningful spectra to be collected on the longer timescale required for electrolysis in the spectroelectrochemical cells. For example, while oxidation of **3.6b** *in situ* caused a bleaching of the characteristic ν(C≡C) band and the observation of new bands in the region of 1930 cm^{-1} and 1500 cm^{-1}, the failure to recover the original spectrum after back reduction suggests that the oxidation event is complicated by subsequent chemical processes.

However, the cationic species produced by one electron oxidation of the most readily oxidised species, **3.7b**, was much more chemically stable, as evidenced by recovery of the original spectrum upon back reduction. In this case, oxidation resulted in the shift of the ν(C≡C) band from 2041 to 1926 cm^{-1} (**Figure 3.3**, **Table 3.2**). The shift in this band of *ca.* 120 cm^{-1}, is somewhat larger than that observed following oxidation of the iron complex $[Fe(C{\equiv}CC_6H_5)(dppe)Cp^*]^{n+}$ (n = 0, 1), although it is comparable to those observed in some of the *para*-functionalised derivatives ($[Fe(C{\equiv}CC_6H_4NH_2)(dppe)Cp^*]^{n+}$ (n = 0, 1) and $[Fe(C{\equiv}CC_6H_4NMe_2)(dppe)Cp^*]^{n+}$ (n = 0, 1), Δ ν(C≡C) ~ 100 cm^{-1}).[49] The radical cation **[3.7b]**$^+$ also displayed a weak

lower energy band at 1595 cm^{-1}, tentatively assigned to one of the anthracene ring ν(CC) modes.

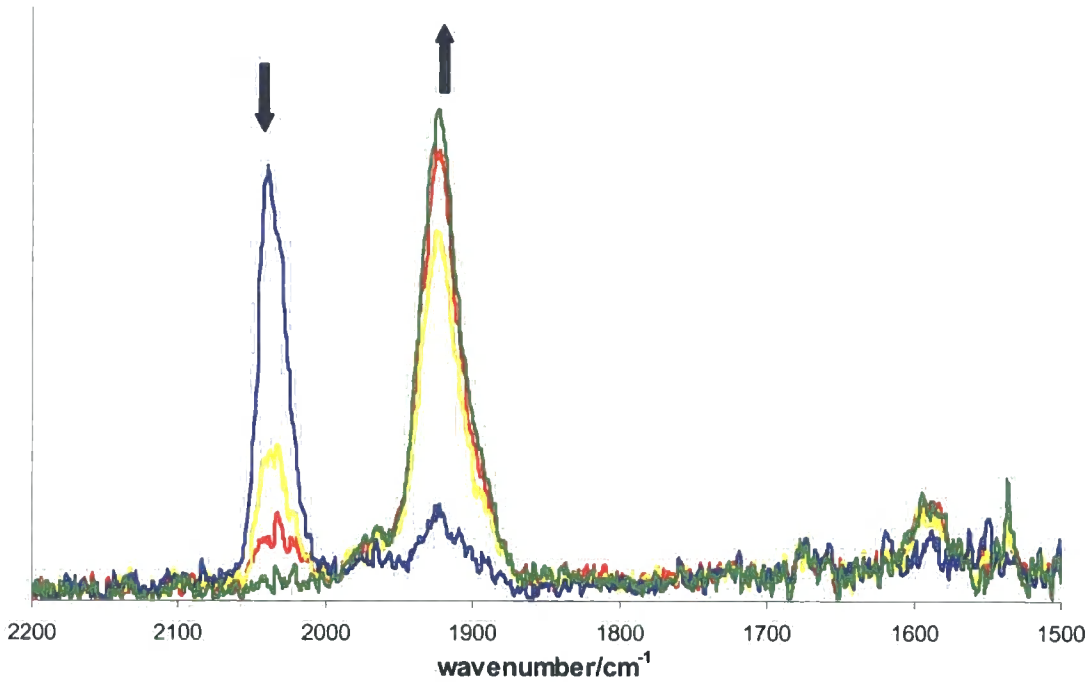

Figure 3.3 Infra-red spectra obtained upon oxidation of **3.7b** → $[\mathbf{3.7b}]^+$

Electrochemical oxidation of the soluble bimetallic complexes was found to be fully chemically reversible within the IR spectroelectrochemical cell, and a shift of the ν(C≡C) bands to lower frequencies was found to accompany oxidation of the parent (36-electron) species to the 35-electron singly-oxidised derivatives. This shift in the observed frequency of the ν(C≡C) bands is consistent with the involvement of the bridging ligand π-system in the redox-active orbital (**Figure 3.4a, Table 3.2**). In the 35-electron species the shoulder on the high energy side of the primary band may be argued as evidence for valence localisation on the IR timescale, or may also be explained by the presence of two distinct vibrational modes. In addition, weak bands were observed in the region 1540-1605 cm^{-1} and assigned to the aromatic ring vibrations in the monocation.

Further oxidation to the 34-electron dicationic species resulted in collapse of the bands in the 1500-1600 cm^{-1} region, and a shift in ν(C≡C) to give a single, relatively low frequency band between 1910-1930 cm^{-1} (**Figure 3.4b**, **Table 3.2**).

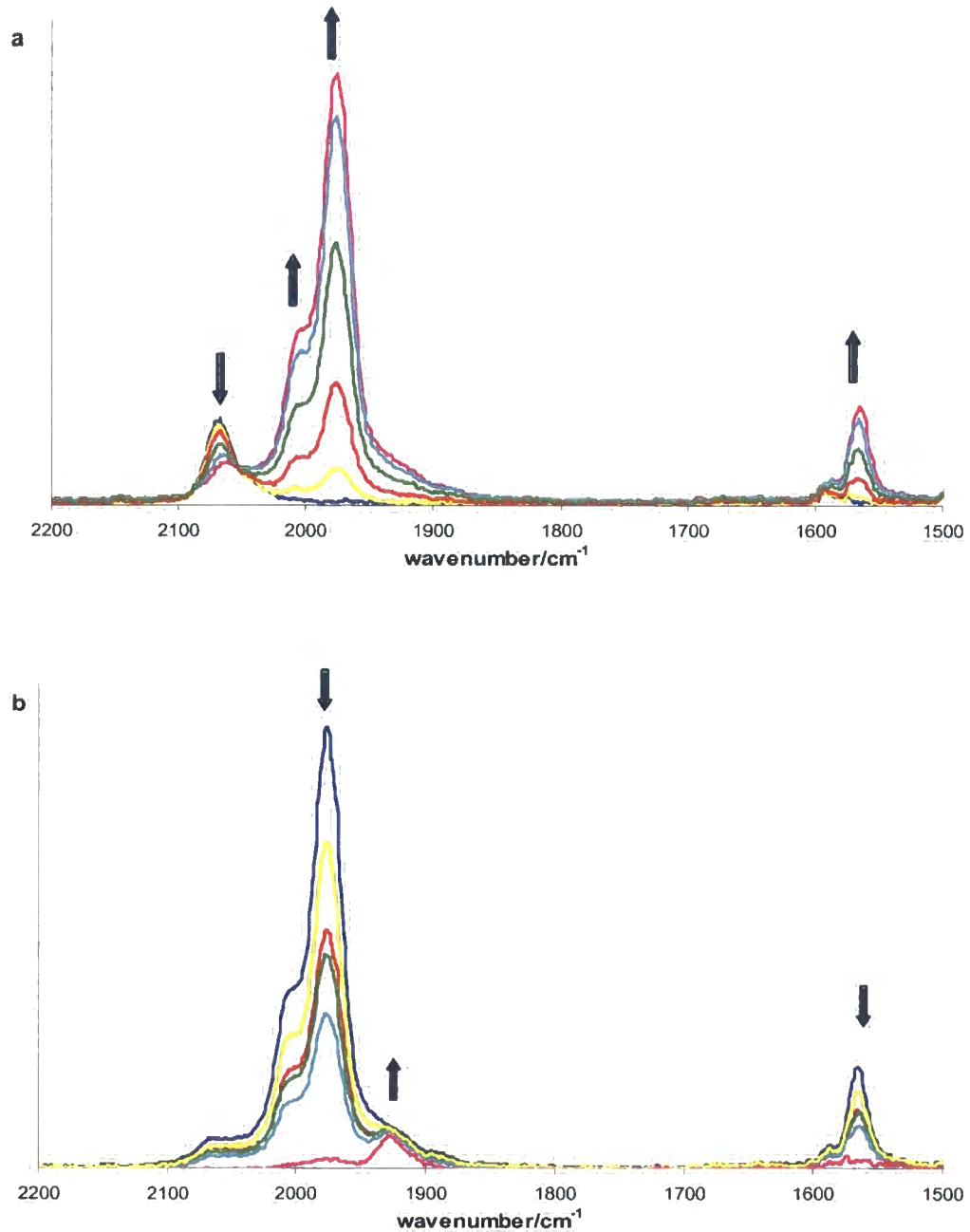

Figure 3.4. Infra-red spectra obtained on **a)** oxidation of **3.8** → $[\mathbf{3.8}]^{+}$ and **b)** oxidation of $[\mathbf{3.8}]^{+}$ → $[\mathbf{3.8}]^{2+}$

With the IR spectroelectrochemical response of the diethynylaryl bridged species clearly indicating involvement of the bridging ligand orbitals in the redox-active orbital, further investigation of the electronic structure was undertaken utilising UV-vis-NIR spectroelectrochemistry.

The electronic spectra of the organic dialkynes **3.11**, **3.12** and **3.13** were characterised by a π-π^* transition in the region 45500-38000 cm^{-1}, which shifted to progressively lower energy with the increasing size of the aromatic hydrocarbon moiety. In addition, **3.11** exhibited a broad band at 37000 cm^{-1}, whilst the more extended aromatic dialkynes exhibited vibrationally-structured π–π^* bands between 28700-31500 cm^{-1} (**3.12**) and 22800-27100 cm^{-1} (**3.13**) associated with transitions localised on the extended aromatic ring systems.

In the neutral bimetallic species, ligand based π-π^* transitions were observed (**3.8b** 27000 cm^{-1}; **3.9b** 22800 cm^{-1}; **3.10b** 18150 cm^{-1}). Upon oxidation to the mono-cation radicals $[\mathbf{3.8b}]^+$, $[\mathbf{3.9b}]^+$ and $[\mathbf{3.10b}]^+$, the electronic spectra display vibrationally-structured bands at lower energy ($\bar{\nu}_{max}$ < 19000 cm^{-1}) (**Figure 3.5**). The profile of these bands are very similar to those of the appropriate aryl radical cation,[50] and are assigned to bridging ligand-centred transitions. The significant shifts of the electronic absorption bands and the vibrational bands associated with the aromatic bridging ligands following oxidation clearly indicate that the orbitals of the dialkyne are significantly involved in the redox process.

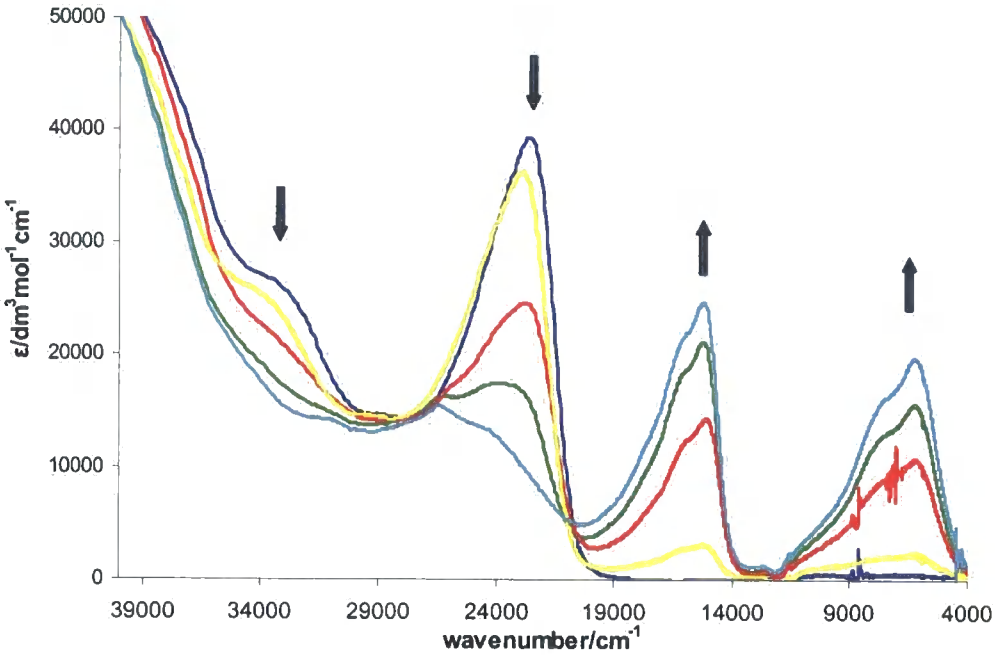

Figure 3.5 UV-vis-NIR spectra obtained upon oxidation of [**3.9b**] → [**3.9b**]$^+$

In addition to the shifts in the UV-vis bands described above, each species **[3.8b]**$^+$, **[3.9b]**$^+$, **[3.10b]**$^+$ also exhibited a series of overlapping absorptions in the NIR region (**Figure 3.5**), which could be deconvoluted into three Gaussian-shaped curves (**Table 3.5**, **Figure 3.7**). The recovery of the original spectrum on back reduction confirms that these transitions are associated with the 35-electron species and not a product of a subsequent chemical reaction. Further oxidation to generate the dications **[3.8b]**$^{2+}$, **[3.9b]**$^{2+}$ and **[3.10b]**$^{2+}$ resulted in collapse of the NIR bands, and a further red-shift of the vibrationally structured lowest energy visible bands (**Figure 3.6**). The electronic spectra of the dications were characterised by one or two bands in the visible region and these bands are probably MLCT/LMCT in nature.

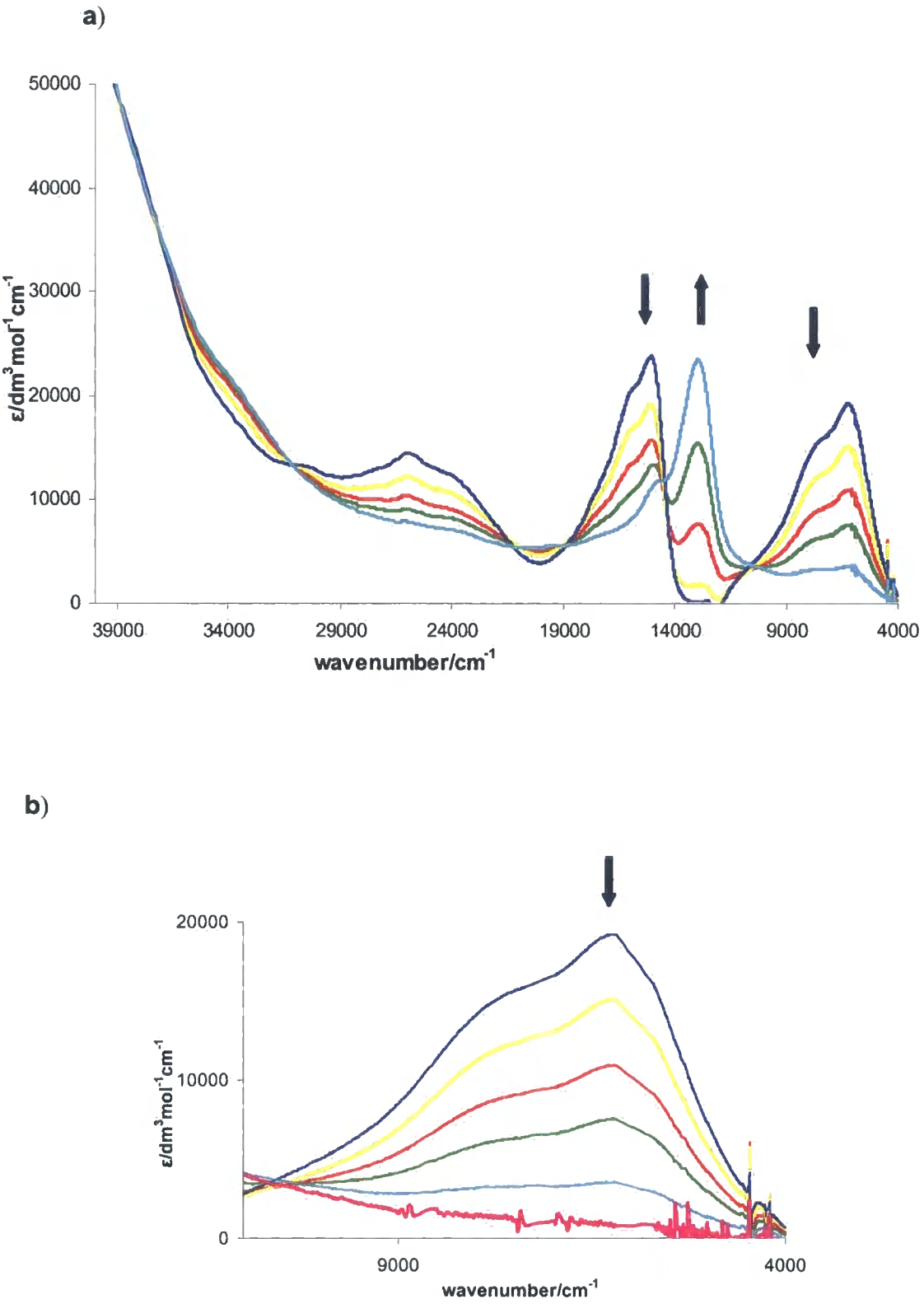

Figure 3.6 a) UV-vis-NIR spectra obtained upon oxidation of $[\mathbf{3.9b}]^{+} \rightarrow [\mathbf{3.9b}]^{2+}$, and **b)** expansion of the NIR region showing the collapse of the NIR band envelope during the redox process.

The radical cations **[3.8b]**$^+$, **[3.9b]**$^+$ and **[3.10b]**$^+$ might be considered as organometallic d^5/d^6 mixed-valence complexes, although, as discussed earlier, the term "mixed-valence" does imply metal-centred localisation of the unpaired electron and hole. The lowest energy (NIR) absorption band found in genuine mixed-valence species can be treated according to the series of relationships derived by Hush, and different treatments apply to valence-trapped (Class II) and delocalised (Class III) species. The NIR transitions in a Class II d^6/d^5 species correspond to photoinduced charge transfer from the d^6 metal site to the hole at the d^5 metal site (i.e. the NIR band is a genuine IVCT band or metal-metal charge transfer, MMCT, transition). Characteristics of Class II species include pronounced solvatochromism (as befits the description as a charge transfer band), and a half-height band-width ($\Delta\bar{\nu}_{1/2}$) that is in agreement with the relationship in Equation 1.5.

$$\Delta\bar{\nu}_{1/2} = (2310\bar{\nu}_{max})^{1/2} \qquad \textbf{Equation 1.5}$$

In a Class III species, in which the unpaired electron is delocalised over both metal sites and the bridging ligand, the notion of IVCT is misleading, and the term "charge resonance band" has been suggested as an alternative descriptor.[51] The half-height band width of these Class III systems is usually less than predicted on the basis of Equation 1.5, an observation which is often taken as a diagnostic test for Class II or Class III assignments.

The results of the deconvolution carried out on the NIR region of the electronic spectra of **[3.8b]**$^+$, **[3.9b]**$^+$ and **[3.10b]**$^+$ are illustrated in **Figure 3.7** (part **a**, **b** and **c** respectively). In each case, the NIR absorption envelope could be deconvoluted into three Gaussian shape curves and each curve treated according to Hush theory for Class II systems. The observed and calculated band widths at half height are reported in **Table 3.4**. For each band, the observed $\bar{\nu}_{1/2}$ is significantly narrower than that

predicted from Hush theory, suggesting that a delocalised description of the mixed-valence state may be most appropriate.

In addition the coupling parameters, V_{ab}, which may by extracted by application of Equation 1.6 to the observed values of $\bar{\nu}_{max}$, were calculated.

$$E_{op} = \bar{\nu}_{max} = 2V_{ab} \qquad \textbf{Equation 1.6}$$

Table 3.4

	$\bar{\nu}_{max}$/cm^{-1}	$\bar{\nu}_{1/2\ obs}$/cm^{-1}	$\bar{\nu}_{1/2\ calc}$/cm^{-1}	V_{ab} (Class III)/cm^{-1}
[3.8b]$^+$				
1	5737	1290	3640	2869
2	7047	1490	4035	3524
3	8090	1370	4323	4045
[3.9b]$^+$				
1	6196	1994	3783	3098
2	7893	1753	4270	3947
3	9497	2901	4684	4749
[3.10b]$^+$				
1	6439	1448	3857	3220
2	7849	2888	4258	3925
3	8688	2638	4478	4344

a)

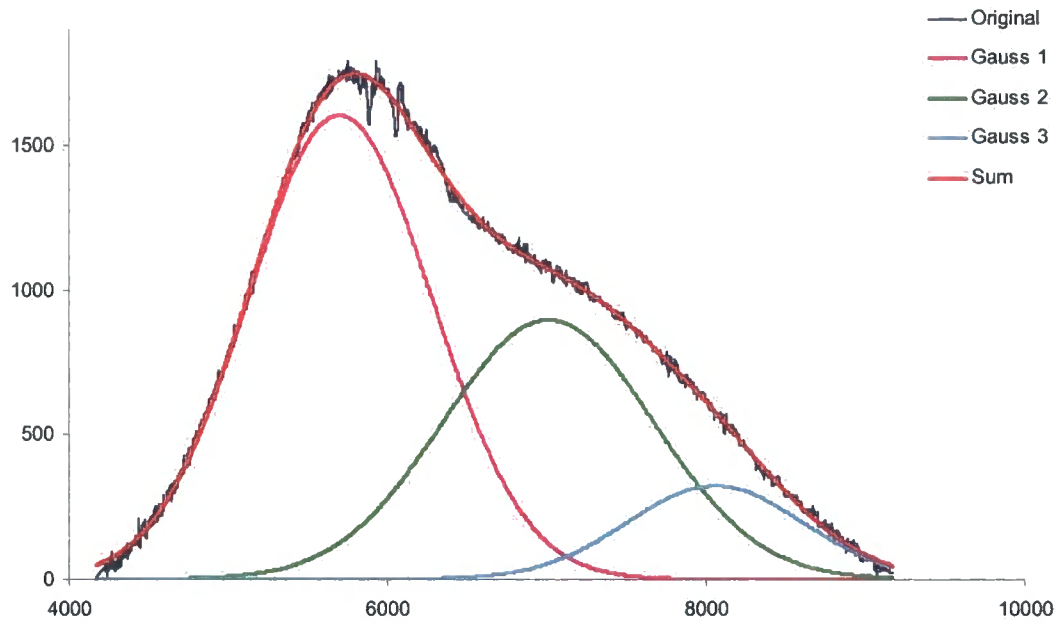
Original
Gauss 1
Gauss 2
Gauss 3
Sum
1500
1000
500
0
4000
6000
8000
10000

b)

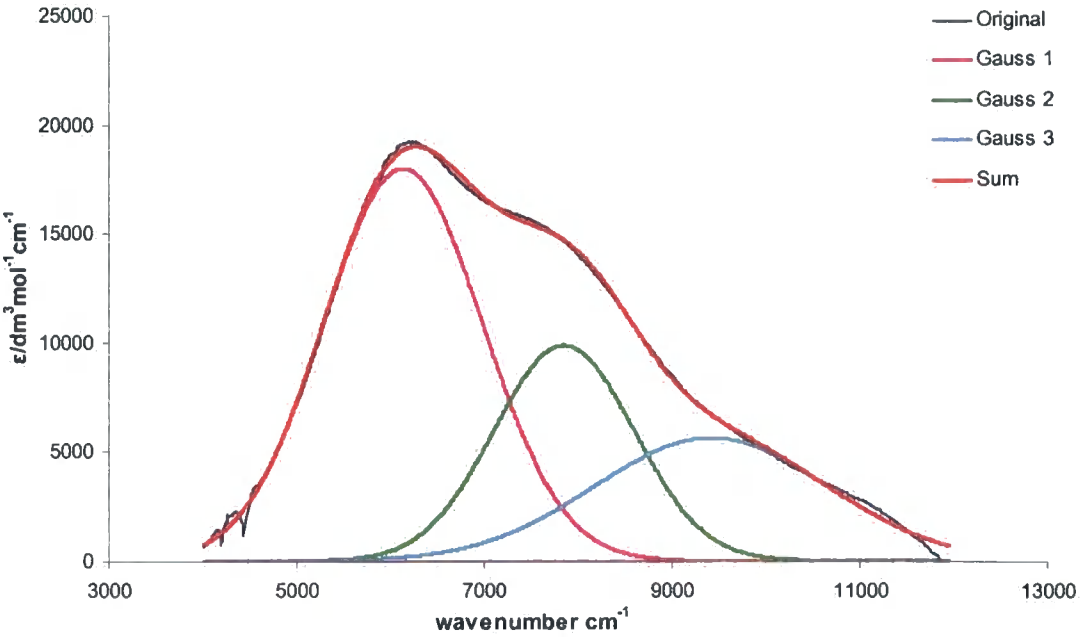
Original
Gauss 1
Gauss 2
Gauss 3
Sum
25000
20000
15000
10000
5000
0
ε/dm3mol-1cm-1
3000
5000
7000
9000
11000
13000
wavenumber cm-1

c)

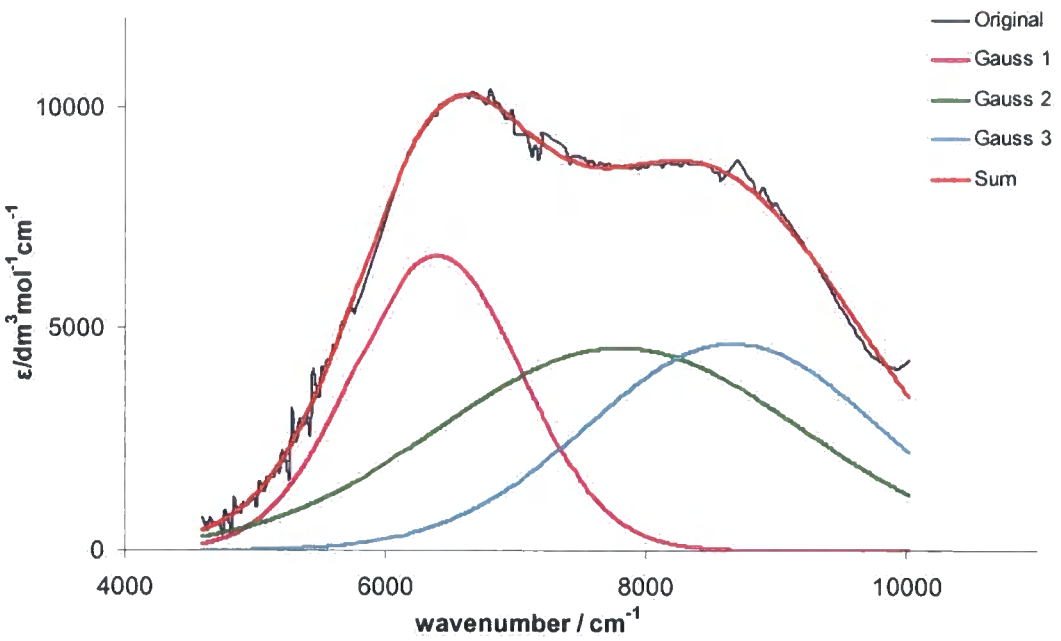

Figure 1.7 Deconvolution of the NIR region of the electronic spectra (original) of **a)** $[\mathbf{3.8b}]^+$, **b)** $[\mathbf{3.9b}]^+$ and **c)** $[\mathbf{3.10b}]^+$, into the three Gaussian-shaped curves (Gauss 1, 2, 3) that may be obtained.

The observation of multiple transitions within the NIR band envelope, as in $[\mathbf{3.8b}]^+$, $[\mathbf{3.9b}]^+$ and $[\mathbf{3.10b}]^+$, is not uncommon in strongly coupled systems.[48, 52] As noted in Chapter 1, Meyer has thoroughly reviewed the properties of compounds at the Class II (localised) and Class III (delocalised) borderline, and remarked that a combination of the low symmetry at the metal sites, spin-orbit coupling (less likely in the lighter transition metal elements) and metal-ligand mixing can all serve to relax the formal selection rules that would otherwise forbid transitions from lower lying filled orbitals to the SOMO.[53] Systems in which a higher degree of symmetry is present at the metal centre, and in which spin-orbit coupling is reduced, should therefore give rise to less 'complicated' electronic spectra and will be discussed further in Chapter 5.

Guided by the electrochemical and spectroelectrochemical results, the Ru(dppe)Cp* series was examined in more detail. On the basis of the electrochemical results $AgPF_6$ was chosen as a convenient chemical oxidising agent with which to prepare the various oxidised species. For example, reaction of **3.8b** with one molar equivalent of $AgPF_6$ in CH_2Cl_2 gave a dark red coloured solution, from which the 35-electron bimetallic species **[3.8b]PF_6** was isolated in good yield by precipitation into diethyl ether. Subsequent reaction of **[3.8b]PF_6** with a further equivalent of $AgPF_6$, or reaction of **3.8b** with two equivalents of the same oxidising agent, gave dark blue **[3.8b][PF_6]$_2$**. Similar procedures afforded **[3.9b][PF_6]$_n$** and **[3.10b][PF_6]$_n$** (n = 1, 2).

Isolation of the chemically oxidised species allowed the UV-Vis-NIR spectra of these to be measured in solvents of different dielectric strength (CH_2Cl_2, thf, CH_3CN), and free of the high electrolyte concentrations necessary for the spectroelectrochemical work. The transitions in the monocations were found to be essentially independent of the solvent environment suggesting that the mixed-valence species are best described in terms of delocalised electronic structure, and supporting the conclusions and methods of analysis above.

Raman spectroscopy

Raman spectroscopy provides a useful vibrational probe complimentary to IR spectroscopy. Raman scattering spectra were obtained from powders, with a Horiba-Jobin-Yvon Raman microscope LabRam HR800 with 633 nm HeNe laser excitation and Peltier cooled (-75 °C) detector (Durham), or with 1064 nm laser and a nitrogen cooled (-133 °C) detector (Horiba-Jobin-Yvon, Lille).

In an effort to more thoroughly link the chromophores responsible for the NIR band envelope with molecular structure, a series of Raman spectra were undertaken with 1064 nm probe wavelength which is in resonance with the blue-edge of the NIR envelope in the singly oxidised species. As stated in Chapter 1, if the sample under study has an absorption band coincident with the excitation frequency then a resonance Raman effect may be observed resulting in significant enhancement of certain Raman bands. In comparing spectra obtained at a wavelength in resonance

with the NIR envelope with those obtained at 633 nm it was hoped to more thoroughly define the parts of the molecule involved in the transitions giving rise to the observed bands in the NIR region. As might be expected the intensities of the C≡C band in the (non-resonant) spectra of the neutral complexes were comparable when probed by either wavelength. In contrast, for the oxidised derivatives, significant differences were observed between spectra obtained at the two wavelengths.

Unfortunately not all complexes were stable under the laser required to obtain the Raman scattering spectra which hampered comparisons. The most stable series was provided by $[\mathbf{3.9b}]^{n+}$ (n = 0, 1, 2). The spectra of the 35-electron monocationic species, $[\mathbf{3.9b}]^{+}$, collected from samples probed at 1064 nm displayed a significant increase in intensity of the C≡C band when compared with the 633 nm spectra. These studies demonstrate the possibility of linking the chromophores responsible for absorption bands in the electronic spectrum with structural features within complexes. The Raman spectra were obtained using the two probe wavelengths available, at Durham and at the Laboratories of Horiba-Jobin-Yvon in Lille; however a tuneable probe laser would allow much greater control over the bands addressed, and would reveal the links between structure and electronic transition more clearly.

Using the 633 nm probe laser, the monometallic complexes **3.5b**-**3.7b** displayed ν(C≡C) bands between 2019 cm^{-1} and 2076 cm^{-1} which followed the trend **3.5b** > **3.6b** > **3.7b** as observed in the IR spectra of these complexes. Compound **3.7b** was amenable to chemical oxidation and the Raman spectrum of the singly oxidised derivative **3.7b**[PF_6] displayed a ν(C≡C) band at a lower energy (1967cm^{-1}), the shift in wavenumber of *ca.* 50 cm^{-1} being somewhat smaller than the shift observed in the analogous IR spectra. The observation of the ν(C≡C) bands same energy as they appear in the analogous IR spectra confirms, here, and in all the Raman spectra reported, the integrity of the samples in the laser.

In the case of the parent materials **3.8b, 3.9a/b, 3.10a/b** strong ν(C≡C) bands were observed in the region 2040-2088 cm^{-1}, these bands displayed trends in position which followed those described above for the IR bands with ν(C≡C) **3.8** > **3.9** > **3.10**. Samples of the chemically oxidised materials (monocations and dications of the Ru(dppe)Cp* series) were studied similarly and again revealed an analogous pattern to that observed for the IR spectra with a general shift of bands to lower frequencies upon oxidation, consistent with a decrease in the formal CC bond order (**Table 3.6**). A number of bands below 1700 cm^{-1} relating to the aromatic portion of the bridging ligand and the supporting metal ligands were also observed and could be identified by comparison with spectra obtained from the corresponding $SiMe_3$-protected dialkynes, dppe and RuCl(dppe)Cp*.

Table 3.6 Raman (ν(C≡C) /cm^{-1}) data for $[\mathbf{3.5b}]^{n+}$-$[\mathbf{3.10b}]^{n+}$ and **3.11-3.13**.[a]

633/1064 nm	**n**		
	0	**1**	**2**
3.5b	2076		
3.6b	2057		
3.7b	2039		
3.8b	2081/2079	[b]/1973	[b]/[b]
3.9b	2060/2058	1967/1964	1919/1914
3.10b	2040/2032	1967/[b]	[b] /1894
3.11	2155		
3.12	2145		
3.13	2135		

[a]not all species could be measured due to decomposition in laser beam. [b]not observed

Theoretical studies

In order to better understand the experimental results from this family of diethynyl(aryl)-bridged bimetallic complexes, DFT level calculations were performed on the model systems $[Ru(PH_3)_2Cp\}_2(\mu\text{-}C{\equiv}CC_6H_4C{\equiv}C)]^{n+}$, $[\mathbf{3.8\text{-}H}]^{n+}$ (**Figure 3.9**) with C_{2v} symmetry imposed,† to minimise computational effort after initial optimisation and energy minimisation steps.[54] The optimised structure (**Table 3.7**) fits well with the structure of other acetylide complexes of the general type Ru(C≡CR)(PP)Cp' that have been structurally characterised,[44, 48, 55] and is also similar to the metrical parameters obtained from the diethynyl anthracene-bridged complex **3.10b**. The good general agreement between the optimised structure and the available experimental data give a high degree of confidence in the accuracy of the calculations and the results that may be drawn from them.

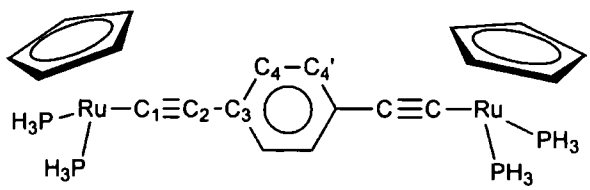

Figure 3.9 The model complex $[\{Ru(PH_3)_2Cp\}_2(\mu\text{-}C{\equiv}CC_6H_4C{\equiv}C)]^{n+}$, **[3.8-H]**, showing labelling scheme

† Symmetry restrictions were imposed in order to minimise computational effort. Studies on similar systems with and without such constraints indicate little difference in the final solution.

Table 3.7 Bond lengths (Å) obtained from the optimised structures of $[\mathbf{3.8\text{-}H}]^{n+}$.

	[3.8-H]	$[\mathbf{3.8\text{-}H}]^{+}$	$[\mathbf{3.8\text{-}H}]^{2+}$ (LS)	$[\mathbf{3.8\text{-}H}]^{2+}$ (HS)
Ru-C(1)	2.033	1.980	1.929	1.953
C(1)-C(2)	1.234	1.247	1.257	1.247
C(2)-C(3)	1.427	1.401	1.379	1.408
C(3)-C(4)	1.416	1.428	1.437	1.420
C(4)-C(4')	1.389	1.376	1.366	1.381
Ru-P	2.301	2.315	2.339	2.348

The MO diagram presented in (**Figure 3.10**) shows the large separation of the HOMO from the LUMO (1.715 eV). The HOMO is also removed from the other occupied orbitals by some 0.8 eV. The HOMO and HOMO-1 from the model system are shown in **Figure 3.11**, and are clearly derived from the orthogonal d-π systems. The HOMO is extensively delocalised over both metal centres, the ethynyl moieties and critically the phenylene group (**Table 3.8**). From **Figure 3.11** it can be seen that this π-orbital is anti-bonding in character with respect to the Ru-C(1), C(2)-C(3) and C(4)-C(4') bonds, and bonding with respect to C(1)-C(2) and C(3)-C(4), in agreement with the valence bond description.

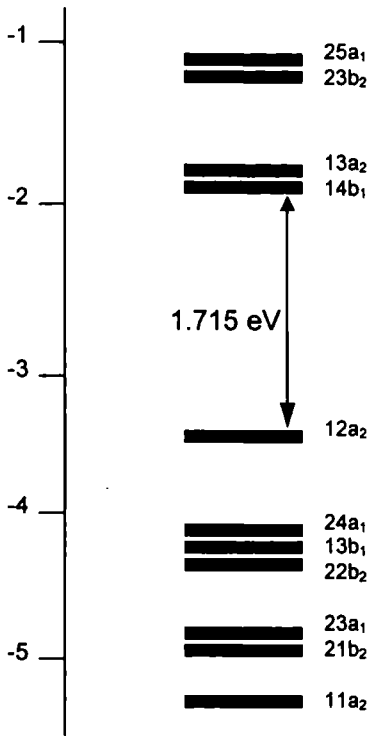

Figure 3.10 Molecular orbital diagram obtained from DFT calculations on **[3.8-H]**

This description of the HOMO points towards the role of the bridging diethynyl benzene ligand, and in particular the extended π-system, in promoting electronic interactions between the remote metal centres. However, in contrast, the HOMO-1, which is comprised of π-type orbitals orthogonal to those in the HOMO, is more extensively localised on the metal centres and the carbon atoms of the C≡C fragment, with negligible contribution from the central phenylene moiety (**Figure 3.11**, **Table 3.8**).

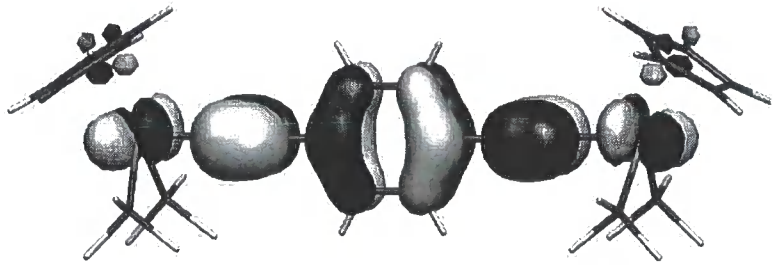

a

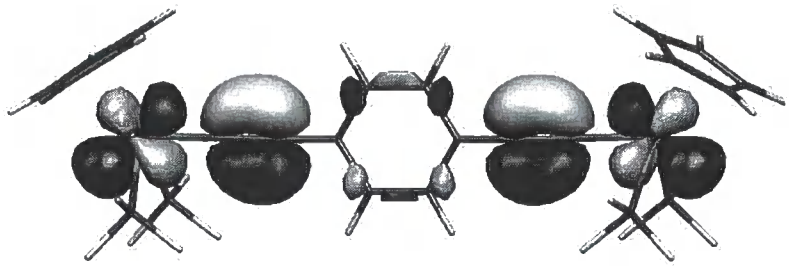

b

Figure 3.11 The HOMO (a) and HOMO-1 (b) calculated for $\{Ru(PH_3)_2Cp\}_2(\mu\text{-}C{\equiv}CC_6H_4CC{\equiv}C)$, **[3.8-H]**. Contour values are ±0.03 [e/bohr^3]$^{1/2}$

Table 3.8 Energy (ε/eV), occupation and localisation (%) of the MOs in the HOMO-LUMO region of **[3.8-H]**

	$13a_2$	**$14b_1$**	**$12a_2$**	**$24a_1$**	**$13b_1$**	**$22b_2$**	**$23a_1$**	**$21b_2$**
ε	-1.83	-1.83	-3.50	-4.27	-4.32	-4.32	-4.97	-4.98
Occupancy	0	0	2	2	2	2	2	2
C(1)	0	0	25	20	7	17	9	9
C(2)	0	0	20	32	29	30	6	8
C(3)	0	0	14	0	1	1	0	0
C(4)	0	0	14	0	9	0	0	0
H_{C4}	0	0	0	0	0	0	0	0
Ru	45	44	22	46	41	48	50	49
PH_3	31	32	1	1	5	2	15	15
Cp	24	24	4	1	8	2	20	19

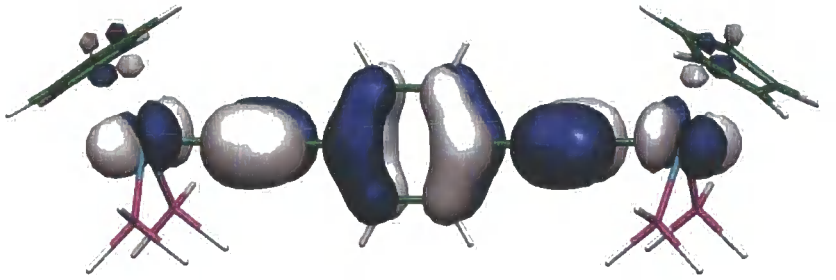

a

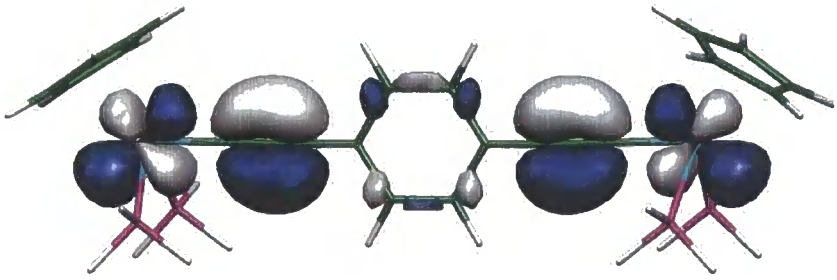

b

Figure 3.11 The HOMO (a) and HOMO-1 (b) calculated for $\{Ru(PH_3)_2Cp\}_2(\mu\text{-}C{\equiv}CC_6H_4CC{\equiv}C)$, **[3.8-H]**. Contour values are ±0.03 $[e/bohr^3]^{1/2}$

Table 3.8 Energy (ε/eV), occupation and localisation (%) of the MOs in the HOMO-LUMO region of **[3.8-H]**

	$13a_2$	**$14b_1$**	**$12a_2$**	**$24a_1$**	**$13b_1$**	**$22b_2$**	**$23a_1$**	**$21b_2$**
ε	-1.83	-1.83	-3.50	-4.27	-4.32	-4.32	-4.97	-4.98
Occupancy	0	0	2	2	2	2	2	2
C(1)	0	0	25	20	7	17	9	9
C(2)	0	0	20	32	29	30	6	8
C(3)	0	0	14	0	1	1	0	0
C(4)	0	0	14	0	9	0	0	0
H_{C4}	0	0	0	0	0	0	0	0
Ru	45	44	22	46	41	48	50	49
PH_3	31	32	1	1	5	2	15	15
Cp	24	24	4	1	8	2	20	19

In order to assess the effects of oxidation on the electronic and physical structure of these molecules, the total electron count was reduced by one. The effects of this oxidation event on the molecule are clear in the resulting optimised structure (**Table 3.7**). Comparisons of the structures of [**3.8-H**] and [**3.8-H**]$^{+}$ reveal a contraction of the Ru-C(1), C(2)-C(3) and C(4)-C(4') bond lengths, and a concomitant elongation of the C(1)≡C(2) and C(3)-C(4) bonds, all of which is consistent with the evolution of a degree of quinoidal character in the bridge. In the case of the doubly oxidised form [**3.8-H**]$^{2+}$ the low-spin configuration was found to be 12.41 eV more stable than the corresponding high-spin state, which can be attributed to the large difference in energy between the HOMO and the other occupied orbitals. The low-spin structure exhibits even more pronounced quinoidal characteristics (**Table 3.7**).

The involvement of the metal centre in the redox process being modelled here is apparent from the Ru-P bond lengths, which become progressively longer as the electron count of the molecule is reduced (**Table 3.7**). As the electron-density available for Ru-P d-π* back-bonding is decreased the Ru-P bond length increases, and it has been shown that the Ru-P bond length is a very sensitive probe of the electronic environment about the metal centre.[56]

Taken together, the changes in structure at the metal and throughout the bridging ligand clearly indicate that oxidation of **3.8-H** and related systems influences the entire Ru-bridge-Ru assembly.

3.3 Discussion

A combination of spectroscopic, electrochemical and theoretical studies has allowed the electronic structure of the diethynylaryl-bridged, bimetallic complexes to be assessed and rationalised. The electrochemical data reveal that the nature of the aromatic portion of the ethynyl ligand plays a significant role in the relative oxidation potentials of the bimetallic species, with both oxidation potentials (E_1 and E_2) decreasing in the order **3.8** > **3.9** > **3.10**. Regardless of the nature of the bridge the first oxidation potential of the binuclear species is significantly lower than the oxidation potential of the corresponding mononuclear model, indicating a much higher-lying HOMO in the case of the bimetallic complexes, and providing qualitative evidence for strong interactions between the metal centres via the bridge.

The shift of the ν(C≡C) bands to progressively lower frequencies, upon oxidation of the parent complexes to the monocationic and dicationic derivatives, provides evidence for the involvement of the bridging ligand π-system in the redox-active orbital of these bimetallic ruthenium complexes.

The changes observed in the UV-vis region of the electronic spectra of the bimetallic species **3.8**, **3.9** and **3.10**, upon oxidation to the monocation, provides further evidence for involvement of the diethynyl aromatic bridging ligand in the redox active orbital. In addition, the presence of overlapping bands in the NIR region of the electronic spectra of $[\mathbf{3.8b}]^+$, $[\mathbf{3.9b}]^+$ and $[\mathbf{3.10b}]^+$, which could be treated according to Hush theory, allows an evaluation of the underlying electronic structure of these 35-electron monocations. The solvent independence of these bands suggests the monocationic species are best described in terms of a delocalised structure.

The similar electrochemical, vibrational and electronic signature of these monocations suggests little variation in the magnitude of electronic coupling through the bridging ligands. Analysis of the lowest energy band obtained by deconvolution of the NIR spectra of $[\mathbf{3.8}]^+$, $[\mathbf{3.9}]^+$ and $[\mathbf{3.10}]^+$ support this, with values of V_{ab} = 2900, 3100 and 3200 cm^{-1} respectively, being obtained.

The Gaussian-shaped bands obtained from the NIR spectra of $[\mathbf{3.8}]^+$, $[\mathbf{3.9}]^+$ and $[\mathbf{3.10}]^+$ are at lower energies than those observed in the electronic spectra of related

C≡CC≡C-bridged species, $[\mathbf{1.23}]^+$ and $[\mathbf{1.24}]^+$. The value of V_{ab} obtained for the lowest energy band in the spectra of $[\mathbf{1.23}]^+$ and $[\mathbf{1.24}]^+$ (0.63 eV, 5100cm^{-1} in each case) is significantly higher than in $[\mathbf{3.8}]^+$, $[\mathbf{3.9}]^+$ and $[\mathbf{3.10}]^+$ indicating a smaller electronic coupling in the aromatic-bridged species compared to the diyndiyl species.

The theoretical results obtained for the model complex $[\mathbf{3.8\text{-}H}]^{n+}$ indicate that oxidation of these complexes influences the entire {Ru}(μ-C≡CXC≡C){Ru} assembly and, together with the spectroscopic and electrochemical data, support a description of the redox active HOMO as being delocalised over both the ruthenium centres and the bridge.

3.4 Experimental Details

General conditions

All reactions were carried out in oven-dried glassware under dry nitrogen as a matter of routine. NMR spectra were recorded on a Bruker Avance 400, Varian VXR-200 or Inova 500 spectrometer and referenced against solvent resonances. IR spectra were recorded on a Nicolet Avatar spectrometer as solutions using solution cells fitted with CaF_2 windows.

Instrumentation

Cyclic voltammograms were recorded with an EG&G PAR Model 283 potentiostat. The CH_2Cl_2 solutions contained 10^{-3} M complex and 0.1 M $[NBu_4]PF_6$ (Aldrich; recrystallised twice from absolute EtOH and dried overnight under vacuum at 80 °C) as supporting electrolyte. The solutions were placed in an airtight single-compartment three-electrode cell equipped with a Pt disk working electrode (0.42 mm^2 apparent electrode surface, polished with a 0.25 μm diamond paste), Pt gauze auxiliary electrode and Ag wire pseudo-reference electrode. In all cases, ferrocene or cobaltocence was used as internal calibrant [$E_{1/2}(FeCp_2/[FeCp_2]^+)$ = +0.46 V vs SCE in CH_2Cl_2; $E_{1/2}(CoCp_2/[CoCp_2]^+$ = -0.87 V vs SCE in CH_2Cl_2]. The IR spectroelectrochemical experiments at variable temperatures were performed with a previously described OTTLE cell positioned in the sample compartment of a Bio-Rad FTS-7 FT-IR spectrometer.[57, 58] The solutions were 5 x 10^{-3} M in analyte and 3 x 10^{-1} M in the supporting electrolyte, $[NBu_4]PF_6$. The UV-Vis-NIR spectroelectrochemical measurements were conducted using an OTE cell similar to that described previously,[59] from CH_2Cl_2 solutions containing 1 x 10^{-1} M $[NBu_4]BF_4$ as supporting electrolyte.

The compounds 1,4-bis(trimethylsilylethynyl)benzene,[60, 61] $Ru(C{\equiv}CC_6H_5)(PPh_3)_2Cp$,[43] 1,4-bis(trimethylsilylethynyl)naphthalene,[32, 61] $Ru(C{\equiv}CC_6H_5)(dppe)Cp^*$,[41] 9,10-bis(trimethylsilylethynyl)anthracene,[32, 61] $RuCl(PPh_3)_2Cp$,[41] and RuCl(dppe)Cp*,[48] were prepared by standard literature routes. Other reagents were purchased and used as received. Solvents were dried and

deoxygenated using an Innovative Technologies Solvent Purification System, and de-gassed prior to use.

*$Ru(C{\equiv}CC_{10}H_7)(PPh_3)_2Cp$ (**3.6a**)*

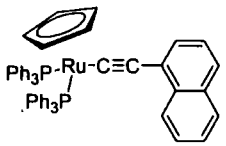

A suspension of $RuCl(PPh_3)_2Cp$ (200 mg, 0.275 mmol), NH_4PF_6 (100 mg, 0.613 mmol) in methanol (20 ml) and $HC{\equiv}CC_{10}H_7$ (50 mg, 0.329 mmol), was heated at reflux for 90 min under a nitrogen atmosphere. The red/orange solution formed was treated with a methanolic solution of NaOMe and the yellow precipitate formed collected, washed with MeOH and hexane and dried to give **3.6a** as a yellow powder (167 mg, 0.232 mmol, 72%). Found: C, 74.33; H, 4.92. $RuC_{53}H_{42}P_2$ requires: C, 75.61; H, 5.03. IR: ν(C≡C) 2057 cm^{-1}. ^1H NMR ($CDCl_3$, 200 MHz): δ 4.59 (s, 5H, Cp); 8.58-7.10 (m, 37H, Ph, $C_{10}H_7$). $^{31}P\{^1H\}$ NMR($CDCl_3$, 81 MHz): δ 51.56 (s, PPh_3). $^{13}C\{^1H\}$ NMR ($CDCl_3$, 126 MHz): 85.32 (s, Cp), 90.95, 114.50 (C≡C), 127.30-139.23 (arom) ES(+)-MS (m/z): 842 [$Ru(C{\equiv}CC_{10}H_7)(PPh_3)_2Cp$].

*$Ru(C{\equiv}CC_{10}H_7)(dppe)Cp^*$ (**3.6b**)*

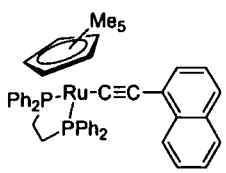

A suspension of RuCl(dppe)Cp* (100 mg, 0.149 mmol), $HC{\equiv}CC_{10}H_7$ (30 mg, 0.197 mmol), and NH_4PF_6 (75 mg, 0.46 mmol) in methanol (20 ml) was heated to reflux under a nitrogen atmosphere (90 min). After cooling the red-orange solution was treated with a methanolic solution of NaOMe and the yellow precipitate formed was collected and washed with MeOH and hexane and dried to give **3.6b** as a yellow powder (83 mg, 0.106 mmol, 71%). Found: C, 72.48; H, 5.81; $RuC_{48}H_{46}P_2$ requires: C, 73.36; H, 5.90. IR: ν(C≡C) 2055 cm^{-1}. ^1H NMR ($CDCl_3$, 200 MHz): δ 1.58 (s, 15H, Cp*); 2.80, 2.14 (m, 4H, CH_2); 8.34-6.74 (m, 27H, Ph, $C_{10}H_7$). $^{31}P\{^1H\}$ NMR

($CDCl_3$, 81 MHz): δ 75.42 (s, dppe) ES(+)-MS (*m/z*): 786[$Ru(C{\equiv}CC_{10}H_7)(dppe)Cp^*$].

$Ru(C{\equiv}CC_{14}H_9)(PPh_3)_2Cp$ (3.7a)

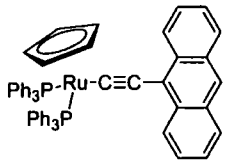

$RuCl(PPh_3)_2Cp$ (200 mg, 0.275 mmol), $Me_3SiC{\equiv}CC_{14}H_9$ (75 mg, 0.275 mmol), were treated with methanol (20 ml) and KF (30 mg, 0.556 mmol). The resulting suspension was heated and the orange solution formed heated at reflux for 2h under a nitrogen atmosphere. The yellow precipitate formed was collected and washed with cold MeOH and hexane and dried to give **3.7a** as a yellow/orange powder (228 mg, 0.256 mmol, 93%). Found: C, 76.04; H, 5.14. $RuC_{57}H_{44}P_2$ requires: C, 76.75; H, 4.97. IR: ν(C≡C) 2042 cm^{-1}. ^1H NMR ($CDCl_3$, 200 MHz): δ 4.49 (s, 5H, Cp); 8.76-7.06 (m, 39H, Ph, $C_{14}H_9$). $^{31}P\{^1H\}$ NMR ($CDCl_3$, 81 MHz): δ 51.24 (s, PPh_3). $^{13}C\{^1H\}$ NMR ($CDCl_3$, 126 MHz): 81.57, (s, C≡) 85.90 (s, Cp), 112.70 (s, C≡), 120.46-139.54 (arom). ES(+)-MS (m/z): 892 [$Ru(C{\equiv}CC_{14}H_9)(PPh_3)_2Cp$].

$Ru(C{\equiv}CC_{14}H_9)(dppe)Cp^*$ (3.7b)

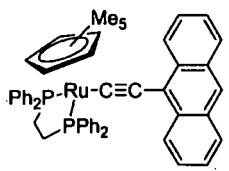

A suspension of $RuCl(dppe)Cp^*$ (100 mg, 0.149 mmol), $Me_3SiC{\equiv}CC_{14}H_9$ (45 mg, 0.164 mmol), and KF (25 mg, 0.430 mmol) in methanol (15 ml) was heated at reflux for 2 hours under a nitrogen atmosphere. The yellow precipitate formed was collected and washed with MeOH and hexane and dried to give **3.7b** as a yellow powder (91 mg, 0.109 mmol, 73%). Found: C, 73.65; H, 5.71. $RuC_{52}H_{48}P_2$ requires: C, 74.71; H, 5.79. IR: ν(C≡C) 2039 cm^{-1}. ^1H NMR ($CDCl_3$, 200 MHz): δ 1.74 (s, 15H, Cp^*); 2.94, 2.17 (m, 4H, CH_2); 7.91-7.09 (m, 29H, Ph, $C_{14}H_9$). $^{31}P\{^1H\}$ NMR ($CDCl_3$, 81 MHz): δ 76.10 (s, dppe). ES(+)-MS (*m/z*): 836 [$Ru(C{\equiv}CC_{14}H_9)(dppe)Cp^*$].

{Ru(dppe)Cp}$_2$(μ-C≡CC$_6$H$_4$C≡C) (**3.8b**)*

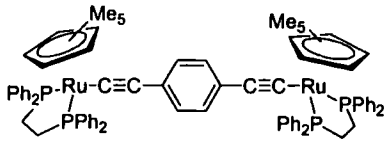

A suspension of RuCl(dppe)Cp* (500 mg, 0.747 mmol), $Me_3SiC{\equiv}CC_6H_4C{\equiv}CSiMe_3$ (270 mg, 0.374 mmol), and KF (100 mg, 1.72 mmol) in methanol (40 ml) was heated at reflux for 1 hour under a nitrogen atmosphere. The yellow precipitate formed was collected and washed with MeOH and hexane and dried to give **3.8b** as a yellow powder (390 mg, 0.280 mmol, 75%). Found: C, 69.17; H, 5.84. $Ru_2C_{82}H_{82}P_4$ requires: C, 70.67; H, 5.93. IR: ν(C≡C) 2067 cm^{-1}. ^{1}H NMR ($CDCl_3$, 200 MHz): δ 1.54 (s, 30H, Cp*); 2.69, 2.05 (m, 8H, CH_2); 7.78-6.55 (m, 44H, Ph, C_6H_4). $^{31}P\{^1H\}$ NMR ($CDCl_3$, 81 MHz): δ 81.77 (s, dppe). $^{13}C\{^1H\}$ NMR (C_6D_6, 126 MHz): 10.10 (s, C_5Me_5), 29.52 (m, CH_2), 89.27 (s, C≡), 92.64 (s, C_5Me_5), 99.65 (s, C≡), 127.31-133.99 (arom). ES(+)-MS (*m/z*): 1394 [{Ru(dppe)Cp*}$_2$(μ-C≡CC$_6$H$_4$C≡C)].

*{Ru(PPh$_3$)$_2$Cp}$_2$(μ-C≡CC$_{10}$H$_6$C≡C) (**3.9a**)*

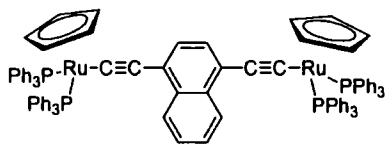

A suspension of $RuCl(PPh_3)_2Cp$ (300 mg, 0.413 mmol), $Me_3SiC{\equiv}CC_{10}H_6C{\equiv}CSiMe_3$ (70 mg, 0.215 mmol), and KF (50 mg, 0.862 mmol) in methanol (20 ml) was heated at reflux for 1 hour under a nitrogen atmosphere. The yellow precipitate formed was collected, washed with MeOH and hexane and dried to give **3.9a** as a yellow powder (312 mg, 0.201 mmol, 97%). IR: ν(C≡C) 2070 cm^{-1}. ^{1}H NMR ($CDCl_3$, 200 MHz): δ 4.39 (s, 10H, Cp); 7.06-7.50 (m, 66H, Ph, $C_{10}H_6$). $^{31}P\{^1H\}$ NMR ($CDCl_3$, 81 MHz): δ 51.45 (s, PPh_3). $^{13}C\{^1H\}$ NMR ($CDCl_3$, 126 MHz): δ 85.52 (Cp), 124.46-134.01 (arom) ES(+)-MS (*m/z*): 1556[{Ru(PPh$_3$)$_2$Cp }$_2$(μ-C≡CC$_{10}$H$_6$C≡C)].

{Ru(dppe)Cp}$_2$(μ-C≡C$C_{10}H_6$C≡C) (**3.9b**)*

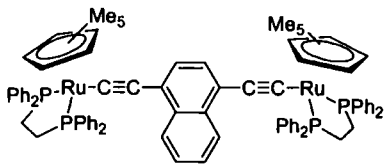

A suspension of RuCl(dppe)Cp* (200 mg, 0.299 mmol), (Me_3Si)C≡C$C_{10}H_6$C≡C($SiMe_3$) (48 mg, 0.151 mmol), and KF (35 mg, 0.60 mmol) in methanol (20 ml) was heated to reflux under a nitrogen atmosphere. On reflux a green solution was formed, the solution was heated at reflux for 90 min and the yellow precipitate formed was collected, washed with MeOH and hexane and dried to give **3.9b** as a yellow powder (135mg, 0.0935 mmol, 63%). Found: C, 69.48; H, 5.76. $Ru_2C_{86}H_{84}P_4$ requires: C, 71.55; H, 5.86. IR: ν(C≡C) 2055 cm^{-1}. ^{1}H NMR ($CDCl_3$, 200 MHz): δ 1.55 (s, 30H, Cp*); 2.80, 2.10 (m, 8H, CH_2); 7.83-7.19 (m, 46H, Ph). $^{31}P\{^1H\}$ NMR ($CDCl_3$, 81 MHz): δ 82.03 (s, dppe). $^{13}C\{^1H\}$ NMR (C_6D_6, 126 MHz): δ 10.51 (s, C_5Me_5), 29.77 (m, CH_2), 92.86 (s, C_5Me_5), 110.19 (C≡), 124.51-137.95 (arom) ES(+)-MS (*m/z*): 1444[{Ru(dppe)Cp*}$_2$(μ-C≡C$C_{10}H_6$C≡C)].

*{Ru(PPh_3)$_2$Cp}$_2$(μ-C≡C$C_{14}H_8$C≡C) (**3.10a**)*

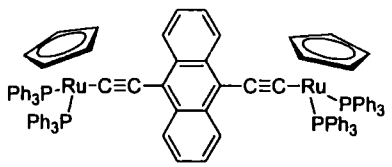

A suspension of RuCl(PPh_3)$_2$Cp (100 mg, 0.138 mmol), $Me_3SiC{\equiv}CC_{14}H_8C{\equiv}CSiMe_3$ (25 mg, 0.069 mmol), and KF (20 mg, 0.345 mmol). Methanol (15 ml) was added and the suspension was heated to reflux under a nitrogen atmosphere. The red precipitate formed was collected and washed with MeOH and hexane and dried to give **3.10a** as a bright red powder (91 mg, 0.0567 mmol, 41%). IR: ν(C≡C) 2035 cm^{-1}. ^{1}H NMR ($CDCl_3$, 200 MHz): δ 4.51 (s, 10H, Cp); 7.64-7.06 (m, 68H, Ph, $C_{14}H_8$). $^{31}P\{^1H\}$ NMR ($CDCl_3$, 81 MHz): δ 51.06 (s, PPh_3). ES(+)-MS (*m/z*): 1606 [{Ru(PPh_3)$_2$Cp }$_2$(μ-C≡C$C_{14}H_8$C≡C)]$^+$.

{Ru(dppe)Cp}$_2$(μ-C≡C$C_{14}H_8$C≡C) (3.10b)*

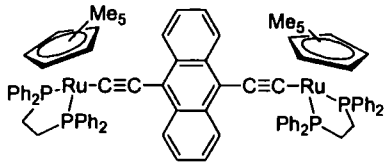

RuCl(dppe)Cp* (500 mg, 0.747 mmol), (Me_3Si)C≡C$C_{14}H_8$C≡C($SiMe_3$) (140 mg, 0.374 mmol), and KF (100 mg, 1.72 mmol) were treated with methanol (40 ml) and the suspension formed was heated at reflux for 40 hours under a nitrogen atmosphere. The red precipitate formed was collected and washed with MeOH and hexane and dried to give **3.10b** as a red/purple powder (451 mg, 0.302 mmol, 81%). Found: C, 67.98; H, 5.56. $Ru_2C_{90}H_{86}P_4$ requires: C, 72.37; H, 5.80. IR: ν(C≡C) 2029 cm^{-1}. ^{1}H NMR (C_6D_6, 200 MHz): δ 1.61 (s, 30H, Cp*); 2.168 (m, 8H, CH_2); 7.69-7.18 (m, 48H, Ph, $C_{14}H_8$). $^{31}P\{^1H\}$ NMR ($CDCl_3$, 81 MHz): δ 82.27 (s, dppe). $^{13}C\{^1H\}$ NMR (C_6D_6, 126 MHz): 10.45 (s, C_5Me_5), 29.77 (m, CH_2), 89.26 (C≡), 93.47 (s, C_5Me_5), 99.60(C≡), 123.49-133.60 (arom) ES(+)-MS (*m/z*): 1494[{Ru(dppe)Cp*}$_2$(μ-C≡C$C_{14}H_8$C≡C)].

Chemically oxidised derivatives

The chemically oxidised species **[3.8b][PF_6]$_n$, [3.9b][PF_6]$_n$ and [3.10b][PF_6]$_n$** (n = 1, 2) were prepared by the same general method. A solution of the neutral complex in CH_2Cl_2 was treated with one (in the case of **[3.8b][PF_6]**, **[3.9b][PF_6]** and **[3.10b][PF_6]**) or two (in the case of **[3.8b][PF_6]$_2$**, **[3.9b][PF_6]$_2$** and **[3.10b][PF_6]$_2$**) molar equivalents of $AgPF_6$. The oxidised species were isolated in essentially quantitative yields by precipitation into diethyl ether. The 34 electron bimetallic species **3.8b][PF_6]$_2$**, **[3.9b][PF_6]$_2$** and **[3.10b][PF_6]$_2$** could also be produced by reaction of **[3.8b]PF_6** **[3.9b][PF_6]** and **[3.10b][PF_6]** respectively, with a further equivalent of $AgPF_6$. Authenticity of the samples was confirmed by comparison of their spectroscopic characteristics with those obtained from the electrochemically generated cations.

3.5 References

1 N. Hagihara and K. Sonogashira, *Adv. Poly. Sci.*, 1980, **41**, 149.

2 S. Takahashi, H. Morimoto, E. Murata, S. Kataoka, K. Sonogashira, and N. Hagihara, *J. Polym. Sci., Polym Chem. Ed.*, 1982, **20**, 565.

3 S. Takahashi, Y. Ohyama, E. Murata, K. Sonogashira, and N. Hagihara, *J. Polym. Sci., Polym Chem. Ed.*, 1980, **18**, 349.

4 S. Takahashi, M. Kariya, T. Yatake, K. Sonogashira, and N. Hagihara, *Macromolecules*, 1978, **11**, 1063.

5 N. J. Long and C. K. Williams, *Angew. Chem. Int. Ed.*, 2003, **42**, 2586.

6 N. J. Long, *Angew. Chem. Int. Ed. Engl.*, 1995, **34**, 21.

7 C. E. Powell and M. G. Humphrey, *Coord. Chem. Rev.*, 2004, **248**, 725.

8 I. R. Whittall, A. M. McDonagh, M. G. Humphrey, and M. Samoc, *Adv. Organomet. Chem*, 1999, **43**, 349.

9 I. R. Whittall, A. M. McDonagh, and M. G. Humphrey, *Adv. Organomet. Chem*, 1998, **42**, 291.

10 M. Younus, A. Köhler, S. Cron, N. Chawdhury, M. R. A. Al-Mandhary, M. S. Khan, J. Lewis, N. J. Long, R. H. Friend, and P. R. Raithby, *Angew. Chem. Int. Ed.*, 1998, **37**, 3036.

11 J. Lewis, M. S. Khan, A. K. Kakkar, B. F. G. Johnson, T. B. Marder, H. B. Fyfe, F. Wittmann, R. H. Friend, and A. E. Day, *J. Organomet. Chem.*, 1992, **425**, 165.

12 N. Chawdhury, A. Köhler, R. H. Friend, M. Younus, N. J. Long, P. R. Raithby, and J. Lewis, *Macromolecules*, 1998, **31**, 722.

13 V. W.-W. Yam, K. K. W. Lo, and K. M.-C. Wong, *J. Organomet. Chem.*, 1999, **578**, 3.

14 L. Oriol and J. L. Serrano, *Adv. Mater.*, 1995, **7**, 348.

15 D. W. Bruce, M. S. Lea, and J. R. Marsden, *Mol. Cryst. Liq. Cryst. Sci. Technol., Sect. A*, 1996, **275**, 183.

16 J. L. Serrano, 'Metallomesogens: Synthesis, Properties and Applications', ed. J. L. Serrano, Wiley, 1996.

17 D. W. Bruce, 'Inorganic Materials', ed. D. W. Bruce and D. O'Hare, Wiley, 1996.

18 M. S. Khan, S. J. Davies, A. K. Kakkar, D. Schwartz, B. Lin, B. F. G. Johnson, and J. Lewis, *J. Organomet. Chem.*, 1992, **424**, 87.

19 R. P. Kingsborough and T. M. Swager, *Prog. Inorg. Chem.*, 1999, **48**, 123.

20 H. B. Fyfe, M. Mlekuz, D. Zargarian, N. J. Taylor, and T. B. Marder, *J. Chem. Soc., Chem. Commun.*, 1991, 188.

21 S. J. Davies, B. F. G. Johnson, M. S. Khan, and J. Lewis, *J. Chem. Soc., Chem. Commun.*, 1991, 187.

22 M. S. Khan, A. K. Kakkar, S. L. Ingham, P. R. Raithby, J. Lewis, B. Spencer, F. Wittmann, and R. H. Friend, *J. Organomet. Chem.*, 1994, **472**, 247.

23 Z. Atherton, C. W. Faulkner, S. L. Ingham, A. K. Kakkar, M. S. Khan, J. Lewis, N. J. Long, and P. R. Raithby, *J. Organomet. Chem.*, 1993, **462**, 265.

24 M. S. Khan, M. R. A. Al-Mandhary, M. K. Al-Suti, A. K. Hisahm, P. R. Raithby, B. Ahrens, M. F. Mahon, L. Male, E. A. Marseglia, E. Tedesco, R. H. Friend, A. Köhler, N. Feeder, and S. J. Teat, *J. Chem. Soc., Dalton Trans.*, 2002, 1358.

25 M. S. Khan, M. R. A. Al-Mandhary, M. K. Al-Suti, T. C. Corcoran, J. P. Attfield, N. Feeder, W. I. F. David, K. Shankland, R. H. Friend, A. Köhler, E. A. Marseglia, E. Tedesco, C. C. Tang, P. R. Raithby, J. C. Collings, K. P. Roscoe, A. S. Batsanov, L. M. Stimson, and T. B. Marder, *New J. Chem.*, 2003, **27**, 140.

26 M. S. Khan, M. K. Al-Suti, M. R. A. Al-Mandhary, B. Ahrens, J. K. Bjernemose, M. F. Mahon, L. Male, P. R. Raithby, R. H. Friend, A. Köhler, and J. S. Wilson, *Dalton Trans.*, 2003, 65.

27 M. S. Khan, M. R. A. Al-Mandhary, M. K. Al-Suti, P. R. Raithby, B. Ahrens, M. F. Mahon, L. Male, C. E. Boothby, and A. Köhler, *Dalton Trans.*, 2003, 74.

28 M. S. Khan, M. R. A. Al-Mandhary, M. K. Al-Suti, N. Feeder, S. Nahar, A. Köhler, R. H. Friend, P. J. Wilson, and P. R. Raithby, *J. Chem. Soc., Dalton Trans.*, 2002, 2441.

29 A. E. Dray, F. Wittmann, R. H. Friend, A. M. Donald, M. S. Khan, J. Lewis, and B. F. G. Johnson, *Synth. Met.*, 1991, **41-43**, 871.

30 A. Köhler, M. Younus, M. R. A. Al-Mandhary, P. R. Raithby, M. S. Khan, and R. H. Friend, *Synth. Met.*, 1999, **101**, 246.

31 A. Köhler, J. S. Wilson, R. H. Friend, M. K. Al-Suti, M. S. Khan, A. Gerhard, and H. Bassler, *J. Chem. Phys.*, 2002, **116**, 9457.

32 M. S. Khan, M. R. A. Al-Mandhary, M. K. Al-Suti, F. R. Al-Battashi, S. Al-Saadi, B. Ahrens, J. K. Bjernemose, M. F. Mahon, P. R. Raithby, M. Younus, N. Chawdhury, A. Köhler, E. A. Marseglia, E. Tedesco, N. Feeder, and S. J. Teat, *Dalton Trans.*, 2004, 2377.

33 P. J. Low, R. L. Roberts, R. L. Cordiner, and F. Hartl, *J. Solid State Electrochem.*, 2005, in press.

34 N. Le Narvor and C. Lapinte, *Organometallics*, 1995, **14**, 634.

35 S. Le Stang, F. Paul, and C. Lapinte, *Organometallics*, 2000, **19**, 1035.

36 F. de Montigny, G. Argouarch, K. Costuas, J. F. Halet, T. Roisnel, L. Toupet, and C. Lapinte, *Organometallics*, 2005, **24**, 4558.

37 F. Coat and C. Lapinte, *Organometallics*, 1996, **15**, 477.

38 M. I. Bruce and A. G. Swincer, *Adv. Organomet. Chem*, 1983, **22**, 59.

39 M. I. Bruce, *Chem. Rev.*, 1991, **91**, 197.

40 P. J. Low and M. I. Bruce, *Adv. Organomet. Chem*, 2001, **48**, 71.

41 M. I. Bruce, C. Hameister, A. G. Swincer, and R. C. Wallis, *Inorg. Synth.*, 1982, **21**, 78.

42 C. Bitcon and M. W. Whiteley, *J. Organomet. Chem.*, 1987, **336**, 385.

43 M. I. Bruce and R. C. Wallis, *Aust. J. Chem.*, 1979, **32**, 1471.

44 M. I. Bruce, B. C. Hall, B. D. Kelly, P. J. Low, B. W. Skelton, and A. H. White, *J. Chem. Soc., Dalton Trans.*, 1999, 3719.

45 O. F. Koentjoro, R. Rousseau, and P. J. Low, *Organometallics*, 2001, **20**, 4502.

46 D. L. Lichtenberger, S. K. Renshaw, and R. M. Bullock, *J. Am. Chem. Soc.*, 1993, **115**, 3276.

47 J. E. McGrady, T. Lovell, R. Stranger, and M. G. Humphrey, *Organometallics*, 1997, **16**, 4004.

48 M. I. Bruce, B. G. Ellis, P. J. Low, B. W. Skelton, and A. H. White, *Organometallics*, 2003, **22**, 3184.

49 R. Denis, L. Toupet, and F. Paul, *Organometallics*, 2000, **19**, 4240.

50 T. Shida, 'Electronic Absorption Spectra of Radical Ions', Elsevier, 1988.

51 B. Badger and B. Brocklehurst, *Trans. Farady Soc.*, 1970, **66**, 2939.

52 M. I. Bruce, K. Costuas, T. Davin, B. G. Ellis, J. F. Halet, C. Lapinte, P. J. Low, M. E. Smith, B. W. Skelton, L. Toupet, and A. H. White, *Organometallics*, 2005, **24**, 3864.

53 K. D. Demadis, C. M. Hartshorn, and T. J. Meyer, *Chem. Rev.*, 2001, **101**, 2655.

54 B. Le Guennic, Ph.D thesis, Université de Rennes 1.

55 M. I. Bruce, P. Hinterding, E. R. T. Tiekink, B. E. Skelton, and A. H. White, *J. Organomet. Chem.*, 1993, **450**, 209.

56 R. L. Cordiner, D. Albesa-Jove, R. L. Roberts, J. D. Farmer, H. Puschmann, D. Corcoran, A. E. Goeta, J. A. K. Howard, and P. J. Low, *J. Organomet. Chem.*, 2005, **690**, 4908.

57 T. Mahabiersing, H. Luyten, R. Nieuwendam, and F. Hartl, *Collect. Czech. Chem. Commun.*, 2003, **68**, 1687.

58 F. Hartl, H. Luyten, H. A. Nieuwenhuis, and G. C. Schoemaker, *Appl. Spectr*, 1994, **48**, 1522.

59 C. M. Duff and G. A. Heath, *Inorg. Chem.*, 1991, **30**, 2528.

60 S. Takahashi, Y. Kuroyama, K. Sonogashira, and N. Hagihara, *Synthesis*, 1980, 627.

61 D. P. Lydon, L. Porres, A. Beeby, T. B. Marder, and P. J. Low, *New J. Chem.*, 2005, **29**, 972.

Chapter 4

4.1 Introduction

The cage of icosahedral *para*-carborane 1,12-$C_2B_{10}H_{12}$ is robust in terms of high thermal and chemical stabilities, only degrading under extreme basic conditions,[1, 2] the robustness of the cage being largely attributed to its much discussed 'three-dimensional aromaticity'.[3-7] This 'three-dimensional aromaticity' has drawn comparisons between carboranyl and phenylene bridges and has prompted several recent investigations of interactions between various organic and metal centres that might be mediated by these carboranyl cages.[8-12] Comparisons of NMR characteristics have been utilised in assessing these interactions as the chemical shift of the nuclei are sensitive to the local magnetic (and hence electronic) environment.[8] Electrochemical properties have also been employed, and when used in conjunction with other techniques have provided an insight into the nature of these interactions.

For example, the electronic properties of the cobalt cluster complex 1,12-$\{Co_2C_2(SiMe_3)(CO)_4(\mu\text{-dppm})\}_2$(1,12-$C_2B_{10}H_{10}$), **4.4**, **Figure 4.2**, were assessed by a combination of structural, electrochemical and computational methods. Electrochemical studies, using both CV and differential pulse methods, revealed two sequential oxidation processes and two sequential reduction processes separated by 105 mV and 80 mV, respectively.[13] These redox processes were qualitatively similar to those of an analogous 1,4-C_6H_4-bridged species,[14] however DFT analysis of the radical cations revealed a different underlying electronic structure in each case. The SOMO of the aryl-bridged species featured considerable aryl π-character, while the SOMO of the carborane-spaced species was essentially localised on the Co_2C_2 clusters. It was concluded that the carborane cluster cage acts as a more or less purely σ-bridge and that electronic interactions between the redox-active Co_2C_2 clusters are mediated by the σ-framework of the carborane cage.[13, 15]

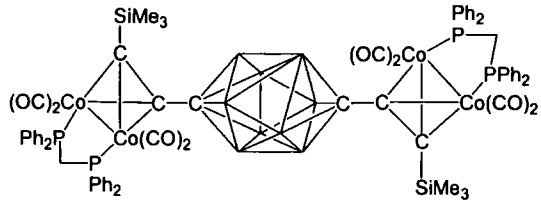

Figure 4.2 The complex 1,12-{$Co_2C_2(SiMe_3)(CO)_4(\mu$-dppm)}$_2$(1,12-$C_2B_{10}H_{10}$), **4.4**

The recent preparation of 1,12-diethynyl carborane has prompted consideration of this three dimensional aromatic analogue of 1,4-diethynyl benzene as a bridging ligand. Whilst the electronic properties of complexes in which 1,4-diethynyl benzene has been utilised as a bridging ligand, between redox active metal centres, have been well explored (see Chapter 1, Chapter 3), less is known about the 1,12-diethynyl carborane spacer as a conduit for electronic delocalisation.

The cyclic voltammetric response of the *para*-carborane complexes 1,10-{$Fe(CO)_2Cp$}$_2$(1,10-$C_2B_8H_8$), **4.1**, and 1,12-{$Fe(CO)_2Cp$}$_2$(1,12-$C_2B_{10}H_{10}$), **4.2** (**Figure 4.1**), were both characterised by distinct oxidation events associated with each $Fe(CO)_2Cp$ group, which was taken by the authors as being suggestive of a degree of interaction between the metal centres.[16, 17] However, the electrochemical response of the corresponding diethynyl complex 1,12-{$Cp(CO)_2FeC{\equiv}C$}$_2$(1,12-$C_2B_{10}H_{10}$), **4.3** (**Figure 4.1**) formed from sequential reaction of 1,12-diethynyl-1,12-$C_2B_{10}H_{10}$ with ^{n}BuLi and $FeCl(CO)_2Cp$, was characterised by an apparently single oxidation event. This observation was attributed to the poor π-orbital overlap of the ethynyl moieties with the carboranyl carbon p-orbital,[11, 17] but whilst chemically sensible the electrochemical data alone cannot support this hypothesis.

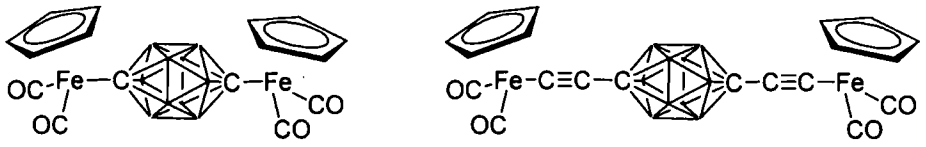

Figure 4.1 The carboranyl-bridged species 1,12-{$Fe(CO)_2Cp$}$_2$(1,12-$C_2B_{10}H_{10}$), **4.2** and 1,12-{$Cp(CO)_2FeC{\equiv}C$}$_2$(1,12-$C_2B_{10}H_{10}$), **4.3**.

Further to these studies and as an extension of the work presented in Chapter 3, the ruthenium-containing complexes $Ru(C{\equiv}C\text{-}CB_{10}H_{10}CH)(dppe)Cp^*$, **4.5**, and 1,12-{$Ru(dppe)Cp^*$}$_2$($\mu$-$C{\equiv}C\text{-}CB_{10}H_{10}C\text{-}C{\equiv}C$), **4.6**, were prepared and their electronic properties evaluated. The work described in Chapter 3 and Chapter 4 allows direct comparison of the properties of carboranyl and phenyl moieties as 'spacers' in bridging diethynyl ligands to be made.

4.2 Results and Discussion

The *in situ* metallation / desilylation methodology described for the synthesis of complexes **3.7-3.10** was employed in the production of **4.5** and **4.6**. Accordingly, reaction of RuCl(dppe)Cp* with $Me_3SiC{\equiv}C\text{-}CB_{10}H_{10}CH$, or $Me_3SiC{\equiv}C\text{-}CB_{10}H_{10}C\text{-}C{\equiv}CSiMe_3$, and catalytic quantities of KF in MeOH afforded the yellow complexes **4.5** and **4.6** in moderate or good yield (**Scheme 4.1**).

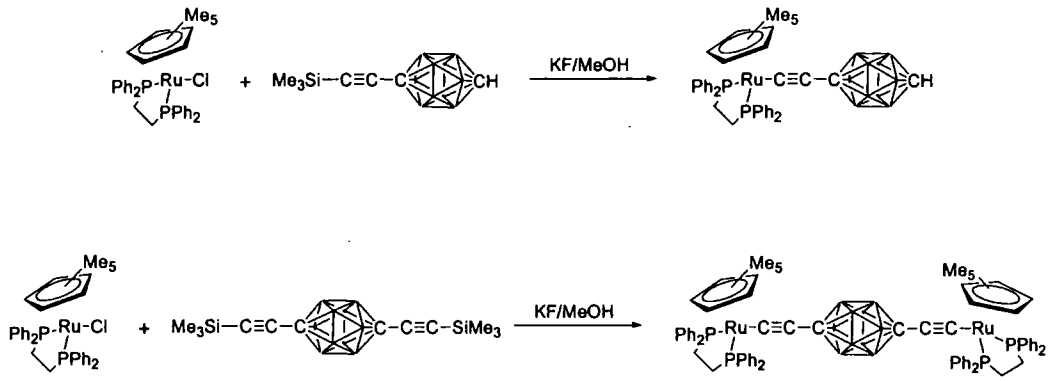

Scheme 4.1 Preparation of $Ru(C{\equiv}C\text{-}CB_{10}H_{10}CH)(dppe)Cp^*$, **4.5**, and 1,12-$\{Ru(dppe)Cp^*\}_2(\mu\text{-}C{\equiv}C\text{-}CB_{10}H_{10}C\text{-}C{\equiv}C)$, **4.6**, *via* an *in situ* metallation / desilylation reaction.

Both complexes were characterised by the usual spectroscopic methods (**Table 4.1**). The ^1H NMR spectra contained overlapping resonances from the aromatic protons of the phosphine phenyl groups. In addition, resonances due to the Cp* ligands were observed at δ 1.45 and 1.49 for **4.5** and **4.6** respectively, and the resonances corresponding to the BH protons at δ 2.00 and 2.30 in **4.5** and 2.11 for **4.6**. For both complexes the ^{31}P NMR spectra were characterised by a single resonance (δ 81.6) at similar chemical shifts to those observed for the related aryl-bridged complexes

(**Table 3.1**). The ^{11}B NMR spectrum of **4.5** displayed two doublets at δ -11.1 and -16.3 ppm corresponding to the boron atoms adjacent to the C-C≡C moiety and those adjacent to the CH apex respectively. By contrast, the ^{11}B NMR spectrum of **4.6** was characterised by a single doublet at -12.4 ppm (**Table 4.1**).

Table 4.1 Selected spectroscopic data for complexes **4.5** and **4.6**

	δ_H Cp* (ppm)[b]	δ_c C_α/C_β (ppm)[c]	δ_p dppe (ppm)[d]	δ_B BH (ppm)[e]	ES(+)-MS
4.5	1.45	[a]	81.6	-11.1, -16.3	802
4.6	1.49	98.68/104.58	81.6	-12.4	1460

[a] not observed. [b] $CDCl_3$, 200 MHz. [c] $CDCl_3$, 126 MHz. [d] $CDCl_3$, 81 MHz. [e] $CDCl_3$, 128 MHz. Details in Experimental Details section.

Coordination of the metal fragments results in a decrease of *ca.* 100 cm^{-1} in the ν(C≡C) frequency, relative to the trimethylsilyl-protected alkyne [ν(C≡C) 2178 cm^{-1}].[12] As observed for the aryl analogues, the IR spectra of the mono- and bi-metallic complexes are very similar, displaying ν(C≡C) bands at 2082 cm^{-1}, this being higher in energy than in any of the complexes **3.5b-3.10b**. A strong ν(BH) band was also observed at 2605 and 2600 cm^{-1} in **4.5** and **4.6**, respectively.

Electrochemical Studies

The electrochemical response of **4.5** was characterised by a single oxidation event at 0.37 V (**Table 4.2**), this being less thermodynamically favourable than the oxidation processes in the related aryl systems, **3.5b-3.7b**.

The cyclic voltammogram of the bimetallic complex **4.6** displayed two reversible, sequential oxidation processes (E_1 and E_2) with a value of $\Delta E = E_2-E_1$ of 100 mV, and correspondingly a value for K_c of 45. Both the first and second oxidation processes were less thermodynamically favourable than all of the aryl-bridged derivatives.

In contrast to the trend observed for the aryl systems in Chapter 3, the first oxidation potential of the binuclear species is slightly higher (15 mV) than the oxidation potential of the corresponding mononuclear model.

Table 4.2 Electrochemical data for **4.5** and **4.6**

	E_1/V	E_2/V	ΔE/mV	K_c
4.5	0.37			
4.6	0.38	0.48	100	45

Spectroelectrochemical Studies

Again, in order to probe the effect of oxidation on the physical and electronic structure of these carborane-bridged species, a series of spectroelectrochemical experiments were undertaken covering the UV-vis-NIR and IR regions of the spectrum. Electrochemical oxidation of the monometallic species **4.5** was fully chemically reversible within the IR spectroelectrochemical cell, as evidenced by the recovery of the original spectrum upon back reduction. The IR spectrum of the neutral derivative was characterised by a single ν(C≡C) band at 2082 cm^{-1} and a band at 2605 cm^{-1} due to the BH bonds of the carborane cage. Oxidation to the 17-electron monocation, $[\mathbf{4.5}]^+$, resulted in a shift to lower energy of the ν(C≡C) band (2014 cm^{-1}) with an accompanying decrease in intensity (**Figure 4.3, Table 4.3**). In contrast, the BH band displays a shift to slightly higher energy, consistent with a slight reduction in electron density in the carborane cage.

Table 4.3 Infra-red data, ν(C≡C) / ν(BH), for $[\mathbf{4.5}]^{n+}$ and $[\mathbf{4.6}]^{n+}$

	n		
	0	**1**	**2**
4.5 ν(C≡C) / ν(BH)	2082 / 2605	2014 / 2614	
4.6 ν(C≡C) / ν(BH)	2082 / 2602	2074, 2002 / 2609	2012 / 2617

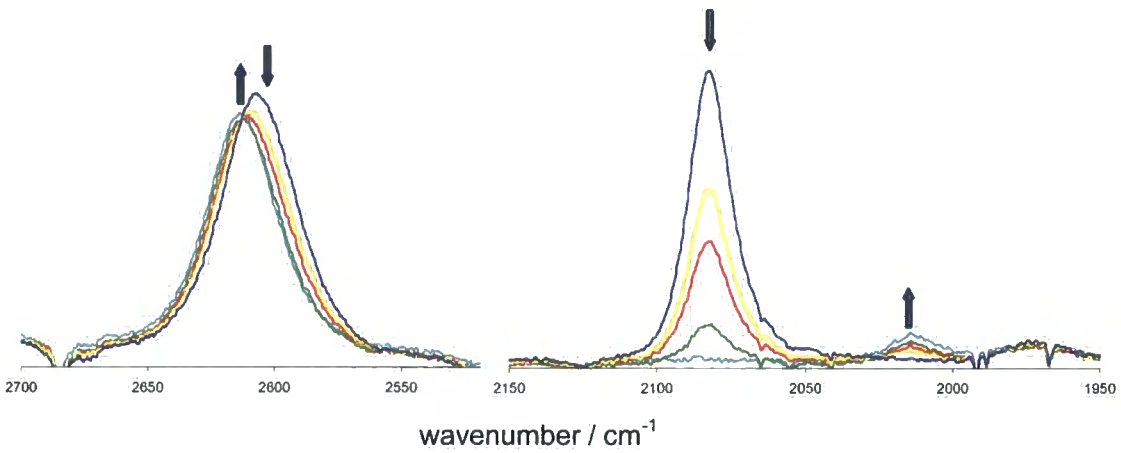

Figure 4.3 Infra-red spectra obtained in the ν(BH) and ν(C≡C) regions upon oxidation of the monometallic complex **4.5** → $[\mathbf{4.5}]^{+}$

The bimetallic species **4.6** also displayed reversible behaviour upon electrochemical oxidation in the IR spectroelectrochemical cell, with the original spectrum being recovered on back reduction of both the mono and dicationic derivatives. The neutral species was characterised by a single ν(C≡C) stretch at the same energy as that observed in **4.5** and a ν(BH) band at 2602 cm^{-1}. Oxidation to the monocation was accompanied by the appearance of two distinct bands in the ν(C≡C) region of the spectrum and a concomitant shift in the ν(BH) band of *ca.* 7 cm^{-1} to higher energy

(**Figure 4.4**). The most intense band in the ν(C≡C) region of the spectrum was of comparable intensity to that of the single band observed in the neutral species and was slightly lower in energy (*ca.* 8 cm^{-1}), a second, less intense band was also observed at 2002 cm^{-1}. Further oxidation to $[\mathbf{4.6}]^{2+}$ was accompanied by a further shift to higher energy of the ν(BH) band and the appearance of only a single, weak ν(C≡C) band, at 2012 cm^{-1}, of very similar energy to that observed in $[\mathbf{4.5}]^{+}$ (**Figure 4.5**).

The changes in IR spectra upon oxidation are consistent with largely isolated metal centres and little or no involvement of the carborane cage in the redox active HOMO. The presence of only a single ν(C≡C) band in the neutral and dicationic derivatives is indicative of the identical oxidation states on each metal centre, and hence the identical environment of each C≡C bond. However, in the monocation two bands are observed, the strongest of which is of similar intensity and position to that observed in the neutral species and the weakest of which is similar in position and intensity to that of the band observed in the dication. This suggests two distinct C≡C environments as a result of differing oxidation states of the metal centres, i.e. localisation of the unpaired electron on the IR timescale. By comparison with the monometallic model complexes $[\mathbf{4.5}]^{n+}$, the monocation $[\mathbf{4.6}]^{+}$ may therefore befit a description of consisting of two distinct halves, one of which is analogous to **4.5** and the second to $[\mathbf{4.5}]^{+}$.

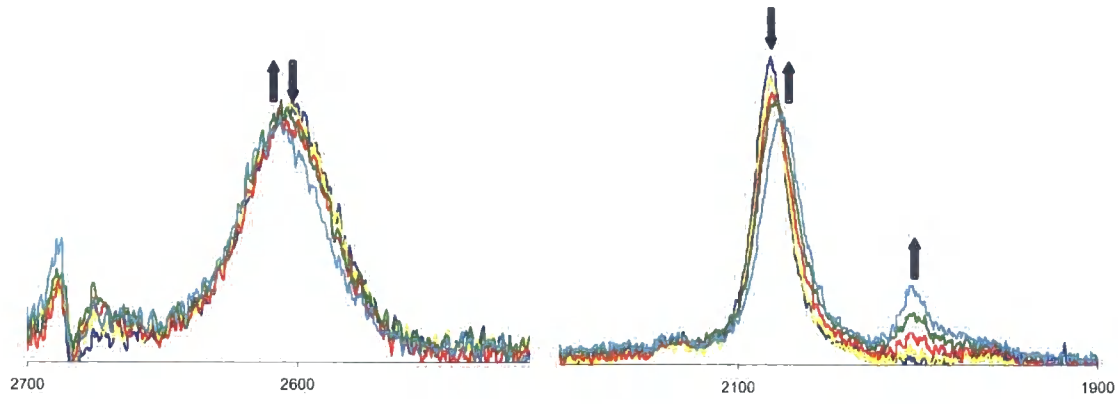

Figure 4.4 Infra-red spectra obtained in the ν(BH) and ν(C≡C) regions upon oxidation of **4.6** → $[\mathbf{4.6}]^{+}$.

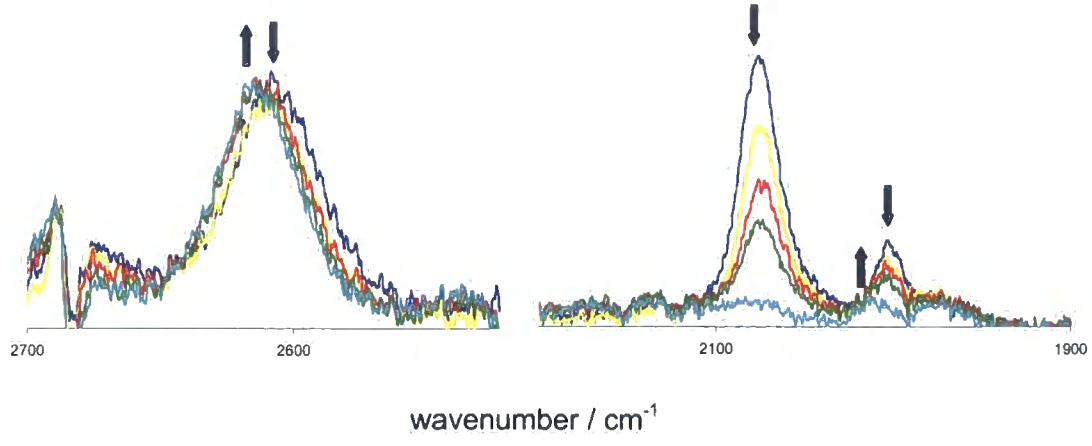

Figure 4.5 Infra-red spectra obtained in the ν(BH) and ν(C≡C) regions upon oxidation of $[\mathbf{4.6}]^{+}$ → $[\mathbf{4.6}]^{2+}$.

Spectroelectrochemical studies of the electronic spectra in the UV-vis NIR region were also undertaken. The electronic spectra of **4.5** was characterised by an intense band at 43500 cm^{-1} with shoulders at 36900 and 30800 cm^{-1}. Oxidation to the 17-electron species $[\mathbf{4.5}]^{+}$ resulted in only a subtle shift in the shape of these bands.

The bimetallic species **4.6** displayed a similar spectral profile to **4.5** with a broad band observed at 37000 cm^{-1}. On oxidation to $[\mathbf{4.6}]^+$ a change in the shape of this band and a shift to slightly higher energy (38500 cm^{-1}) was observed, accompanied by the appearance of two further bands in the visible region at 19600 and 15400 cm^{-1} respectively. In addition to the changes in the UV-vis region, $[\mathbf{4.6}]^+$ exhibited a series of overlapping absorptions in the NIR region (**Figure 4.6**). In a similar manner to the aryl systems **3.8-3.10b** this band envelope could be deconvoluted to give three Gaussian-shaped curves (**Figure 4.7**, *vide infra*).

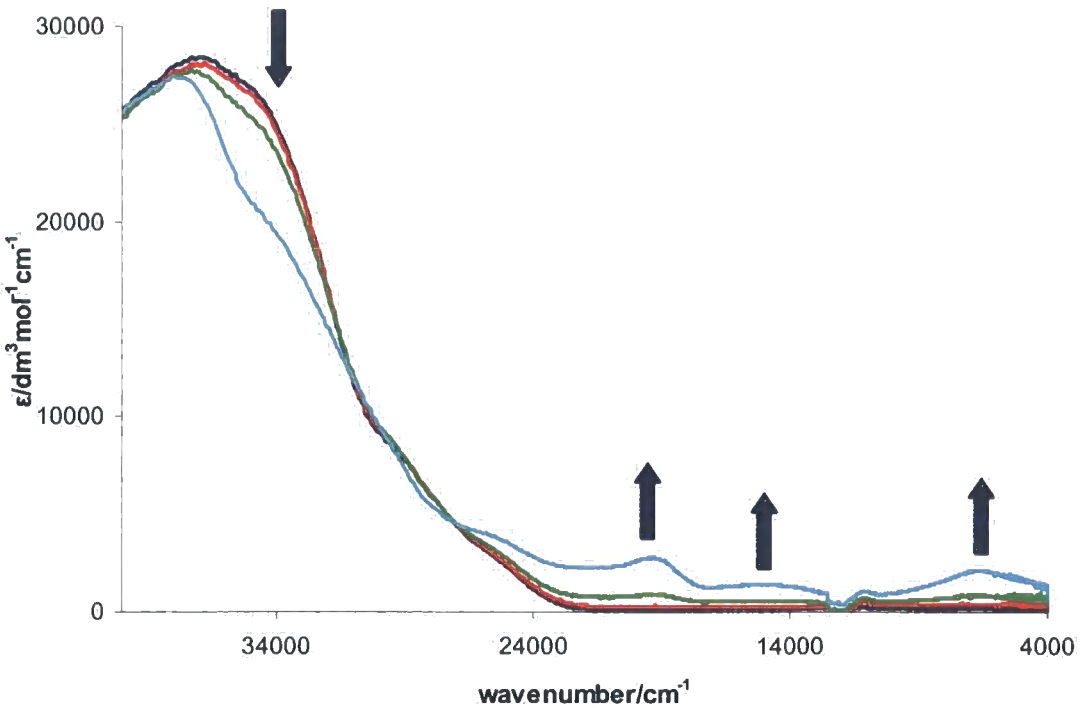

Figure 4.6 UV-vis-NIR spectra obtained upon oxidation of **4.6** → $[\mathbf{4.6}]^+$.

On further oxidation to the dication the highest energy band was shifted to 34500 cm^{-1}, and the bands at 19600 and 15400 cm^{-1} that were present in $[\mathbf{4.6}]^+$, were also shifted to slightly lower energy (19200 and 14900 cm^{-1}, respectively). In addition, collapse of the bands in the NIR region of the spectrum was observed.

The results of the deconvolution applied to the NIR region of the electronic spectrum of $[\mathbf{4.6}]^+$ are illustrated in **Figure 4.7**. As for the aryl-bridged systems, $[\mathbf{3.8b}]^+$-$[\mathbf{3.10b}]^+$, the NIR absorption envelope could be deconvoluted into three Gaussian-shaped bands. The individual curves were treated according to Hush theory for Class II systems and the observed and calculated (Equation 1.5) band widths at half height are reported in **Table 4.4**.

$$\Delta\bar{\nu}_{1/2} = (2310\bar{\nu}_{max})^{1/2} \qquad \textbf{Equation 1.5}$$

Table 4.4. Parameters associated with the Gaussian-shaped bands obtained from deconvolution of the NIR region of $[\mathbf{4.6}]^+$

Band	$\bar{\nu}_{max}$/cm^{-1}	$\bar{\nu}_{1/2}$ obs/cm^{-1}	$\bar{\nu}_{1/2}$ calc/cm^{-1}
1	5426	2202	3540
2	6978	1676	4015
3	8410	2018	4408

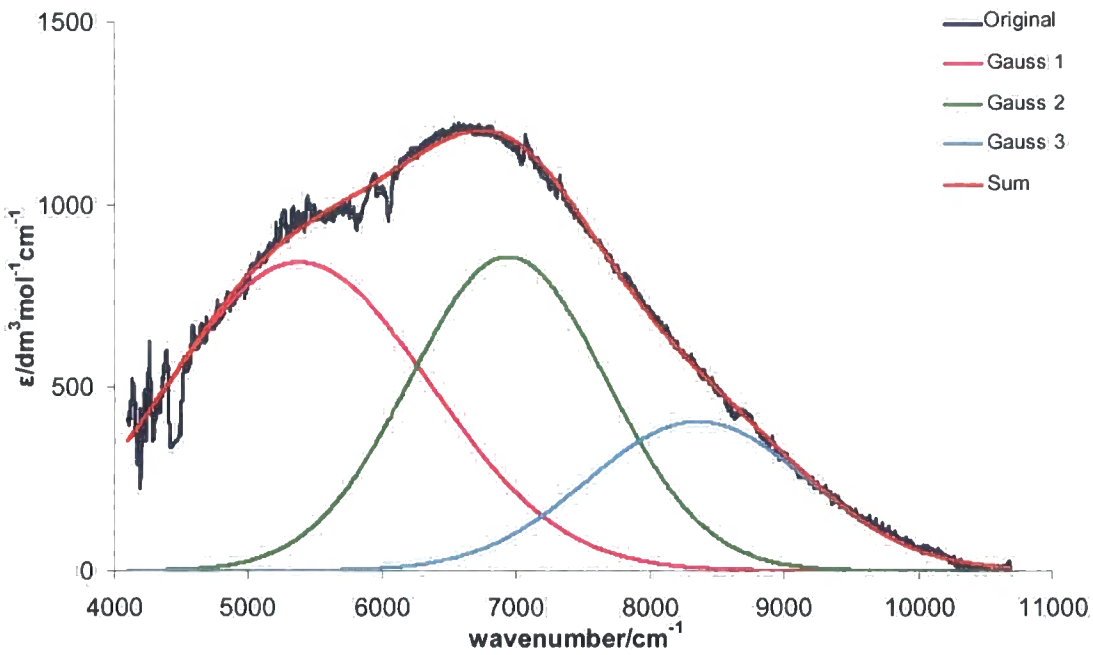

Figure 4.7 Deconvolution of the NIR region of the electronic spectra of $[\mathbf{4.6}]^{+}$ into the three Gaussian-shaped curves that may be obtained

As discussed in Chapter 1, the observation of multiple NIR transitions in mixed-valence systems that display low local symmetry at the organometallic termini, is not uncommon, and the validity of applying Hush-type analysis in extensively delocalised systems is a subject for debate. Values for V_{ab} of 2700, 3500 and 4200 cm^{-1} for bands 1, 2 and 3 respectively, can be obtained by Equation 1.6 if Class III behaviour is assumed. Alternatively, assuming Class II behaviour, and using Equation 1.4, gives values of 170, 160 and 140 cm^{-1} (using the Ru-Ru separation obtained from DFT optimised geometries as the approximate charge transfer distance, *vide infra*). In order to rationalise the experimental results obtained for $[\mathbf{4.6}]^{n+}$ in terms of the electronic structure of the complexes, DFT calculations were performed on model complexes.

Theoretical Studies

DFT level calculations were performed on the model complex $[\{Ru(PH_3)_2Cp\}_2(\mu\text{-}C{\equiv}CCB_{10}H_{10}C{\equiv}C)]^{n+}$ **[4.6-H]**$^{n+}$, **Figure 4.8**, with C_{2h} symmetry imposed,[†] after initial optimisation and energy minimisation steps, in order to minimise computational effort.[18] The optimised structure (**Table 4.5**) fits well with the determined structures of other acetylide complexes of the type Ru(C≡CR)(PP)Cp',[19-21] diethynyl carboranes,[12] and diethynyl carborane-bridged metal complexes,[22, 23] giving a high degree of confidence in the accuracy of the results that may be drawn from them.

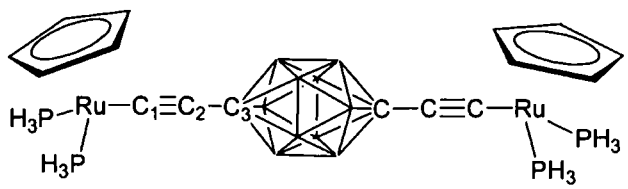

Figure 4.8 The model complex $[\{Ru(PH_3)_2Cp\}_2(\mu\text{-}C{\equiv}CC_6H_4C{\equiv}C)]$, **[4.6-H]**, showing labelling scheme.

Table 4.5 Bond lengths (Å) obtained from the optimised structures of **[4.6-H]**$^{n+}$.

	[4.6-H]	**[4.6-H]$^{+}$**	**[4.6-H]$^{2+}$ (LS)**	**[4.6-H]$^{2+}$ (HS)**
Ru-C(1)	2.029	1.984	1.970	1.963
C(1)-C(2)	1.233	1.242	1.252	1.248
C(2)-C(3)	1.438	1.428	1.427	1.434
C(3)-B[a]	1.732	1.728	1.730	1.725
B-B'[a]	1.773[b]/1.760[c]	1.780/1.757	1.784/1.756	1.785/1.755
Ru-P	2.294	2.318	2.340	2.341

[a] average distances [b] distances between boron atoms bonded to the same carbon atom [c] B-B intra-cluster distances

[†] Symmetry restrictions were imposed in order to minimise computational effort. Studies on similar systems with and without such constraints indicate little difference in the final solution.

The MO diagram illustrated in **Figure 4.9** demonstrates the large energy separation (2.219 eV) between the HOMO and LUMO. An analysis of the energies and composition of the MOs of the neutral species allows information on the structural changes that occur upon oxidation of **[4.6-H]** to $[\mathbf{4.6\text{-}H}]^{n+}$ to be obtained. The composition of the frontier orbitals are presented in **Table 4.6**.

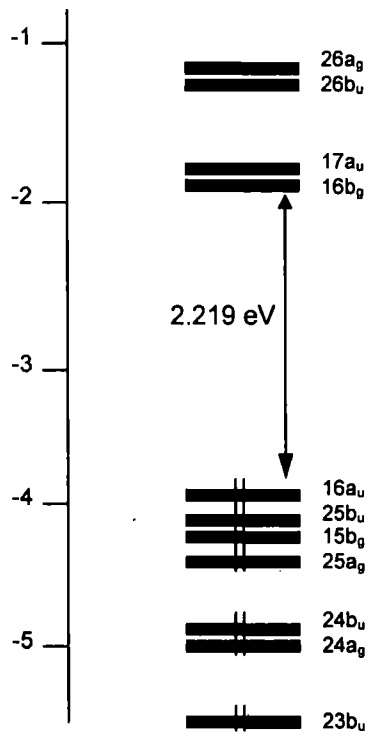

Figure 4.9 Molecular orbital diagram obtained from DFT calculations on **[4.6-H]**

Table 4.6 Energy (ε/eV), occupation and localisation (%) of the MOs in the HOMO-LUMO region of **[4.6-H]**

	$17a_u$	$16b_g$	$16a_u$	$25b_u$	$15b_g$	$25a_g$	$24b_u$	$24a_g$
ε	-1.89	-1.89	-4.11	-4.27	-4.33	-4.50	-4.98	-5.04
Occ	0	0	2	2	2	2	2	2
C(1)	0	0	16	19	8	10	9	9
C(2)	0	0	30	29	27	23	7	11
C(3)	0	0	0	0	2	1	0	0
B	0	0	3	3	4	1	0	0
H_{BH}	0	0	0	0	0	0	0	0
Ru	44	44	43	44	47	55	45	47
PH_3	32	32	2	3	4	5	16	15
Cp	24	24	6	2	8	5	23	18

The HOMO and HOMO-1 from the model system are shown in **Figure 4.10** and are clearly derived from the orthogonal d-π systems of the metal centres and C≡C moieties. The HOMO is localised primarily on the Ru-C≡C fragments with a contribution of 43, 16 and 30% on Ru, C(1) and C(2) respectively. The HOMO-1 level is characterised in much the same way with contributions of 44, 19 and 29 % on Ru, C(1) and C(2) respectively in this case. It can be seen in **Figure 4.10** that the HOMO and HOMO-1 are antibonding in character with respect to Ru-C(1), bonding with respect to C(1)-C(2) and display essentially no contribution from the atoms of the carborane fragment. The structural changes that occur on oxidation are readily interpreted in terms of the localisation and nodal properties of these orbitals which do not differ significantly in the mono- and di-cation.

Comparison of the structures of **4.6-H** and $[\mathbf{4.6\text{-}H}]^+$ reveal a significant contraction of the Ru-C(1) bond length and an accompanying elongation of the C(1)-C(2) bond on reduction of the electron count by one, with much smaller changes observed within the cage itself. In the case of the doubly oxidised species $[\mathbf{4.6\text{-}H}]^{2+}$ the similar geometries of the low spin $[(25b_u)^2\ (16a_u)^0]$ and high spin $[(25b_u)^1\ (16a_u)^1]$ electronic

configurations arise from the similar nodal properties of the $16a_u$ and $25b_u$ orbitals. In contrast to the phenylene system the high spin triplet state is calculated to be more stable (2.61 eV) than the low spin state.

The contribution of backbonding interactions to the Ru-P bond makes this bond length a sensitive probe of the electronic environment around the metal centre.[24] In $[\mathbf{4.6\text{-}H}]^{n+}$ the Ru-P bond lengths become progressively longer as the electron count of the complex is reduced, consistent with the involvement of the metal centre in the redox processes being modelled and hence the redox-active orbital.

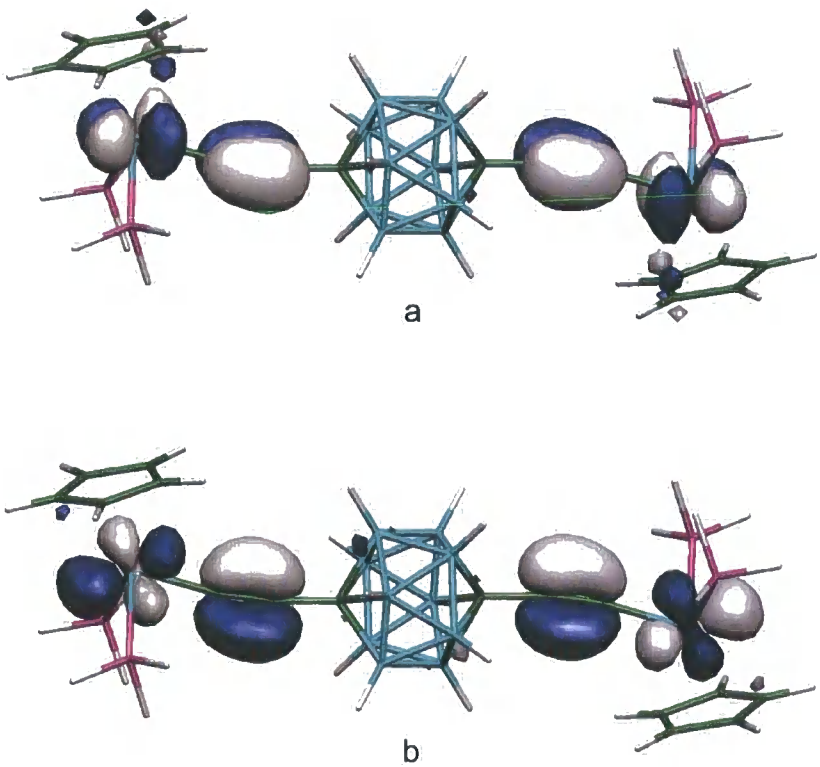

Figure 4.10 The HOMO (**a**) and HOMO-1 (**b**) of [**4.6-H**] calculated for $[Ru(PH_3)_2Cp]_2(\mu\text{-}C{\equiv}CCB_{10}H_{10}CC{\equiv}C)$. Contour values are ± 0.03 $[e/bohr^3]^{1/2}$

4.3 Conclusion

The changes in structure observed at the metal and in certain fragments of the bridging ligand clearly indicate that in contrast to the phenylene system, oxidation of **4.6-H** does not affect the entire Ru-bridge-Ru assembly. On the basis of the results obtained from DFT calculations, it can be concluded that the carborane has limited involvement in the redox-active orbital. On the basis of the IR and UV-vis-NIR spectroscopic data, $[\mathbf{4.6}]^{+}$ may be described as a weakly-coupled Class II 'mixed-valence' compound, however given the appreciable contribution of the C≡C fragments to the redox active orbitals, and the extensive mixing of the metal d and C≡C π orbitals the appropriateness of the term 'mixed-valence' in the description of this system can be debated.

4.4 Experimental Details

General conditions.

All reactions were carried out in oven-dried glassware under dry nitrogen as a matter of routine. NMR spectra were recorded on a Bruker Avance 400, Varian VXR-200 or Inova 500 spectrometer and referenced against solvent resonances. IR spectra were recorded on a Nicolet Avatar spectrophotometer as solutions using solution cells fitted with CaF_2 windows.

Instrumentation.

Cyclic voltammograms were recorded with an Eco Chemie Autolab PGstat controlled by a PC running GPES v.4.9 for Windows. The electrochemical cell used was an EG & PARC micro cell fitted with a nitrogen feed. Ferrocene or decamethylferrocene were used as internal calibrant [$E_{1/2}(FeCp_2/[FeCp_2]^+)$ = +0.46 V vs SCE in CH_2Cl_2; $E_{1/2}(FeCp^*_2/[FeCp^*_2]^+$ = -0.02 V vs SCE in CH_2Cl_2]. The IR spectroelectrochemical experiments were performed with a previously described OTTLE cell positioned in the sample compartment of a Nicolet Avatar spectrometer,[25, 26] from CH_2Cl_2 solutions containing 1 x 10^{-1} M $[NBu_4]BF_4$ as the supporting electrolyte. The UV-Vis-NIR spectroelectrochemical measurements were conducted using an OTE cell similar to that described previously,[27] from CH_2Cl_2 solutions containing 1 x 10^{-1} M $[NBu_4]BF_4$ as supporting electrolyte.

The compounds $Me_3SiC{\equiv}C\text{-}CB_{10}H_{10}CH$,[28] and $Me_3SiC{\equiv}C\text{-}CB_{10}H_{10}C\text{-}C{\equiv}CSiMe_3$[12] were prepared by literature routes. Other reagents were purchased and used as received. Solvents were dried and deoxygenated using an Innovative Technologies Solvent Purification System, and de-gassed prior to use.

$Ru(C{\equiv}CC_2B_{10}H_{11})(dppe)Cp^*$ (4.5)

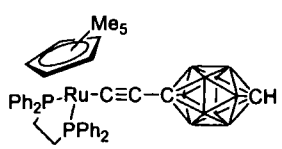

A suspension of RuCl(dppe)Cp* (160 mg, 0.224 mmol), $Me_3SiC{\equiv}CC_2B_{10}H_{11}$ (60 mg, 0.249 mmol), and KF (25 mg, 0.431 mmol) in methanol (20 ml) was heated at

reflux for 1 hour under a nitrogen atmosphere. The yellow precipitate formed was collected, washed with cold MeOH and hexane and dried to give **4.5** as a yellow powder (49mg, 0.062 mmol, 28 %). IR: ν(C≡C) 2082 cm^{-1}, ν(BH) 2605 cm^{-1}. ^{1}H NMR ($CDCl_3$, 200 MHz): δ 1.45 (s, 30H, Cp*); 2.56, 2.11 (m, 8H, CH_2); 2.00, 2.30 (2s, 11H, $C_2B_{10}H_{11}$); 7.01-7.58 (m, 40H, Ph). $^{31}P\{^{1}H\}$ NMR ($CDCl_3$, 81 MHz): δ 81.6 (s, dppe). ^{11}B NMR ($CDCl_3$, 128 MHz): δ -11.1 (d, 5B, J_{BH} = 156 Hz, B2-6), -16.3 (d, 5B, J_{BH} = 164 Hz). $^{13}C\{^{1}H\}$ NMR ($CDCl_3$, 126 MHz): δ 10.12 (C_5Me_5), 92.85 (C_5Me_5) 125.6-133.79 (arom). ES(+)-MS (*m/z*): 802 [{Ru(C≡C$C_2B_{10}H_{11}$)(dppe)Cp*}+H], 825 [{Ru(C≡C$C_2B_{10}H_{11}$)(dppe)Cp*}+Na].

{Ru(dppe)Cp}$_2$(μ-C≡C$C_2B_{10}H_{10}$C≡C) (**4.6**)*

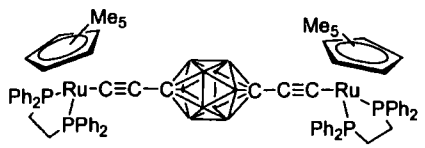

A suspension of RuCl(dppe)Cp* (100 mg, 0.149 mmol), $Me_3SiC{\equiv}CC_2B_{10}H_{10}C{\equiv}CSiMe_3$ (25 mg, 0.075 mmol), and KF (35 mg, 0.603 mmol) in methanol (20 ml) was heated at reflux for 3 hours under a nitrogen atmosphere. The yellow precipitate formed was collected, washed with MeOH and hexane and dried to give **4.6** as a yellow powder (84mg, 0.0576 mmol, 77%). Found: C, 59.89; H, 6.01. $Ru_2C_{78}H_{88}P_4B_{10}$ requires: C, 64.18; H, 6.08. IR: ν(C≡C) 2082 cm^{-1} ν(BH) 2600 cm^{-1}. ^{1}H NMR ($CDCl_3$, 200 MHz): δ 1.49 (s, 30H, Cp*); 2.52, 2.25 (m, 8H, CH_2); 2.109 (s, 10H, $C_2B_{10}H_{10}$); 7.01-7.58 (m, 40H, Ph). $^{31}P\{^{1}H\}$ NMR ($CDCl_3$, 81 MHz): δ 81.6 (s, dppe). ^{11}B NMR ($CDCl_3$, 128 MHz): δ -12.4 (d, 10B, J_{BH} = 132, $C_2B_{10}H_{10}$). $^{13}C\{^{1}H\}$ NMR (C_6D_6, 126 MHz): δ 10.20 (C_5Me_5), 29.31 (m, CH_2), 92.80 (C_5Me_5), 98.68, 104.58 (C≡C), 128.82-133.88 (arom): ES(+)-MS (*m/z*): 1460 [{Ru(dppe)Cp*}$_2$(μ-C≡C$C_2B_{10}H_{10}$C≡C)].

4.5 References

1 D. C. Busby and M. F. Hawthorne, *Inorg. Chem.*, 1982, **21**, 4101.

2 M. A. Fox, A. E. Goeta, A. K. Hughes, and A. L. Johnson, *J. Chem. Soc., Dalton Trans.*, 2002, 2132.

3 J. Aihara, *J. Am. Chem. Soc.*, 1978, **100**, 3339.

4 A. J. Stone and M. J. Alderton, *Inorg. Chem.*, 1982, **21**, 22971.

5 R. B. King, *Russ. Chem. Bull.*, 1993, **42**, 1283.

6 B. M. Gimarc and M. Zhao, *Inorg. Chem.*, 1996, **35**, 825.

7 G. A. Olah, G. K. S. Prakash, R. E. Williams, L. E. Field, and K. Wade, 'Hypercarbon Chemistry', Wiley, 1987.

8 M. A. Fox, J. A. H. MacBride, R. J. Peace, and K. Wade, *J. Chem. Soc., Dalton Trans.*, 1998, 401.

9 D. G. Allis and J. T. Spencer, *Inorg. Chem.*, 2001, **40**, 3373.

10 D. G. Allis and J. T. Spencer, *J. Organomet. Chem.*, 2000, **614-615**, 309.

11 P. Kaszynski, S. Pakhomov, and V. G. Young Jr., *Collect. Czech. Chem. Commun.*, 2002, **67**, 1061.

12 A. S. Batsanov, M. A. Fox, J. A. K. Howard, J. A. H. MacBride, and K. Wade, *J. Organomet. Chem.*, 2000, **610**, 20.

13 M. A. Fox, M. A. J. Paterson, C. Nervi, F. Galeotti, H. Puschmann, J. A. K. Howard, and P. J. Low, *Chemical Communications*, 2001, 1610.

14 D. Osella, L. Milone, C. Nervi, and M. Ravera, *Eur. J. Inorg. Chem*, 1998, 1473.

15 B. Le Guennic, K. Costuas, J. F. Halet, C. Nervi, M. A. J. Patterson, M. A. Fox, R. L. Roberts, D. Albesa-Jove, H. Puschmann, J. A. K. Howard, and P. J. Low, *C. R. Chimie*, 2005, **8**, 1883.

16 T. W. Bitner, T. J. Wedge, M. F. Hawthorne, and J. I. Zink, *Inorg. Chem.*, 2001, **40**, 5428.

17 T. J. Wedge, A. Herzog, R. Huertas, M. W. Lee, C. B. Knobler, and M. F. Hawthorne, *Organometallics*, 2004, **23**, 482.

18 B. Le Guennic, Ph.D thesis, Université de Rennes 1.

19 M. I. Bruce, B. C. Hall, B. D. Kelly, P. J. Low, B. W. Skelton, and A. H. White, *J. Chem. Soc., Dalton Trans.*, 1999, 3719.

20 M. I. Bruce, B. G. Ellis, P. J. Low, B. W. Skelton, and A. H. White, *Organometallics*, 2003, **22**, 3184.

21 M. I. Bruce, P. Hinterding, E. R. T. Tiekink, B. E. Skelton, and A. H. White, *J. Organomet. Chem.*, 1993, **450**, 209.

22 J. Vicente, M.-T. Chicote, M. M. Alvarez-Falcon, M. A. Fox, and D. Bautista, *Organometallics*, 2003, **22**, 4792.

23 H. Jude, H. Disteldorf, S. Fischer, T. J. Wedge, A. M. Hawkridge, A. M. Arif, M. F. Hawthorne, D. C. Muddiman, and P. J. Stang, *J. Am. Chem. Soc.*, 2005, **127**, 12131.

24 R. L. Cordiner, D. Albesa-Jove, R. L. Roberts, J. D. Farmer, H. Puschmann, D. Corcoran, A. E. Goeta, J. A. K. Howard, and P. J. Low, *J. Organomet. Chem.*, 2005, **690**, 4908.

25 T. Mahabiersing, H. Luyten, R. Nieuwendam, and F. Hartl, *Collect. Czech. Chem. Commun.*, 2003, **68**, 1687.

26 F. Hartl, H. Luyten, H. A. Nieuwenhuis, and G. C. Schoemaker, *Appl. Spectr*, 1994, **48**, 1522.

27 C. M. Duff and G. A. Heath, *Inorg. Chem.*, 1991, **30**, 2528.

28 L. I. Zakharin, A. I. Kovrelov, and V. A. Ol'shevskaya, *Izv. Akad. Nauk. SSSR, Ser. Khim.*, 1986, **6**, 1388.

Chapter 5

5.1 Introduction

Complexes of the type L_xM-C≡C-X-C≡C-ML_x where X is an organometallic spacer such as ferrocene, an aromatic organic spacer, or a 'three-dimensional' aromatic spacer, such as 1,12-$C_2B_{10}H_{10}$, have been discussed in previous chapters. The introduction of a metallic 'spacer' directly in to the conjugated bridging ligand has also been a topic of interest for quite some time.[1-6] The resulting complexes L_xM-C≡C-M'L'_x-C≡C-ML_x serve as models for an ever increasing family of metallopolymers,[7] while the presence of a rigid rod structure, and polarisable π-systems has also raised interest in these systems as potential NLO chromophores and liquid crystal materials.[8-16] In keeping with the themes of this thesis, the influence of the metallic spacers on the ground-state electronic structure, and consequently the role played by the metallic bridge in mediating "electronic interactions" between other metal centres located at the termini, will be briefly reviewed here, together with a summary of the key synthetic pathways to the compounds of general interest. The general topic of metal-containing polymers has been extensively reviewed on several occasions,[7, 8, 17-20] and the interested reader is referred to these summaries.

The introduction of a diethynyl platinum motif as the spacer, as in **5.1** (**Figure 5.1**), was not found to promote any electrochemically detectable interactions between the remote ferrocene moieties. Similarly, in the case of *trans*-{RuCl(dppe)$_2$}$_2$(μ-C≡CPt(PBu$_3$)$_2$C≡C), **5.2** (**Figure 5.1**), only a single, apparently two electron, oxidation process was observed for the $Ru^{II/III}$ couples.[1] The introduction of a mercury centre into the conjugated carbon chain in **5.3** (**Figure 5.1**) also served to sever electrochemically detectable interactions between Ru(dppe)Cp* fragments along the chain, this result being attributed to the lack of a Hg contribution in the HOMO, on the basis of DFT calculations.[21]

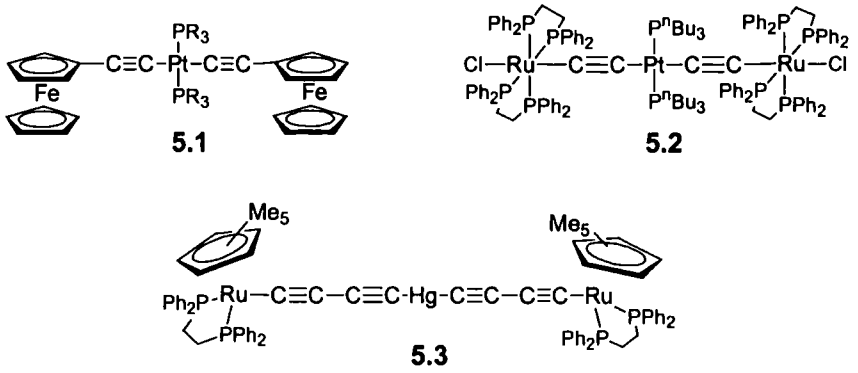

Figure 5.1

Octahedral metal centres have been found to mediate more pronounced interactions in the ground state. For the series of ruthenium bridged complexes *trans*-$[Ru(C{\equiv}CFc)_2(dppx)_2]$ (dppx = dppm (**5.4a**);[22-24] dppe (**5.4b**)[25]) cyclic voltammetric studies revealed three chemically reversible oxidation processes, with similar results also being observed in a related manganese system.[26]

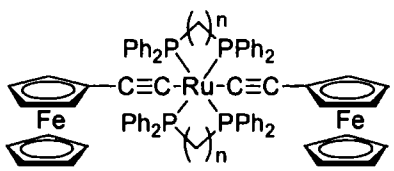

n = 1, **5.4a** n = 2, **5.4b**

Figure 5.2

These processes were assigned to the sequential oxidation of the ferrocene moieties (ΔE *ca.* 200 mV), and the Ru^{II}/Ru^{III} couple, by comparison with the oxidation potentials of model materials. The mono- and di-cationic derivatives $[\mathbf{5.4a}]^+$ and $[\mathbf{5.4a}]^{2+}$ were each found to exhibit at least two bands in the NIR region, which were not present in the neutral complex and which were assigned to a localised d-d

transition, associated with Fe^{III}, and to the $Ru^{II} \rightarrow Fe^{III}$ electron transfer processes.[24] Extension of the carbon bridge from yndiyl (C≡C) to diyndiyl (C≡CC≡C) resulted in a reduced separation of the ferrocene-based oxidation events (ΔE 139 mV),[25] but still supports the observation that, despite the increase in Fe...Fe separation, the metallocarbon backbone is more effective than the pure carbon bridge at promoting electronic interactions in this series. Wolf has proposed a three state model to account for this observation.[24]

The bis(acetylide) complexes, $M(C{\equiv}CR)_2(PP)_2$, can also be considered as fragments related to metal-containing polymers such as $[Ru(CO)_2(P^nBu_3)_2\text{-}C{\equiv}C\text{-}C_6H_4\text{-}C{\equiv}C\text{-}]_n$ (**3.1**) and $[Ru(depe)_2\text{-}C{\equiv}C\text{-}C_6H_4\text{-}C{\equiv}C\text{-}]_n$ (**3.2**) discussed in Chapter 3 and related ruthenium- and iron-containing polymers *trans*-$[M(PP)_2(C{\equiv}C\text{-}X\text{-}C{\equiv}C)_n]$.[27-31]

Consequently, the chemistry of ruthenium bis(acetylide) complexes has been thoroughly explored and a number of routes to complexes of the type $Ru(C{\equiv}CR)_2(PP)_2$ have been developed. For example, the reaction of $RuCl_2(dppm)_2$ with $LiC{\equiv}CC{\equiv}CSiMe_3$ in Et_2O was reported to produce either *trans*-$[Ru(C{\equiv}CC{\equiv}CSiMe_3)_2(dppm)_2]$ (**5.5a**), or the related mono-substituted complex *trans*-$[Ru(Cl)(C{\equiv}CC{\equiv}CSiMe_3)(dppm)_2]$.[32] Although the complexes *trans*-$[Ru(C{\equiv}CR)(CO)_2(PEt_3)_2]$ (R = $C{\equiv}CSiMe_3$, **5.6a**; C_6H_5, **5.6b**; H, **5.6c**; $SiMe_3$, **5.6d**; C≡CH, **5.6e**; $C(CH_3)_3$, **5.6h**) could also be prepared from reaction of $RuCl_2(CO)_2(PEt_3)_2$ and the appropriate lithiated acetylenes $LiC{\equiv}CR$,[33, 34] the dppe analogue of **5.5a**, *trans*-$[Ru(C{\equiv}CC{\equiv}CSiMe_3)_2(dppe)_2]$ (**5.7a**), could not be obtained by this route. However, **5.7a** was prepared *via* deprotonation, by NEt_3, of an intermediate vinylidine formed from the reaction of $RuCl_2(dppe)_2$ with $HC{\equiv}CC{\equiv}CSiMe_3$ in the presence of $NaPF_6$.[35]

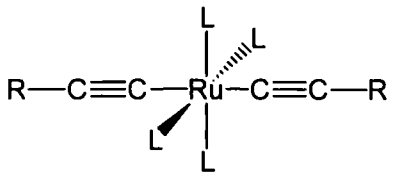

	L_4	R	
5.5	$(dppm)_2$	**a)**	$C{\equiv}CSiMe_3$
5.6	$(PEt_3)_2(CO)_2$	**b)**	C_6H_5
5.7	$(dppe)_2$	**c)**	H
5.8	$(PMe_3)_4$	**d)**	$SiMe_3$
5.9	$(depe)_2$	**e)**	$C{\equiv}CH$
5.10	$(P^nBu_3)_2(CO)_2$	**f)**	$C_6H_4C_6H_4SnMe_3$
5.11	$(dmpe)_2$	**g)**	$C_6H_4C{\equiv}CH$
		h)	$C(CH_3)_3$
		i)	$C_6H_4OMe_3$
		j)	$C_6H_3(CF_3)_2$

Figure 5.4 Ruthenium bis(acetylide) complexes $Ru(C{\equiv}CR)_2L_4$. Selected spectroscopic data are presented in **Table 5.1**.

The complexes *trans*-$[Ru(C{\equiv}CC_6H_5)_2(PMe_3)_4]$ (**5.8b**) and *trans*-$[Ru(C{\equiv}CC_6H_4C_6H_4C{\equiv}CSnMe_3)_2(PMe_3)_4]$ (**5.8f**) have been produced by the reaction of $RuCl_2(PMe_3)_4$ with the appropriate trimethylstannyl-protected acetylide ligand and displayed a characteristic single $\nu(C{\equiv}C)$ band in the IR spectra.[31] In a similar manner, trimethylstannyl-protected acetylide ligands were utilised in the production of the ruthenium bis(acetylide) complexes *trans*-$[Ru(C{\equiv}CC_6H_5)_2L_4]$ (L_4 = $(dppm)_2$, **5.5b**; $(dppe)_2$, **5.7b**; $(depe)_2$, **5.9b**; $(P^nBu_3)_2(CO)_2$, **5.10b**).[27, 29, 30]

Table 5.1 Selected spectroscopic data for **5.5-5.11**

	ν(C≡C) / cm^{-1}	^{31}P NMR δ / ppm	reference
5.5a	2107	-3.0	32
5.5b	2069	-144.7	30
5.6a	2165, 2121	20.1	33, 34
5.6b	2093	21.0	33, 34
5.6c	1944	19.9	33, 34
5.6d	2021	19.9	33, 34
5.6e	2137	20.0	33, 34
5.6h	2033	18.2	33, 34
5.7a	2166, 2109, 1993	53.6	35
5.7b	2061	88.0	29
5.8b	2055	-3.1	36
5.8f	2053	-3.2	36
5.9b	2043	51.3	36
5.9g	2049	52.3	36
5.9h	2063	52.3	36
5.9i	2056	51.3	36
5.9j	2029	50.5	36
5.10b	2093	[a]	27
5.11b	[a]	40.8	36
5.11h	[a]	40.0	36

[a] not reported

The complex **5.9b** could also be prepared by the reaction of $RuH_2(depe)_2$ and $HC{\equiv}CC_6H_5$ or by the reaction of $RuCl_2(depe)_2$ with the $HC{\equiv}CC_6H_5$ in the presence of sodium methoxide. This latter route was also utilised in the production of the related complexes *trans*-[$Ru(C{\equiv}CR)_2(depe)_2$] (R = $C_6H_4C{\equiv}CH$, **5.9g**; $C(CH_3)_3$, **5.9h**; C_6H_4OMe, **5.9i**; 3,5-$(CF_3)_2$-C_6H_3, **5.9j**). The dmpe complexes $Ru(C{\equiv}CC_6H_5)_2(dmpe)_2$, **5.11b**, and $Ru(C{\equiv}CC(CH_3)_3)_2(dmpe)_2$, **5.11h** could also be prepared by the reaction of $RuH_2(dmpe)_2$ and the appropriate terminal alkyne in

methanol.[36] The *trans* configuration of these ruthenium bis(acetylide) complexes was confirmed by the presence of a single resonance in the ^{31}P NMR and a single ν(C≡C) band due to the ruthenium-coordinated acetylide fragments (**Table 5.1**).

Whilst the synthetic chemistry of the ruthenium derivatives of this class of compounds has been thoroughly explored the analogous iron chemistry is distinctly less well developed. For example, although ruthenium complexes featuring aryl phosphines are common, only iron complexes featuring phosphite or alkyl phosphine as supporting ligands are known.

The series of iron bis(acetylide) complexes $Fe(dmpe)_2(C{\equiv}CR)_2$ (R = C_6H_5 **5.12b**, $C_6H_4C{\equiv}CH$ **5.12g**, $C(CH_3)_3$ **5.12h**, $C_6H_3(C{\equiv}CH)_2$ **5.12k**, CH_3 **5.12l**, $C(CH_3)CH_2$ **5.12m**) have been prepared by the reaction of $FeH_2(dmpe)_2$ and the appropriate terminal acetylide.[37, 38] The related complexes $Fe(C{\equiv}CC_6H_5)_2(depe)_2$ **5.13b**[28] and $Fe(C{\equiv}CC_6H_5)_2(dbpe)_2$ **5.14b**[39] were prepared from the reaction of $FeCl_2(depe)_2$ or $FeCl_2(dbpe)_2$ and $Me_3SnC{\equiv}CC_6H_5$. The *trans* disposition of the acetylide fragments around the iron centre was again confirmed by the presence of a single ν(C≡C) in the infra-red spectrum and only a single ^{31}P NMR resonance in each case (**Table 5.2**).

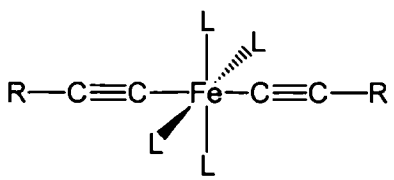

	L_4		R
5.12	$(dmpe)_2$	**b)**	C_6H_5
5.13	$(depe)_2$	**g)**	$C_6H_4C{\equiv}CH$
5.14	$(dbpe)_2$	**h)**	$C(CH_3)_3$
5.15	$(P(OMe)_3)_4$	**k)**	$C_6H_3(C{\equiv}CH)_2$
5.16	$(P(OEt)_3)_4$	**l)**	CH_3
5.17	$(PPh(OEt)_2)_4$	**m)**	$C(CH_3)CH_2$
		n)	$C_6H_4CH_3$

Figure 5.5 Iron bis(acetylide) complexes $Fe(C{\equiv}CR)_2L_4$

The electronic spectra of **5.12-5.14** displayed electronic absorption bands in the UV-vis region, associated with MLCT-type transitions, and with ligand based π-π^* transitions. These π-π^* transitions, which were found at lower energy than those in the appropriate terminal acetylene, were taken as evidence for extended conjugation in these complexes. The electrochemical response of **5.12b** was characterised by the observation of two distinct redox processes by cyclic voltammetry.[40] The first, observed at -0.16 V (vs SCE) in CH_2Cl_2 solution was attributed to the Fe^{II}/Fe^{III} couple and a second process which was not fully reversible was attributed to the Fe^{III}/Fe^{IV} couple.

Table 5.2 Selected spectroscopic data for **5.12-5.17**

	ν(C≡C) / cm^{-1}	**^{31}P NMR δ / ppm**	**λ_{max} / nm**	**reference**
5.12b	2037	64.7	259, 364	37
5.13b	2035	76.0	258, 375	28
5.14b	2038	72.8	256, 374	39
5.12g	2037, 2016	67.9	222, 284, 413	37
5.12h	2059	69.4	350	37
5.12k	2033	66.5	250, 405	37
5.12l	2075	69.5	232, 400	37
5.12m	[a]	69.1	336, 240	38
5.15b	2064	165.0	[a]	41
5.15n	2072	163.9	[a]	41
5.16b	2063	162.3	[a]	41
5.16n	2064	162.5	[a]	41
5.16h	2072	163.4	[a]	41
5.17b	2060	181.8	[a]	41
5.17n	2061	181.7	[a]	41

[a] not reported

An interesting variation on these general synthetic methods has been described by Albertin *et al.*, with the reaction of $FeCl_2$ with lithiated acetylenes, carried out in the presence of an excess of a phosphite being shown to give *trans*-[$Fe(C{\equiv}CR)_2(L)_4$] (L = $P(OMe)_3$, R = C_6H_5, **5.15b**, $C_6H_4CH_3$, **5.15n**; $P(OEt)_3$, R = C_6H_5, **5.16b**, $C_6H_4CH_3$, **5.16n**, $C(CH_3)_3$ **5.16h**; $PPh(OEt)_2$, R = C_6H_5, **5.17b**, $C_6H_4CH_3$, **5.17n**) (**Table 5.2**).[41]

The summary above highlights the useful role chemical transformations involving metal-halide bonds play in the preparation of acetylide complexes. In the design of extended systems, particularly those in which a high degree of chemical functionality is desired, the chemoselective reaction of each halide in a generic MX_2L_4 precursor is important. In general terms, such selectivity can be achieved through careful control of the reaction stoichiometry, and synthetic routes to the bis(acetylide) complexes described above may also be used in the production of related complexes in which only one acetylide ligand is attached to the group 8 metal centre.

For example, the complex $Cl(P^nBu_3)_2(CO)_2Ru$-C≡C-*p*-C_6H_4-C_6H_4-*p*-C≡C-$Ru(CO_2)(P^nBu_3)_2Cl$ was prepared from the reaction of $RuCl_2(CO)_2(P^nBu_3)_2$ and $Me_3SnC{\equiv}C$-*p*-C_6H_4-C_6H_4-*p*-$C{\equiv}CSnMe_3$,[27] and, in a similar manner to that used in the production of **5.5-5.7**, the appropriate lithium acetylide $Li(C{\equiv}C)_nSiMe_3$ has been used in the preparation of *trans*-[$Cl(dppe)_2Ru(C{\equiv}C)_nSiMe_3$] (n = 1-4) and *trans*-[$Cl(dppm)_2Ru(C{\equiv}C)_2SiMe_3$].[32, 35] Perhaps the most common route to these species is *via* a vinylidine intermediate, with, for example, the complexes *trans*-[$RuCl(C{\equiv}CR)L_4$] (L_4 = $(dppm)_2$, R = C_6H_5, $C_6H_4C{\equiv}CH$, H, CH_3, $C(CH_3)_3$, $C_6H_3(C{\equiv}CH)_2$, $C_6H_4NO_2$, $C_6H_4C_6H_4NO_2$, $C_6H_4CH{=}CHC_6H_4NO_2$; L_4 = $(dppe)_2$, R = C_6H_5, $SiMe_3$, C_6H_4-*p*-C_6H_5, C_6H_4-*p*-CH_3, C_6H_4-*p*-NO_2, C_6H_3-*o*-CH_3-*p*-NO_2; L_4 = $(P(OEt)_3)_4$, R = C_6H_5, $C_6H_4CH_3$, $C_6H_4C{\equiv}CH$, $SiMe_3$, $C(CH_3)_3$, COOMe; L_4 = $(P(OMe)_3)_4$, R = C_6H_5, $C_6H_4CH_3$, $C_6H_4C{\equiv}CH$, C_6H_4I, $C_6H_4C{\equiv}CSiMe_3$, $C_6H_4C{\equiv}CC_6H_5$) being prepared *via* reaction with the appropriate terminal acetylene, and deprotonation of the intermediate vinylidine formed.[30, 35, 42-49]

Again, the chemistry of the iron derivatives is less well developed although a number of synthetic routes to mono acetylides have been reported. The high pressure reaction of $FeH_2(dmpe)_2$ and $HC{\equiv}CC_6H_5$ in toluene has been utilised to produce the

monosubstituted complex $FeH(C{\equiv}CC_6H_5)(dmpe)_2$,[50] and the related complex $FeCl(C{\equiv}CC_6H_5)(dmpe)_2$ has been prepared by the reaction of $FeCl_2(dmpe)_2$ with $HC{\equiv}CC_6H_5$ in methanol.[51] The deprotonation of a vinylidine intermediate has also been utilised in the preparation of *trans*-$[FeCl(C{\equiv}CC_6H_4NO_2)\{(R,R)diph\}_2]$.[52]

The preparation of unsymmetrically-substituted metal bis(acetylide) complexes as donor-metal-acceptor systems has attracted interest due to the possibility of utilising such complexes in NLO applications.[10, 11, 45, 53, 54] The synthesis of these asymmetrically-substituted materials is not, however, always straightforward. For example, whilst the symmetrically-substituted rhodium complexes *trans*-$[Rh(PMe_3)_3(H)(C{\equiv}CR)_2]$ can be readily prepared,[55] the asymmetrically-substituted derivatives could not be obtained in a pure form. The presence of the symmetrically-substituted counterparts in attempts to prepare the unsymmetrical systems was attributed to alkyne exchange, in the intermediate of the reaction, with free alkyne.[56]

The preparation of group 8 systems bearing differing acetylide ligands is greatly simplified by the availability of both mono acetylide complexes, $MX(C{\equiv}CR)L_4$, and intermediary stable vinylidine complexes, and accordingly a number of asymmetrically-substituted iron, ruthenium and osmium compounds have been reported. The reaction of *trans*-$[Ru(C{\equiv}CC_6H_5)Cl(dppm)_2]$ with the terminal acetylene $HC{\equiv}CC_6H_4NO_2$ in the presence of $NaPF_6$ and NEt_3 resulted in the formation of $[Ru(C{\equiv}CC_6H_5)(C{\equiv}CC_6H_4NO_2)(dppm)_2]$.[57] This complex could also be prepared by the reaction of the monosubstituted vinylidine complex *trans*-$[Ru(=C=C(H)C_6H_5)Cl(dppe)_2][PF_6]$ with the terminal acetylene, $HC{\equiv}CC_6H_4NO_2$, in the presence of $NaPF_6$ and NEt_3.[43, 47] This route, from the appropriate monosubstituted vinylidine, was also utilised to produce the related complexes *trans*-$[Ru(C{\equiv}CR)(C{\equiv}CR')(dppe)_2]$ (R = C_6H_5, R' = ^nBu; R = ^nBu, R' = $C_6H_4NO_2$; R = C_6H_4OMe, R' = $C_6H_4NO_2$).[43] An alternative route from the mixed ammonia alkynyl ruthenium precursor *trans*-$[Ru(C{\equiv}CR)(NH_3)(dppe)_2]$ has also been shown to produce the complexes *trans*-$[Ru(C{\equiv}CR)(C{\equiv}CR')(dppe)_2]$ (R = C_6H_5, R' = ^nBu, $C_6H_4NO_2$; R = ^nBu, R' = C_6H_5, $C_6H_4NO_2$) by reaction with the appropriate terminal acetylene $HC{\equiv}CR'$ in methanol.[58]

The use of protected alkynes has been exploited in the production of these unsymmetrical systems by the reaction of metal chloro-mono-acetylides with trimethylstannyl-protected alkynes. The reaction of *trans*-[M(C≡CR)Cl(dppm)$_2$] (M = Ru, Os) with $Me_3SnC{\equiv}CR'$ in the presence of CuI gave the bis(acetylide) complexes *trans*-[Ru(C≡CR)(C≡CR')(dppm)$_2$] (R = $C_6H_4NO_2$, R' = $C_6H_4CH_3$, C_6H_5, $C_6H_4NO_2$; R = C_6H_5, R' = $C_6H_4CH_3$) and *trans*-[Os(C≡CR)(C≡CR')(dppm)$_2$] (R = $C_6H_4NO_2$, R' = C_6H_5, $C_6H_4CH_3$; R = C_6H_5, R' = $C_6H_4CH_3$).[47]

The preparation of asymmetrically-substituted iron analogues has also been reported, with the complexes, *trans*-[Fe(C≡CR)(C≡CR')(dmpe)$_2$] (R = C_6H_5, R' = C_6H_5, $C_6H_4OCH_3$, ^{t}Bu, $SiMe_3$, $(CH_2)_4C{\equiv}CH$; R = $C_6H_4OCH_3$, R' = $C_6H_4OCH_3$, ^{t}Bu, $(CH_2)_4C{\equiv}CH$, 1-adamantyl), being produced by the photochemically induced metathesis reactions of acetylido methyl complexes, *trans*-[Fe(dmpe)$_2$(C≡CR)(CH$_3$)] in the presence of an excess of the appropriate terminal alkyne.[59]

Whilst, to date, there has been much interest in the use of *trans*-bis(acetylide) complexes as structural or electronic bridges, the symmetry and redox properties of d^6 complexes, *trans*-[MY(C≡CR)L$_4$] (Y = halide, C≡CR) have, so far, been under exploited in studies of d^5/d^6 mixed-valence bimetallic complexes. As highlighted in Chapter 1, the origin of multiple overlapping bands in the NIR region of d^5/d^6 mixed-valence complexes of the type L_xM^{II}-B-$M^{III}L_x$ has been addressed by Meyer.[60] In Meyer's treatment the NIR transitions are considered to arise from a combination of inter-valence charge transfer (IVCT) processes from the M^{II} (d^6) metal to the oxidised M^{III} (d^5) centre and of formally forbidden d-d transitions at the M^{III} centre (**Figure 5.3**). A combination of the low symmetry of these pseudo-octahedral metal centres, spin-orbit coupling and extensive overlap between the metal orbitals and those of the bridging ligand results in these transitions becoming allowed, and consequentially, multiple bands in the NIR region of the spectrum. Many systems in the literature, and also those presented in this thesis, feature half sandwich metal fragments. The multiple transitions which these systems give rise to in the NIR region of their electronic spectra, are clearly demonstrated in the preceding chapters, Chapter 3 and Chapter 4. Employing systems with greater local octahedral symmetry

and perhaps also lighter metal centres (to minimise spin orbit coupling) offers one way of approaching the task of simplifying the NIR spectra of 'mixed-valence' species derived from bimetallic, organometallic complexes.

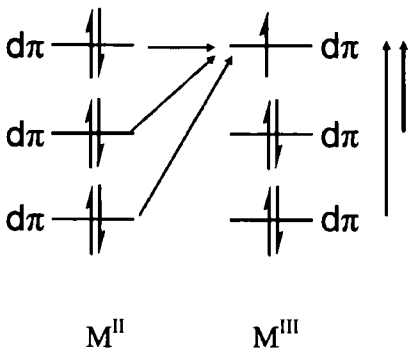

Figure 5.3

The above summary illustrates the availability of a wide range of comparable octahedral iron and ruthenium complexes. However, whilst many examples of air-stable ruthenium complexes bearing aryl phosphine supporting ligands are known, the smaller metal centre in the iron derivatives has prompted the use of smaller, more electron donating, alkyl phosphines. The inherent air sensitivity of these phosphines, the lower oxidation potential of the resulting iron complexes, and the greater synthetic difficulties that result from their sensitivity to ambient conditions, limits the attraction of these compounds to many workers in the field. In this chapter some explorations of the acetylide chemistry of the $Fe(dppe)_n$ fragment are described. The resulting complexes, which are air stable, yet oxidised at moderate potentials, provide a convenient entry point to the acetylide chemistry of the octahedral iron fragment.

5.2 Results and Discussion

The complex $FeCl_2(dppe)$ is conveniently and reproducibly obtained from the reaction of anhydrous $FeCl_2$ and dppe.[61, 62] Whilst one report describes the synthesis of a white solid reported to be $FeCl_2(dppe)_2$ from the reaction of anhydrous $FeCl_2$ and 2.1 equivalents of dppe,[63] and a second has reported the presence of a compound proposed to be $FeCl_2(dppe)_2$ in the product mixture from the reaction of $FeH_2(dppe)_2$ with $SiCl_3H$,[64] subsequent studies have failed to reproduce these results, with only mixtures of $FeCl_2(dppe)$ and the free ligand being obtained.[61] In the subsequent years it seems to have been generally accepted that the iron centre is too small to accommodate the bulky dppe ligand. However, $FeCl_2(dppe)_2$ has been crystallographically characterised within a solid solution of $[FeCl_2(dppe)_2][Fe_2(CO)_2Cl_4]$ formed from the reaction of $FeCl_2.4H_2O$ and dppe under a carbon monoxide atmosphere,[6] and Field has also recently reported the preparation of the iron chloride $FeCl_2(bpe6)_2$ featuring the relatively bulky ligand 1,2-bis(phosphorinan-1-yl)ethane (bpe6).[65] In light of this ambiguity, the preparation of $FeCl_2(dppe)_2$ was re-investigated here.

Reaction of anhydrous $FeCl_2$ with dppe in various stochiometric ratios (1:2-1:4) gave almost uniformly $FeCl_2(dppe)$ which could be separated from excess phosphine by extraction of the free ligand with hot hexane. Curiously, water had little effect on this reaction and $FeCl_2(dppe)$ could also be obtained in good yields from the reaction of $FeCl_2.nH_2O$ and two equivalents of dppe, suggesting that it may be possible to further simplify the preparation of $FeCl_2(dppe)$ directly from laboratory grade ferrous chloride. However, on one occasion a 10 g scale reaction of $FeCl_2$ and two equivalents of dppe afforded a deep green solid (**5.18**), which may possibly be related to the light green material reported by Baker and Lutz as being $FeCl_2(dppe)$.[62] The ^1H NMR spectrum of compound **5.18** measured in $CDCl_3$ and CD_2Cl_2 displayed a broad peak in the aromatic region but the $^{31}P\{^1H\}$ spectrum could not be obtained and the compound was insoluble in other common deuterated solvents. ES+ mass spectrometry was inconclusive with only a peak at m/z = 887, consistent with the fragment ion $[Fe(dppe)_2Cl]^+$, being observed. Whilst **5.18** reacted in a manner

consistent with its formulation being $FeCl_2(dppe)_2$ (*vide infra*) all attempts to re-prepare this material have failed and the definitive preparation of $FeCl_2(dppe)_2$ awaits further investigation.

As an alternative route to iron bis(acetylide) complexes featuring the bulky dppe ligand, the reaction of the well characterised complex $FeCl_2(dppe)$, with two equivalents of a terminal alkyne and one equivalent of dppe, in the presence of $NaPF_6$ and Et_3N, was investigated. The reactions were carried out in CH_2Cl_2, in the presence of Et_3N, between room temperature and the reflux point of the solvent, during which time the suspended solids dissolved and solutions with colours ranging from deep orange to purple were obtained. After removal of the solvent the products *trans*-$Fe(C{\equiv}CR)_2(dppe)_2$ were obtained in low to moderate yields by extraction of the residue with toluene, or by chromatography, and subsequent crystallisation (**Scheme 5.1, Figure 5.6**).

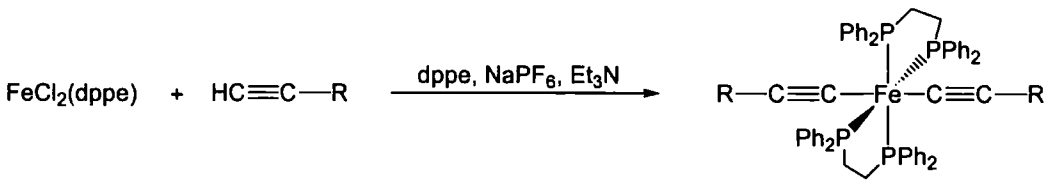

Scheme 5.1 Preparation of the iron bis(acetylide) complexes *trans*-$[Fe(C{\equiv}CR)_2(dppe)_2]$

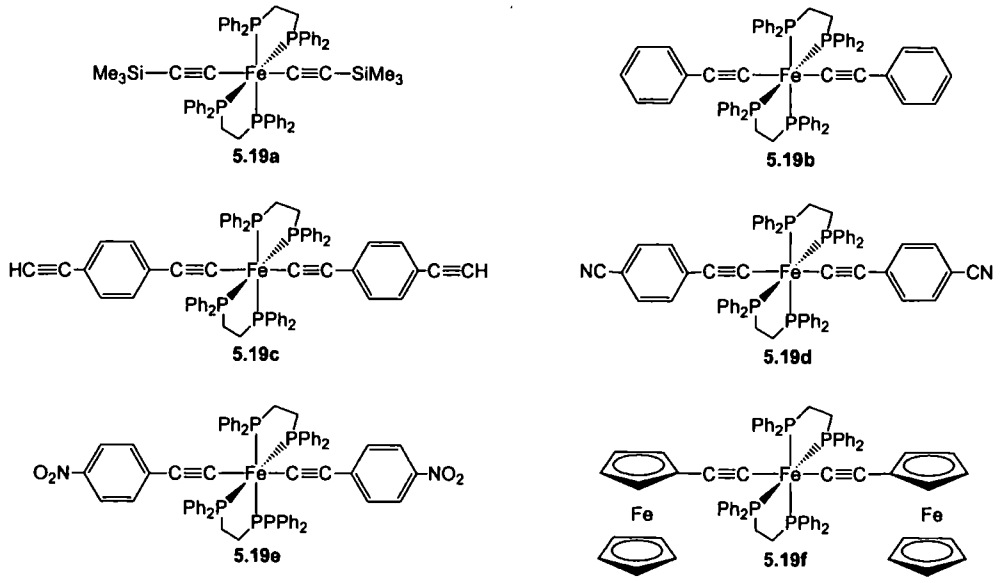

Figure 5.6 The complexes produced by the route illustrated in **Scheme 5.1**

The identities of the complexes **5.19a-f** were established from spectroscopic data, electrochemical responses (**Table 5.3**) and single crystal X-ray diffraction studies in the case of **5.19a** and **5.19b**.

Table 5.3 Selected spectroscopic and electrochemical data for compounds **5.19a-f**

	^{31}P NMR δ/ppm	ν(C≡C)/cm^{-1} [f]	ES+ MS	$E_{1/2}$/V
5.19a	34.3[e]	1970	1046 $[M]^+$	0.035
5.19b	-11.34[e]	2046	1054 $[M]^+$	0.030
5.19c	-11.7[e]	2045[a]	1102 $[M]^+$	0.080
5.19d	62.9[e]	2061, 2030w[b]	1105 $[M+1]^+$	0.550
5.19e	49.4[e]	2033, 2010sh[c]	998$[M-(C{\equiv}CC_6H_4NO_2)]^+$	0.140
5.19f	-12.50[e]	2049	[d]	0.530/0.670

[a] ν(C≡CH) 2024, [b] ν(CN) 2226, 2205w [c] ν(NO) 1525, 1348 [d] not observed. [e] $CDCl_3$, 81 MHz. [f] as solutions in CH_2Cl_2.

The chemical shift of the singlets observed in the ^{31}P NMR spectra of **5.19a-5.19e** displayed sensitivity to the electronic nature of the acetylide substituent with the resonance moving to higher frequency with the increased electron withdrawing ability of the R group. The complexes displayed lower values of the chemical shifts than those observed in the related dmpe and depe analogues. With the exception of **5.19a**, the energy of the ν(C≡C) bands of these complexes falls within the small range, 2033-2061 cm^{-1}. The low value of ν(C≡C) observed for **5.19a** may be due to hyperconjugation of the acetylide and silicon moieties.

The electrochemical response of each of the compounds **5.19a-5.19e** was characterised by a single, chemically reversible oxidation event. The phenyl acetylide derivative, **5.19a**, was oxidised at a higher potential than the dmpe analogue **5.12b**, consistent with the presence of the more electron-releasing alkyl phosphine in the latter. The cyclic voltammogram of the ethynyl ferrocene derivative **5.19f** displayed at least two overlapping waves. Differential pulse voltammetry reveals two broad peaks at 0.530 and 0.670 V, but these were not well resolved.

Structural Studies

Complexes **5.19a** and **5.19b** were characterised by single crystal X-ray diffraction studies using crystals grown by slow evaporation of a saturated solution of the complex in toluene.

The molecular structure of **5.19a** is shown in **Figure 5.7**. Selected bond lengths and angles are listed in **Table 5.4** and experimental details in **Table 5.7**. The molecular structure reveals the two acetylide ligands are coordinated with a *trans* disposition about the iron centre. The Fe-P bond lengths lie within the range 2.2364(9)-2.2836(9) Å, and the iron acetylide distances are 1.941(3) and 1.928(3) Å. The coordination geometry of the iron centre displays only small deviations from that expected for octahedral coordination with angles between mutually *cis* ligands in the range 81.35(8)-99.16(8)° and those between *trans* ligands from 175.71(3)-178.45(11)°. The acetylide C≡C bond lengths are experimentally indistinguishable at 1.233(4) and

1.239(4) Å. The Si-C≡C-Fe-C≡C-Si chain is essentially linear with angles of 173.8(3)-178.45(11)° observed along the length of the chain (**Table 5.4**).

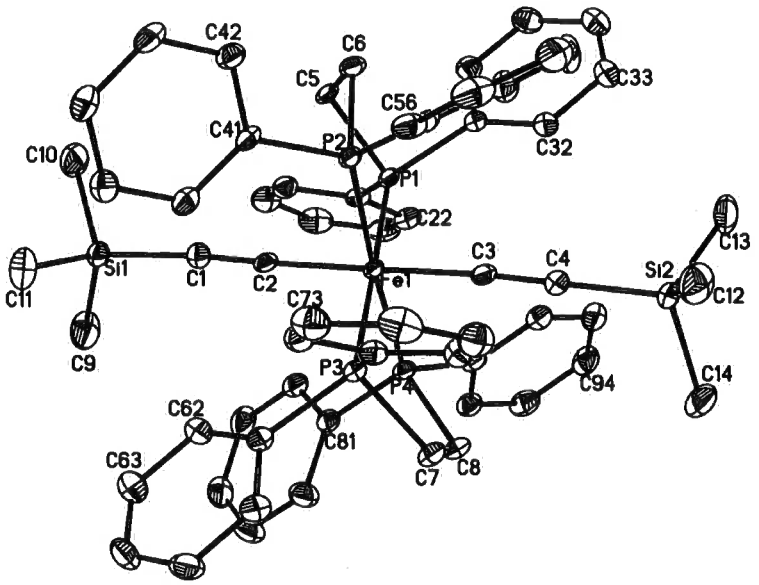

Figure 5.7 Molecular structure of **5.19a** showing the labelling scheme. Thermal ellipsoids are shown at 50% probability. Hydrogen atoms have been omitted for clarity.

Table 5.4 Selected bond lengths (Å) and angles (°) for **5.19a**

Si(1)-C(1)	1.826(3)	Si(1)-C(1)-C(2)	173.8(3)
C(1)-C(2)	1.233(4)	C(1)-C(2)-Fe(1)	177.9(2)
C(2)-Fe(1)	1.941(3)	C(2)-Fe(1)-C(3)	178.45(11)
Fe(1)-C(3)	1.928(3)	Fe(1)-C(3)-C(4)	176.2(2)
C(3)-C(4)	1.239(4)	C(3)-C(4)-Si(2)	175.2(3)
C(4)-Si(2)	1.813(3)	P(1)-Fe(1)-P(2)	84.72(3)
Fe(1)-P(1)	2.2836(9)	P(1)-Fe(1)-P(3)	177.70(3)
Fe(1)-P(2)	2.2784(9)	P(1)-Fe(1)-P(4)	95.45(3)
Fe(1)-P(3)	2.2763(9)	P(1)-Fe(1)- C(2)	81.35(8)
Fe(1)-P(4)	2.2364(9)	P(1)-Fe(1)- C(3)	99.16(8)
Si(1)-C(9)/(10)/(11)	1.869(3)/1.876(4) /1.866(3)	P(2)-Fe(1)- C(2)	89.27(8)
Si(2)-C(12)/(13)/(14)	1.868(4)/1.867(3) /1.867(3)	P(2)-Fe(1)- C(3)	89.32(8)
		P(2)-Fe(1)- P(4)	175.71(3)

The molecular structure of **5.19b** is shown in **Figure 5.8**. Selected bond lengths and angles are listed in **Table 5.5** and experimental details in **Table 5.7**. In contrast to **5.19a**, the iron centre in the 'phenyl acetylide' complex **5.19b** rests on an inversion centre. The two acetylide ligands are coordinated with a mutually *trans* disposition about the iron centre. The Fe-P bond lengths are 2.2720(4) and 2.2849(4) Å and the iron acetylide distances are 1.9297(15) Å. The coordination geometry of the iron centre displays only small deviations from that expected for octahedral coordination, with angles between mutually *cis* ligands in the range 80.81(4)-99.19(4)°. The acetylide C≡C bond lengths are 1.223(2) Å. The Si-C≡C-Fe-C≡C-Si chain is linear and displays C(2)-C(1)-Fe(1) and C(1)-C(2)-C(11) bond angles of 177.28(13) and 177.76(16)°, respectively.

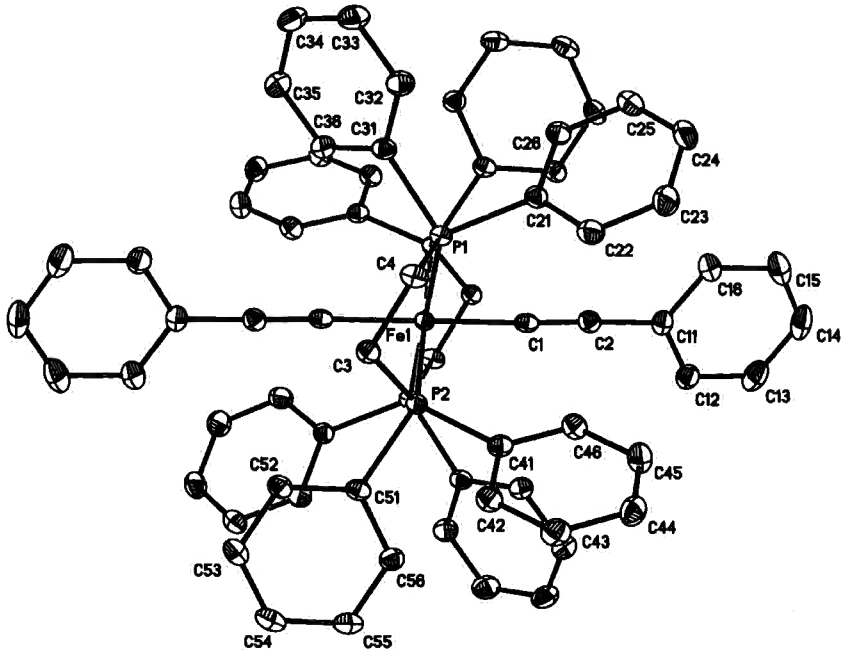

Figure 5.8 Molecular structure of **5.19b** showing the labelling scheme. Thermal ellipsoids are shown at 50% probability. Hydrogen atoms have been omitted for clarity.

Table 5.5 Selected bond lengths (Å) and angles (°) for **5.19ab**

C(1)#1-Fe(1)	1.9297(15)	C(1)#1-Fe(1)-C(1)	180.0
Fe(1)-C(1)	1.9297(15)	C(2)-C(1)-Fe(1)	177.28(13)
C(1)-C(2)	1.223(2)	C(1)-C(2)-C(11)	177.76(16)
C(2)-C(11)	1.432(2)	C(1)-Fe(1)-P(1)	89.34(4)
Fe(1)-P(1)	2.2720(4)	C(1)-Fe(1)-P(1)#1	90.66(4)
Fe(1)-P(2)	2.2849(4)	C(1)#1-Fe(1)-P(2)	80.81(4)
		C(1)-Fe(1)-P(2)	99.19(4)
		P(1)-Fe(1)-P(2)	83.362(13)
		P(1)-Fe(1)-P(1)#1	180.0
		P(1)-Fe(1)-P(2)#1	96.639(13)
		P(2)-Fe(1)-P(2)#1	180.0

Symmetry transformations used to generate equivalent atoms: #1 -x,-y,-z

The molecular structures of **5.19a** and **5.19b** therefore display metrical parameters similar to each other and to those observed in related structures such as $Fe(C{\equiv}CC_6H_5)_2(dmpe)_2$, **5.12b**,and $Fe(C{\equiv}CC_6H_5)_2(depe)_2$, **5.13b** (**Table 5.6**).

The increase in the Fe-P bond distance in **5.13b** compared with **5.12b** was attributed to the increased steric requirements of the bulkier chelating ligand.[37] The further increase observed in **5.19b** is consistent with this trend but may also be due to the greater electron donating ability of the dmpe and depe ligands compared with dppe. As mentioned in Chapter 3, the M-P bond length has been shown to be very sensitive probe of the electronic environment about the metal centre,[66] with reductions in electron-density available for M-P d-π^* back-bonding leading to increased M-P bond lengths.

Table 5.6 Selected bond lengths for **5.12b**, **5.13b**, **5.19a** and **5.19b**.

	5.12b	**5.13b**	**5.19a**	**5.19b**
Fe-C≡	1.925(6)	1.918(3)	1.941(3)	1.9297(15)
			1.928(3)	
Fe-P	2.191(3)	2.222(1)	2.2364(9)-	2.2720(4)
	2.180(5)	2.231(1)	2.2836(9)	2.2849(4)
C≡C	1.209(9)	1.222(4)	1.233(4)	1.223(2)
			1.239(4)	
≡C-E	1.438(9)	1.435(4)	1.826(3)	1.432(2)
			1.813(3)	

5.3 Outlook

The reaction of $FeCl_2(dppe)$, with terminal alkynes and one equivalent of dppe in the presence of $NaPF_6$ and Et_3N, has been utilised to produce octahedral iron bis(acetylide) complexes which are air stable and oxidised at moderate potentials. It is worth noting that reaction of **5.18** with the appropriate terminal alkynes in CH_2Cl_2 containing $NaPF_6$ and NEt_3, but no additional dppe, also affords **5.19a-f** in moderate to good yields.

The compound $Fe(C{\equiv}CC_6H_4C{\equiv}CH)_2(dppe)_2$ offers an obvious entry point to polymetallic chemistry. Given the wealth of chemistry associated with the ruthenium and osmium analogues of this type of system,[9, 29, 45, 47, 67-72] the availability of this compound provides the possibility for the preparation of, not only directly comparable iron systems, but also a range of heterometallic examples, and whilst $FeCl_2(dppe)_2$ remains elusive, $FeCl_2(dppe)$ provides a convenient entry point to air stable crystalline iron *trans* bis(acetylide) complexes.

5.4 Experimental Details

General conditions

All reactions were carried out in oven-dried glassware under dry nitrogen as a matter of routine. Solvents were dried and deoxygenated using an Innovative Technologies Solvent Purification System, and de-gassed prior to use. NMR spectra were recorded on a Bruker Avance 400, Varian VXR-200 or Inova 500 spectrometer and referenced against solvent resonances. IR spectra were recorded on a Nicolet Avatar spectrometer as solutions using solution cells fitted with CaF_2 windows.

Instrumentation

Cyclic voltammograms were recorded with an Eco Chemie Autolab PGstat controlled by a PC running GPES v.4.9 for Windows. The electrochemical cell used was an EG & PARC micro cell fitted with a nitrogen feed. In all cases, ferrocene or cobaltocence was used as an internal calibrant [$E_{1/2}(FeCp_2/[FeCp_2]^+)$ = +0.46 V vs SCE in CH_2Cl_2; $E_{1/2}(CoCp_2/[CoCp_2]^+$ = -0.87 V vs SCE in CH_2Cl_2]. Solvents were dried and, in some cases, deoxygenated using an Innovative Technologies Solvent Purification System. All solvents were de-gassed prior to use as a matter of routine precaution.

General procedure

A solution of $FeCl_2$(dppe), 1 molar equivalent of dppe, 2.5 equivalents of $NaPF_6$ and 2 equivalents of the appropriate terminal alkyne, in CH_2Cl_2, was treated with Et_3N and refluxed for 60 min over which time the solution darkened and a deep orange to deep purple solution was formed. The solution was cooled, the solvent removed and the residue, washed with hot hexane, and redissolved in the minimum of CH_2Cl_2. The solution was filtered to remove any residual salt, the solvent removed and the residue extracted with toluene or purified by chromatography. In the case of **5.19e-f** purification was less straightforward although the compounds could be identified from their spectral data.

trans-*[Fe(dppe)$_2$(C≡CSiMe$_3$)$_2$]* ***(5.19a)***

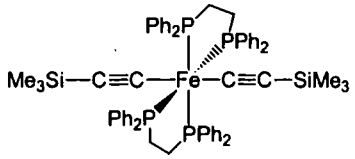

Red crystals suitable for X-ray structural analysis were obtained by slow evaporation of a saturated toluene solution of the complex. Yield = 46%. ^{1}H NMR ($CDCl_3$, 200 MHz): -0.12 (s, 18H, $SiMe_3$); δ 1.76, 2.14 (m, 8H, CH_2); 6.93-7.55 (m, 40H, Ph). $^{31}P\{^1H\}$ NMR ($CDCl_3$, 81 MHz): δ 34.3 (s, dppe). $^{13}C\{^1H\}$ NMR (CD_2Cl_2, 126 MHz): δ 1.54 (s, $SiMe_3$); 127.35-135.58 (m, Ph). ES(+)-MS (*m/z*): 1046 $\{[Fe(dppe)_2(C{\equiv}CSiMe_3)_2]^+\}$. IR: ν(C≡C) 1970 cm^{-1}

trans-*[Fe(dppe)$_2$(C≡CC$_6$H$_5$)$_2$]* ***(5.19b)***

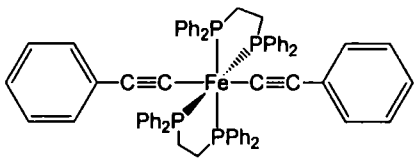

Red crystals suitable for X-ray structural analysis were obtained by slow evaporation of a saturated toluene solution of the complex. Yield = 30%. ^{1}H NMR ($CDCl_3$, 200 MHz): δ 2.24, 2.48 (br, 8H, CH_2); 7.01-7.94 (m, 50H, Ph, C_6H_5). $^{31}P\{^1H\}$ NMR ($CDCl_3$, 81 MHz): δ -11.4 (s, dppe). ES(+)-MS (*m/z*): 1054 $\{[Fe(dppe)_2(C{\equiv}CC_6H_5)_2]^+\}$. IR: ν(C≡C) 2046 cm^{-1}

trans-*[Fe(dppe)$_2$(C≡CC$_6$H$_4$C≡CH)$_2$]* ***(5.19c)***

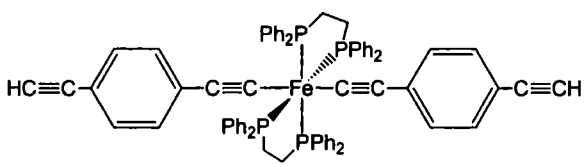

Orange powder, yield = 43 %. ^{1}H NMR ($CDCl_3$, 200 MHz): δ 2.26, 2.43 (m, 8H, CH_2); 2.01 (s, 2H, C≡CH); 6.61-7.69 (m, 48H, Ph, C_6H_4). $^{31}P\{^1H\}$ NMR ($CDCl_3$, 81 MHz): δ -11.7 (s, dppe). ES(+)-MS (*m/z*): 1102 $\{[Fe(dppe)_2(C{\equiv}CC_6H_4C{\equiv}CH)_2]^+\}$. IR: ν(C≡C) 2045, 2024 cm^{-1}

trans-*[Fe(dppe)$_2$(C≡CC$_6$H$_4$CN)$_2$]* ***(5.19d)***

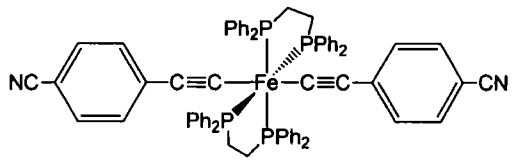

Orange powder, yield = 47 %. ^{1}H NMR ($CDCl_3$, 200 MHz): δ 2.29, 2.52 (m, 8H, CH_2); 6.74-7.77 (m, 48H, Ph, C_6H_4). $^{31}P\{^1H\}$ NMR ($CDCl_3$, 81 MHz): δ 62.9 (s, dppe). ES(+)-MS (*m/z*): 1105 {[Fe(dppe)$_2$(C≡CC$_6$H$_4$CN)$_2$ +H]$^+$}. IR: ν(C≡C), 2061, 2030w cm^{-1}, ν(C≡N) 2226, 2205w.

trans-*[Fe(dppe)$_2$(C≡CC$_6$H$_4$NO$_2$)$_2$]* ***(5.19e)***

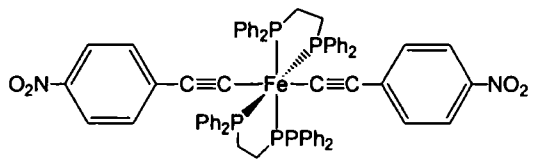

Dark purple powder, yield = 26%. ^{1}H NMR ($CDCl_3$, 200 MHz): δ 2.28, 2.22 (m, 8H, CH_2); 6.82-8.21 (m, 48H, Ph, C_6H_4). $^{31}P\{^1H\}$ NMR ($CDCl_3$, 81 MHz): δ 49.39 (s, dppe). ES(+)-MS (*m/z*): 998 {[Fe(dppe)$_2$(C≡CC6H4NO2)]$^+$}. IR: ν(C≡C) 2033, 2010sh cm^{-1}, ν(NO_2) 1525, 1348 cm^{-1}.

trans-*[Fe(dppe)$_2$(C≡CFc)$_2$]* ***(5.19f)***

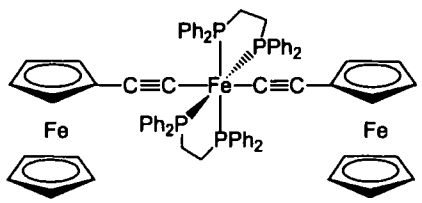

Deep orange powder, yield = 34 %. ^{1}H NMR ($CDCl_3$, 81 MHz): δ.2.027 (br, 8H, CH_2); 4.15-4.92 (m, 18H, Fc Cp); 6.43-7.71 (m, 40H, Ph). $^{31}P\{^1H\}$ NMR ($CDCl_3$, 81 MHz): δ -12.5 (s, dppe). IR: ν(C≡C) 2046 cm^{-1}.

Preparation of ***5.18***

A suspension of $FeCl_2.4H_2O$ (3.1 g, 15.59 mmol) in Me_3SiCl (30 ml) was heated at reflux for 4 hours under a nitrogen atmosphere after which time the grey $FeCl_2$ (1.9g, 14.99 mmol, 96%) was collected and dried.

A suspension of $FeCl_2$ (1.9g 14.99 mmol) and dppe (13.3 g, 33.42 mmol) in Et_2O (200 ml) was stirred under a nitrogen atmosphere for 14 hours. The green precipitate formed was filtered washed in hot hexane and dried to give **5.18** (12.9g, 13.98 mmol, 93%) as a green powder. ^1H NMR: ($CDCl_3$, 200 MHz) δ 9.13 (br, Ph); (CD_2Cl_2, 200 MHz) δ 9.59 (br, Ph). ES(+)-MS (*m/z*):887 $[FeCl(dppe)_2]^+$.

Table 5.7 Crystallographic Data for **5.19a** and **5.19b**

Identification code	**5.19a**	**5.19b**
Empirical formula	$C_{69}H_{74}FeP_4Si_2$	$C_{82}H_{74}FeP_4$
Formula weight	1139.19	1239.14
Temperature	120(2) K	120(2) K
Wavelength	0.71073 Å	0.71073 Å
Crystal system	Triclinic	Monoclinic
Space group	$P\bar{1}$	$P2_1/c$
a	13.653(4) Å	10.5938(5) Å
b	14.188(4) Å	22.9402(11) Å
c	18.843(5) Å	13.4451(7) Å
α	91.669(6)°.	90°.
β	107.707(5)°.	102.985(2)°.
γ	117.933(5)°.	90°.
Volume	3007.3(15) $Å^3$	3183.9(3) $Å^3$
Z	2	2
Density (calculated)	1.258 Mg/m^3	1.293 Mg/m^3
Absorption coefficient	0.438 mm^{-1}	0.384 mm^{-1}
F(000)	1204	1304
Crystal size	0.38 x 0.22 x 0.1 mm^3	0.40 x 0.14 x 0.10 mm^3
Theta range for data collection	1.16 to 30.55°.	1.78 to 30.51°.
Index ranges	$-19\leq h\leq 19$, $-20\leq k\leq 20$, $-26\leq l\leq 26$	$-15\leq h\leq 14$, $-26\leq k\leq 32$, $-19\leq l\leq 19$
Reflections collected	32796	29902
Independent reflections	17458 [R(int) = 0.0355]	9708 [R(int) = 0.0390]
Completeness	98.5 % to theta = 27.50°	100.0 % to theta = 30.00°
Absorption correction	Semi-empirical from equivalents	None
Max. and min. transmission	0.957 and 0.699	
Refinement method	Full-matrix least-squares on F^2	Full-matrix least-squares on F^2
Data / restraints / parameters	17458 / 0 / 692	9708 / 0 / 542
Goodness-of-fit on F^2	1.205	1.023
Final R indices [$I>2\sigma(I)$]	R1 = 0.0651, wR2 = 0.1696	R_1 = 0.0408, $_wR_2$ = 0.1006
R indices (all data)	R1 = 0.0945, wR2 = 0.1947	R1 = 0.0603, wR2 = 0.1101
Largest diff. peak and hole	1.314 and -1.265 $e.Å^{-3}$	0.843 and -0.349 $e.Å^{-3}$

5.5 References

1 O. Lavastre, J. Plass, P. Bachmann, S. Gusemi, C. Moinet, and P. H. Dixneuf, *Organometallics*, 1997, **16**, 184.

2 W.-Y. Wong, G.-L. Lu, K.-F. Ng, K.-H. Choi, and Z. Lin, *J. Chem. Soc., Dalton Trans.*, 2001, 3250.

3 W.-Y. Wong, K.-Y. Ho, and K.-H. Choi, *J. Organomet. Chem.*, 2003, **670**, 17.

4 D. Osella, R. Gobetto, C. Nervi, M. Ravera, R. D'Amato, and M. V. Russo, *Inorg. Chem. Commun.*, 1998, **1**, 239.

5 D. Osella, L. Milone, C. Nervi, and M. Ravera, *J. Organomet. Chem.*, 1995, **488**, 1.

6 W. Weng, T. Bartik, M. Brady, B. Bartik, J. A. Ramsden, A. M. Arif, and J. A. Gladysz, *J. Am. Chem. Soc.*, 1995, **117**, 11922.

7 R. P. Kingsborough and T. M. Swager, *Prog. Inorg. Chem.*, 1999, **48**, 123.

8 N. J. Long, *Angew. Chem. Int. Ed. Engl.*, 1995, **34**, 21.

9 N. J. Long and C. K. Williams, *Angew. Chem. Int. Ed.*, 2003, **42**, 2586.

10 C. E. Powell and M. G. Humphrey, *Coord. Chem. Rev.*, 2004, **248**, 725.

11 M. P. Cifuentes and M. G. Humphrey, *J. Organomet. Chem.*, 2004, **689**, 3968.

12 I. R. Whittall, A. M. McDonagh, and M. G. Humphrey, *Adv. Organomet. Chem*, 1998, **42**, 291.

13 I. R. Whittall, A. M. McDonagh, M. G. Humphrey, and M. Samoc, *Adv. Organomet. Chem*, 1999, **43**, 349.

14 D. W. Bruce, 'Inorganic Materials', ed. D. W. Bruce and D. O'Hare, Wiley, 1996.

15 D. W. Bruce, M. S. Lea, and J. R. Marsden, *Mol. Cryst. Liq. Cryst. Sci. Technol., Sect. A*, 1996, **275**, 183.

16 J. L. Serrano, 'Metallomesogens: Synthesis, Properties and Applications', ed. J. L. Serrano, Wiley, 1996.

17 L. Oriol and J. L. Serrano, *Adv. Mater.*, 1995, **7**, 348.

18 I. Manners, *Angew. Chem. Int. Ed. Engl.*, 1996, **35**, 1602.

19 P. Nguyen, P. Gomez-Elipe, and I. Manners, *Chem. Rev.*, 1999, **99**, 1515.

20 B. J. Holliday and T. M. Swager, *Chem. Commun.*, 2005, 23.

21 M. I. Bruce, J. F. Halet, B. Le Guennic, B. E. Skelton, M. E. Smith, and A. H. White, *Inorg. Chim. Acta*, 2003, **350**, 175.

22 M. C. B. Colbert, J. Lewis, N. J. Long, P. R. Raithby, A. J. P. White, and D. J. Williams, *J. Chem. Soc., Dalton Trans.*, 1997, 99.

23 N. D. Jones and M. O. Wolf, *Organometallics*, 1997, **16**, 1352.

24 Y. Zhu, O. Clot, M. O. Wolf, and G. P. A. Yap, *J. Am. Chem. Soc.*, 1998, **120**, 1812.

25 C. Lebreton, D. Touchard, L. Le Pichon, A. Daridor, L. Toupet, and P. H. Dixneuf, *Inorg. Chim. Acta*, 1998, **272**, 188.

26 A. G. Belen'kaya, F. M. Dolgushin, M. G. Peterleitner, P. V. Petrovskii, and V. V. Krivykh, *Russ. Chem. Bull.*, 2002, **51**, 170.

27 M. S. Khan, A. K. Kakkar, S. L. Ingham, P. R. Raithby, J. Lewis, B. Spencer, F. Wittmann, and R. H. Friend, *J. Organomet. Chem.*, 1994, **472**, 247.

28 B. F. G. Johnson, A. K. Kakkar, M. S. Khan, and J. Lewis, *J. Organomet. Chem.*, 1991, **409**, C12.

29 Z. Atherton, C. W. Faulkner, S. L. Ingham, A. K. Kakkar, M. S. Khan, J. Lewis, N. J. Long, and P. R. Raithby, *J. Organomet. Chem.*, 1993, **462**, 265.

30 C. W. Faulkner, S. L. Ingham, M. S. Khan, J. Lewis, N. J. Long, and P. R. Raithby, *J. Organomet. Chem.*, 1994, **482**, 139.

31 S. J. Davies, B. F. G. Johnson, J. Lewis, and P. R. Raithby, *J. Organomet. Chem.*, 1991, **414**, C51.

32 L. Dahlenburg, A. Weiβ, M. Bock, and A. Zahl, *J. Organomet. Chem.*, 1997, **541**, 465.

33 Y. Sun, N. J. Taylor, and A. J. Carty, *Organometallics*, 1992, **11**, 4293.

34 Y. Sun, N. J. Taylor, and A. J. Carty, *J. Organomet. Chem.*, 1992, **423**, C43.

35 S. Rigaut, J. Perruchon, L. Le Pichon, D. Touchard, and P. H. Dixneuf, *J. Organomet. Chem.*, 2003, **670**, 37.

36 L. D. Field, A. V. George, D. C. R. Hockless, G. R. Purches, and A. H. White, *J. Chem. Soc., Dalton Trans.*, 1996, 2011.

37 L. D. Field, A. V. George, E. Y. Malouf, I. H. M. Slip, and T. W. Hambley, *Organometallics*, 1991, **10**, 3842.

38 I. E. Buys, L. D. Field, A. V. George, and T. W. Hambley, *Aust. J. Chem.*, 1997, **50**, 159.

39 J. Lewis, M. S. Khan, A. K. Kakkar, and P. R. Raithby, *J. Organomet. Chem.*, 1992, **433**, 135.

40 L. D. Field, A. V. George, F. Laschi, E. Y. Malouf, and P. Zanello, *J. Organomet. Chem.*, 1992, **435**, 347.

41 G. Albertin, S. Antoniutti, E. Bordignon, E. D. Ministro, S. Ianelli, and G. Pelizzi, *J. Chem. Soc., Dalton Trans.*, 1995, 1783.

42 G. Albertin, S. Antoniutti, E. Bordignon, and M. Granzotto, *J. Organomet. Chem.*, 1999, **585**, 83.

43 D. Touchard, P. Haquette, S. Guesmi, L. Le Pichon, A. Daridor, L. Toupet, and P. H. Dixneuf, *Organometallics*, 1997, **16**, 3640.

44 C. E. Powell, M. P. Cifuentes, J. P. Morrall, R. Stranger, M. G. Humphrey, M. Samoc, B. Luther-Davies, and G. A. Heath, *J. Am. Chem. Soc.*, 2003, **125**, 602.

45 S. K. Hurst, M. P. Cifuentes, A. M. McDonagh, M. G. Humphrey, M. Samoc, B. Luther-Davies, I. Asselberghs, and A. Persoons, *J. Organomet. Chem.*, 2002, **642**, 259.

46 P. Haquette, N. Pirio, D. Touchard, L. Toupet, and P. H. Dixneuf, *J. Chem. Soc., Chem. Commun.*, 1993, 163.

47 M. Younus, N. J. Long, P. R. Raithby, J. Lewis, N. A. Page, A. J. P. White, D. J. Williams, M. C. B. Colbert, A. J. Hodge, M. S. Khan, and D. G. Parker, *J. Organomet. Chem.*, 1999, **578**, 198.

48 A. M. McDonagh, I. R. Whittall, M. G. Humphrey, B. E. Skelton, and A. H. White, *J. Organomet. Chem.*, 1996, **519**, 229.

49 N. J. Long, A. J. Martin, F. Fabrizi de Biani, and P. Zanello, *J. Chem. Soc., Dalton Trans.*, 1998, 2017.

50 L. D. Field and A. V. George, *J. Organomet. Chem.*, 1993, **454**, 217.

51 L. D. Field, A. V. George, and T. W. Hambley, *Inorg. Chem.*, 1990, **29**, 4565.

52 A. M. McDonagh, M. P. Cifuentes, M. G. Humphrey, S. Houbrechts, J. Maes, A. Persoons, M. Samoc, and B. Luther-Davies, *J. Organomet. Chem.*, 2000, **610**, 71.

53 A. M. McDonagh, M. P. Cifuentes, I. R. Whittall, M. G. Humphrey, M. Samoc, B. Luther-Davies, and D. C. R. Hockless, *J. Organomet. Chem.*, 1996, **526**, 99.

54 R. D'Amato, A. Furlani, M. Colapietro, G. Portalone, M. Casalboni, M. Falconieri, and M. V. Russo, *J. Organomet. Chem.*, 2001, **627**, 13.

55 H. B. Fyfe, M. Mlekuz, D. Zargarian, N. J. Taylor, and T. B. Marder, *J. Chem. Soc., Chem. Commun.*, 1991, 188.

56 J. P. Rourke, G. Stringer, P. Chow, R. J. Deeth, D. S. Yufit, J. A. K. Howard, and T. B. Marder, *Organometallics*, 2002, **21**, 429.

57 A. M. McDonagh, I. R. Whittall, M. G. Humphrey, D. C. R. Hockless, B. E. Skelton, and A. H. White, *J. Organomet. Chem.*, 1996, **523**, 33.

58 D. Touchard, S. Guesmi, L. Le Pichon, A. Daridor, and P. H. Dixneuf, *Inorg. Chim. Acta*, 1998, **280**, 118.

59 L. D. Field, A. J. Turnbull, and P. Turner, *J. Am. Chem. Soc.*, 2002, **124**, 3692.

60 K. D. Demadis, C. M. Hartshorn, and T. J. Meyer, *Chem. Rev.*, 2001, **101**, 2655.

61 J. E. Barclay, G. J. Leigh, A. Houlton, and S. J., *J. Chem. Soc., Dalton Trans.*, 1998, 2865.

62 W. A. Baker and P. M. Lutz, *Inorg. Chim. Acta*, 1976, **5**, 5.

63 M. Aresta, P. Giannoccaro, M. Rossi, and A. Sacco, *Inorg. Chim. Acta*, 1971, **5**, 115.

64 R. V. Parish and B. F. Riley, *J. Chem. Soc., Dalton Trans.*, 1979, 482.

65 L. D. Field, I. P. Thomas, P. Turner, and T. W. Hambley, *Aust. J. Chem.*, 2000, **53**, 541.

66 R. L. Cordiner, D. Albesa-Jove, R. L. Roberts, J. D. Farmer, H. Puschmann, D. Corcoran, A. E. Goeta, J. A. K. Howard, and P. J. Low, *J. Organomet. Chem.*, 2005, **690**, 4908.

67 O. Lavastre, M. Even, P. H. Dixneuf, A. Pacreau, and J.-P. Vairan, *Organometallics*, 1996, **15**, 1530.

68 S. Guesmi, D. Touchard, and P. H. Dixneuf, *Chem. Commun.*, 1996, 2773.

69 S. K. Hurst, M. P. Cifuentes, and M. G. Humphrey, *Organometallics*, 2002, **21**, 2353.

70 M. Younus, N. J. Long, P. R. Raithby, and J. Lewis, *J. Organomet. Chem.*, 1998, **570**, 55.

71 M. C. B. Colbert, J. Lewis, N. J. Long, P. R. Raithby, M. Younus, A. J. P. White, D. J. Williams, N. N. Payne, L. Yellowlees, D. Beljonne, N. Chawdhury, and R. H. Friend, *Organometallics*, 1998, **17**, 3034.

72 A. J. Hodge, S. L. Ingham, A. K. Kakkar, M. S. Khan, J. Lewis, N. J. Long, D. G. Parker, and P. R. Raithby, *J. Organomet. Chem.*, 1995, **488**, 205.

Appendix 1

Appendix 1: Additional Crystal Structures

During the course of this Ph.D a number of additional crystal structures have been elucidated through the use of single crystal X-ray diffraction. Details of these structures, together with a brief description of the chemistry associated with them, will be presented in this appendix.

A.1 $Co_2(\mu\text{-}\eta^2\text{-}Me_3SiC_2C{\equiv}SiMe_3)(CO)_4(\mu\text{-}dppm)$

Cobalt octacarbonyl, $Co_2(CO)_8$, and phosphine-substituted derivatives such as $Co_2(CO)_6(\mu\text{-}dppm)$, readily coordinate to alkynes RC≡CR' through the displacement of two carbonyl ligands to give tetrahedral Co_2C_2 clusters of general form $Co_2(\mu\text{-}RC_2R')(CO)_4(L_2)$ (L = CO, phosphine). The electrochemical response of the hexacarbonyl derivatives is characterised by a one-electron, diffusion-controlled reduction, which is often complicated by subsequent fast chemical reactions arising from cleavage of the Co-Co bond.[1] The use of bis(diphenylphosphino)methane (dppm) results in the oxidation becoming more chemically reversible, and as such, coordination of $Co_2(CO)_6(\mu\text{-}dppm)$ to ethynyl moieties provides a readily accessible redox and spectroscopic probe, with which to asses electronic structure.[2-4] The spectral and electrochemical properties of the heterometallic complexes $Co_2\{\mu\text{-}Me_3SiC{\equiv}CC_2C{\equiv}C[Ru(PPh_3)_2Cp]\}(CO)_4(dppm)$ and $Co_2\{\mu\text{-}Me_3SiC_2C{\equiv}CC{\equiv}C[Ru(PPh_3)_2Cp]\}(CO)_4(dppm)$ indicated a significant electronic interaction between the mononuclear fragment and the metallocarbon cluster core which was attributed to strong filled orbital – filled orbital interactions along the length of the $Ru(C{\equiv}C)_nC_2Co_2$ fragment, giving rise to a delocalised HOMO with significant Ru, C≡C, and cluster character.[2]

Complex **A.1** was prepared as part of a study in to the preparation of analogous complexes containing both Co_2C_2 clusters and octahedral ruthenium centres. Crystals of $Co_2(\mu\text{-}\eta^2\text{-}Me_3SiC_2C{\equiv}SiMe_3)(CO)_4(\mu\text{-}dppm)$ suitable for diffraction studies were grown by slow diffusion of hexane into a concentrated dichloromethane solution of

A.1. Red, block-shaped crystals were obtained on slow diffusion of the solvents at room temperature. Data collection was carried out on a crystal with dimensions 0.35 x 0.15 x 0.06 mm^3, at a temperature of 120(2) K. A total of 28280 reflections were collected over a theta range of 1.99 to 26.99°. The unit cell was determined as being monoclinic and the space group as $P2_1/c$. The data was corrected for absorption using SADABS and solved by direct methods. The hydrogen atoms were geometrically placed and refined isotropically. Anisotropic thermal parameters were refined for all non-hydrogen atoms. The final refinement factors were $R_1 = 0.0572$, $_wR_2 = 0.0789$ and S = 1.026. Crystallographic data is collected in **Table A.5**, selected bond lengths and angles are summarised in **Table A.1**. The molecular structure of **A.1** is illustrated in **Figure A.1**.

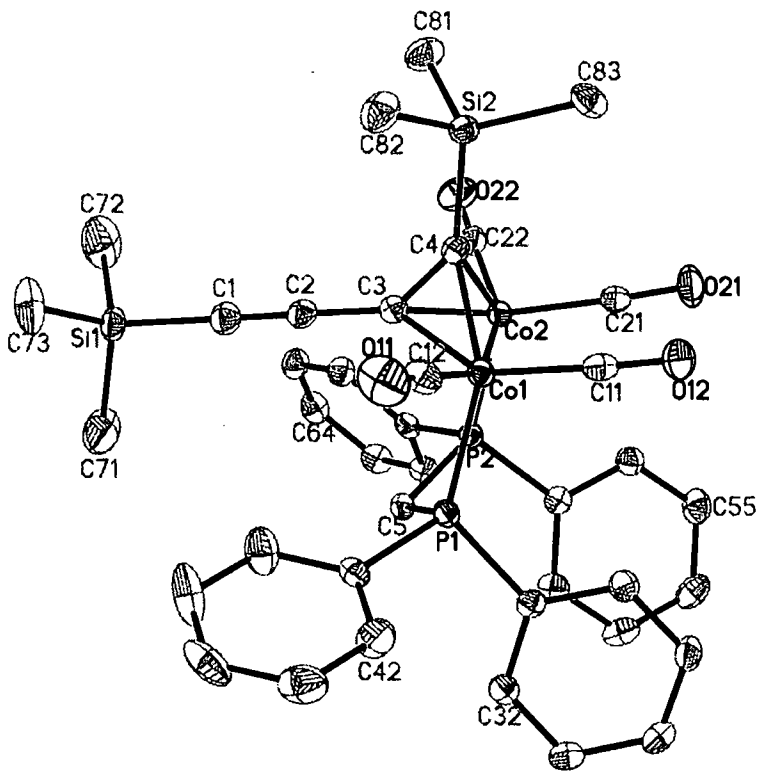

Figure A.1. Molecular structure of **A.1** showing labelling scheme. Ellipsoids are shown at the 50% probability level. Hydrogen atoms have been omitted for clarity.

The molecular structure shows features common to this type of complex (**Table A.1**.) The Co(1) Co(2) and C(3) C(4) separations of 2.4783(6) Å and 1.353(3) Å respectively, and the Co-C bond lengths 1.965(2)-1.974(2) Å are typical for this type of cluster.[2, 5, 6] The Si(1)-C(1)-C(2)-C(3) fragment is essentially linear and displays bond lengths typical of the triple, C(1)-C(2), and single, C(2)-C(3), bonds associated with alkyne chains.

Table A.1 Selected bond lengths (Å) and angles (°) for **A.1**

Si(1)-C(1)	1.835(3)	C(2)-C(1)-Si(1)	178.6(2)
C(1)-C(2)	1.213(3)	C(1)-C(2)-C(3)	176.7(3)
C(2)-C(3)	1.404(3)	C(2)-C(3)-C(4)	139.7(2)
C(3)-C(4)	1.353(3)	C(3)-C(4)-Si(2)	140.41(19)
C(4)-Si(2)	1.845(2)	Co(1)-Co(2)-P(1)	96.36(2)
Co(1)-C(3)	1.965(2)	Co(2)-Co(1)-P(2)	97.17(2)
Co(1)-C(4)	1.966(2)		
Co(2)-C(3)	1.965(2)		
Co(2)-C(4)	1.974(2)		
Co(1)-Co(2)	2.4783(6)		

A.2 $(FcC{\equiv}C)_3C$-OH

The chemistry and properties of complexes featuring conjugated bridging ligands is of immense contemporary interest. Whilst the majority of studies have been concerned with linear systems, more recently branched systems have attracted much interest. For example, organometallic hyper-branched dendritic systems, featuring branched ligands derived from 1,3,5-trisubstituted benzene cores, have been the focus of studies exploring, in particular, the optical properties of such systems.[7-14]

Organometallic complexes featuring branched all-carbon ligands such as η^1-bonded tetraethynylethene ligands have also been prepared but are much less common. Diederich and co-workers have reported platinum derivatives, such as the complex shown in **Figure A.2**, and investigated the potential of such systems as materials for non-linear optics.[15]

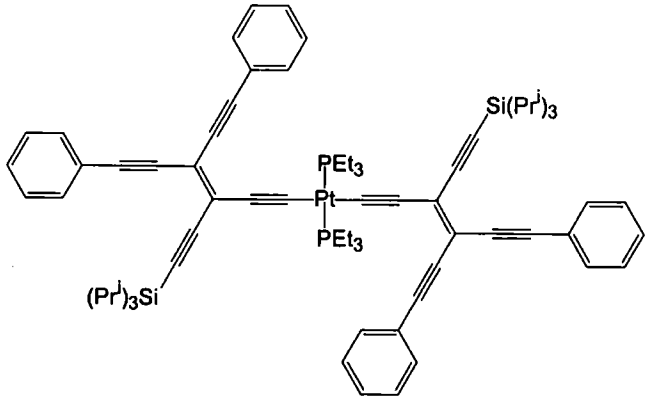

Figure A.2

Studies of the ^{13}C spectra of a series of substituted tris(ethynyl)methyl cations $[(RC{\equiv}C)_3C]^+$ (R = Ph, $SiMe_3$, alkyl groups), prepared in superacidic media, have indicated that the positive charge is extensively delocalised into the ethynyl groups, however attempts to isolate the cation have been unsuccessful.[16]

A facile synthesis of triethynyl methanol derivatives has been developed in the Low group and, in an attempt to prepare a stabilised C_7^+ cation, ferrocene centres were introduced into the general triethynyl methanol framework. The complex **A.2** was prepared by the reaction of ethynyl ferrocene with ethyl ferrocene propiolate as shown in **Scheme A.1**. The presence of the more electron donating Fc groups may serve to stabilise the cations which may be formed from these systems.

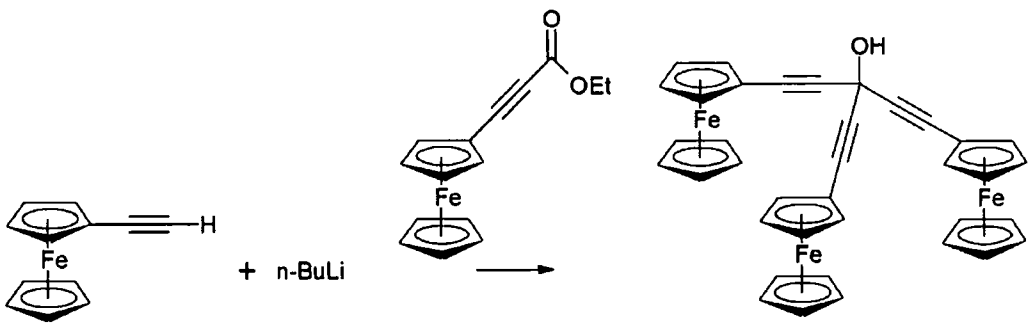

Scheme A.1. Synthesis of **A.2**, $(FcC{\equiv}C)_3C\text{-}OH$ (Fc = Ferrocenyl)

Crystals suitable for diffraction studies were grown by slow diffusion of hexane into a concentrated CH_2Cl_2 solution of **A.2**. Orange, needle-shaped crystals were obtained on slow diffusion of the solvents at room temperature. Data collection was carried out on a crystal with dimensions 0.3 x 0.15 x 0.1 mm^3, at a temperature of 120(2) K. A total of 20740 reflections were collected over a theta range of 1.08 to 27.48°. The unit cell was determined as being monoclinic and the space group as $P2_1/c$. The data was solved by direct methods. The hydrogen atoms were geometrically placed and refined isotropically. Anisotropic thermal parameters were refined for all non-hydrogen atoms. The final refinement factors were $R_1 = 0.0554$, $_wR_2 = 0.0755$ and S = 0.896. Crystallographic data is collected in **Table A.5**, Important bond lengths and angles are summarised in **Table A.2**. The molecular structure of **A.2** is illustrated in **Figure A.3**.

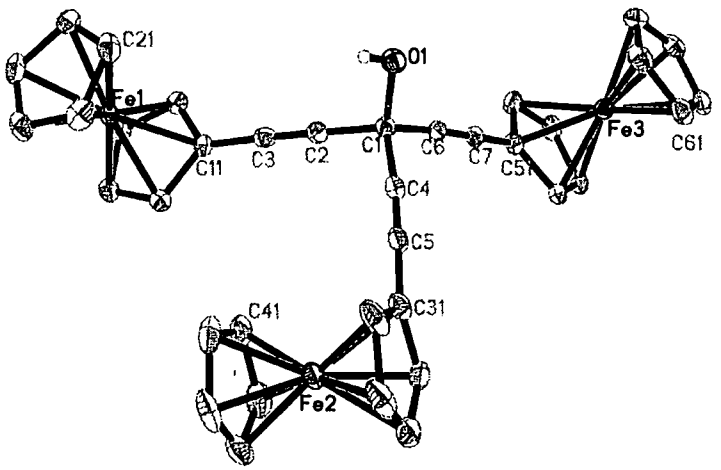

Figure A.3. Molecular structure of **A.2** showing labelling scheme. Ellipsoids are shown at the 50% probability level. Hydrogen atoms have been omitted for clarity

Table A.2 Selected bond lengths (Å) and angles (°) for **A.2**

O(1)-C(1)	1.432(3)	O(1)-C(1)-C(2)	110.28(18)
C(1)-C(2)	1.490(3)	C(1)-C(2)-C(3)	179.0(3)
C(2)-C(3)	1.188(3)	C(2)-C(3)-C(11)	177.8(2)
C(3)-C(11)	1.434(3)	O(1)-C(1)-C(4)	112.10(18)
C(1)-C(4)	1.489(3)	C(1)-C(4)-C(5)	175.0(3)
C(4)-C(5)	1.182(3)	C(4)-C(5)-C(31)	177.9(3)
C(5)-C(31)	1.435(3)	O(1)-C(1)-C(6)	106.98(18)
C(1)-C(6)	1.482(3)	C(1)-C(6)-C(7)	175.8(2)
C(6)-C(7)	1.187(3)	C(6)-C(7)-C(51)	176.0(2)
C(7)-C(51)	1.431(3)	C(2)-C(1)-C(4)	108.13(19)
		C(2)-C(1)-C(6)	110.23(18)
		C(4)-C(1)-C(6)	109.11(19)

The molecular structure of **A.2** displays similar metrical parameters to the related structures of ferrocenylpropargyl alcohol[17] and 1,1'-bis(2-hydroxy-2-methylbut-3-yn-4-yl)ferrocene.[18, 19] The ethynyl chains display the long–short–long bond alternation typical of acetylenic moieties. The three pendant ethynylferrocene groups and OH group describe an almost tetrahedral geometry about C(1) with bond angles of approximately 109° (**Table A.2**). The ethynyl chains are essentially linear, with bond angles of 175.8-179.0 °.

A.3 $RuCl_2(dppe)_2$

Complex **A.3** was prepared as part of a study in to the preparation of complexes containing octahedral ruthenium centres featuring ethynyl ligands. The molecular structure of $RuCl_2(dppe)_2$ has been reported a number of times previously, however a different polymorph was found in this case.

Yellow, plate-shaped single crystals of **A.3** suitable for X-ray diffraction were obtained by slow diffusion of hexane into a concentrated CH_2Cl_2 solution of the complex at room temperature. Data collection was carried out on a crystal with dimensions 0.14 x 0.10 x 0.04 mm^3, at a temperature of 120(2) K. A total of 8599 reflections were collected over a theta range of 2.13 to 27.48°. The unit cell was determined as being triclinic and the space group as $P\bar{1}$. The data was corrected for absorption using SADABS and solved by direct methods. The hydrogen atoms were geometrically placed and refined isotropically. Anisotropic thermal parameters were refined for all non-hydrogen atoms. The final refinement factors were $R_1 = 0.0537$, $_wR_2 = 0.1134$ and S = 1.014. Crystallographic data is collected in **Table A.5.** Selected crystallographic details, together those of the related polymorphs, and selected bond lengths and angles of **A.3** are summarised in **Table A.3**. The molecular structure of **A.3** is illustrated in **Figure A.4**.

The molecular structure of **A.3** displays similar geometrical parameters to the previously reported polymorphs.[20-24] The two chloride ligands, together with the two bidentate dppe ligands display pseudo-octahedral geometry around the ruthenium centre.

Table A.3 a) bond lengths (Å) and angles (°) of **A.3** and **b)** selected crystallographic details of **A.3** and related polymorphs

a)

Ru(1)-P(1)	2.3872(11)	P(2)-Ru(1)-P(2)#1[a]	180.0
Ru(1)-P(2)	2.3580(14)	P(2)-Ru(1)-P(1)	97.88(4)
Ru(1)-Cl(1)	2.4338(12)	P(2)-Ru(1)-P(1)#1[a]	82.12(4)
P(1)-C(1)	1.877(4)	P(1)-Ru(1)-P(1)#1[a]	180.0
P(2)-C(2)	1.844(4)	P(2)-Ru(1)-Cl(1)#1[a]	85.11(5)
C(1)-C(2)#1[a]	1.531(6)	P(1)-Ru(1)-Cl(1)#1[a]	96.74(4)
		P(2)-Ru(1)-Cl(1)	94.89(5)
		P(1)-Ru(1)-Cl(1)	83.26(4)
		Cl(1)-Ru(1)-Cl(1)#1[a]	180.0

[a]Symmetry transformations used to generate equivalent atoms: #1 -x,-y+2,-z+1

b)

	A.3	KICZUR[b]	POGNEE[b]	QEKPEB[b]	RALLUL[b]	SASWAK[b]
Space group	$P\bar{1}$	$C2/c$	$P2_1/c$	$P2_1$	$P\bar{1}$	$P2_1/c$
a / Å	10.064(2)	27.995	23.713	13.3497	12.4021	11.371(3)
b / Å	10.362(2)	13.85	11.156	17.9236	14.1049	13.458(2)
c / Å	12.902(3)	13.265	17.595	20.345	19.9913	17.232(3)
α / °	68.75(3)	90.0	90	90	100.8105	90.0
β / °	70.11(3)	105.38	103.23	93.505	102.5588	96.02(2)
γ / °	89.32(3)	90.0	90	90	111.4494	90.0
Volume / Å^3	1169.6(4)	4959.1	4531.1	4858.9	3036.6	2622.5(9)
Z	1	4	4	4	2	2
Reference		20	21	22	24	23

[b]CCDC reference code

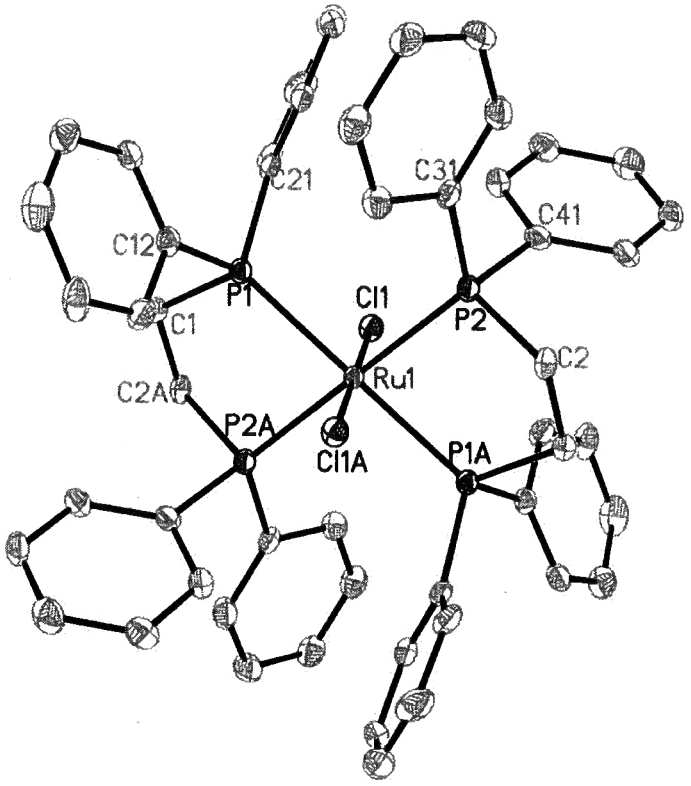

Figure A.4 Molecular structure of A.3 showing labelling scheme. Ellipsoids are shown at the 50% probability level. Hydrogen atoms have been omitted for clarity

A.4 $[\{Ru(PPh_3)_2Cp\}_2(\mu\text{-}C{\equiv}CC_6H_4CN)][PF_6]$

Complex **A.4** was prepared as part of an investigation of the coordination and organometallic chemistry of a number of unusual cyanocarbons.[25] The complexes $[Ru\{\eta^1(N)\text{-}N{\equiv}CC{\equiv}CPh\}(PPh_3)_2Cp][PF_6]$ and the cyanoacetylide complex $Ru(C{\equiv}CC{\equiv}N)(PPh_3)_2Cp$ have been described previously,[26] in the course of extending these studies to other half-sandwich metal systems, and exploring the nature of the M-N≡CC≡CR bonding interaction, a range of spectroscopic, electrochemical and structural parameters from simple nitrile complexes of general form $[M(N{\equiv}CR)(L_2)(\eta^5\text{-}C_5R'_5)]^+$, and related complexes, were assessed.[25]

Complex **A.4** was prepared from the reaction of 4-ethynylbenzonitrile and two equivalents of $RuCl(PPh_3)_2Cp$ in the presence of NH_4PF_6 and subsequent treatment with NaOMe to deprotonate the intermediate vinylidene, (**Scheme A.4**) and could also be produced from the reaction of the related monometallic complex $Ru(C{\equiv}CC_6H_4C{\equiv}N)(PPh_3)_2Cp$ with one equivalent of $RuCl(PPh_3)_2Cp$.[25]

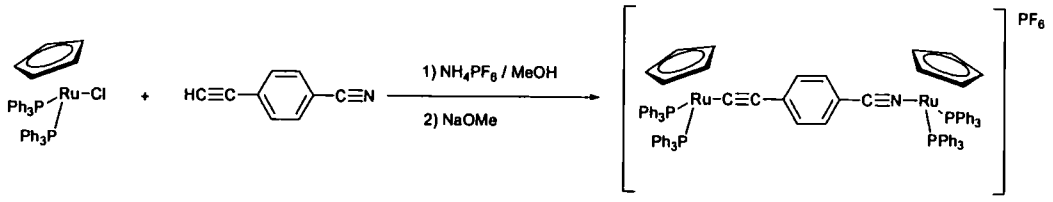

Scheme A.2 Preparation of **A.4**

Single crystals of **A.4** suitable for X-ray diffraction were obtained by slow diffusion of hexane into a concentrated acetone solution of the complex salt. Data collection was carried out on a crystal with dimensions 0.32 x 0.12 x 0.04 mm^3, at a temperature of 120(2) K. A total of 42161 reflections were collected over a theta range of 1.24 to 30.42°. The unit cell was determined as being triclinic and the space group as $P\bar{1}$. The data was solved by direct methods. The hydrogen atoms were geometrically placed and refined isotropically. Anisotropic thermal parameters were

refined for all non-hydrogen atoms. The final refinement factors were R_1 = 0.0630, $_wR_2$ = 0.1082 and S = 0.927. Crystallographic data is collected in **Table A.5.** Selected bond lengths and angles are summarised in **Table A.4**, together with those of some closely related species reported earlier. The molecular structure of **A.4** is illustrated in **Figure A.4.**

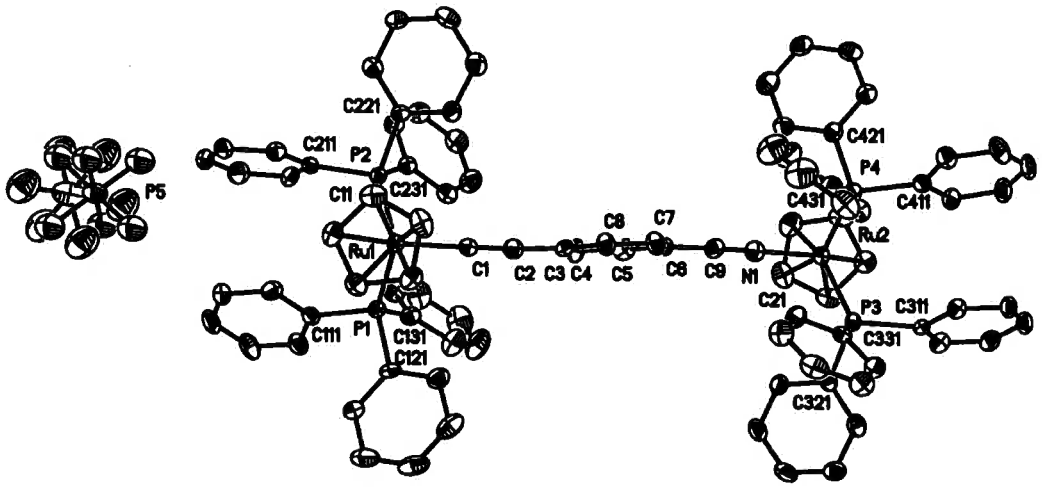

Figure A.5 Molecular structure of **A.4** showing labelling scheme. Ellipsoids are shown at the 50% probability level. Hydrogen atoms have been omitted for clarity

It is interesting to examine the features of the mixed acetylide/nitrile bridging ligand present in **A.4**, and the structural data from $[Ru(NCC_6H_5)(PPh_3)_2Cp][PF_6]$, **A.5**, $Ru(C{\equiv}CPh)(PPh_3)_2Cp$, **A.6** and $Ru(C{\equiv}CC_6H_4C{\equiv}N)(PPh_3)_2Cp$, **A.7** to provide a comparison of the metrical parameters associated with the M-C≡CR and M-N≡CR motifs.

Each metal centre in the bimetallic species **A.4** adopts the expected arrangement of Cp and PPh_3 ligands, displaying, together with the acetylide or nitrile fragment, the pseudo-octahedral geometry expected in these half sandwich complexes. The plane in which the aromatic ring of the bridging ligand lies almost bisects the P-Ru-P angle at each metal centre, providing an extended conjugation pathway between d_π orbitals

on each metal centre. The C(9)≡N(1) and C(1)≡C(2) bond lengths in **A.4** are essentially identical to those observed in the respective model mononuclear complexes. However, within the C(3)-C(8) ring system there is some evidence for a degree of quinoidal character, an observation which is supported by the short C(2)-C(3) [1.419(7) Å] and C(6)-C(9) [1.415(7) Å] bond lengths.

Compound [ref]	**A.5** [25]	**A.6** [27, 28]	**A.7** [25]	**A.4**
Ru-E	2.037(1)	2.016(3) / 2.017(5)	2.011(2)	1.994(5)‡ 2.020(5)†
E≡C	1.145(2)	1.215(4) / 1.214(7)	1.219(3)	1.201(7)‡ 1.146(6)†
C-C_{ipso}	1.440(2)	1.456(4) / 1.462(8)	1.432(3)	1.419(7)‡ 1.415(7)†
Ru-P(1)	2.334(1)	/ 2.229(3)	2.3134(5)	2.2903(14)‡ 2.3104(14)†
Ru-P(2)	2.335(1)	/ 2.228(3)	2.3031(5)	2.3046(13)‡ 2.3218(14)†
Ru-E-C	171.70(12)	178.0(2) / 177.7(4)	175.43(18)	172.7(4)‡ 172.0(4)†
E-C-C_{ipso}	177.84(16)	171.9(3) / 170.6(5)	175.1(2)	175.1(5)‡ 177.2(5)†
P(1)-Ru-P(2)	97.46(1)	/ 100.9(1)	102.21(2)	99.59(5)‡ 97.25(5)†

‡ Data from acetylide coordinated metal centre † Data from nitrile coordinated metal centre

A comparison of the Ru(1)-P(1, 2) bond lengths [2.290(1), 2.305(1) Å] with the Ru-P bond lengths of Ru(C≡CPh)(PPh_3)$_2$Cp, **A.6** [2.229(3), 2.228(3) Å], reveals an elongation of the Ru(1)-P(1, 2) in **A.4**. In contrast, comparison of the Ru(2)-P(3, 4) bond lengths [2.310(1), 2.322(1) Å] with the Ru-P bond lengths of **A.5** [2.334(1), 2.335(1) Å] reveal a contraction of the bond, with the Ru-P bonds on the nitrile coordinated metal centre being amongst the shortest reported for this class of complex. When taken as a whole, these structural parameters provide clear evidence for the donation of electron density from Ru(1) to Ru(2) *via* the polarised σ-bond framework of the ethynylbenzonitrile bridge.

A.5 Crystallographic Data

Table A.5 Crystallographic data for **A.1-A.4**

	A1	A2
Empirical formula	$C_{39}H_{40}Co_2O_4P_2Si_2$	$C_{37}H_{28}Fe_3O$
Formula weight	808.69	656.14
Temperature	120(2) K	120(2) K
Wavelength	0.71073 Å	0.71073 Å
Crystal system	Monoclinic	Monoclinic
Space group	$P2_1/c$	$P2_1/c$
a	12.291(3) Å	18.7771(4) Å
b	30.730(6) Å	11.0288(2) Å
c	11.846(2) Å	13.3869(3) Å
α	90°.	90°.
β	117.91(3)°.	91.4430(10)°
γ	90°.	90°.
Volume	3953.7(14) $Å^3$	2771.40(10) $Å^3$
Z	4	4
Density (calculated)	1.359 Mg/m^3	1.573 Mg/m^3
Absorption coefficient	1.018 mm^{-1}	1.580 mm^{-1}
F(000)	1672	1344
Crystal size	0.35 x 0.15 x 0.06 mm^3	0.3 x 0.15 x 0.1mm^3
Theta range for data collection	1.99 to 26.99°.	1.08 to 27.48 °.
Index ranges	$-14\leq h\leq 15$, $-39\leq k\leq 31$, $-15\leq l\leq 15$	$-24\leq h\leq 20$, $-14\leq k\leq 13$, $-16\leq l\leq 17$
Reflections collected	28280	20740
Independent reflections	8596 [R(int) = 0.0498]	6369 [R(int) = 0.0717]
Completeness	99.8 % to theta = 26.99°	100.0 % to theta = 27.48°
Absorption correction	Semi-empirical from equivalents	None
Max. and min. transmission	1 and 0.835225	
Refinement method	Full-matrix least-squares on F^2	Full-matrix least-squares on F^2
Data / restraints / parameters	8596 / 0 / 448	6369 / 0 / 371
Goodness-of-fit on F^2	1.026	0.896
Final R indices [$I>2\sigma(I)$]	R1 = 0.0347, wR2 = 0.0696	R1 = 0.0335, wR2 = 0.0697
R indices (all data)	R1 = 0.0572, wR2 = 0.0789	R1 = 0.0554, wR2 = 0.0755
Largest diff. peak and hole	0.471 and -0.340 $e.Å^{-3}$	0.462 and -1.384 $e.Å^{-3}$

	A3	A4
Empirical formula	$RuCl_4P_4C_{53}H_{50}$	$Ru_2P_5F_6O_2NC_{97}H_{86}$
Formula weight	1053	1768.66
Temperature	120(2) K	120(2) K
Wavelength	0.71073 Å	0.71073 Å
Crystal system	Triclinic	Triclinic
Space group	$P\bar{1}$	$P\bar{1}$
a	10.064(2) Å	13.5570(18) Å
b	10.362(2) Å	18.406(3) Å
c	12.902(3) Å	18.554(2) Å
α	68.75(3)°.	63.479(2)°.
β	70.11(3)°.	79.126(2)°.
γ	89.32(3)°.	82.183(3)°.
Volume	1169.6(4) $Å^3$	4061.2(9) $Å^3$
Z	1	2
Density (calculated)	1.496 Mg/m^3	1.446 Mg/m^3
Absorption coefficient	0.738 mm^{-1}	0.536 mm^{-1}
F(000)	540	1816
Crystal size	0.14 x 0.10 x 0.04 mm^3	0.32 x 0.12 x 0.04 mm^3
Theta range for data collection	2.13 to 27.48°.	1.24 to 30.42°.
Index ranges	$-11\leq h\leq 13$, $-11\leq k\leq 13$, $-16\leq l\leq 16$	$-18\leq h\leq 18$, $-25\leq k\leq 25$, $-25\leq l\leq 26$
Reflections collected	8599	42161
Independent reflections	5287 [R(int) = 0.0482]	21594 [R(int) = 0.0846]
Completeness	98.6 % to theta = 27.48°	98.8 % to theta = 27.50°
Absorption correction	Semi-empirical from equivalents	None
Max. and min. transmission	0.971 and 0.898	
Refinement method	Full-matrix least-squares on F^2	Full-matrix least-squares on F^2
Data / restraints / parameters	5287 / 0 / 288	21594 / 0 / 1026
Goodness-of-fit on F^2	1.014	0.927
Final R indices [$I>2\sigma(I)$]	R1 = 0.0537, wR2 = 0.1134	R1 = 0.0630, wR2 = 0.1082
R indices (all data)	R1 = 0.0844, wR2 = 0.1266	R1 = 0.1687, wR2 = 0.1436
Largest diff. peak and hole	0.964 and -1.589 $e.Å^{-3}$	0.888 and -0.625 $e.Å^{-3}$

A.6 Experimental Details

Diffraction data were collected on Bruker 3-circle diffractometers with SMART APEX, SMART 6K or SMART 1K CCD area detectors, using graphite-monochromated sealed-tube Mo Kα radiation. The data collection was carried out at 120 K or 250 K (for **3.10b**) using cryostream (Oxford cryosystem) open flow N_2 cryostats. Reflection intensities were integrated using the saint V6.45 program or saint V6.02a.[29, 30]

The crystal structures were solved using direct-methods and refined by full matrix least-squares against F^2 of all data using shelxtl software.[31] All non-hydrogen atoms were refined in anisotropic approximation, except the benzene solvent molecules in **3.10b** the atoms of which were isotropically refined. Hydrogen atoms were either located by a difference map (**5.19b**) or placed in calculated positions and refined isotropically using a riding model.

The PF_6 anion is disordered in compound **A.4**. In the crystal structure of **3.10b**, one benzene molecule is disordered between two positions, partially populated with occupancies of *ca.* 0.55 and 0.45.

A.7 References

1 M. Arewgoda, P. H. Reiger, B. H. Robinson, J. Simpson, and S. J. Visco, *J. Am. Chem. Soc.*, 1982, **104**, 5633.

2 P. J. Low, R. Rousseau, P. Lam, K. A. Udachin, G. D. Enright, J. S. Tse, D. D. M. Wayner, and A. J. Carty, *Organometallics*, 1999, **18**, 3885.

3 R. P. Aggarwal, N. G. Connelly, M. C. Crespo, B. J. Dunne, P. M. Hopkins, and A. G. Orpen, *J. Chem. Soc., Dalton Trans.*, 1992, 655.

4 J. Lewis, B. Lin, M. S. Khan, M. R. A. Al-Mandhary, and P. R. Raithby, *J. Organomet. Chem.*, 1994, **484**, 161.

5 T. J. Snaith, P. J. Low, R. Rousseau, H. Puschmann, and J. A. K. Howard, *J. Chem. Soc.,Dalton Trans*, 2001, 292.

6 M. I. Bruce, P. J. Low, M. Z. Ke, B. D. Kelly, B. W. Skelton, M. E. Smith, A. H. White, and N. B. Witton, *Aust. J. Chem.*, 2001, **54**, 453.

7 M. P. Cifuentes, M. G. Humphrey, J. P. Morrall, M. Samoc, F. Paul, C. Lapinte, and T. Roisnel, *Organometallics*, 2005, **24**, 4280.

8 N. J. Long, A. J. Martin, F. Fabrizi de Biani, and P. Zanello, *J. Chem. Soc., Dalton Trans.*, 1998, 2017.

9 T. Weyland, C. Lapinte, G. Frapper, M. J. Calhorda, J.-F. Halet, and L. Toupet, *Organometallics*, 1997, **16**, 2024.

10 T. Weyland, K. Costuas, L. Toupet, J.-F. Halet, and C. Lapinte, *Organometallics*, 2000, **19**, 4228.

11 I. R. Whittall, M. G. Humphrey, S. Houbrechts, J. Maes, A. Persoons, S. Schmid, and D. C. R. Hockless, *J. Organomet. Chem.*, 1997, **544**, 277.

12 T. Weyland, I. Ledoux, S. Brasselet, J. Zyss, and C. Lapinte, *Organometallics*, 2000, **19**, 5235.

13 M. S. Khan, D. J. Schwartz, N. A. Pasha, A. K. Kakkar, B. Lin, P. R. Raithby, and J. Lewis, *Z. Anorg. Allg. Chem.*, 1992, **616**, 121.

14 S. H.-F. Chong, S. C.-F. Lam, V. W.-W. Yam, N. Zhu, K.-K. Cheung, S. Fathallah, K. Costuas, and J.-F. Halet, *Organometallics*, 2004, **23**, 4924.

15 F. Diederich, R. Faust, V. Gramlich, and P. Seiler, *J. Chem. Soc., Chem. Commun.*, 1994, 2045.

16 G. A. Olah, R. Krishnamurti, G. K. S. Prakash, D. P. Loker, and K. B. Loker, *J. Org. Chem.*, 1990, **55**, 6061.

17 L. Dufková, I. Císařová, P. Štepnička, and M. Kotora, *Eur. J. Org. Chem.*, 2003, 2882.

18 H. Schottenberger, K. Wurst, and M. R. Buchmeiser, *J. Organomet. Chem.*, 1999, **584**, 301.

19 A. D. Woods, G. Alcalde, V. B. Golovko, C. M. Halliwell, M. J. Mays, and J. M. Rawson, *Organometallics*, 2005, **24**, 628.

20 T. S. Lobana, R. Singh, and E. R. T. Tiekink, *J. Coord. Chem.*, 1990, **21**, 225.

21 J. R. Polam and L. C. Porter, *J. Coord. Chem.*, 1993, **29**, 109.

22 R. M. Stoop, C. Bauer, P. Setz, M. Worle, T. Y. H. Wong, and A. Mezzetti, *Organometallics*, 1999, **18**, 5691.

23 C.-W. Chang, P.-C. Ting, Y.-C. Lin, G.-H. Lee, and Y. Wang, *J. Organomet. Chem.*, 1998, **553**, 417.

24 F. R. Fronczek, H. Breaux, T. G. McBride, and R. S. Srivastava, *Private Communication*, 2001, data obtained from Cambridge Structural Database.

25 R. L. Cordiner, D. Albesa-Jove, R. L. Roberts, J. D. Farmer, H. Puschmann, D. Corcoran, A. E. Goeta, J. A. K. Howard, and P. J. Low, *J. Organomet. Chem.*, 2005, **690**, 4908.

26 R. L. Cordiner, D. Corcoran, D. S. Yufit, A. E. Goeta, J. A. K. Howard, and P. J. Low, *Dalton Trans.*, 2003, 3541.

27 M. I. Bruce, M. G. Humphrey, M. R. Snow, and E. R. T. Tiekink, *J. Organomet. Chem.*, 1986, **314**, 213.

28 J. M. Wisner, T. J. Bartczak, and J. A. Albers, *Inorg. Chim. Acta*, 1985, **100**, 115.

29 saint V6.45, Bruker AXS, Madison, WI, USA, 2001.

30 saint V6.02a, Bruker AXS, Madison, WI, USA, 2000.

31 shelxtl, version 5.10, Bruker AXS, Madison, WI, USA, 1997.